FAMU-FSU COLLEGE OF ENGINEERING
DEPARTMENT OF CIVIL ENGINEERING
TALLAHASSEE, FLORIDA 32310

Excellence With Caring

Final Report

DRILLED SHAFT UNDER TORSIONAL LOADING CONDITIONS

Submitted to

Florida Department of Transportation

By

Kamal Tawfiq, Ph.D., P.E.
Principal Investigator

Department of Civil Engineering

WPI 0510704
Contract # B-9191
FSU Contract # 6120-519-39

June 12, 2000

TECHNICAL REPORT STANDARD TITLE PAGE

1. Report No.	2. Government Accession No.	3. Recipient's Catalog No.
4. Title and Subtitle **Drilled Shaft Under Torsional Loading Conditions**		5. Report Date **January 20, 2000** 6. Performing Organization Code
7. Author(s) Kamal Tawfiq, Ph.D., P.E.		8. Performing Organization Report No.
9. Performing Organization Name and Address : **FAMU-FSU College of Engineering Department of Civil Engineering Tallahassee, Fl 32301**		10. Work Unit No. 11. Contract or Grant No. Contract # B-9191
12. Sponsored Agency Name and Address **Florida Department of Transportation Research Center 605 Suzanne Street, M.S. 30 Tallahassee, Fl 32301**		13. Type of Report and Period Covered Oct. 1996 - Sep. 1999 14. Sponsoring Agency Code
15. Supplementary Note **Prepared in cooperation with the Federal Highway Administration; FDOT Project Manager : Dr. Sastry Putcha**		

16. Abstract

This study was directed toward investigating the effect of the combined modes of loading on the stress distribution along the shaft and determining the torsional capacity of the foundation. Additionly, it was decided to include the effect of the method of construction on the load transfer of the shaft. Using different types of slurry fluids in drilled shaft construction could impact the shear resistance of the soil surrounding the shaft. To achieve our objectives, the study was divided into three phases. The first phase involved thorough laboratory testing on scaled shafts subjected to torsional loads in cohesionless soil. A special testing device was assembled for this purpose. Also the conventional direct shear test was used to determine the shear friction of soil saturated with different types of slurries. Slurry saturation of soil was completed in a testing setup developed exclusively for this study. In this setup the degree of slurry penetration in the soil could easily be determined. The rate of penetration was found to be much higher in polymer slurries as compared with the regular mineral slurries. However, for the mineral slurries, the rate of fluid loss in attapulgite slurry was higher than the bentonite. Also it was found that polymer slurry concentration has a great effect on the rate of fluid loss. High concentrations as 1 to 200 by weight produced penetration rates that were comparable to those obtained from the mineral slurries. This ratio, however, was four times higher than the manufacturers recommended value. Although this finding had been followed in our field testing on a full scale drilled shaft, the outcome performance of the mineral slurry was not satisfactory because of the fact that a regular pump was not able to discharge the high concentration polymer slurry from the boreholes which caused and extended delay when poring the concrete.

In the second phase of the study a through numerical analysis was performed to explore the pattern of the stress distribution along a drilled shaft (4' diameter x 20' length). The three dimensional finite element simulation could give an insight on how lateral stresses evolve when torsional loads are applied simultaneously with the lateral loads and overturning moments. The loads applied in the FE modeling were similar to those used by the FDOT on single and double arm assemblies. Using this technique it was possible to simulate cases of orthogonal loads and moment produced by the two arm assembly. Such type of analysis was not possible using the traditional design methods. The third phase involved full scales tests on three drilled shafts (4' diameter x 20' length). These shafts were constructed using dry method, bentonite slurry, and mineral slurry. The dry hole shaft was used as a control test to compare with the performance of the other methods of construction. A fourth shaft was set between the three shafts to act as a support structure for the applied lateral and torsional loads. The testing arrangement used in this study was the first of its kind, since literature search could produce any full scale torsional testing on drilled shafts. Through the trial and error, it was possible to come up with a loading head for the three shafts and a load supporting unit for the fourth one. Schematics of this setup are present in this study. Results for the full scale testing supported the laboratory findings that the method of construction has a profound influence on the maximum capacity of the drilled shaft under torsional load. The mineral slurry shaft experienced the lowest torsional capacity; while the dry shaft could sustain much higher loads. The modes of failure in the three shafts were also varied. The dry shaft suffered a structural failure that was noticeable from the 45° concrete cracking which developed at torsional load of about 480,000 ft.lb. The bentonite shaft failed at the foundation level and that was evident for the rotational slip of the shaft at torsional load of about 280,000 ft.lb. The polymer slurry shaft failed at a torsional load that was similar to the dry one. As opposed to the dry shaft, some rotational displacement was recorded, but the final failure occurred in the concrete and it was similar to the dry shaft. The field test demonstrated that various types of slurries may produce different magnitudes of torsional capacities in the drilled shaft. Therefore, using bentonite slurry would necessitate using a reduction factor of 0.5 when estimating the soil-shaft frictional resistance. Also, it was found that the existing FDOT methods underestimate d the capacity of the drilled shafts used in the field testing . The ultimate capacities of the shafts were higher than those predicted by the FDOT methods.

Finally, to fulfill our main objectives in determining the capacity of the drilled shaft, it was certain that formulating a closed form solution approach would narrow the gap between the findings of this study and the results obtained from the existing simplified methods. Accordingly, the option was to incorporate the actual stress distribution along the drilled shaft from lateral loads and overturning moments in determining the torsional capacity of the shaft. Considering the most complicated case of loading when double arm assembly is constructed, the orthogonal lateral loads and moments were distributed on the shaft according to AASHTO requirements for the wind load analysis on double arm assembly. Using this distribution, it was possible to adapt the subgrade reaction method to develop a lateral stress distributions along the drilled shaft that was similar to those obtained from the finite element simulations. Consequently, the developed method was formulated in a MathCAD add-in routine where variables can easily be input and a quick solution to the problem could be obtained. It should be noted that the main concern of the developed method was to estimate the maximum capacity of the shaft and not to predict the magnitude of the torsional deformation. The reason for this constrain was that the soil reaction was bounded by the passive resistance of the material. Along the drilled shaft , it was not allowed to for the stress distribution to exceed the upper limit value set by the passive resistance of the soil. Using this method it was possible to correspond the shaft capacities obtained from field testing. A comparative study was done to demonstrate the variations in the shaft resistance to torsional loading using all the available methods.

17. Key Words **Drilled d Shaft, Slurry, Deep Foundation**	18. Distribution Statement No restriction. This document is available to the public through the National Technical Information Service, Springfield Va 22161	
19. Security Classif. (of this report) Unclassified	20. Security Calssif. (of this page) Unclassified	21. No. of Pages 185 pages

DISCLAIMER

The opinions findings and conclusions expressed in this publication are those of the authors and not necessarily those of the Florida Department of Transportation and the Federal Highway Administration.

Prepared in cooperation with the Florida Department of Transportation and the Federal Highway Administration.

FDOT does not endorse any commercial products mentioned in this report.

ACKNOWLEDGMENTS

The Principal Investigator would like to express his sincere regards to the Florida Department of Transportation represented by **Dr. Sastry Putcha,** State Construction Geotechnical Engineer, for managing this project and for providing his assistant and guidance to successfully complete the study. Thanks also to Rodolfo Ruiz, and Hubert Broughton, graduate research assistants, who conducted the field and laboratory testing and analysis of results. Dr. Primus Mtenga has also assisted in formulating the MathCAD solution for the suggested method. Financial support was provided by the Florida Department of Transportation this support is gratefully acknowledged. The Department of Civil Engineering at FAMU-FSU College of Engineering has made it possible by providing the laboratory facilities for this project.

TABLE OF CONTENTS

EXECUTIVE SUMMARY

The Florida Department of Transportation methods to analyze drilled shafts under torsional loading utilize the limit equilibrium approach for the soil surrounding the shaft. Additionally, these methods consider a simple torsional mode of loading only. The effect of the lateral loads on the torsional capacity is not included. In this study an attempt was done to include more than one mode of loading and to consider the method of construction in the analysis of the ultimate torsional capacity. Accordingly, the study was divided into three stages that included laboratory and field testing as well as finite element analysis. The first stage of the study concerned about the constitutive behavior of the soil penetrated with different types of mineral and polymer slurries. The effect of slurry penetration on the frictional resistance of cohesionless soil the interaction of soil-shaft material was included in the study. In the second stage, different tests were conducted on scaled model shaft subjected to torsional and lateral loads. Findings from these efforts were utilized to devise a full scale torsional testing on three drilled shafts constructed using dry borehole, bentonite and polymer slurries.

Results from these tests indicated that drilled shaft with simple torsional load tended to underestimate the actual capacity. Adding lateral loading to the shaft would increase its torsional capacity. An applied lateral load equivalent to the applied torque could increase the torsional resistance by 2 folds. Increasing the lateral load beyond the torque magnitude did not appreciate the torsional resistance. The limited full scale field tests showed that the method of construction has a great influence on the ultimate capacity of the shafts. For the first drilled shaft with dry borehole, the ultimate torsional capacity was almost twice as for the shaft constructed using bentonite slurry. Also, the dry hole shaft capacity was close that of the polymer slurry.

The presence of the bentonite filter cake even after eight months from construction was the main factor behind the reduction in the torsional capacity of the second shaft. Traces of the polymer slurry were found on the third shaft after eight month from construction.

Based on the results of the study, a new procedure was developed to determine the torsional capacity of drilled shaft under torsional and lateral loading. This procedure is based on the p-y curve method and it was formulated using the MathCAD platform. This platform was chosen to provide a compatibility with the FDOT method for designing mast arm structure. The new procedure for drilled shaft capacity was compared with the available FDOT methods.

SUMMARY

Several approaches were suggested for designing drilled shaft under torsional loading conditions. As for the axial and lateral loading, the design methodology of drilled shafts under torsional loading can be grouped into two schools of thought. The first one is based on the assumptions that the foundation soil behaves as a linear or nonlinear elastic material. The second school pertains to the limit equilibrium method where the ultimate capacity of the shaft is governed by the shear strength of the foundation soil. Methods of analyses utilized by the Florida Department of Transportation including District 5, District 7, and the main office methods can be categorized under the second approach.

The FDOT solutions assume rigid-plastic behavior of the material surrounding drilled shaft. Based on this assumption, the torsional resistance of a shaft evolved from the conventional lateral earth pressure theory. The addition of the base resistance comes from assumptions similar to those developed for the Vane Shear test. Therefore, it can be said that both the side friction and the base resistance are obtained from two different methods. The main differences in the FDOT approaches lie in the prediction of the lateral earth pressure coefficient (K_o) and in the stress distribution at the base.

The FDOT methods as well as those described in the literature lack some major understanding of the actual stress distribution in the soil along the drilled shaft. When torsional, axial and lateral loads are simultaneously applied, the lateral stresses should be different than those for the simple torsional case. Such loading combination can be developed from a mast arm assembly subjected to wind loads. The FDOT approaches oversimplify the problem to the level of assuming a simple torsional loading on the shaft from which a triangular stress distribution is developed along the shaft. Also, the FDOT approaches do not consider the effect of slurry fluids on the soil-shaft

frictional resistance. The use of slurries in construction would definitely affect the soil-structure interaction of the drilled shafts. These concerns among others, were thoroughly investigated in this study. The study was divided into three segments namely, laboratory testing, numerical simulation and full scale field experimentations. The laboratory investigation involved two phases. The first phase included the study of the frictional behavior of soil-concrete block samples. The conventional direct shear test was used in this phase. Soil samples were tested under dry and wet conditions. The wet samples were prepared from soils penetrated with mineral and polymer slurries.

During construction the open boreholes are often stabilized by using mineral slurries. According to the FDOT specifications, the slurry should not remain in the borehole for more than 36 hours. At this time span, the borehole must be filled with concrete. However, in 36 hours of slurry exposure, the soil surrounding the borehole could easily be inundated by the slurry. The slurry saturation in addition to the development of the filter cake along the sides of the borehole would eventually affect the perimeter load transfer of the drilled shaft. Knowing that a new generation of slurries represented by various types of polymers, it was necessary to investigate the effect of such materials on the frictional capacity of the drilled shaft. Accordingly, it was decided to device a new testing setup to investigate the rate of slurry penetration of in the cohesionless soil. After the completion of the slurry penetration, soil samples were procured from the device and transferred to the direct shear test. The lower box of the direct shear test was modified to accommodate a 5in x 5in concrete block. The direct shear test was then conducted according to the standard procedure. Results from these tests indicated that soil penetrated with mineral slurries exhibited the lowest frictional resistance followed by polymer slurries. Even among the mineral slurries, it was found that soils penetrated with attapulgite slurry showed higher frictional resistance than those of bentonite slurry. However, filter cakes from bentonite and attapulgite demonstrated the same

reduced frictional characteristics. The thicknesses of the filter cakes layers were higher in the attapulgite slurry than the bentonite. The larger attapulgite filter cake thickness was attributed to the weak fluid retention in the attapulgite particles as compared to the bentonite clay. Additionally, it was found that increasing the polymer slurry concentrations would reduce the fluid loss in the cohesionless soil. To have a compared rate of fluid loss with the mineral slurry, it was found that polymer slurries with concentrations of 1 to 200 would produce identical rates. This concentration ratio is about four times higher that what the polymer industry recommends. Although it is possible to produce such concentrations in the field, it was found however, that pumping out 1 to 200 slurry during concrete placement may not be any easy task.

The second phase of the laboratory study involved testing scaled models of the drilled shaft. Several concrete shafts were prepared with a ratio of 1/12. A special testing device was built in the laboratory to facilitate testing the scaled models. In this device the loading arrangements were set enable testing the shafts under pure torsional shear as well as combined loading of torsion and lateral loads. Using this device, one can test a scaled shaft under dry and submerged soil conditions. The method of load application was controlled strain for which loads were applied at constant rates. Testing results from this phase indicated that lateral loading on drilled shafts increases the torsional resistance of the foundation. The higher the lateral load the more frictional resistance was developed. Testing under pure torsional load produced the most conservative torsional resistance. The effect of the slurry was very noticeable when results were compared with testing in a dry soil. Mineral slurry exhibited the lowest torsional resistance followed by the polymer slurry. High concentrations of attapulgite produced thicker filter cakes and reduced the friction tremendously. Lower attapulgite concentrations showed improved frictional resistance over bentonite slurries. Polymer slurries with concentrations up to 1 to 400 exhibited similar torsional resistance. Increasing the concentration

levels (1 to 200) caused about 15 percent reduction in the frictional capacity. It was found, however, that by increasing the concentration levels of the polymer slurries, the rate of fluid loss can be better reduced to the those experienced by the mineral slurries.

Numerical simulation of a 4 ft diameter and 20 ft length drilled shaft was performed using a three dimensional finite element analysis. The soil was modeled as a nonlinear elastic plastic material using Druker and Pragar yield criterion. The shaft material was modeled as brick concrete elements with steel reinforcement scheme similar to the actual full scale shaft. The soil along the shaft was divided into layer. The stiffness characteristics of each layer was increased with the depth of the shaft. Such modeling was done in order to simulate the actual soil conditions and to avoid having a uniform stiffness along the shaft. Contact elements between shaft surface and surrounding soil were selected with contact stiffness similar to those obtained from the direct shear testing. The main purpose of the numerical simulation was to have a through insight on the actual stress distribution along the drilled shaft.

Solutions from the FEA modeling were then used to modify the p-y curve method so that lateral stresses, overturning moments from different directions on the mast arm assembly were superimposed to produce identical stresses. The new proposed method was then verified using a three full scaled drilled shaft tests at a selected site. One of the field tests was conducted on shaft constructed using the dry method, i.e. without using any slurry fluid. The other two test were conducted on shafts constructed using miner and polymer slurries. A fourth shaft was also constructed to serve as a supporting point for the applied loads. A special shaft-head assembly was designed for the purpose of applying torsional loading. Although this testing arrangement was not a common standard setup, it is recommended that in the future a similar setup can be used to test drilled shaft under combined lateral, overturning, and torsional loads.

Field testing results showed that when no slurries were used the drilled shaft exhibited a large resistance to the applied torque and the mode of failure was predominantly a structural failure. The maximum toque that cased the structural failure was about 480,000 ft.lb In case of mineral slurry the shaft capacity reached about 280,000 ft.lb. The failure of the shaft in this case was at the foundation soil where a noticeable shaft slippage was observed. At the maximum applied torque, the loading arm experience large rotation. On the other hand, the capacity of the third shaft constructed with polymer slurry attained values similar to the dry shaft. Also, the polymer slurry shaft experienced structural failure identical to the dry one.

These results indicated that the lowest torsional resistance was for the bentonite slurry shaft. A reduction factor of 50% of the ultimate field capacity corresponded the results obtained from the laboratory shear tests. The capacity of the third shaft constructed with polymer slurry, exhibited a larger torsional capacity similar to the dry shaft.

Finally, to fulfill the main objectives in determining the capacity of the drilled shaft, it was certain that formulating a closed form solution approach would narrow the gap between the findings of this study and the results obtained from the existing simplified methods. Consequently, the option was to consider the the actual stress distribution along the drilled shaft from lateral loads and overturning moments in determining the torsional capacity of the shaft. Considering the most complicated case of loading when double arm assembly is constructed, the orthogonal lateral loads and moments were distributed on the shaft using AASHTO requirements for the wind load analysis on a double arm assembly. Using this distribution, it was possible to adapt the subgrade reaction method to develop a lateral stress distributions along the drilled shaft that was similar to those obtained from the finite element simulations. Then, the developed method was formulated in a MathCAD add-in routine where variables can easily be input and a quick solution to the problem

could be obtained. It should be noted that the main concern of the developed method was to estimate the maximum capacity of the shaft and not to predict the magnitude of the torsional deformation. The reason for this constrain was that the soil reaction was bounded by the passive resistance of the material. Along the drilled shaft , it was not allowed to for the stress distribution to exceed the upper limit value set by the passive resistance of the soil. Using this method it was possible to correspond the shaft capacities obtained from field testing. A comparative study was done to demonstrate the variations in the shaft resistance to torsional loading using all the available methods.

CHAPTER 1

1.1 Introduction

The purpose for this study was to determine the drilled shaft behavior under combined axial, lateral and torsional loading conditions. Commonly these loading conditions are developed in a mast arm assembly when subjected to wind forces. Even though mast arms produce combination of loads, the critical loading mode in this case is the torsional load.

Such loading conditions have produced a failure at the foundation level at one of the assemblies in Miami, Florida **(Figure 1.1)**. Although it was not a catastrophic failure, its occurrence has raised the question of how do we count for more than one mode of loading when designing drilled shafts. Whether this shaft was to support a mast arm assembly or any other structure, it was found that the knowledge of how the shaft reacts to torsional loads has been grossly oversimplified to a level that other simultaneous Axial, lateral and overturning loads and moments are consistently ignored. This oversight should not be acceptable when the advancements in the hardware and software technology have reached to a stage where more sophisticated techniques such as numerical simulation can be utilized to have an insight on the actual stress distribution along such foundations.

The effect of the construction methods using slurry fluids on the frictional characteristics of soil-shaft interaction was also of concern in this study. Effects of construction procedure could result in a faulty structure. To overcome the adverse effect of using the slurry, the Florida Department of Transportation, **FDOT**, requires that boreholes stabilized with mineral slurries be cleaned from the filter cake layer that accumulates on the sides and the bottom of the boreholes. The cleaning

procedure should take place immediately before placing the concrete in the open holes. However, trimming the soft filter cake layer does not always improve the borehole conditions. This is due to the fact that some of the slurry fluid may seep in the surrounding soil layers especially when cohesionless soils are encountered. Such slurry penetration has not been considered in the past. The penetration problem has become more serious by introducing a new generation of fluids called polymer slurry. This type of slurries do not form any filter cake in the boreholes and hence, the fluid loss in these holes is expected to be much higher than those of the mineral slurries. Saturating the adjacent soil with a viscous fluid may severe the perimeter load transfer of the drilled shafts. This consideration will be addressed in this study. A special testing setup was devised in this study to simulate the slurry penetration under various fluid concentrations and hydrostatic pressures. The aim was to identify the influenced area along the boreholes.

Friction reduction factors should be considered when mineral or polymer slurries are used in construction. Such factors may vary depending on the slurry and the soil types. This investigation was limited to two types of mineral slurries namely, bentonite and attapulgite, and two polymer slurries commercially known Supermud and KB slurries. Also, cohesionless soil samples were chosen to represent the soil conditions in the State of Florida.

1.2 Background

Among other factors, load transfer in drilled shafts depends on the type of the shaft material and the surrounding soils. A major component of the load transfer capacity of a drilled shaft in cohesionless soil is the frictional resistance of the soil. The friction in turn depends on the octahedral stresses in the soil. These stresses are developed due to a combination of the self weight

of the soil and the superimposed stresses. Knowing the actual stresses distribution in the soil along the drilled shaft will facilitate the prediction of the ultimate shaft capacity. Many stress distribution schemes have been suggested. In general, stress distributions along drilled shafts can be summed into two main groups. The first group involves all the schemes which are based on the theory of elasticity. The advantage of assuming elastic behavior of the soil-structure interaction is that the load versus deformation relationships can be established. The second group of analytical methods depends on the assumptions of the plastic behavior of the soil. The foundation soil is assumed to behave as a rigid-plastic material where at a certain load the material undergoes untenable deformation **(Figure 1.2).** In the second groups the ultimate shaft capacity is governed by the strength of the soil material. If deformation is of a concern, then the first group of analysis should be considered.

The following sections present in details methods of analysis of drilled shafts subjected to torsional and lateral loading. Both modes of loading were treated in literature using either load-deformation methods which pertain to the first group or the limit equilibrium methods which are encompassed in the second group.

1.3 Shaft Behavior Under Torsional Loads

Poulos (1975b) presented an elastic analysis for the determination of the response of a single cylindrical drilled shaft subjected to torsion. He investigated the torsional relationships for both a uniform soil and a soil in which shear modulus and shaft - soil adhesion increases linearly with depth. **Figure 1.3** illustrates the problem considered in terms of loading, drilled shaft geometry and soil parameters.

The method of analysis is similar to that previously employed for analysis of axial and lateral drilled shaft response (Poulos and Davis, 1968, and Poulos, 1971). It involves the use of elastic theory for computing the soil rotation at the mid-point of each element in terms of the unknown interaction stresses. The corresponding drilled shaft rotations are then expressed in terms of these interaction stresses by considering the drilled shaft as a circular rod. Under conditions where the soil-drilled shaft interface remains elastic, the soil and drilled shaft rotation equations are solved in conjunction with a static equilibrium equation to obtain the interaction stress and thus the drilled shaft rotation. The foregoing method was modified to simulate nonlinear relationships between torque and twist by considering elastic-perfectly plastic behavior of the soil after slippage occurs between the drilled shaft and soil. Based on the above quasi-elastic analysis, Poulos presented parametric solutions for the drilled shaft-head torque-twist relationship. For a uniform diameter drilled shaft, the drilled shaft-head rotation (twist), φ_o, of a drilled shaft subjected to torque T_0 may be expressed as follows:

For uniform soil

$$\varphi_o = (T_o / G_s d^3) .(I_\varphi / F_\varphi) \qquad \textbf{1.1}$$

For linearly increasing shear modulus and drilled shaft-soil adhesion

$$\varphi_o = (T_o / N_G d^4) .(I_{\varphi'} / F_{\varphi'}) \qquad \textbf{1.2}$$

in which

G_s	=	Soil shear modulus
I_φ	=	Influence factor for elastic rotation in uniform soil
F_φ	=	Correction factor for drilled shaft-soil slip in uniform soil
$I_{\varphi'}$	=	Influence factor for elastic rotation in soil with linearly increasing shear modulus
$F_{\varphi'}$	=	Correction factor for drilled shaft-soil slip in soil with linearly increasing shear modulus
N_G	=	Rate of increase of shear modulus with depth (e.g.,$G_s = N_G$ depth), and
d	=	Diameter of drilled shaft.

The above factors are functions of drilled shaft length, L, drilled shaft diameter, d, and a relative rotational stiffness factor K_T. The factors can be evaluated using **Figure 1.4**

The approach suggested by Poulos is restricted to the analysis of drilled shaft-head torque and twist behavior only and does not permit computation for the dissipation of torsional stresses with depth. In addition, the method is limited from the point of view of its applicability to drilled shafts embedded in uniform soil (constant shear modulus) and in soil with linearly increasing shear modulus. Furthermore, the elastic analysis does not permit relaxation of shear at the drilled shaft-soil interface after slippage has occurred, resulting in errors in the non-linear range (O'Neill and Dutt, 1976).

Earlier work in the development of a mathematical model to simulate the mechanism of torsionally loaded drilled shafts was undertaken by O'Neill (1964, 1969). He established a closed form differential equation solution for the drilled shaft-head torque and twist relationship for the case in which both the drilled shaft and the soil in which the drilled shaft is embedded are assumed to have linear torque-twist properties.

Figure 1.5 illustrates a deformed increment representing a free body element from a torsionally linear cylindrical drilled shaft embedded in a torsionally linear soil. The closed-form solution of the differential equation under known boundary conditions results in equations relating torque distribution as a function of depth and drilled shaft-head torque and twist in terms of soil and drilled shaft properties. These relationships may be expressed as:

$$T(Z) = T_o e^{-Z\sqrt{\beta\lambda}} \qquad \textbf{1.3}$$

$$(T / \theta)_{\text{Drilled shaft Head}} = \sqrt{\lambda / \beta} \qquad \textbf{1.4}$$

where:

J_o = The torque applied at the top of the drilled shaft

β = The reciprocal of the product of the drilled shaft material shear modulus, G_p and its polar moment of inertia, J (i.e., the reciprocal of the torsional stiffness of the drilled shaft)

λ = A function of the torsional restraint of the soil = $4\pi r^2 G_s$

r = Radius

G_s = Shear modulus of the soil

An example of torque dissipation for this linear interaction problem with an applied torque at the top of the drilled shaft is shown in **Figure 1.6.**

The above linear interaction problem is based on the assumption that the torsional restraint of the soil can be represented for all rotations and for all depths by a single parameter, A. However, the boundary effects near the top of the drilled shaft could possibly preclude the use of a value for **A** which is constant with depth, and drilled shaft-soil bond failure or shear failure in the soil could negate the use of a value for A which is constant with rotation (O'Neill, 1964). Furthermore, a soil which exhibits near-linear torsional resistance properties at small rotation is highly non-linear near failure. Therefore, if the analysis is limited to small rotations, Equations 1.3 and 1.4 yield reasonable results.

In order to include the non-linearities described, O'Neill (1964) introduced a discrete element model that simulates torsional behavior of a circular, prismatic drilled shaft. A three-element portion of that model is shown in **Figure 1.7**.

It is seen that the mechanical model is composed of rigid elements connected by torsional springs with spring constants K_i expressed in-lb/radian, where the subscript i designates a particular

element. Each of these springs represents a concentrated torsional stiffness proportional to the average JG_p between points on the real drilled shaft. The constant of proportionality is 1/h, where h is the incremental length, or the distance between centers. It should be noted that the spring constants are permitted to vary from one element to another, thus allowing simulation of a drilled shaft with variable cross-section and/or shear modulus. These springs can be used to simulate nonlinear twist behavior as well.

A typical soil resistance curve for one element is shown in **Figure 1.8**. It is assumed that in the mechanical model the non-linear torsional resistance of the soil can be represented partially by a spring constant S_i in-lb/radian, and partially by a fixed moment M_{oi}. Parameter S_i and M_{oi} are assumed to be functions only of the rotation of the ith element and, thus, independent of the behavior of all other elements.

The soil resistance for some rotation θi of the ith element can be seen to be equal to M_{oi} plus the product of the rotation of the element and the slope Si of the curve at θi. The soil resistance curve is drawn so that a positive rotation produces a negative soil moment, indicating that the resisting moment acts opposite in sense to the direction of rotation. Since M_{oi} and Si may vary from element to element, the model can be used to simulate drilled shafts embedded in soil whose properties vary with depth. The real drilled shaft can be represented by any number of elements or increments. Boundary conditions consist of specified torque at any element desired.

1.4 Response of Soil to Torsional Loading

The solution of the general mode T for the soil drilled shaft interaction due to torsional loading is based on the premise that the individual torque-twist properties of the, soil and drilled shaft are known. However, very little information is presently available on criteria describing , torsional load transfer from the drilled shaft to the soil Following is a review of the present state-of the art in terms of concepts and criteria governing the torsional load transfer mechanism.

Cadling and Odenstad (l950) first advanced a formula for the soil shear strain corresponding to the measured values, of the torque and twist by the vane shear device as reviewed below. In **Figure 1.9** are shown two views of a typical rigid cylinder embedded in a homogenous material enclosed by a cylindrical container and subjected to a rotational moment around its longitudinal axis. in order to simplify the analysis, the following assumptions are made:

1- The rupture surface is a circular cylinder surrounding the drilled shaft.
2- The shear stress distribution is uniform across the whole rupture surface.

Based on the principles of statics, the magnitude of torque can be expressed as:

$$T = 2\pi L r_i^2 \tau i \qquad 1.5$$

where L is the embedded length of the cylinder; ri is any radius and τi is the shearing stress at radius ri. It follows then, that at the surface of the cylinder the total torque is given by

$$T_o = 2\pi L r_o^2 \tau o\ 1 \qquad 1.6$$

Equating the right-hand expression of Equations 1.5 and 1.6, the following relationship results:

$$\tau_i = (r_o)^2/(r_i)^2\ \tau_o \qquad \mathbf{1.7}$$

Substituting the shearing strain, γ, from the formula $= \gamma G_s$ in which G_s is the soil modulus

$$\gamma_i = (r_o)^2/(r_i)^2\ \gamma_o \qquad \mathbf{1.8}$$

where γ is the shear strain at the surface of the cylinder.

Referring to **Figure 1.10** the shearing strain for any soil element at a radius ri from the center of rotation is given by or, by ignoring products of differentials and simplifying

$$\gamma_i = -r_i \, d\theta/dr_i \qquad \textbf{1.9}$$

Combining Equations 1.8 and 1.9,

$$d\theta/dr_i = -(r_o^2/r_i^3)\ \gamma_o \qquad \textbf{1.10}$$

Integrating both sides of Equation 1.10 between limits defined by the boundaries shown on **Figure 1.9** where ri becomes large, an expression is established for relating the shearing strain, γo, at the surface of a rotating cylinder with the angle of rotation θ. This expression is

$$\theta = \gamma o /2 \qquad \textbf{1.11}$$

Equations1.6 and 1.11 thus represent the torsional restraint of the soil over the length L of a rigid cylinder in terms of the soil shear stress-strain properties at the surface.

For determining the torque-twist curve for the soil, Tucker (1960) proposed the following form representing the soil shear stress-strain characteristics

$$\gamma = A\tau^n \qquad \textbf{1.12}$$

where γ is the unit shearing strain due to a unit shearing stress, τ. The parameters A and n are properties of the material.

Substituting Equation 1.12 in Equation 1.9 and solving the resulting differential equation between the limits defined by the boundaries of the problem, an expression for the angle of rotation at the surface of the cylinder, similar to Equation 1.11 is obtained.

$$\theta = (½\ n)\ A\ \tau_o^{\ n} \qquad \textbf{1.13}$$

The vales of A and n are not directly obtainable, but the torque -twist curves from rotational tests performed on soil samples in the laboratory, such as vane shear tests on clays, can be plotted on log-log paper to obtain these values (Tucker, 1960).

Ha (1976), based on the work by Tucker (1960) and O'Neill (1964), resented guidelines for determining soil torque-twist curves for clay. Criteria presented by Ha are primarily based on Equations 1.6 and 1.13 and the use of rotational shear tests performed on soil samples in the laboratory or in situ. The following is a summary of the procedure outlined for developing soil torque-twist curves for drilled shafts embedded in clay:

1. Draw a logarithmic plot of the results of a vane shear test with the angle of rotation as abscissa and corrected shear stress as ordinate **(Figure 1.11)** and obtain the parameters A and n.
2. Employing Equations 1.6and 1.13, generate the soil torque-twist curve for each increment of the drilled shaft.

Bjerrum (1972) recommends the modification of measured shear strength values from high speed rotational tests in soft clays to respond to low rate of field loading conditions. Based on this, Ha proposed the use of Bjerrum's correction factor (related to the plasticity index of the soil) to the vane shear test results. The procedure just outlined serves to provide only a rough prediction of the torsional response of a drilled shaft and is limited to clay soils

Other Methods

Saul (1968), in his general method of analysis for three-dimensional drilled shaft foundations, proposed a simple criterion for estimating the soil-pile interaction due to torsional loads by considering the drilled shaft as a semi-infinite shaft on an elastic foundation. The criterion representing reaction of the drilled shaft may be expressed as

$$T(z) / \theta(z) = (\delta K_T) (JG/L_e) \qquad \textbf{1.14}$$

which $T(z)$ = Torque present in the drilled shaft at any depth, Z.
$\theta(z)$ = Rotation of the drilled shaft at any depth Z
δ = End restraint condition; 0, for hinged connection; 1, for a fixed connection,
K_T = Combined shape and participation factor; 1, for end bearing drilled shafts, and 2, for friction drilled shafts,
J = Polar moment of inertia of the drilled shaft,
G = shear modulus of the drilled shaft material,
L_e = the effective drilled shaft length,

Equation 1.14 is limited to the linear case and does not consider soil conditions except indirectly through L_e. The determination of L_e is, however, left to the judgement of the user.

Another alternative, probably the most straight forward and accurate practical method for the determination of torsional soil resistance, would be the direct in situ measurement of torque versus twist using full scale test drilled shafts. In this way, the effects of driving upon the drilled shaft- soil adhesion could be investigated while the soil disturbance would closely correspond to that found in the actual foundation drilled shaft. This technique, although accurate, is usually far more expensive than calculating soil resistance versus twist from a laboratory evaluation of **A** and **n**. It is because of these practical limitations (from the economic point of view) and scarcity of information regarding torsional soil-drilled shaft response in granular media, that the main objectives of the research described herein was to study the mechanism of torsional load transfer and the characteristics of torsionally loaded drilled shafts in granular soil.

1.5 Current Drilled Shaft Torsional Designs Methods In Florida

Currently, there are three major methods of drilled shaft design employed by the Florida Department of Transportation. These methods are categorized as follows: the Structures Design Office Method (of the Central Office), the District 5 Method, and the District 7 Method. The Structures Design

Office Method is the more commonly used design method by engineers in the FDOT.

1.5.1 Structures Design Office Method

The Structures Design Office Method was developed based on the assumptions that the drilled shaft is subjected to a simple torsional load and that the soil behaves as a rigid plastic material. The method can be applied for cases of drilled shafts in cohesive or cohesionless soils. Stratified soil can also be considered in this method providing that the length of the shaft be divided into distances equal to the depths of the soil layers. The FDOT Structural Design Method can be used as an add in MathCAD application and is known as MASARM. For cohesionless soil the method can be used as follows:

$$T_s = (K_o \cdot \gamma \cdot 0.5\, L^2) \cdot \pi \cdot D \cdot \tan\delta \cdot 0.5D \qquad \textbf{1.15}$$

Where,

T_s = side torsional resistance, ft-kips,
K_o = at rest lateral earth pressure coefficient,
γ = effective soil unit weight, lb/ft^3,
L = length of drilled shaft foundation, ft,
D = diameter of drilled shaft foundation, ft,
δ = friction angle at the soil-concrete interface, in the case of drilled foundations it is equal to the internal friction angle of the soil, φ of embedded soil.

Additionally, the base torsional resistance can be estimated as:

$$T_b = W \cdot \tan\delta \cdot 0.33D \qquad \textbf{1.16}$$

Where, T_b = base torsional resistance, ft-kips,
W = weight of the drilled shaft foundation, kips,
D = diameter of the drilled shaft foundation,
δ = friction angle at the soil-concrete interface, in the case of drilled foundations it is equal to the internal friction angle of the soil, φ of embedded soil.

After determining the side and base frictional resistance, the total torsional capacity of a drilled shaft is

$$T_{total} = T_s + T_b \quad \textbf{1.17}$$

1.5.2 District 5 Method

In this method the ultimate skin friction (Qs) from the SHAFTUF program is utilized to determine the side friction of the drilled shaft. accordingly the side torsional resistance equals

$$T_s = Q_s\,(D/2) \quad \textbf{1.18}$$

Also the base torsional resistance is computed as the following:

$$T_b = 0.67\,.\,(W + A_y)\,.\,\tan(0.67\,\varphi)\,.\,(D/2) \quad \textbf{1.19}$$

Where, W = the weight of the deep drilled shaft, lbs,
A_y = vertical loading upon the drilled shaft, lbs.

The total resistance is the summation of the side and the base torsional resistance.

Also District 5 proposed that O'Neil and Hassan approach for shaft under axial loading can also be used. They suggested the following for cohesionless soil:

$$f_s = \sigma_{vz}\,.\,\beta \quad \textbf{1.20}$$

Where: σ_{vz} = effective vertical stress
β = load transfer ratio and it can be estimated as:
For $N_{SPT} > 15$ $\quad \beta_{nominal} = 1.5 - 0.135\sqrt{z} \quad 1.2 \geq \beta_{nominal} \geq 0.25$
For $N_{SPT} < 15$ $\quad \beta = (N/15)\,.\,\beta_{nominal}$.

Where: z = depth below ground surface, ft

The total side friction can be described as

$$Q_s = \pi\,.\,D\,.\,L\,.\,f_s \quad \textbf{1.21}$$

The base resistance to torsional loading is

$$Q_b = 0.67\,.\,(W + A_y)\,.\,\tan(\delta) \quad \textbf{1.22}$$

The total torsional resistance equals

$$T = Q_s \cdot (D/2) + Q_b \cdot (D/2) \quad \textbf{1.23}$$

1.5.3 District 7 Method

This method is literally based on the α method. Accordingly, the unit friction can be expressed as:

$$fs = \alpha \cdot C + \boldsymbol{\sigma} \cdot \mathbf{K} \cdot \tan\delta \quad \textbf{1.24}$$

where

α = the adhesion factor,
C = the average cohesion for the soil stratum of interest,
σ_v = effective vertical stress on the segment of the shaft,
δ = effective friction angle at the soil concrete interface (usually taken as ½f - ⅔f).
K = coefficient of lateral earth pressure, values close to K_o are generally recommended and

$$\mathbf{K_o = (1 - \sin\varphi)\sqrt{OCR}} \quad \textbf{1.25}$$

OCR = the over consolidation ratio,

The total base resistance is determined as

$$Q_s = 0.67 \cdot (W + A_y) \cdot \tan(\delta) \quad \textbf{1.26}$$

W, A_y, and δ are the same as previously defined. From the equations the total torsional side resistance along the shaft can be obtained using

$$T_s = p \cdot L \cdot \sum f_s \cdot D/2 \quad \textbf{1.27}$$

Where:

P = circumferential area of drilled shaft foundation, pD,
L = length of drilled shaft foundation, ft,
D = diameter of drilled shaft, ft.

The total base resistance to torsion can be obtained by

$$T_b = Q_b(0.67 \cdot D) \quad \textbf{1.28}$$

The total torsional resistance is equal to the sum of the side and the base torsional resistance. Assumptions involved in the four FDOT methods are presented in **Figures 1.12 and 1.13**.

1.6 Illustrative Example

To demonstrate the applicability of the FDOT methods in determining drilled shaft resistance to torsional loading Lai (1997) presented a comparison of the four methods in a solved problem format. Assuming a hypothetical drilled shaft situation similar to a typical one used in the construction of mast arm assembly in Florida (L = 25' and D = 4'), the various torsional capacities in cohesionless soil (γ = 120 pcf, φ = 30°) are presented in **Table 1.1**.

Table 1.1 Summary of Drilled Shaft Capacity using FDOT Methods

Axial Load A_y = 4437.2 lb		Torsional Load , M_t = 170600 ft.lb			
Depth to Water Table (ft)	Method	Side Resistance Ts (ft.lb)	Base Resistance Tb (ft.lb)	Total Resistance, T (ft.lb)	Factor of Safety
0	SDO	130594	36276	166870	0.978
	District 5	268080	25283	293400	1.72
	District 5M	178900	15672	194600	1.14
	District 7	224600	29760	254400	1.49
15	SDO	272070	36276	308346	1.81
	District 5	268080	25283	293400	1.72
	District 5M	178900	21440	200300	1.17
	District 7	445400	29760	475100	2.78

District 5M is the modified method using β method.

1.7 Shaft Behavior Under Lateral Loads

Lateral loads and moments may act on drilled shafts in addition to the torsional loads. The two drilled shaft head fixity conditions - free-head and fixed headed may occur in practice. **Figure 1.14** shows the combined loading conditions on a drilled shaft of a mast arm assembly. For simplicity it is possible to superimpose all the loads on the drilled shaft **(Figure 1.15)**. However, loading condition such as lateral load and overturning moment should be considered when estimating the lateral soil pressure along the shaft **(Figure 1.16)**. As for the loads the deformation modes can also be superimposed.

Lateral shaft capacity can be determined using one of the following two criteria:

2. Allowable lateral load is obtained by dividing the ultimate (failure) load by an adequate factor of safety
3. Allowable lateral load is corresponding to an acceptable lateral deflection.

The smaller of the two above values is the one actually adopted as the design lateral load. Examples of the first category are Brinch Hansen's Method (1961) and Broms' Method (1964 a,b). Methods of the second category include modulus of subgrade reaction approach (Reese and Matlock, 1956) and elastic approach (Poulos, 1971a and b).

The Brinch Hansen's method is based on earth pressure theory and has the advantage that it is:

1. Applicable for c - φ soils
2. Applicable for layered system

However, this method suffers from disadvantages that it is

1. Applicable only for short drilled shafts

2. Requires trial-and-error solution to locate point of rotation

Broms' Method is also based on earth pressure theory, but simplifying assumptions are made for distribution of ultimate soil resistance along the drilled shaft length. This method has the advantage that it is:

1. Applicable for short and long drilled shafts
2. Considers both purely cohesive and cohensionless soils
3. Considers both free-head and fixed-head drilled shafts that can be analyzed separately

However, this method suffers from disadvantages that:

1. It is not applicable to layered system
2. It does not consider c-φ soils

In the modulus of subgrade reaction approach it is assumed that soil reacts as a series of independent linearly elastic springs. This method has the advantage that:

1. It is relatively simple
2. It can incorporate factors such as nonlinearity, variation of subgrade reaction with depth, and layered systems
3. It has been used in the practice for a long time

Therefore, a considerable amount of experience has been gained in applying the theory to practical problems. However, this method suffers from disadvantages that:

1. It ignores continuity of the soil
2. Modulus of subgrade reaction is not a unique soil property hut depends on the foundation size and deflections.

On the other hand, the elastic solution by Poulos, (1971a and b) assumes the soil as as an ideal elastic continuum. The method has the advantage that:

1. It is based on a theoretically more realistic approach,
2. It can give solutions for varying modulus with depth and layered system.

However, this method suffers from disadvantages that:

1. It is difficult to determine appropriate strains in a field problem and the corresponding soil moduli
2. It needs more field verification by applying theory to practical problems.

1.7.1 Acceptable Deflection at Working Lateral Load

In most situations, the design of drilled shafts to resist lateral loads is based on acceptable lateral deflection rather than the ultimate lateral capacity. The two generally used approaches of calculating lateral deflections are:

1. Subgrade reaction approach (Reese and Matlock, 1956, Matlock and Reese 1960)
2. Elastic continuum approach (Poulos, 1971a and b)

Subgrade Reaction Approach: This approach treats a laterally loaded drilled shaft as a beam on elastic foundation **(Figure 1.17 b, c)**. It is assumed that the beam is supported by a Winkler soil model according to which the elastic soil medium is replaced by a series of infinitely closely spaced independent and elastic springs. The stiffness of these springs k_h (also called the modulus of horizontal subgrade reaction) can be expressed as follows **(Figure 1.17 d):**

$$k_h = p / y \qquad \textbf{1.29}$$

where

p = the soil reaction per unit length of drilled shaft

y = the drilled shaft deformation and *kh* has the units of force length2

Palmer and Thompson (1948) employed the following form to express the modulus of a horizontal subgrade reaction:

$k_x = k_h (x / L)^n$ **1.30**

where

k_h = value of k~ at x = L or tip of the drilled shaft

x = any point along drilled shaft depth

n = a coefficient equal to or greater than zero

The most commonly used value of n for sands and normally consolidated clays under long-term loading is unity. For overconsolidated clays i is taken zero. According to Davisson and Prakash (1963). a more appropriate value of ii will be 1.5 for sands and 0.15 for clays under undrained conditions.

For the value of n = 1, the variation of k_h with depth is expressed by the following relationship:

$k_h = n_h . x$ **1.31**

where n_h is the constant of modulus of subgrade reaction. This applies to cohensionless soils and normally consolidated clays where these soils indicate increased strength with depth due to overburden pressures and the consolidation process of the deposition. Typical values are listed in **Table 1.2.** For the value of n = 0, the modulus will be constant with depth and this assumption is most appropriate for drilled shafts in overconsolidated clays.

The soil reaction vs. deflection relationship for real soils is nonlinear and Winkler's idealization would require modification. This can be done by using p t curves approach. The behavior of a drilled shaft can thus be analyzed by using the equation of an elastic beam supported on an elastic

foundation and is given by the following equation:

$$EI\,(d^4y/dx^4) + p = 0 \qquad \textbf{1.32}$$

where
E = modulus of elasticity of drilled shaft
I = moment of inertia of drilled shaft section
p = soil reaction which is equal to (k_h y)

Equation (1.32) can be rewritten as follows:

$$(d^4y/dx^4) + (k_h\, y / EI) = 0 \qquad \textbf{1.33}$$

Elastic Continuum Approach: The determination of deflections and moments of drilled shafts subjected to lateral loads and moments based on the theory of subgrade reaction is unsatisfactory as the continuity of the soil mass is not taken into account. The behavior of laterally loaded drilled shafts for soil as an elastic continuum has been examined by Poulos (1971 a, and b). Although this approach is theoretically more realistic, one of the major obstacles in its application to the practical problem is the realistic determination of soil modulus E_s ($k_h \approx E_s$). Also. the approach needs more field verification by applying the theoretical concept to practical problems. Therefore, only the basic theoretical concepts and some solutions, for this approach will be described here. These concepts will be helpful in comparing this approach with the subgrade reaction approach.

Theoretical Basis Theoretical basis for the elastic continuum approach solution is as follows:

1. As shown in **Figure 1.18**, the drilled shaft is assumed to be a thin rectangular vertical strip of width B, length L, and constant flexibility **El.** The drilled shaft is divided into (n + 1) elements of equal lengths except those at the top and tip of the drilled shaft, which are of length (δ/2)
2. To simplify the analysis, possible horizontal shear stresses developed between the soil and the sides of the drilled shaft are not taken into account.

3. Each element is assumed to be acted on by a uniform horizontal force ***P,*** which is assumed constant across the width of the drilled shaft.
4. The soil is assumed to be an ideal, homogeneous, isotropic, semi-infinite elastic material, having a Young's modulus E_s and Poisson's ratio ν_s ,which are unaffected by the presence of the drilled shaft.

In the purely elastic conditions within the soil, the horizontal displacements of the soil and of the drilled shaft are equal along the drilled shaft. In this analysis, Poulos (1971) equates soil and drilled shaft displacements at the element centers. For the two extreme elements (the top and the tip), the displacements are calculated. By equating soil and drilled shaft displacements at each uniformly spaced points along the drilled shaft and by using appropriate equilibrium conditions an unknown horizontal displacement at each element can be obtained.

1.8 Drilled Shaft Construction Using Slurries

1.8.1 Mineral Slurries

Slurries used in drilled shaft construction are usually prepared from two types of clay minerals. The first one in known as bentonite slurry and is widely used by other industries in various engineering and non engineering applications. The second type of slurry is made up of attapulgite clay which can be found Florida and southern Georgia. Attapulgite clay is rarely used in other places also its supply is limited to tow manufacturing facilities in these two states.

1.8.2 Bentonite Slurries

Bentonite is a sodium montmorillonite clay named after its a primary deposit nearby the city of Fort Benton, Wyoming. Bentonite has proven to have many uses and is very common material in various geotechnical engineering applications. For mineral slurries, bentonite is more commonly used than attapulgite. Bentonite has high swelling capabilities and plastic properties. It is a colloidal mineral with liquid limits reaching 500%. It is classified as a sodium montmorillonite with the following chemical structure, $(OH)_4\ Si_8\ (Al_{3.34}Na_{0.66})O_{20}$. Particle sizes for typical bentonite samples are 10Å in thickness and with long axis being 2 mm. The bentonite slurry is highly viscous and opaque. In drilled shaft construction, bentonite is mixed with water to form a viscous slurry fluid. The slurry is then applied to stabilize the borehole sides. Stabilization is induced by the hydrostatic pressure of the high density - viscosity slurry which acts against the lateral earth pressure in the hole. Before concrete placement, the sides are cleaned from the accumulations of the filter cake that adhere to the sides and the bottoms of the holes. The presence of the filter cake layer may adversely impact the load transfer mechanism of the drilled shaft. Certain procedures are usually followed in the field to inspect the properties of the slurry to insure its performance during and after the drilling stage.

1.8.3 Attapulgite Slurries

Attapulgite is a rare type of clay mineral with only a few mining sites in the entire world. Attapulgite minerals are formed of double chain bands of silica tetrahedra. They can be described as a fine thread like morphology with diameter between 50 and 100Å and lengths between 4 and 5 mm. Attapulgite displays the following chemical structure, $(OH_2)_4(OH)_2Mg_5Si_8O_{20}\cdot 4H_2O$. Attapulgite is favorably, but not often, used in drilling because of its high stability suspension in

saline environments. When mixed with water, the attapulgite slurry form a highly viscous substance . The application of attapulgite slurry is the same for the bentonite slurry.

1.8.4 Polymer Slurries

Polymer slurries, unlike, mineral slurries are not of a suspended particulate nature. Polymer slurries also behave differently than mineral slurries during application. The main difference between polymer and mineral slurries in drilled shaft construction is the formation of the filter cake in case of mineral slurries. The presence of this layer may help in reducing the rate of fluid loss in the borehole. To achieve the same performance for the polymer slurries, the concentrations of the fluids have to be increased. However, the absence of the filter cake may ease the process of borehole cleaning before concrete placement.

1.8.5 KB SlurryPro CDP

One type of polymer slurry is a water- soluble vinyl acetate-maleic polymer. It is mixed by weight in typical concentration of 1 g solid polymer to 1000 g water. For research purposes the range of the concentrations will be between 0.5:1000 and 2:1000. The polymer mix is of a granular structure and forms a high viscosity fluid when added to water. However, it the fluid is not thoroughly mixed clumps of gelatin will form and suspend in water leaving the fluid non-homogeneous. The fluid is transparent, and the transparency is not altered by fluctuated concentrations.

1.8.6 PDSCo Supermud

The second polymer slurry to be tested is prepared from a highly concentrated liquid. It an emulsified form of polymer material which mixes more readily than dry granular polymer materials. It is mixed with water according to volume. Typical practice recommends mixing 1 mL of polymer to 800 mL of water. During research the concentrations were varied between 1:200 and 1:800. Again the viscosity is adjustable with varying concentrations. This polymer, however, forms a translucent fluid instead of transparent. Translucency increases with increasing concentrations.

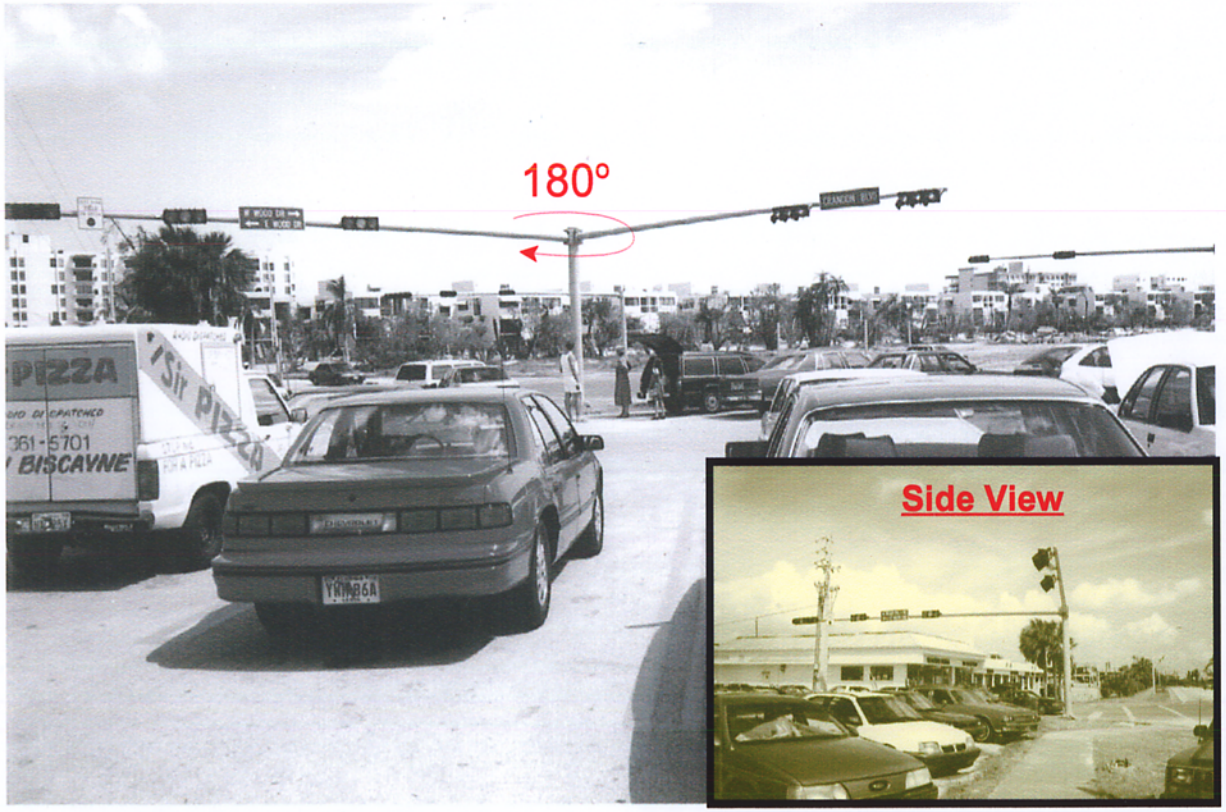

Figure 1.1 Torsional Failure at the Foundation Level.

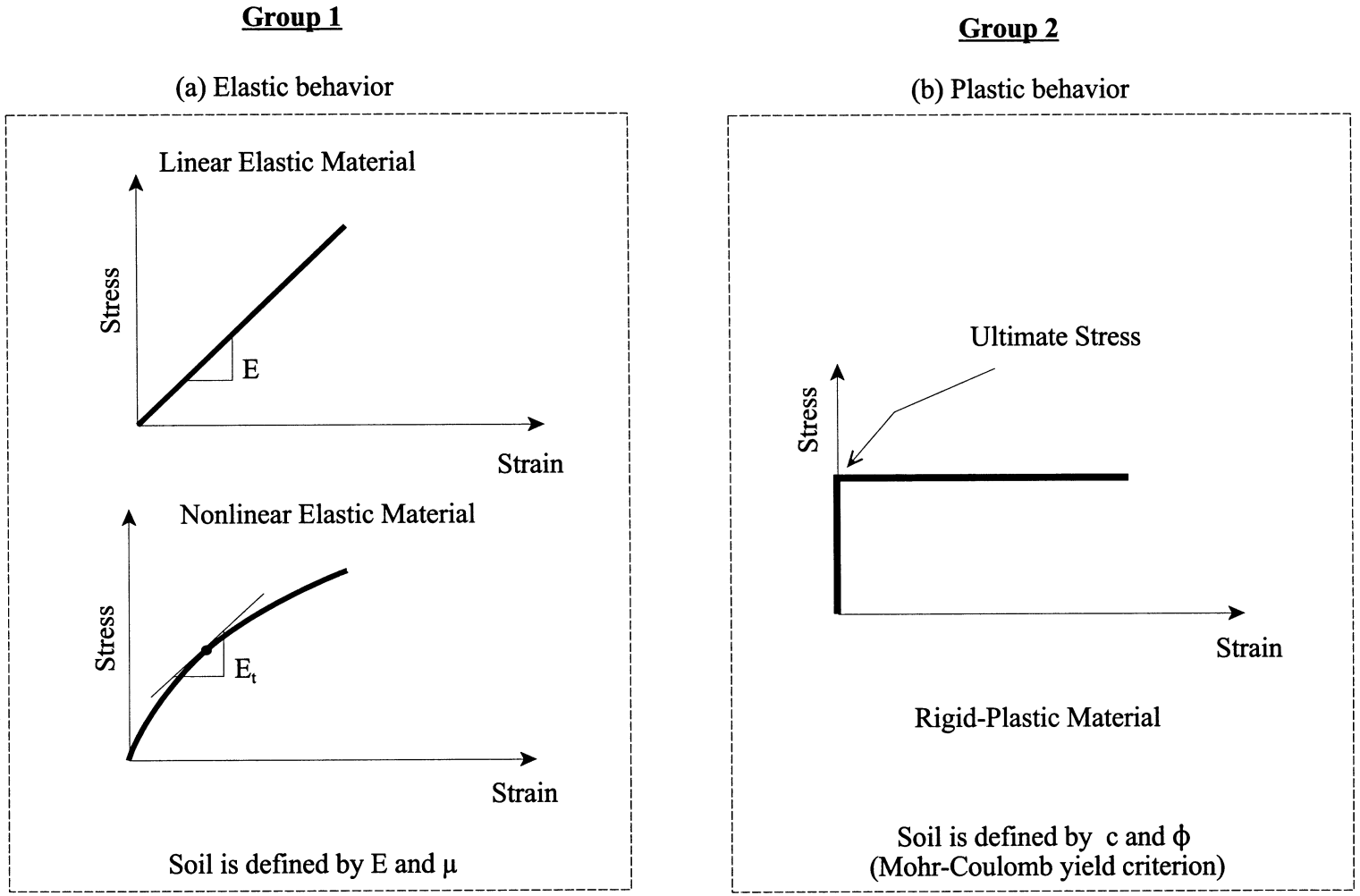

Figure 1.2 Assumptionso of the stress vs. Strain behavior of the soil (a) Deformation methods, (b) Limit equilibrium methods.

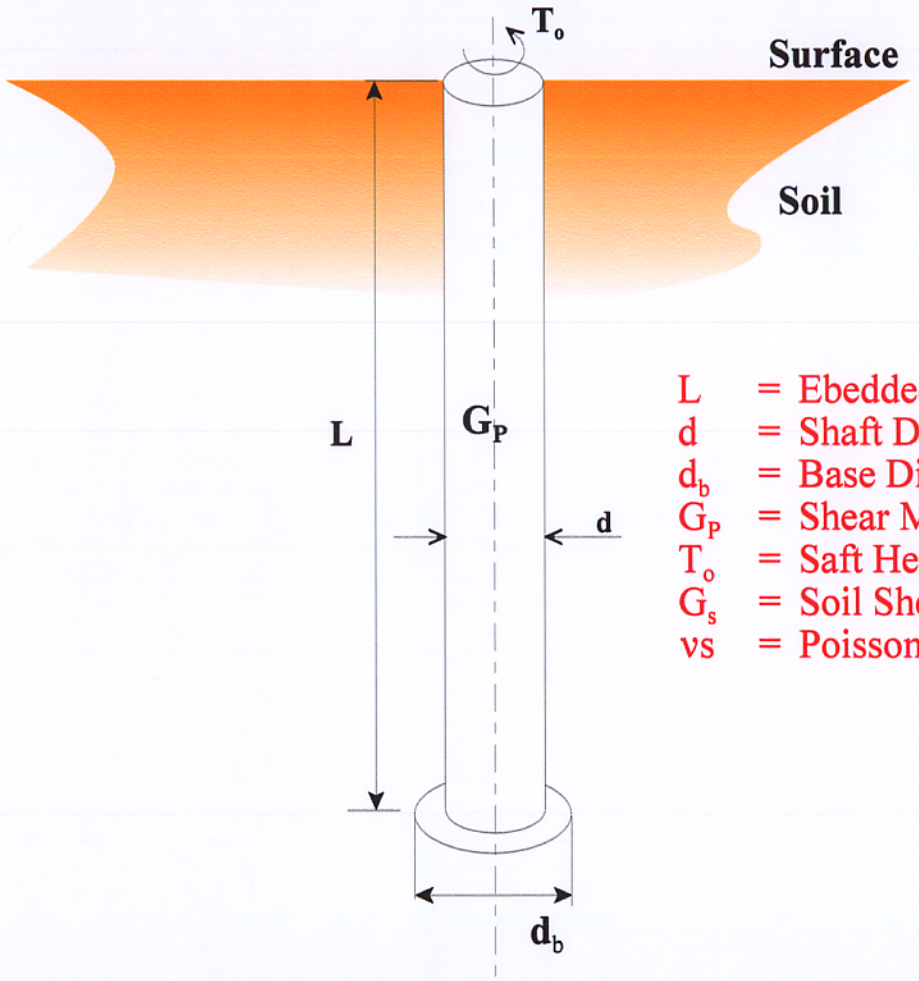

L = Ebedded Shaft Length
d = Shaft Diameter
d_b = Base Diameter
G_P = Shear Modulus pd Shaft Material
T_o = Saft Head Torque
G_s = Soil Shear Modulus
νs = Poisson's Ration for soil

Figure 1.3 Illustration defining Torsional Soil -Shaft Problem (Poulos, 1975b)

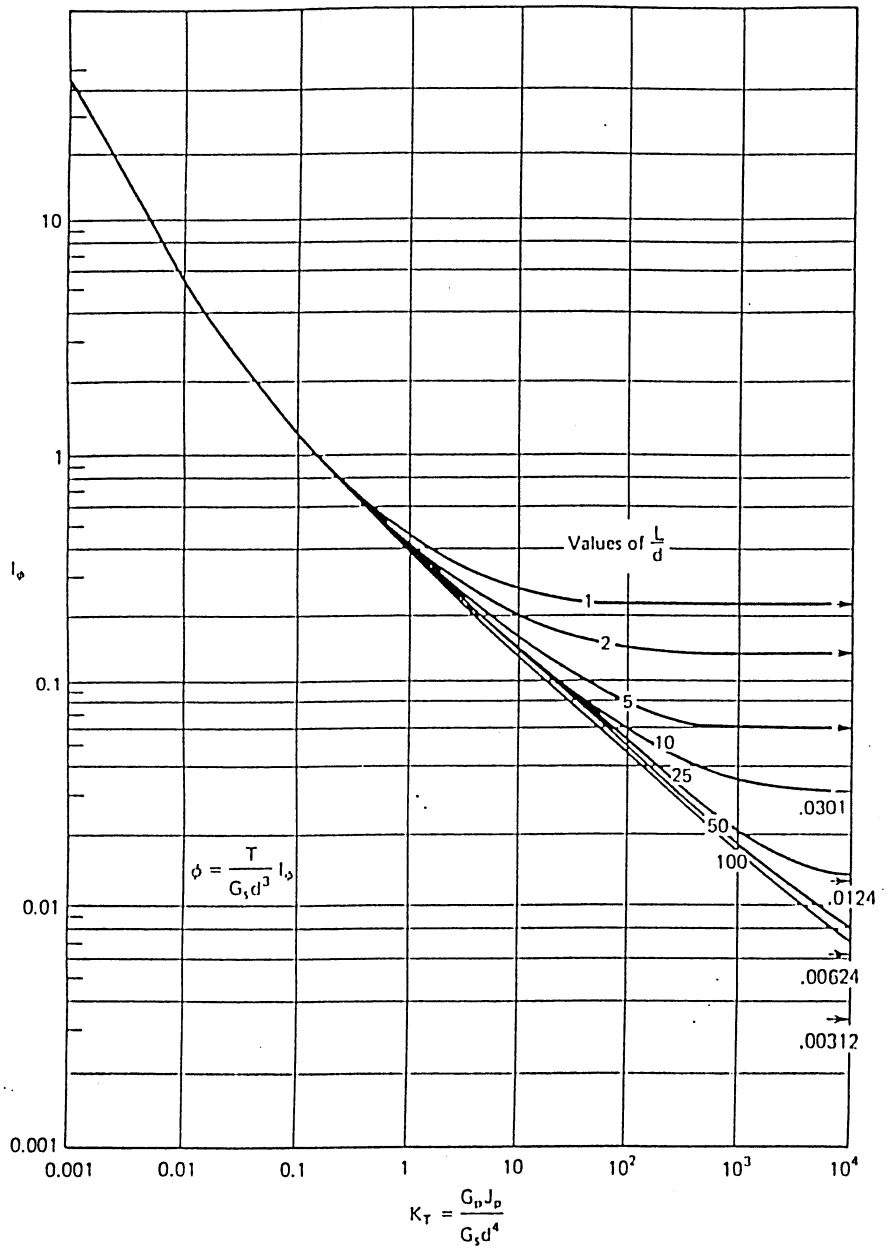

(a) Influence Factor for Constant Gs

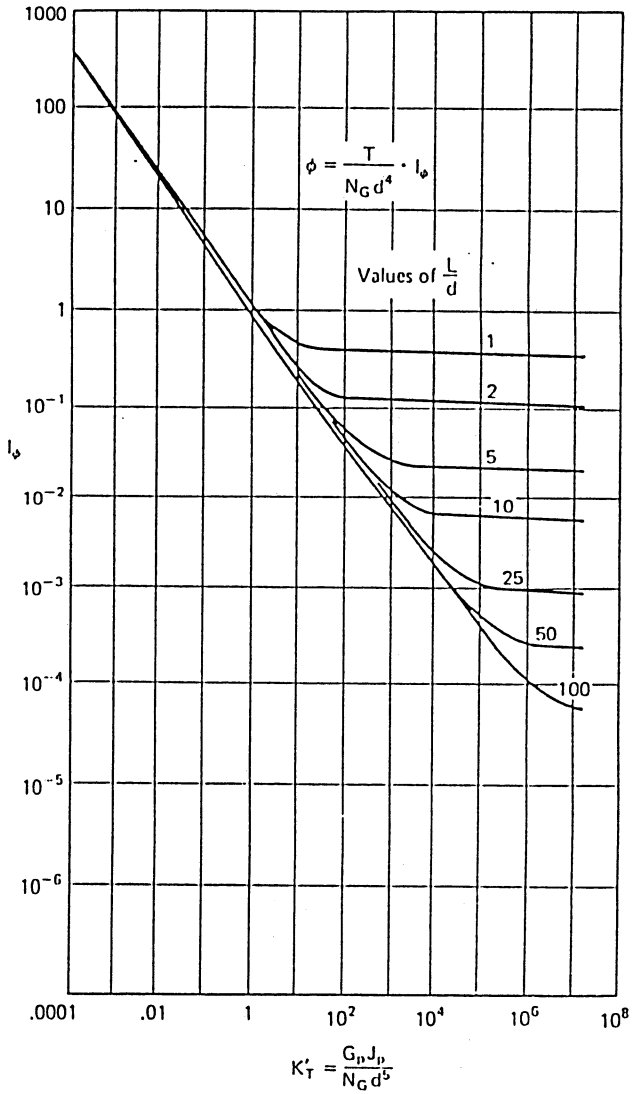

(b) Influence Factor for Linearly Increasing Gs

Figure 1.4 Functional Values of Factors for Torsional Behavior of Circular Pile (Poulos, 1975b)

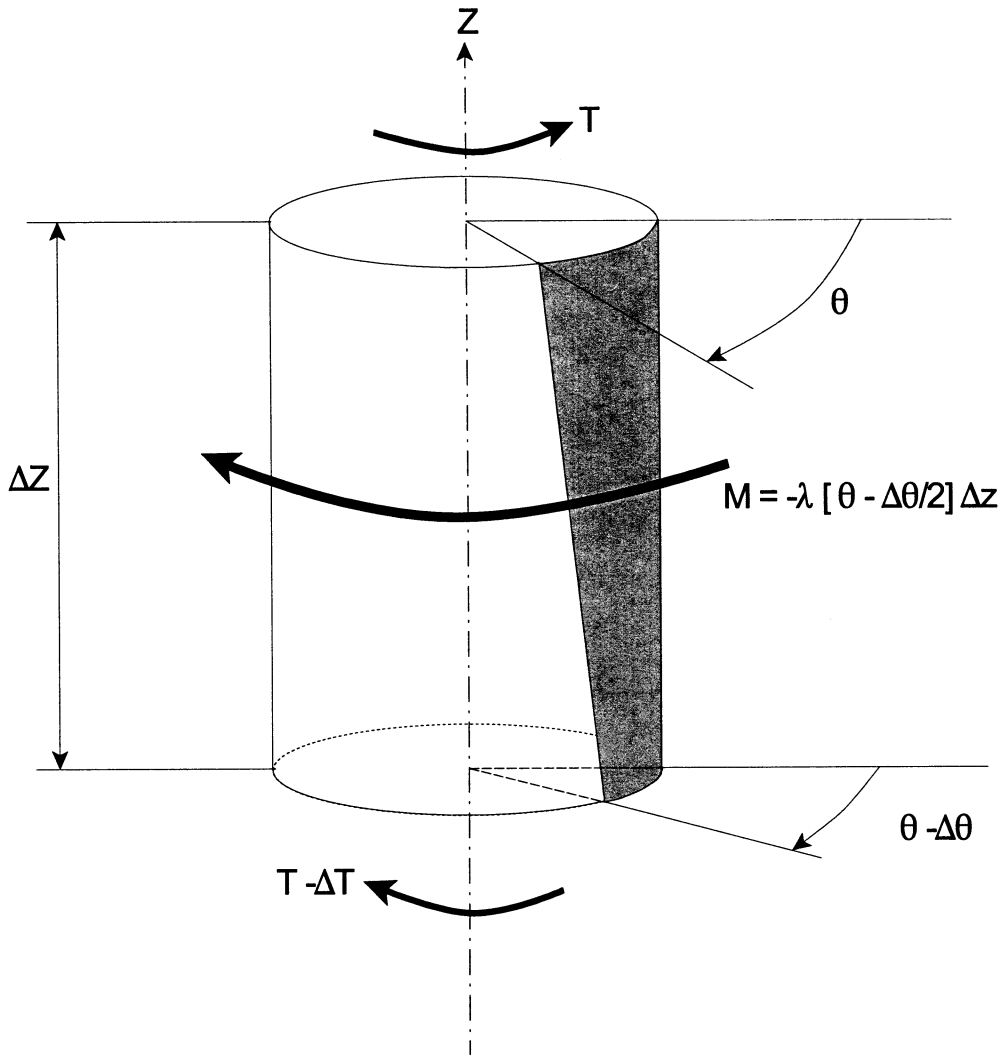

Figure 1.5 Deformed Increment of a Continuous Torsionally Loaded Pile (O'Neill, 1964)

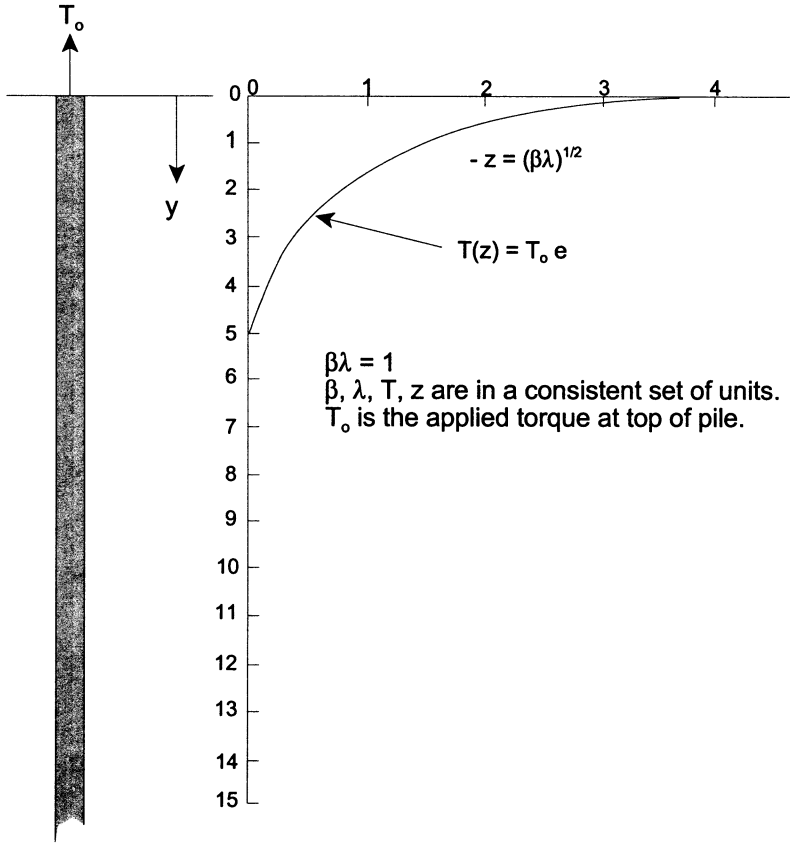

Figure 1.6 Torque vs. Depth as Obtained from the Closed Form Solution (O'Neill, 1964)

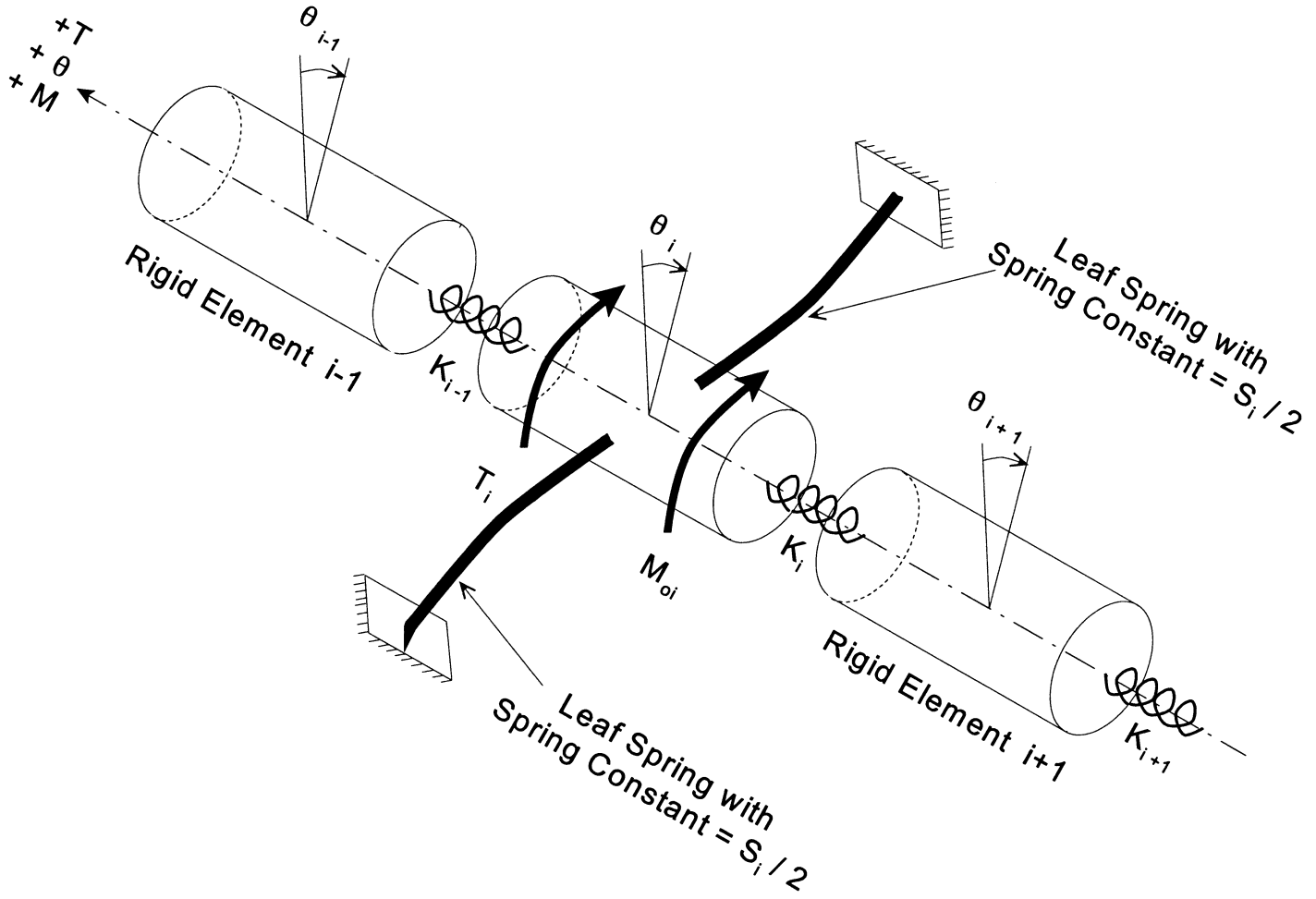

Figure 1.7 Mechanical Finite Element Model of Torsional Loaded Pile for Simulating Torque - Twist Behavior (O'Neill, 1964)

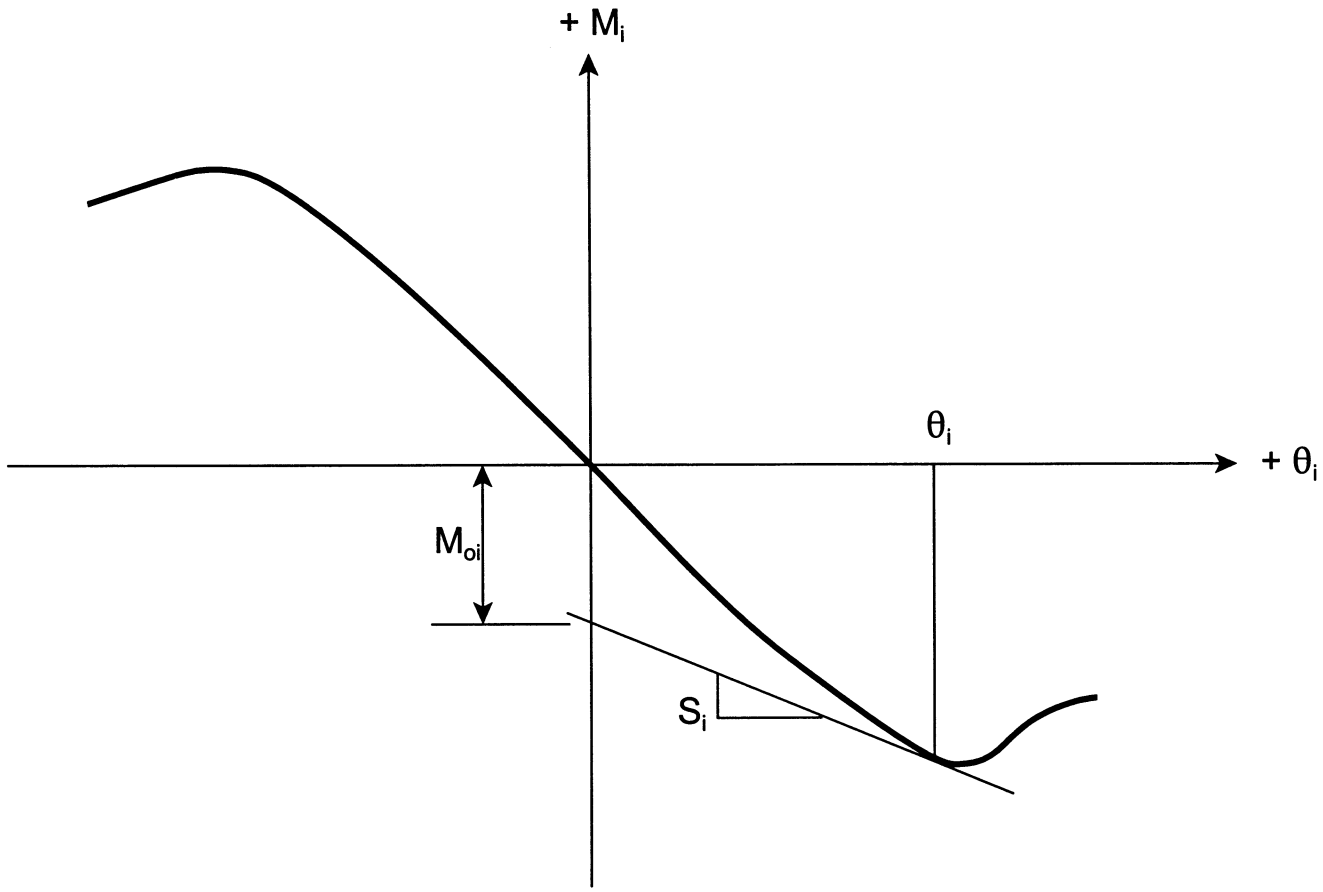

Figure 1.8 Soil Resistance Curve at Station i, Showing Significance of Si and Moi (O'Neill, 1964)

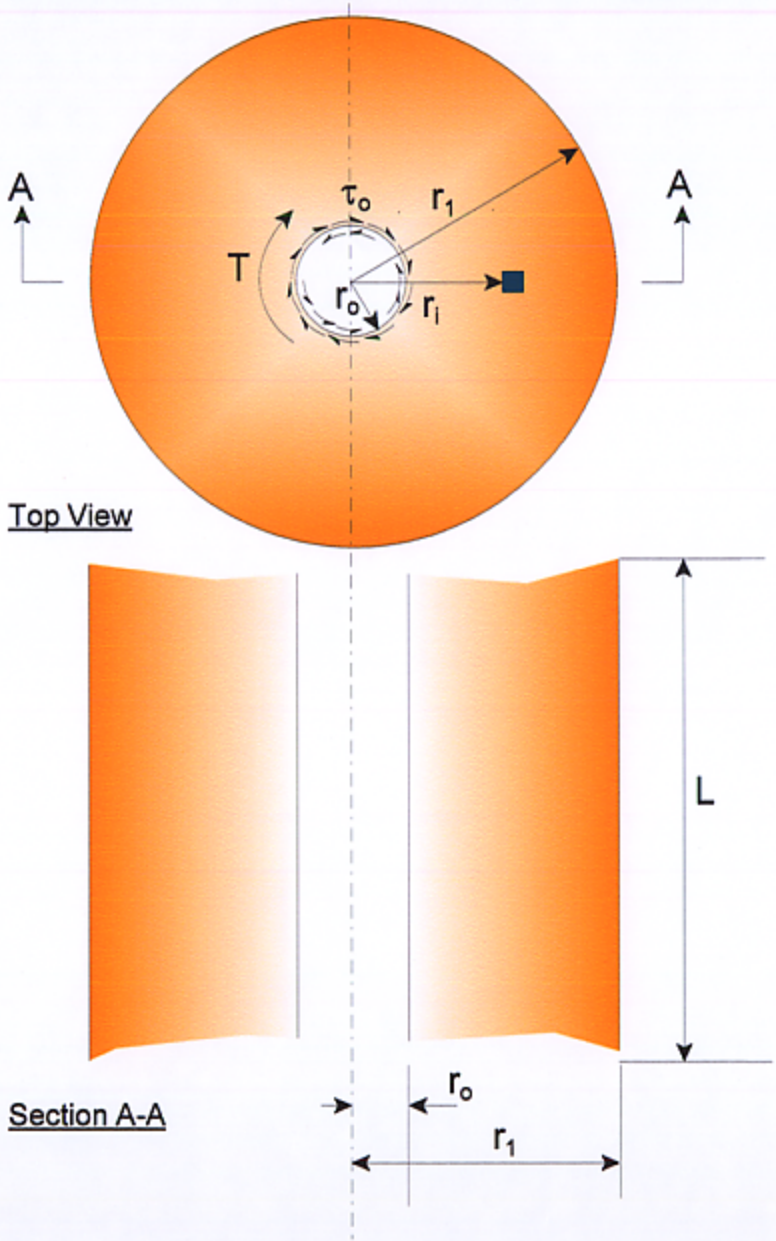

Figure 1.9 Cylindrical Section Embedded in Soil Medium and Subjected to Rotational Moment (Dutt 1976)

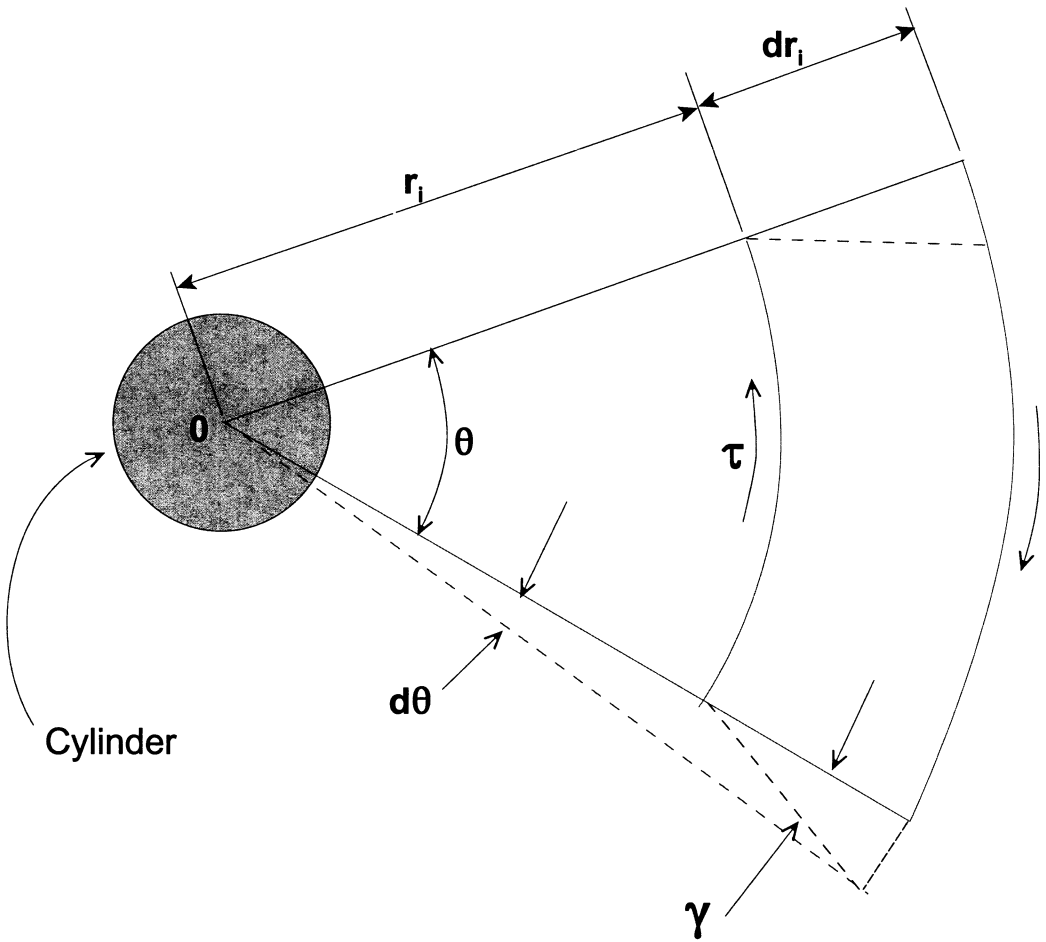

Figure 1.10 Shearing Deformation of a Soil Element (Dutt 1976)

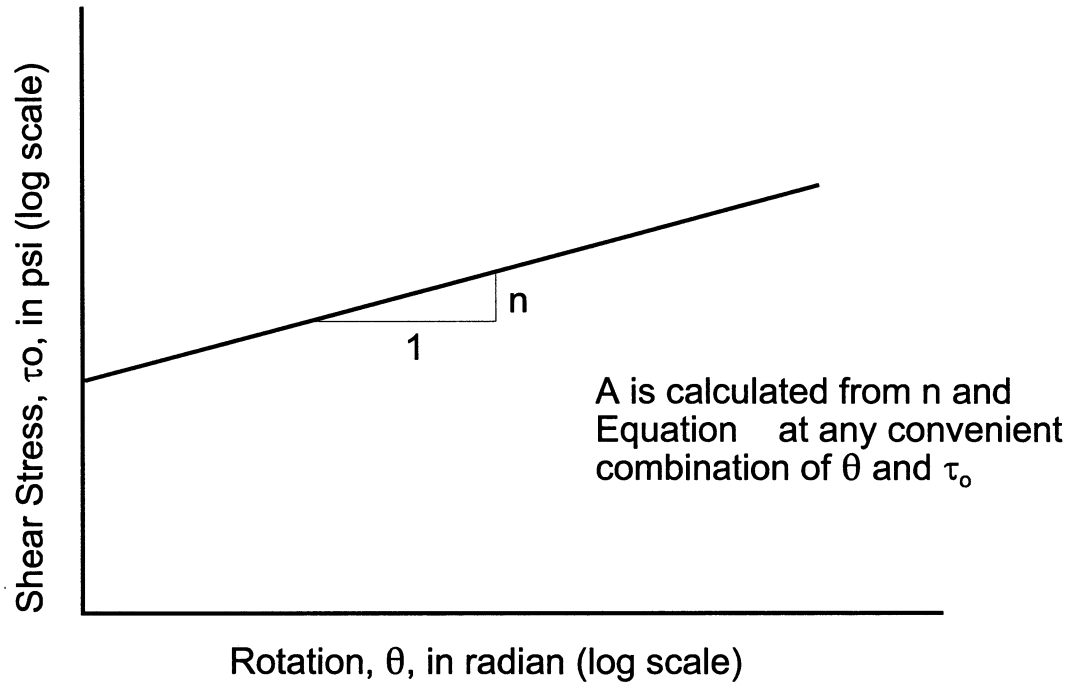

Figure 1.11 Logarithmic Representation of Rotation Test Results (Ha, 1976)

Ultimate Shaft Capacity = Side Friction + Base Friction

$$Q_t = Q_b + Q_s$$

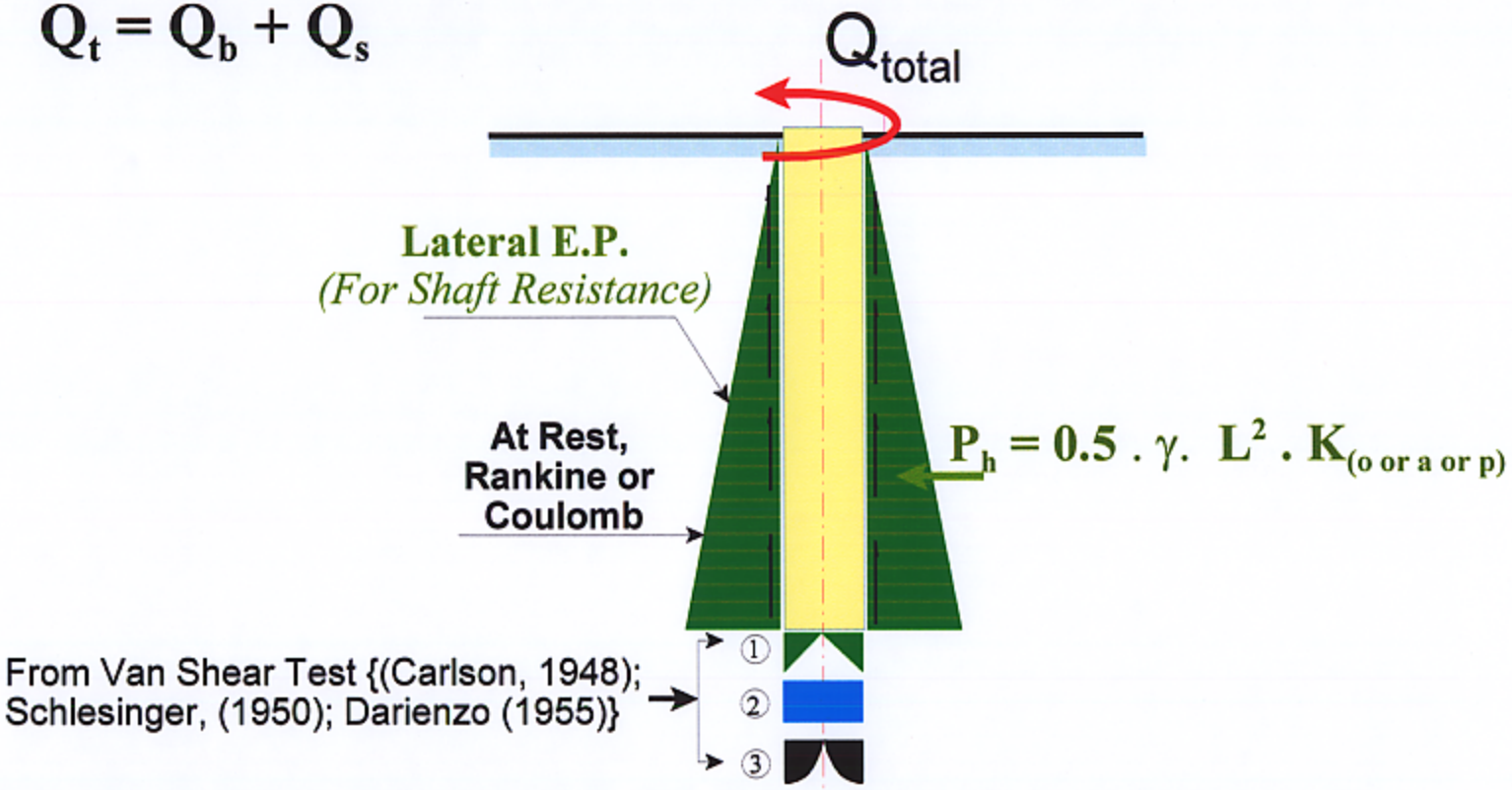

Figure 1.12 Florida Department of Transportationnn Methods for Torsional Resistance of Drilled Shaft

Shaft Resistance

$$T_s = [0.5\ \gamma\ L^2\ K_o \tan\delta]\ \pi\ D$$
$$T_s = \pi\ D\ L\ (s_v\ \beta) \quad \ldots\ \beta \text{ Method}$$

Base Resistance

T_b = W tan δ (D/3) ..... Main Office
T_b = 3/8 W tan δ (2D/3) ..... Dis. 7
T_b = 2/3 W tan 2/3ϕ (D/2) ..... Dis. 5

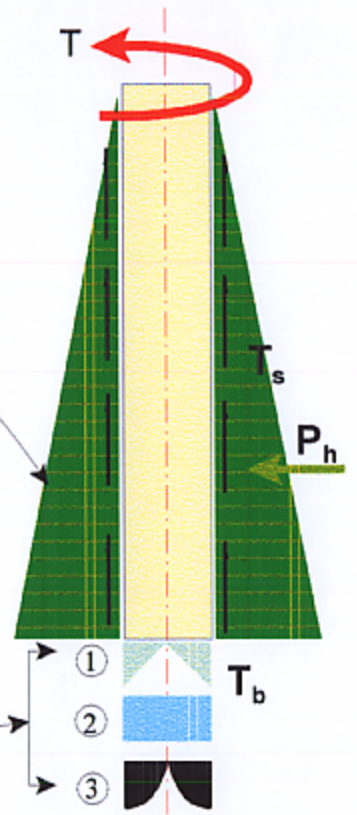

Figure 1.13 Florida Department of Transportationnn Methods for Side and Base Friction

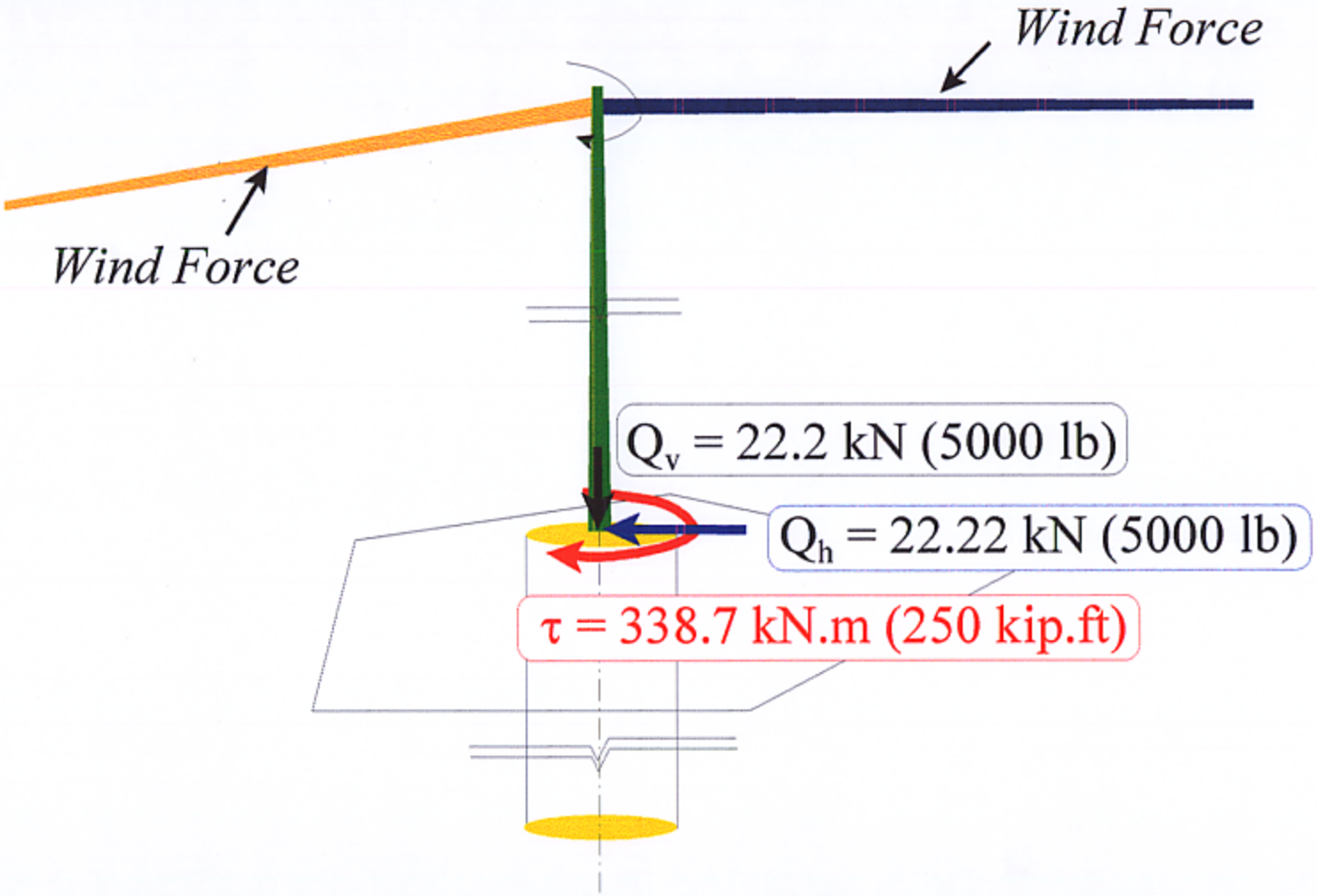

Figure 1.14 Typical values of Axial, Lateral, and Torsional Loads on a Mast Arm Assembly

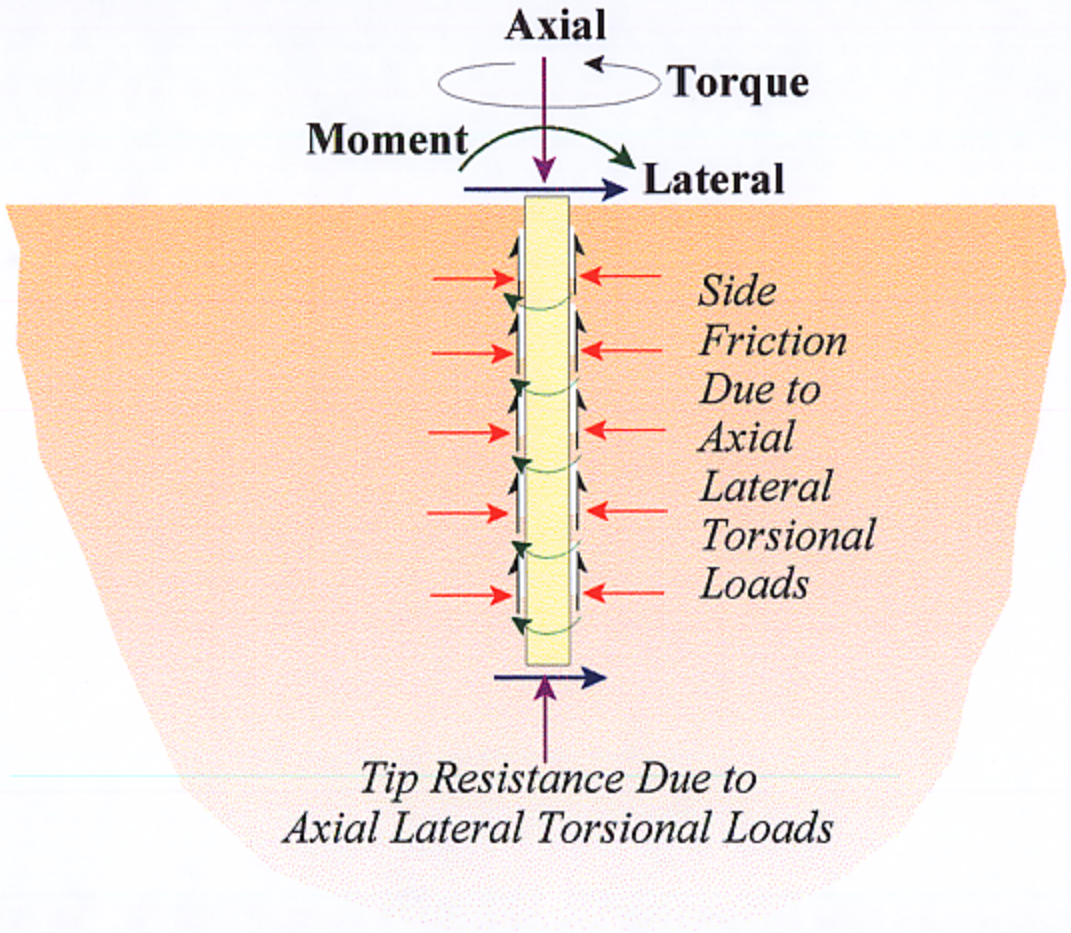

Figure 1.15 Drilled Shaft Under combined Loading Conditions

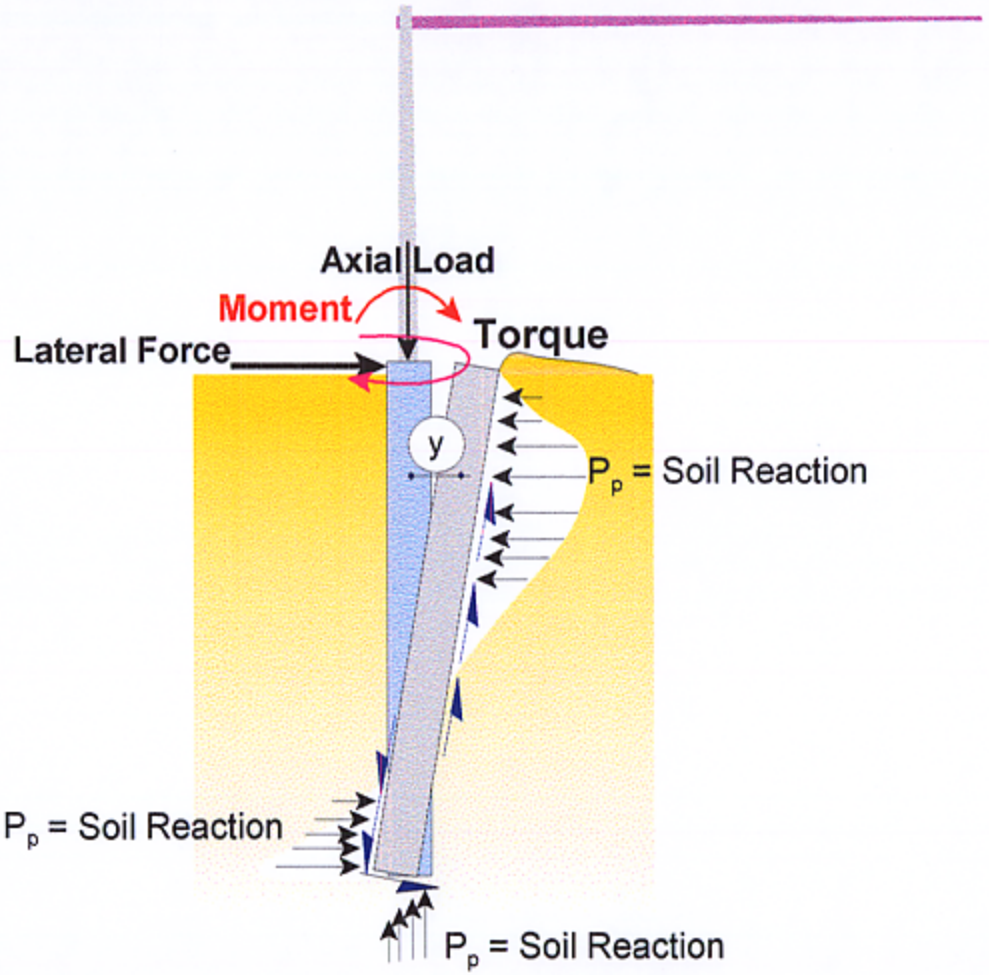

Figure 1.16 Soil Reaction Due to Lateral Loads and Overturning Moments of Mast Arm Assembly

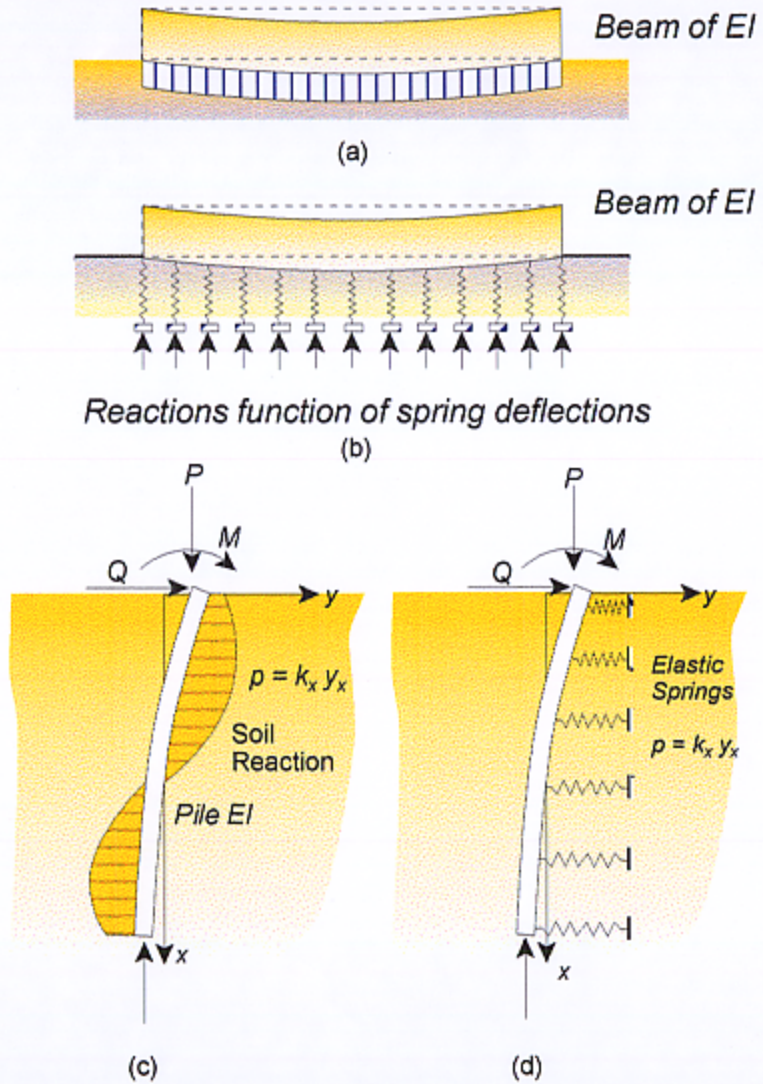

Figure 1.17 Behavior of Laterally Loaded Shaft: Subgrade Reaction Approach. (a) Beam on Elastic Foundation, (b) Winkler's Idealization, (c) Loaded Shaft in Soil, (d) Laterally Loaded Shaft on Springs.

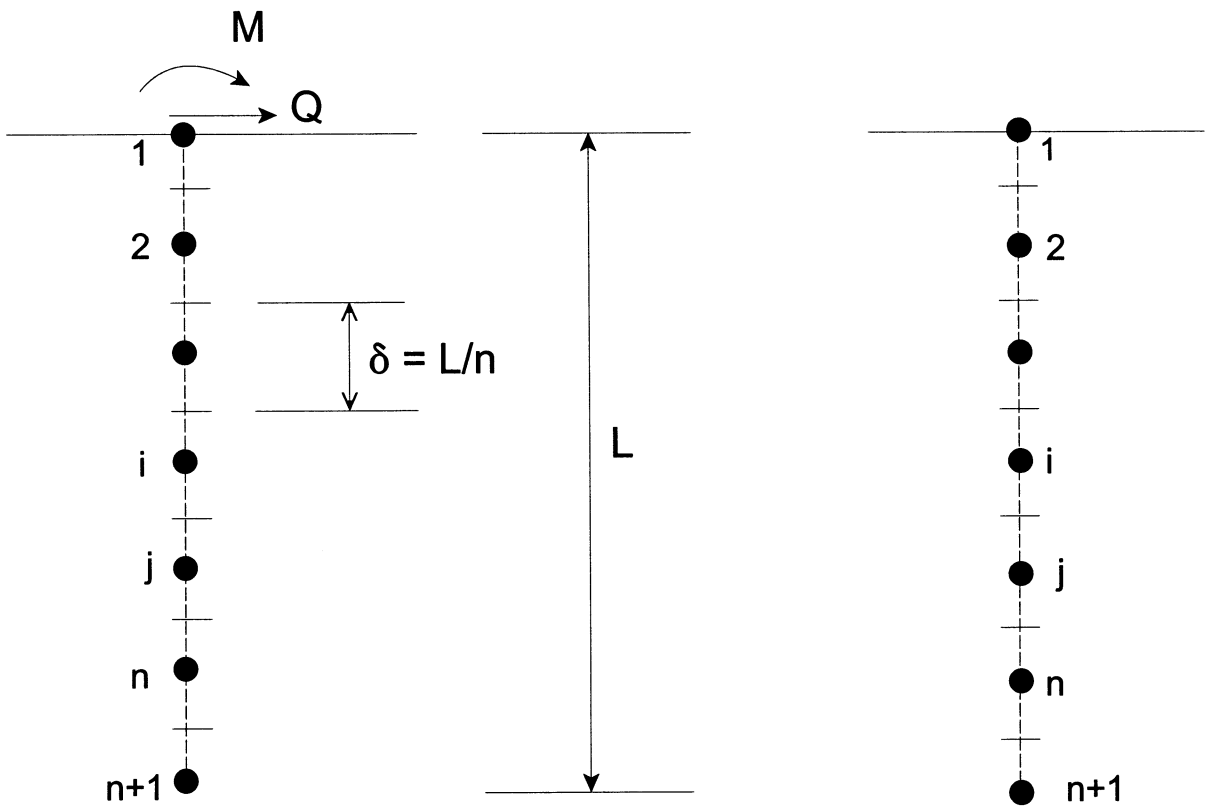

Figure 1.18 Stresses Acting on (a) Shaft, (b) Soil Adjacent to Shaft (Poulos, 1971a)

CHAPTER 2

TEST PROCEDURES AND EQUIPMENT

2.1 Penetration Tests

During the construction of drilled shafts, slurries are often utilized to stabilize boreholes. The presence of the slurry in the borehole prevents the walls of the boring from collapsing by exerting a hydrostatic pressure that is larger than the earth pressure along the borehole sides. The slurry remains in the hole until the concrete placement. FDOT Specifications require that the maximum time between excavation and concrete placement shall not exceed 36 hours after which time over-rimming is required. From the time of slurry application to concrete placement, the slurry fluid tends to penetrate into the soil pores. The extent of this penetration is not usually considered either in the design and analysis or during construction. The rate of penetration may be predictable but the effect of the penetration is not know.

Changing the soil-shaft frictional behavior may cause changes in the over whole performance of the shaft including the perimeter load transfer and the base bearing capacity. The presence of the slurry fluid in the soil around the shaft may induce such a change. The purpose of this phase of the study is to determine the rate of mineral and polymer slurry penetration in cohesionless soil. Also it was sought to infer the extent of fluid penetration into the soil. An organizational chart showing the sequence of the laboratory testing followed in this phase is presented in **Figure 2.1.**

To fulfill these objectives, it was decided to develop a technique capable of determining the penetration rate for any type of slurry. Since no standard device was available to realize such

measurement, a special testing apparatus was fabricated at FAMU-FSU College of Engineering where slurry penetration can be detected under various hydrostatic pressures similar to those encountered in the boreholes.

2.2 Testing Setup and Materials

2.2.1 Slurry Penetration Test

The apparatus used for testing of slurry penetration was devised so that slurry fluid as well as air pressure can sequentially be poured in the pressure chamber. The apparatus consists of a plexiglass pressure chamber of 10" diameter by 11.5" height and 0.5" thick. The base and the top of the chamber were 14" x 14" plexiglass plates with 2" thickness. At the base contained a 0.5" diameter drainage valve to discharge out the penetrated slurry **(Figure 2.2)**. The top plate was also furnished with two valves. One was to pour the slurry in the chamber and the other was to apply the air pressure. The apparatus was positioned on metal container to collect the discharged slurry.

The testing procedure for the slurry penetration was first started with placing the cohesionless soil sample (**Figure 2.3**) in the chamber in layers. each layer was about 1" thick and was tamped with 40 blows. The thicknesses of the layers and the number of blows per layer was kept constant through out the testing program. The aim of such procedure was to have reproducible samples for both mineral and polymer slurries. Once the soil layers reached the mid height of the cell, the testing setup was weighed and the soil unit weight of the soil sample was recorded for that test. The next step was to cover the chamber with the top plate and firmly fasten the setup with four 0.5" long bolts which passed through both the base and the top plates **(Figure 2.4)**.

Then a tap water was poured on the sample in the chamber to saturate the soil before starting the penetration test. The water precipitated on the soil in the chamber and started to flow out from the base valve. At that instant the air pressure was applied at 2 psi to speed up the water flow in the soil. After ensuring the saturation of the soil, liquid valve was opened again and the slurry was poured until it filled the remaining volume of the cell. The valve was then closed and the air pressure was applied. The hydrostatic pressures use in the study were 5 psi, 8 psi, and 10 psi. These values were equivalent to an average of 12', 19' and 24' head of the slurry.

Then the elevation readings of the slurry at specified time intervals were recorded to track the rate of slurry penetration in the soil. The time intervals were 15 sec, 30 sec, 1 min, 2 min, 4 min, 8 min, 15 min, 30 min, 1 hr, 2 hr, 4 hr, 8 hr, 16, hr, 32 hr, etc. until the slurry has fully penetrated the soil. It should be noted that the minimum time was 36 hours for the test. After 36 hours the test was terminated **(Figure 2.5a)**. At the end of testing, the thickness of the filter cake layer was measured and recorded **(Figure 2.5 b and c)**. The slurries used in testing composed of bentonite, attapulgite, KB Slurry Pro CDP, and SuperMud. Contrary to the mineral slurries, samples form polymer slurries did not show any filter cake formation on the surface. The effect of the polymer slurry on the soil, however, was more obvious especially at high concentration levels. The soil samples after testing exhibited viscous consistency. While for the mineral slurries the soil appeared to behave like a like a wet sand.

Some provisions were taken before and after each test. Among these provisions was the application of the high vacuum grease on the chamber wall before placing the sand sample. This application would minimize the flow of slurry at the boundaries between the soil and the walls. It was observed

during the preliminary stages of this test that no traces of slurry were found at the middle of the soil sample, and that most of the slurry was flowing along the wall of the chamber. This phenomena necessitated the grease application. Also, a 20 micrometer filter paper was used underneath the soil sample to evenly distribute the discharge of the slurry. Another provision was considered when preparing both the mineral and polymer slurries. In both cases the slurries were thoroughly mixed in a mixer and then colored using drops of food color to facilitate identifying the different types of slurry and to be able to trace the penetration of he slurry in soil **(Figure 2.6)**.

The viscosities of the slurries used in testing were tested using the conventional Marsh funnel test **(Figure 2.7)**. In addition to the Zahn cup test. The second technique was used for it simplicity, speediness, and the amount of slurry samples needed for testing. The Zahn cup may more practical than the Marsh funnel when testing limited amounts of fluids. The required volume for the Marsh funnel test should be more that a liter per test. Having a large number of tests such as the current study required as many samples as possible to cover different concentrations and repetition of testing. Therefore, it was more feasible to use the Zahn cup for viscosity measurements.

2.2.2 Simulation of the Slurry Penetration Through Soil

To have a better understanding of the concept of slurry penetration in cohesionless soil, it was decided to construct a scaled model borehole and to observe the flow of slurry as it progressed. The scaled model setup for the slurry behavior in a borehole was accomplished using a wide glass tank (6' wide x 4' height and 6" width) from which the slurry flow could be observed from the side glass. The progress of the flow through the soil was captured using a digital camera **(Figure 2.8).** The

digital images were then filtered on the computer to detect features that could not be noticeable. The wet front of the slurry in the soil could easily be detected with the filtered images **(Figure 2.9).** Also, the formation of the filter cake on the side walls in case of mineral slurries could be distinguished from the digital images **(Figure 2.10).** In case of polymer slurry applications, the wet from was easily detected but no filter cake was noticed **(Figure 2.11).** The scaled simulation of the borehole confirmed the some of the results obtained from the one dimensional flow test described above.

In addition to the glass tank, the torsional test setup devised for the scaled drilled shaft was also used in observing the progress of the slurry penetration and the formation of the filter cake on the side walls **(Figure 2.12).** The advantage of using the torsional test setup was to understand the process cleaning the filter cake from the boreholes before concrete placement in the field. The cleaning process of the boreholes was emulated in the torsional test setup by trimming the filter cake deposits. The extent of this process could easily demonstrated to show that traces of the filter cake would always remain in the boreholes regardless how thorough was the process **(Figure 2.13).**

2.2.3 Direct Shear Tests

The direct shear test was performed to determine the frictional characteristics of the cohesionless soil used in the study and the soil-concrete interaction. In addition to the dry soil samples used in testing, samples from the slurry penetration tests. These soil samples were saturated with the mineral and polymer slurries and were obtained directly from the pressure chamber immediately after concluding the penetration tests. The slurry saturated samples were also used for the soil-concrete block testing **(Figure 2. 14).**

For the soil-concrete block shear test, the lower half of the direct shear box was replaced with a 4" x 4" square plain concrete block The thickness of the block was 0.5". These dimensions were chosen to fit the block in the direct shear and to position the upper half of the shear box which contained the soil sample **(Figure 2.15)**. The roughness of the shaft surface block was closely duplicated in the concrete blocks. This roughness would add to the frictional resistance through the soil-shaft interlock. This kind of interaction would elevate the frictional resistance of the soil-concrete to that of the soil internal friction angle. All direct shear tests were performed at normal stress of 31.5 psi was used. Testing procedure followed in this phase of the study was similar to the conventional direct shear test. The rate of shear displacement was chosen to be **0.02 in./min**. For all the tests the horizontal and the vertical displacements were simultaneously recorded.

2.2.4 Scaled Model Torsion Test

Upon completion of the penetration tests and the direct shear tests, the torsional resistance of a scaled shaft model of a 20" long and 4" diameter was carried out using a special setup that was designed and fabricated at the machine shop of FAMU-FSU College of Engineering **(Figure 2.16)**.

The testing setup consisted of a 4' diameter and 5' depth steel chamber. The chamber was furnished with a strain control loading system for which a continuous load application could be exerted on the shaft at a constant rate of loading. The loading configuration which could be applied was torsional, lateral, and axial loading. A combination of these loads could also be employed **(Figure 2.17)**. This arrangement of load application could not be created by any other commercially testing devices; therefore, it was decided to devise the system locally to simulate the actual loading conditions on mast arm assemblies.

To apply the constant rate of loading, it was decided to supply the loading wheel with two 20 gallon buckets. When the torsional test started, a tap water equally poured in the buckets. The rate of flow and, hence, the rate of loading **(0.02 ft-lb/sec)**, was predetermined using a water valve at each bucket.

The scaled shaft was made of plain concrete at a scale of 1" equal 1'. The surface of the shaft was roughened to simulate the case of what might be produced in the field where shaft surfaces reflect the roughness of the open borehole. The load application was done through a square metal key fitted at the top of the shaft and attached to a wheel where a string was pulled by the two water buckets. The torsional displacement was recorded through a dial indicator and a scale attached to the inner surface of the steel chamber. At another occasion when both torsional and lateral loads were simultaneously applied, two digital displacement gages were used. The soil used in the torsional testing was the same as for the slurry penetration tests.

Other arrangements were also provided in the steel chamber to facilitate sample preparation, watering/de-watering the soil, and to measure the lateral deformation of the shaft at the base. To produce a saturated sample and to densify the soil under its own weigh so that soil would hold close the shaft. The process of submerging and de watering the tank was an essential step before starting any torsional test, because of the fact that drilling the hole to place the shaft may produce some disturbance in the soil around the shaft, it was found that forcing the sides on the shaft could better be achieved be consolidating the soil in the tank (**Figure 2.18**).

The detailed steps for the torsion test on the scaled model are described bellow:

1. *Fill the barrel of the torsion apparatus to the top with sand while adding water to the barrel simultaneously.*
2. *Vibrate the soil for 5 minutes and siphon water from system using the piezometer.*
3. *Remove the torsion wheel from the system.*
4. *Drive the 4" PVC soil extraction device to the desired elevation and remove the soil and the device from the system.*
5. *Set the shaft concentrically into the hole and set the torsion wheel over the shaft setting the key into the model with the pointer at 0°. Raise the water table of the system to the surface of the soil through the piezometer.*
6. *Apply a pressure of 1 psi surrounding the model at the surface of the soil to aid collapse.*
7. *Once the soil has collapsed upon the shaft, remove the pressure and the siphon the water from the system through the piezometer.*
8. *Weigh each bucket and before conducting the test.*
9. *Connect the water tubes to each bucket and then connect the main tube to the apparatus.*
10. *Record the initial reading on the calibrated wall.*
11. *Turn on the water flow and note the time.*
12. *Record the degree on the calibrated wall to which the shaft points at every thirty seconds intervals.*
13. *Continue to take readings until the modal shaft rotates more than the calibrated section of the barrel (120°). Also, take readings at the times where the model shows large rotational movements if the time is between specified intervals.*
14. *When the test ends, note the time that the shaft rotated beyond 120°.*
15. *Turn off the water flow and note the time that the water stops flowing to the buckets.*
16. *Measure the final weights of the buckets.*
17. *Prepare to run the next test by removing all soil from the barrel.*

Additional torsional tests were conducted on the scaled shaft where the friction at the base was eliminated by using a greased metal plate. The aim was to determine the frictional capacity of the shaft with regard to the side friction only without the contribution of the base friction. After placing the greased metal plate at the bottom of the borehole and placing the shaft on the plate, the rest of the procedure for the torsional test was the same as described above.

Another set of tests were performed on the shaft with the side friction being eliminated and the torsional capacity was due to the base friction only. In this case the borehole was not collapsed on the shaft as for Step 6.

Mineral and polymer slurries were also used in these tests. The boreholes were filled with the slurry before placing the shaft. In each case the slurry fluid remained in the hole for about 36 hours. After this time the slurry was siphoned and the filter cake layer (if any) was removed by rimming it with 4" plastic tube.

A set of torsional tests were performed agin after the shaft rotated. These testes were called the **residual resistance capacity tests**. In this test, the shaft was brought to its original position before testing and then the torsional load was applied again. The purpose of this tests was to determine the the residual capacity in the shaft if any remedial action was taken by rotating the shaft back to it original position. This remedial action was taken in the case of the failed shaft shown in **Figure 1.1**. The mast arm was rotated 180° to its original position. Such a correction measure needed to be investigated so that the frictional characteristics of the displaced shaft should remain the same as for the newly constructed shaft.

2.3 Field Testing of Full Scale Drilled Shafts

2.3.1 Site Characterization

To fulfill the objectives of this study it was necessary to conduct full scale testing on drilled shaft similar in the geometrical properties to those used for the mast arm situations. Four drilled shaft were constructed at a selected site at FAMU-FSU College of Engineering where water table was below the foundation level (> 20 ft). To prepare for the construction of the shafts, a thorough site investigation was carried out by Ardaman Associates, Tallahassee, Florida. Four soil borings were drilled at the site to 25' depth and were located at the locations of the proposed drilled shafts **(Appendix B).** The soil at the site was predominantly sandy silt (SM) with 5% to 18% fines. For

sample number 4 at 4.5' depth the fine content was about 45%. At depths from 17.5''to 25' the soil was mostly poorly graded sand to silty sand SP-SM **(Figure 2.19 to 2.21)**. Direct shear testing on soil samples obtained from the site indicated that the angle of friction of the soil, φ, ranged from 28° to 32°. Also the natural moisture contents, w_c, for those samples were ranged from 12.% to 25.6%. The cohesion, c, of the samples ranged from 0 to 200 lb/ft^2. Additional cone penetration, CPT, dilatometer sounding tests were conducted at the site to have a full scope of the soil behavior along the proposed shafts (**Appendix B**).

After the site investigation, the drilled shaft construction crew started the drilling operation preparing for the shaft construction. Meanwhile, the four cages of the steel reinforcement of the drilled shafts were prepared at the site and instrumented with embedded rosette strain gages. The embedded gages were located at certain depths along the shaft length in order to record the torsional strains during loading process. Each drilled shaft was furnished with additional 2" PVC tube as a contingency step if the strain gages failed and additional instrumentation was needed. Also each shaft was provided with a tiltmeter PVC tube supplied by Ardaman Associates, Inc. for measuring the lateral displacement of the shaft during testing.

To test the shafts under the combined mode of lateral, overturning and torsional loads, a special 11' rigid arm was constructed. The loading arm consisted of 12" x 12" section and 5/8" thick **(Figure 2.22)**. The arm was filled with concrete to improve its rigidity and minimize the structural deflection. The arm was designed to be fitted on each tested shaft at its predetermined position. The same arm was used in testing the three full scale shafts. On each shaft a bulky steel head was fabricated and affixed to the shaft head with 24" length by 2' in diameter steel bolts.

Twelve of these bolts were embedded in the shaft at the configuration shown in. The size, embedment and locations of the bolts were designed to carry a maximum torque of 510 kip.ft. This capacity was larger than any estimated torque values supplied by the FDOT. It was anticipated that this torsional moment, the shaft might either fail at the structure level or at the foundation level through rotational slip. The torsional slip of the shaft was determined not to exceed 180 kip.ft. This capacity was based on the FDOT main office procedure.

Applying the lateral loads on the drilled shafts was done through a hydraulic jack supported horizontally on a steel angle. The lateral load was transferred to the loading arm through a 1" diameter ball bearing and a socket plate. The arrangement of the testing was the dry shaft first followed by the bentonite and then the polymer shaft. The designations of the shafts came from the method of construction of each shaft. In the first shaft no slurries were used during construction. In the second and third shaft, bentonite and polymer slurry were used, respectively.

During construction, the bentonite slurry was mixed is a special tank and then pumped in the designated borehole. The polymer slurry was Super Mud and was mixed in-hole while pouring the water. The percentage mixing was left for the contractor since there were no guidelines on the proper amount of polymer needed to add to the water. The only measure that was taken during this stage was determining the Marsh funnel viscosity of the slurry and trying to be higher that 45 sec/quarter. The test was run several time ti ensure the target viscosity. After filling the borehole with the slurries a 18 hr waiting period was passed before starting concrete placement. After 18 hr it was noticed that the level of the polymer slurry dropped to about 3.75' from the starting level, and about 3' for the bentonite slurry. This drop could be translated to about 9.5 ft^3 of fluid loss for the

polymer slurry. Although it was not a significant quantity but when it was associated with a slurry of viscosity of 70 sec/quarter, the question that might arise what would be the fluid loss if the viscosity was 45 sec/quarter. The answer could be derived from the laboratory slurry penetration test described above.

For the polymer slurry hole it was not possible to steadily pumping the fluid out while placing the concrete. The rate of slurry discharge was much less than the rate of pumping in the concrete. Such performance was not expected because the same pump was used to discharge out the bentonite slurry during concrete placement. This observation was noted to be aware of any future operation so that the viscosity of the polymer slurry should not exceed 45 sec. if the fluid loss was not of a concern. The two relationships, viscosity vs. fluid loss and viscosity vs. concrete displacement must be addressed before starting the construction.

Before starting the torsional testing, four laser devices were mounted on the load supporting shaft, and the tested shaft. One laser beam was placed on the support shaft, and another devise on the loading are, and two devises at the top of the tested shaft. This arrangement was accompanied with four foam boards located at 20' distance fro the testing setup. Each laser beam was aimed at a foam board so that any induced rotational displacement upon loading could be magnified by a larger movement on the foam boards. Therefore each 0.04 in on the board would be equal to 0.004 in at the edge of the shaft. This rotation was equivalent to an angle of 0.000167 rad or 0.0047°. Such a resolution could be possible if an LVDT was placed directly on the shaft. However, having the conventional displacement gages supported on the shaft directly might subject them the movement of the earth around the shaft, and hence, affecting the net displacement of the shaft.

All the shafts were loaded using controlled rate of loading, and the displacements, strain levels, and load magnitudes were simultaneously recorded. The dry shaft sustained the largest load as compared with the mineral and polymer shaft. The maximum load reached in the dry shaft was 490 kip.ft at which structural failure took place. The bentonite slurry shaft was loaded to 280 kip.ft and suffered rotational slip without any structural failure. The polymer slurry shaft showed similar behavior as for the dry shaft and failed structurally at 480 kip.ft. However, the soil around the polymer slurry shaft was excavated to about 4.5 feet below the ground surface when no appreciable rotational movement was recorded from the laser beam readings.

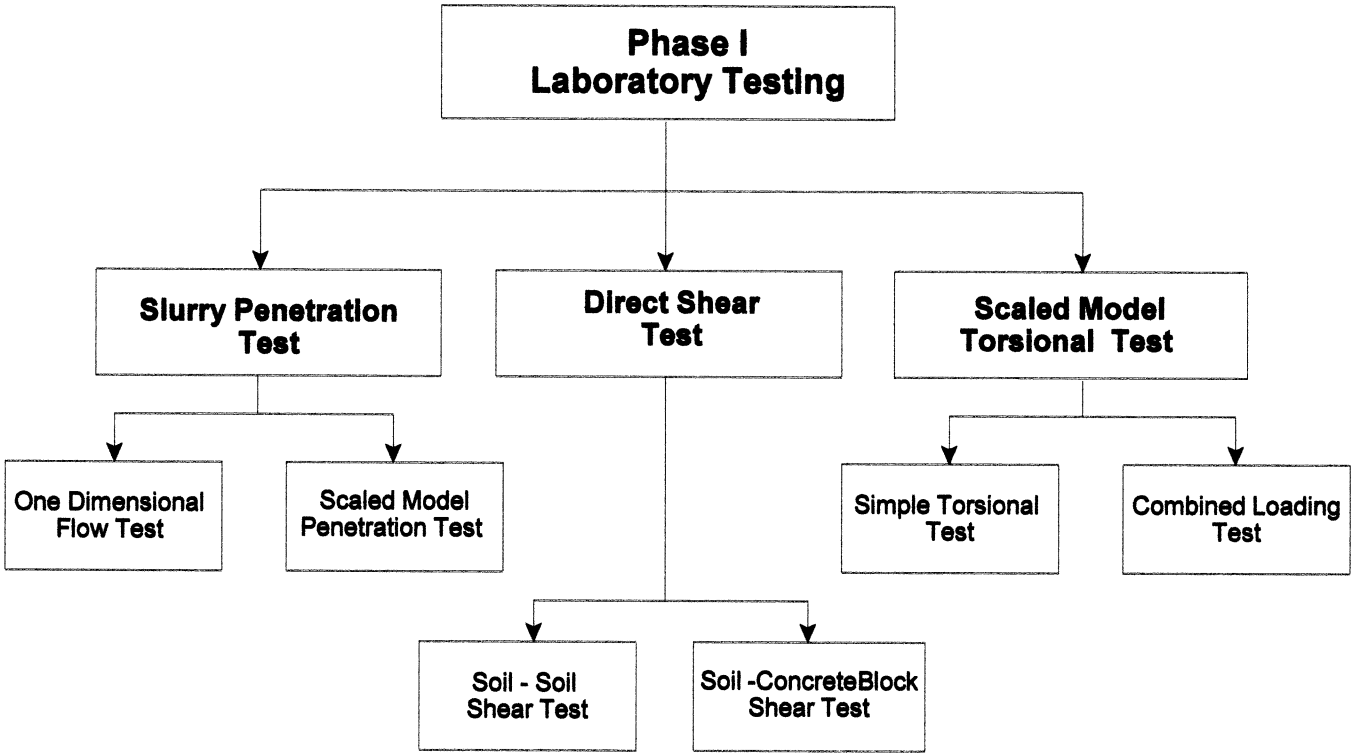

Figure 2.1 Sequence of Laboratory Test Followed in this Study

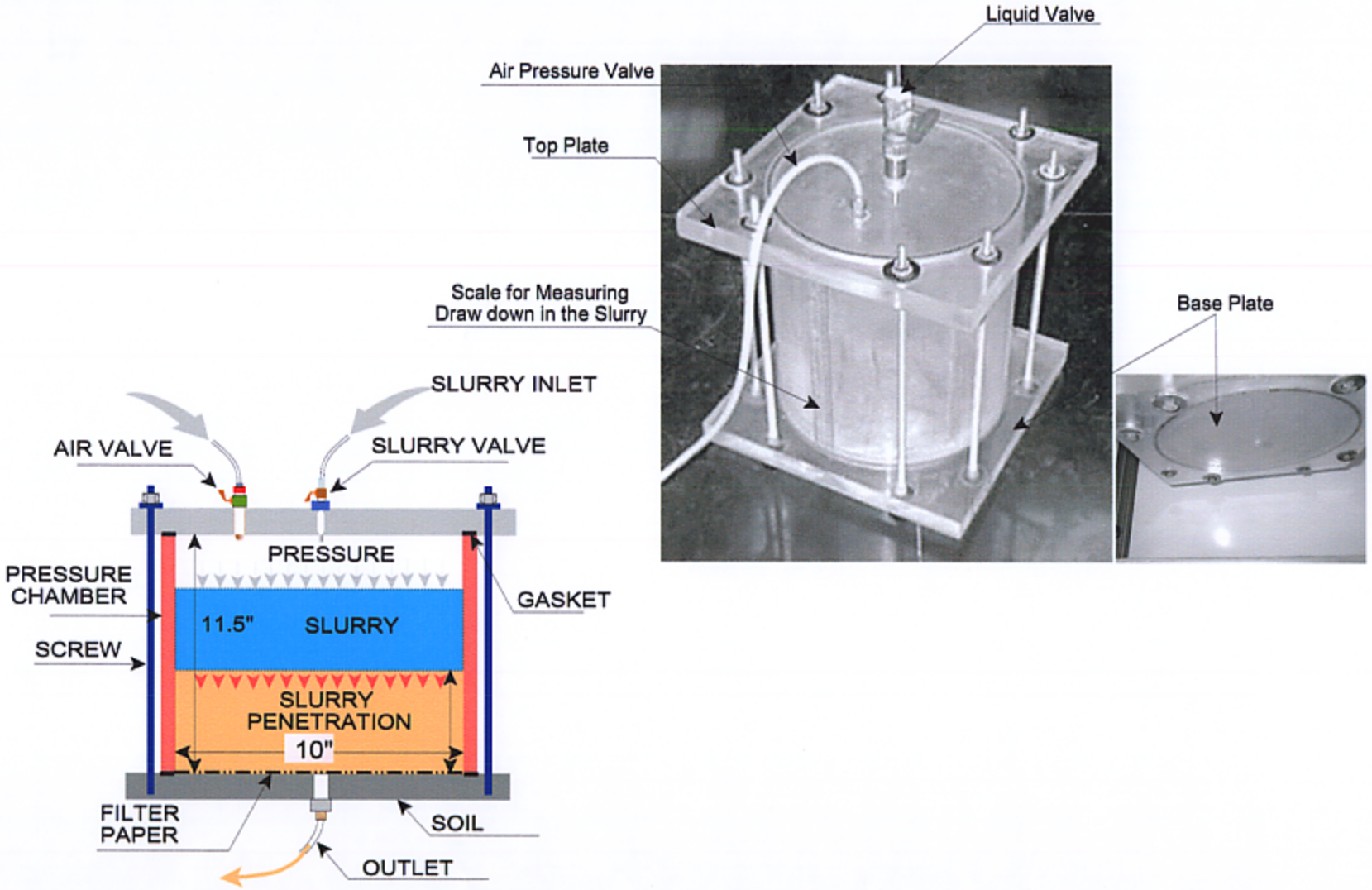

Figure 2.2 Slurry Fluid Penetration Apparatus

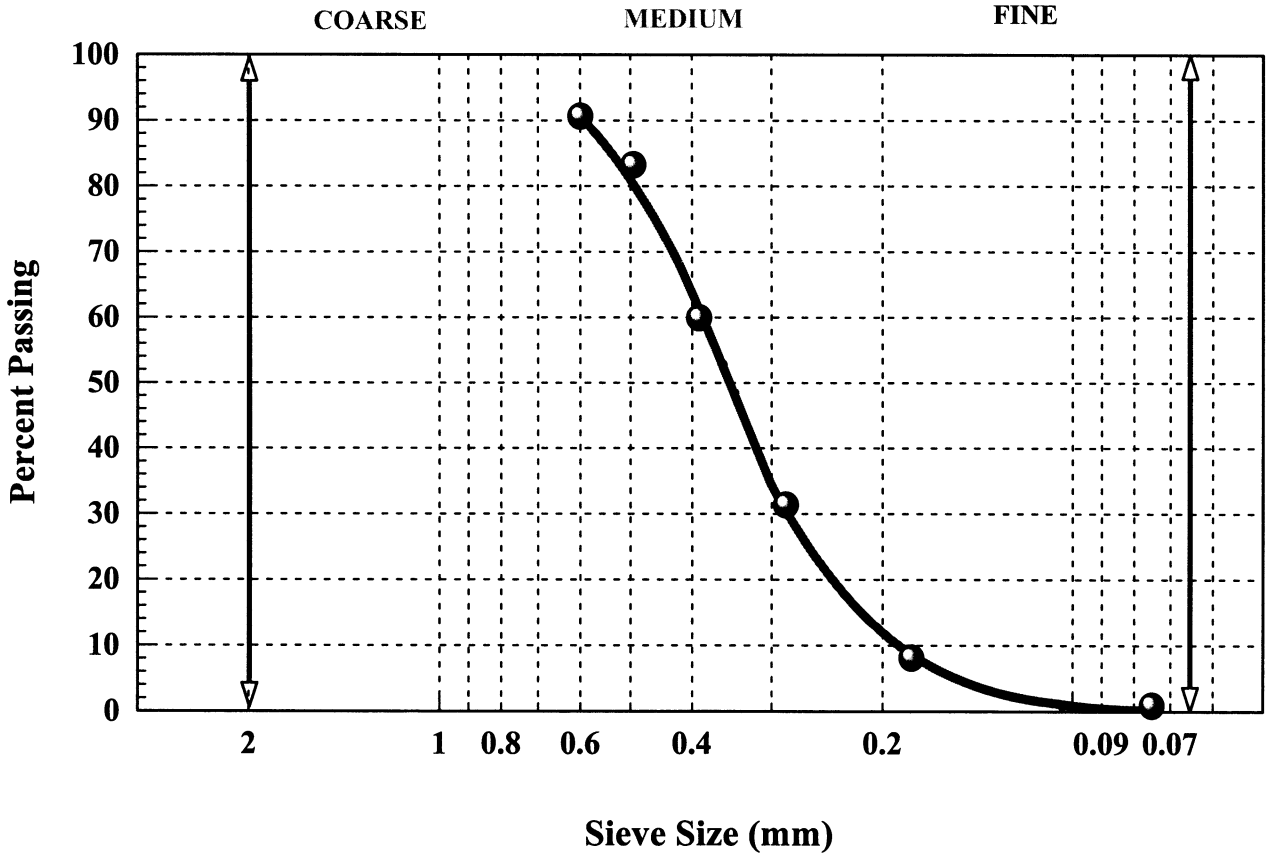

Figure 2.3 Grain Size Distribution of the Soil Used in Testing

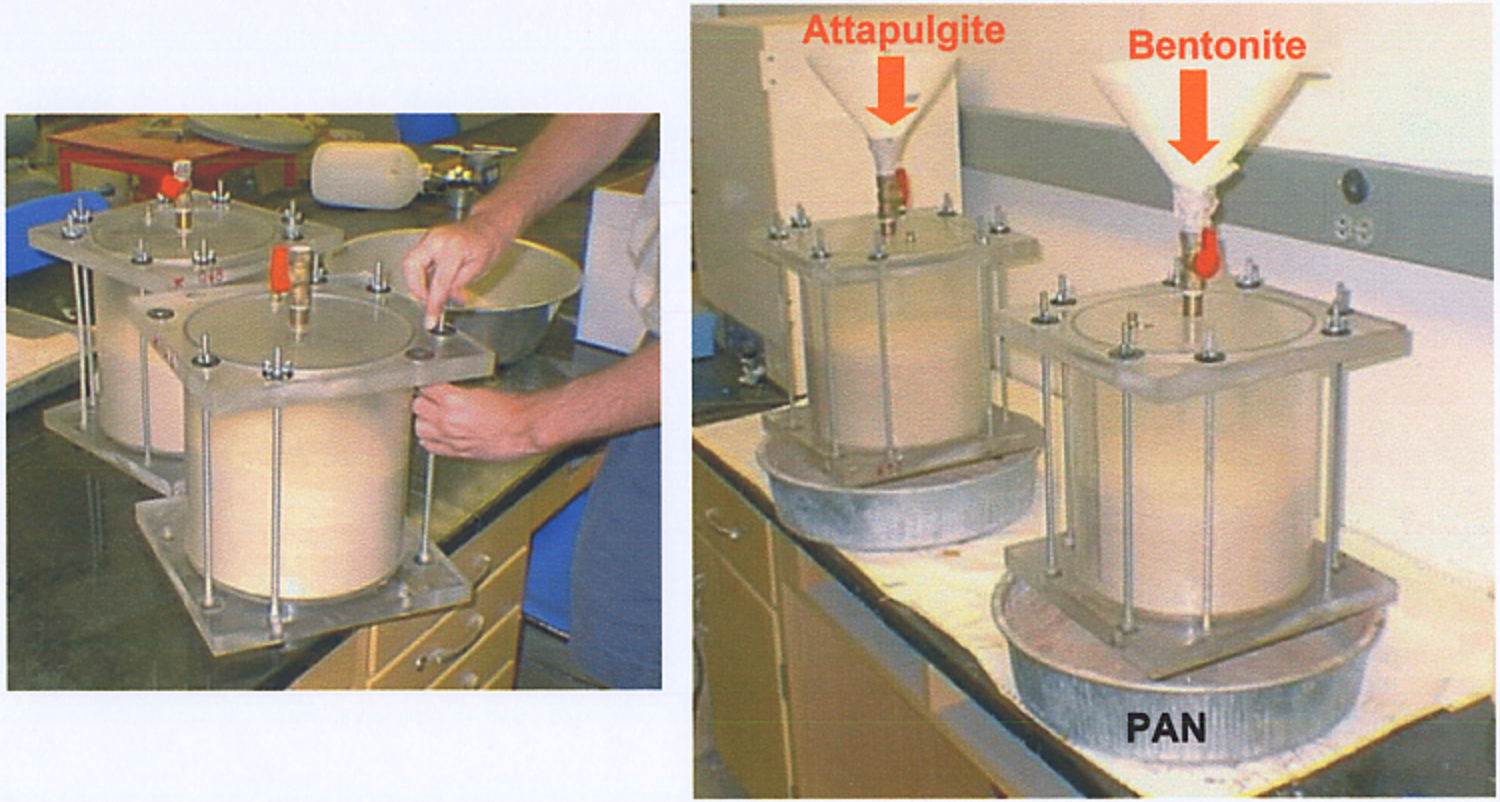

Figure 2.4 Assembling the Slurry Fluid Penetration Apparatus

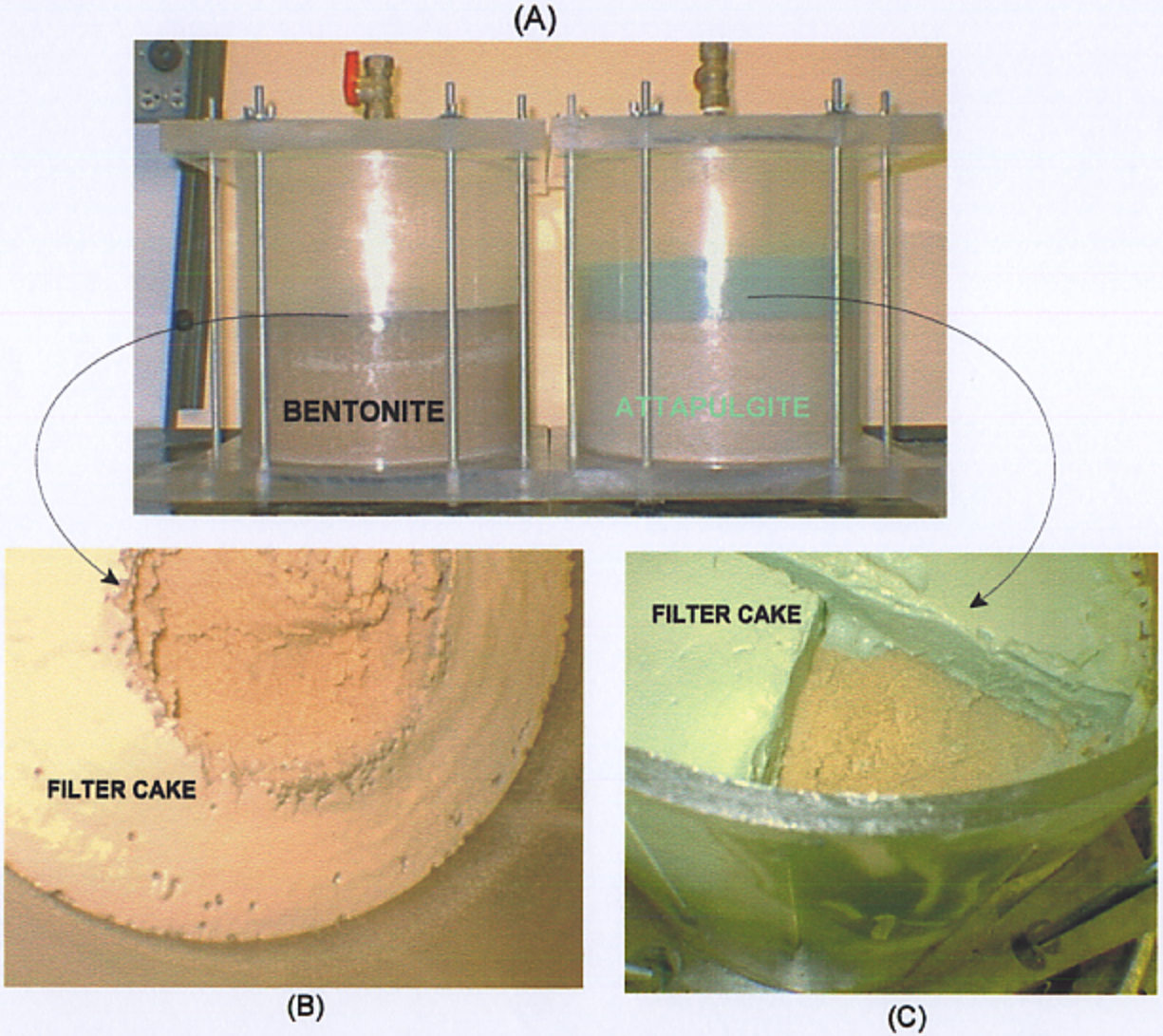

Figure 2.5 (a) Formation of the Filter Cake at the end of Testing, (b) Formation of the Bentonite Filter Cake with Low Clay Concentration, (c) Formation of the Attapulgite Filter Cake with High Clay Concentration.

Figure 2.6 Coloring Mineral and Polymer Slurries for the Slurry Penetration Testing

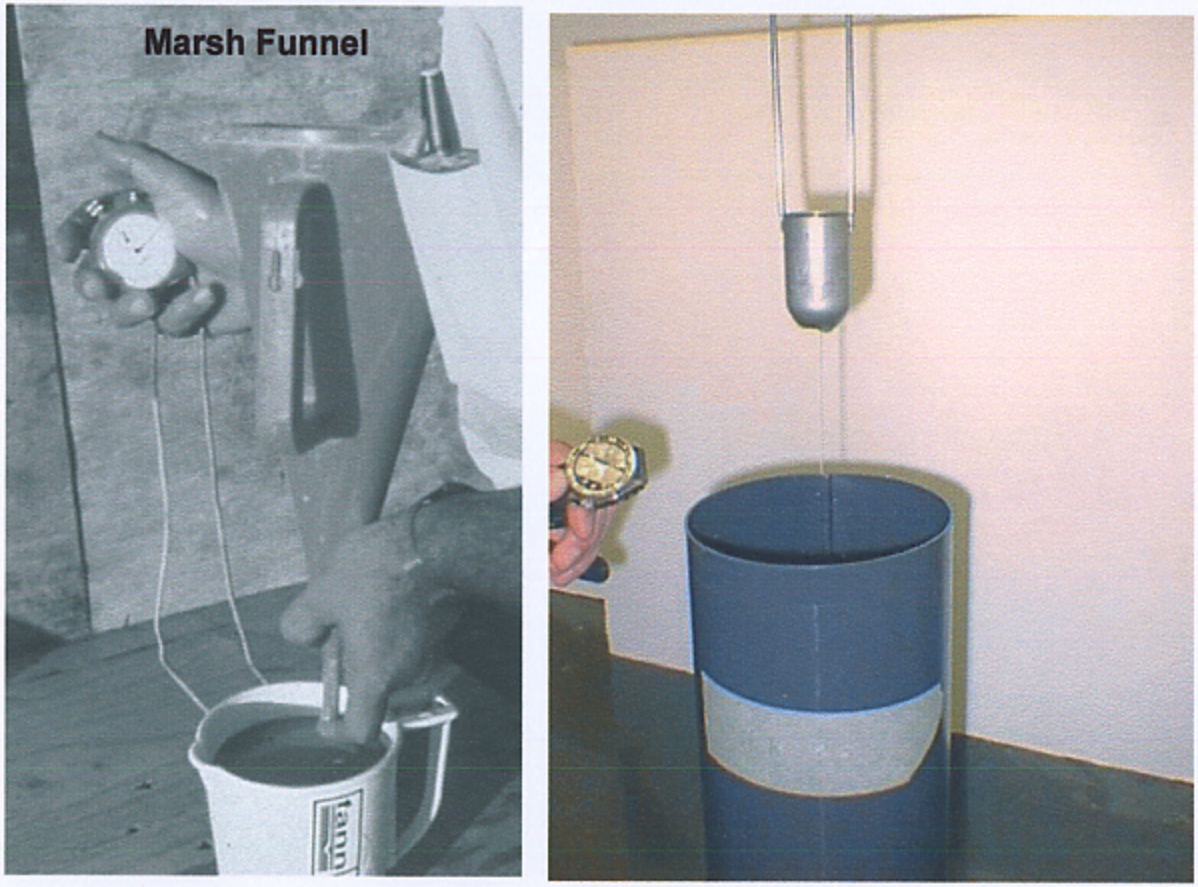

Figure 2.7 Marsh Funnel and Zan Cup Test For Slurry Viscosity Measurements

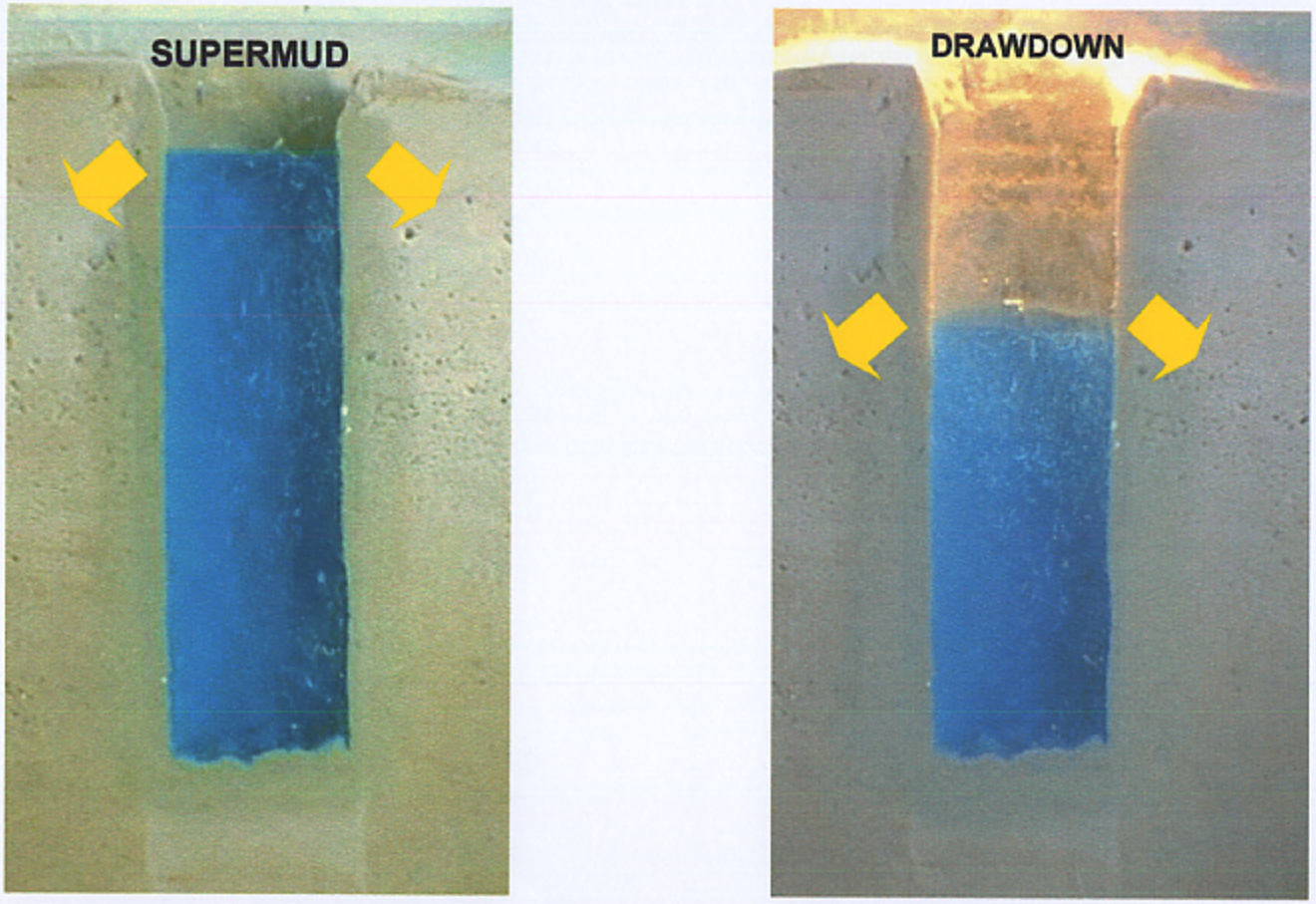

Figure 2.8 Progress of Polymer Slurry Penetration through the Soil in the Scaled Borehole Test.

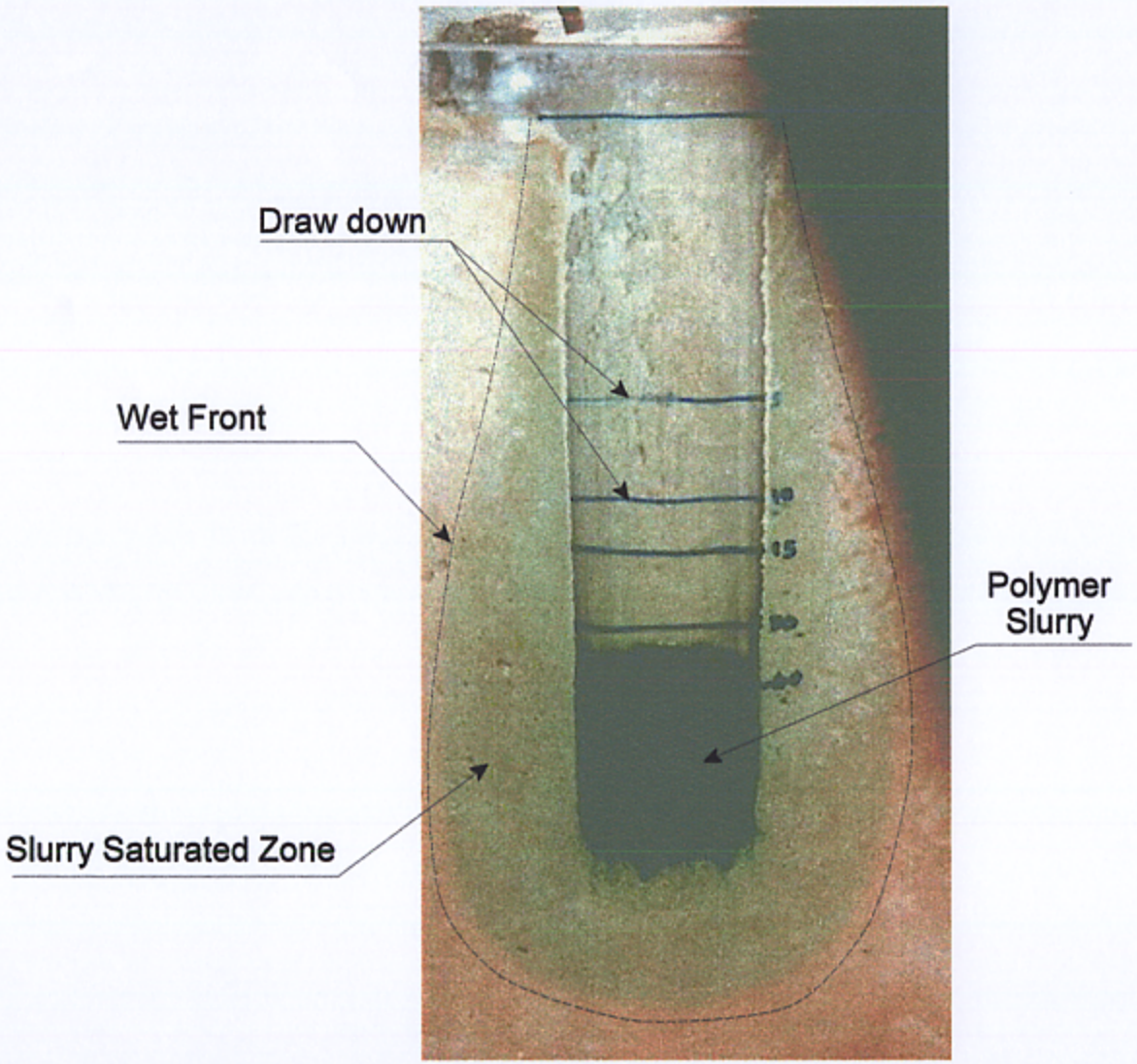

Figure 2.9 Digital Image of the Drawdown of the Polymer Slurry in the Borehole and the formation of the wet Fornt.

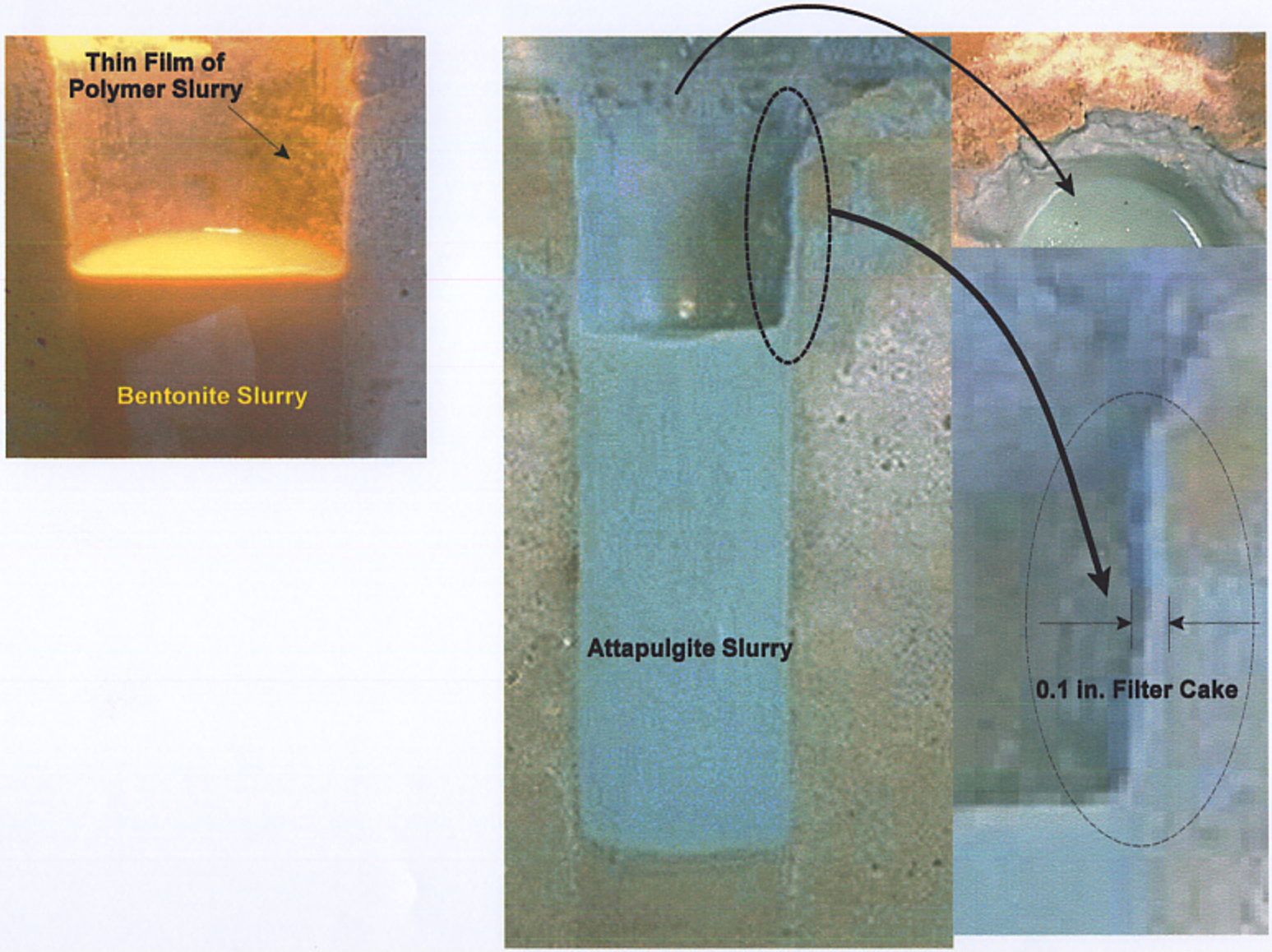

Figure 2.10 Formation of the Filter Cake on the Side of the Scaled Borehole.

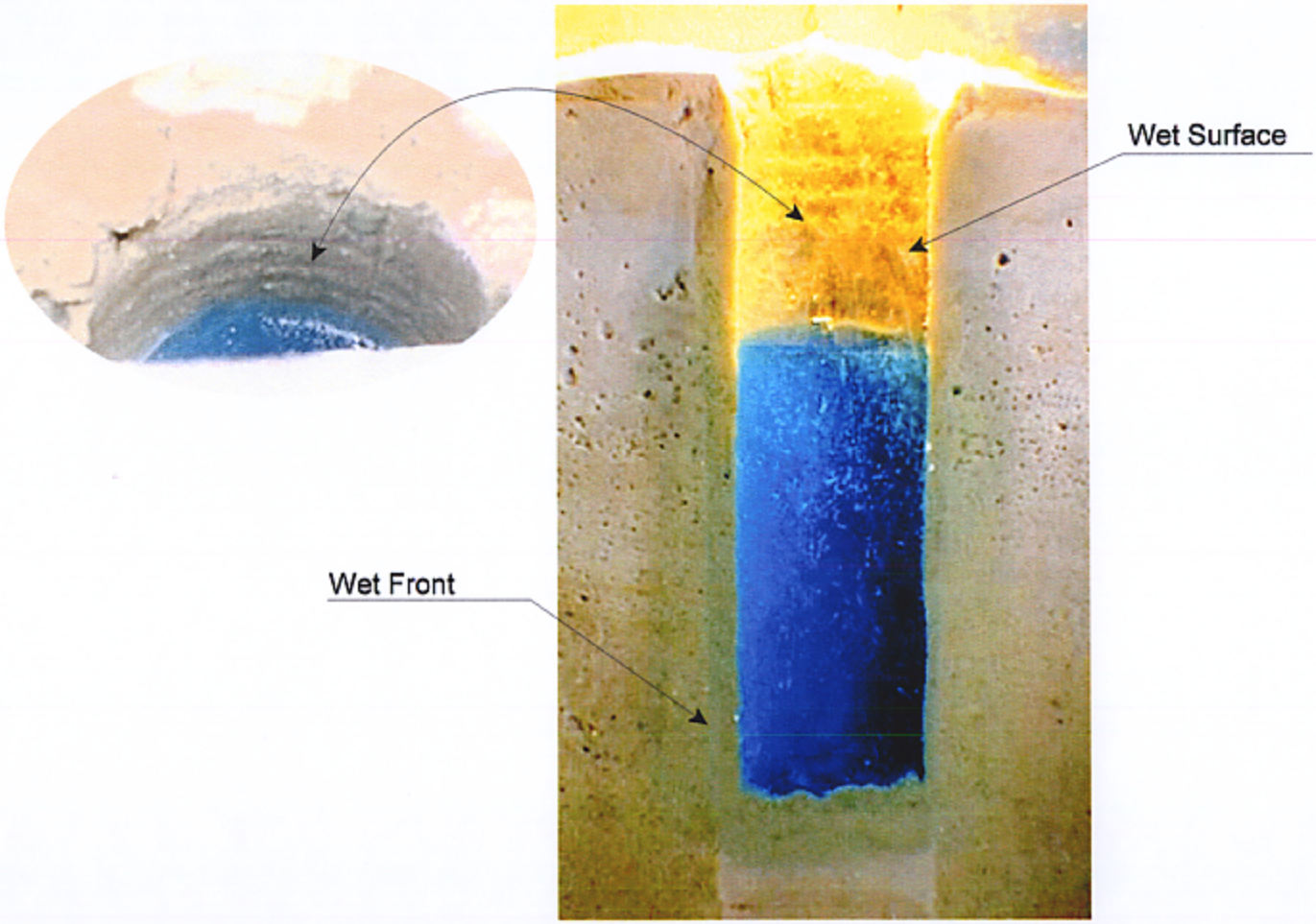

Figure 2.11 Polymer Slurry Showing Wet Side Walls in the Borehole.

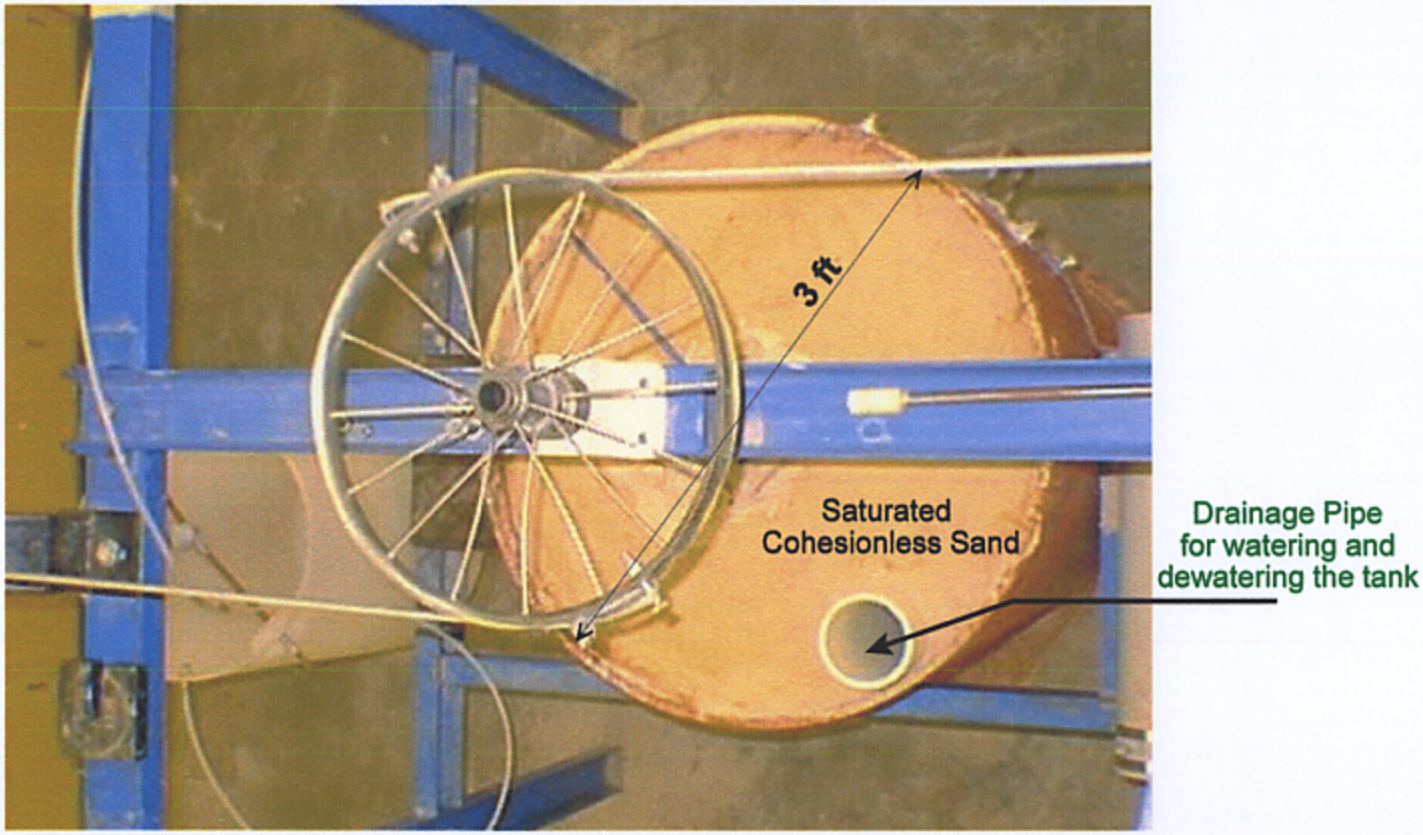

Figure 2.12 Torsional Tetsing Setup Used for the Slurry Penetration Test.

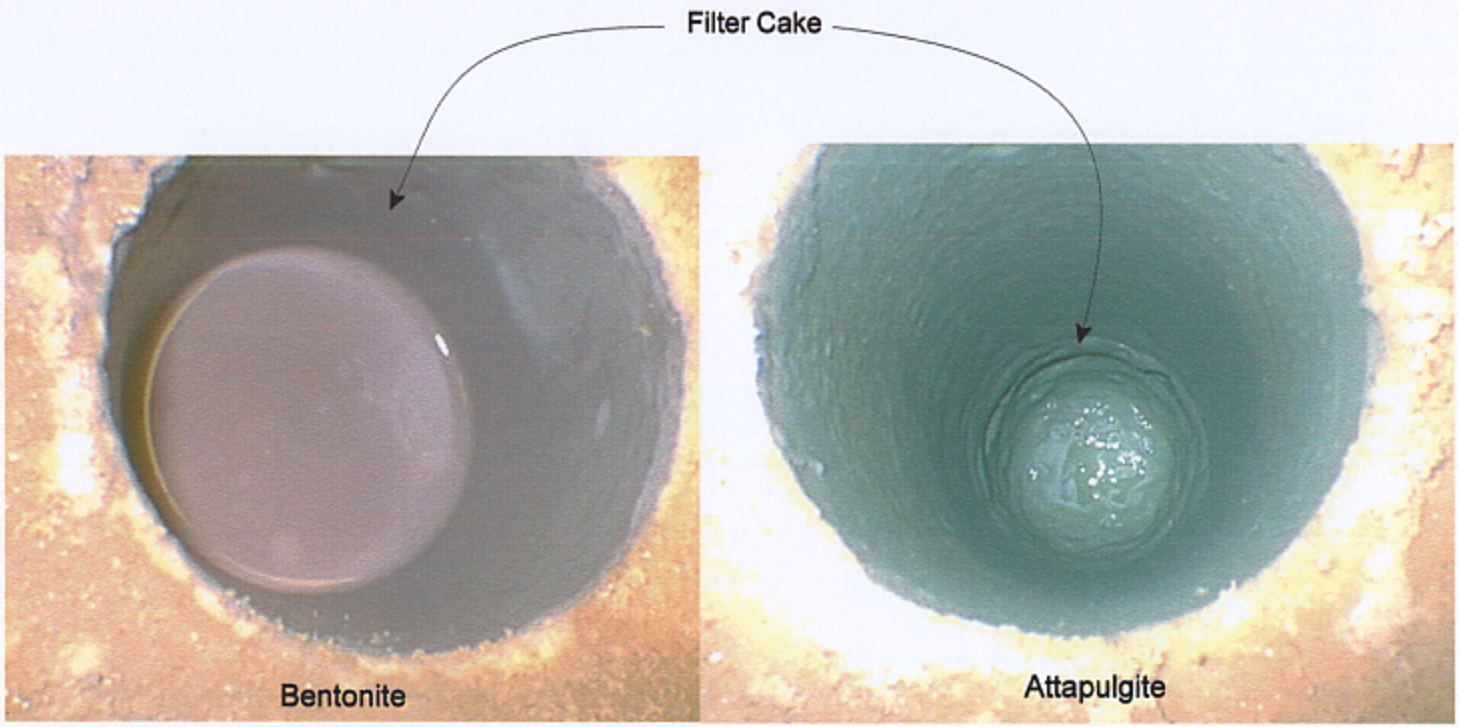

Figure 2.13 Formation of the Filter Cake on a Scaled Borehole Filled with Bentonite Slurry .

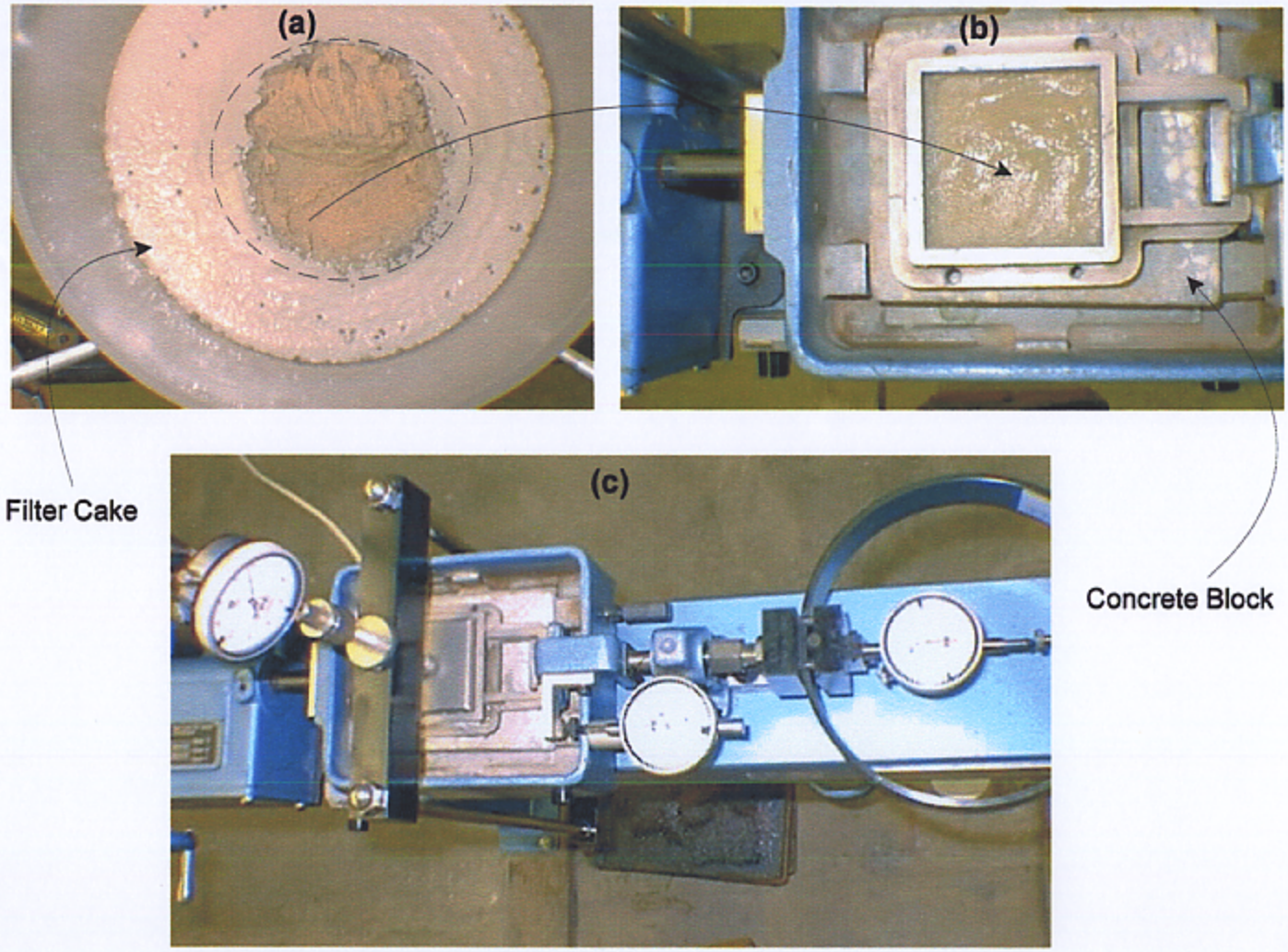

Figure 2.14 (a)Soil Sample Saturated with Mineral Slurry; (b)Placement of the Soil Sample in the Upper Shear Box; (c) Direct Shear Apparatus

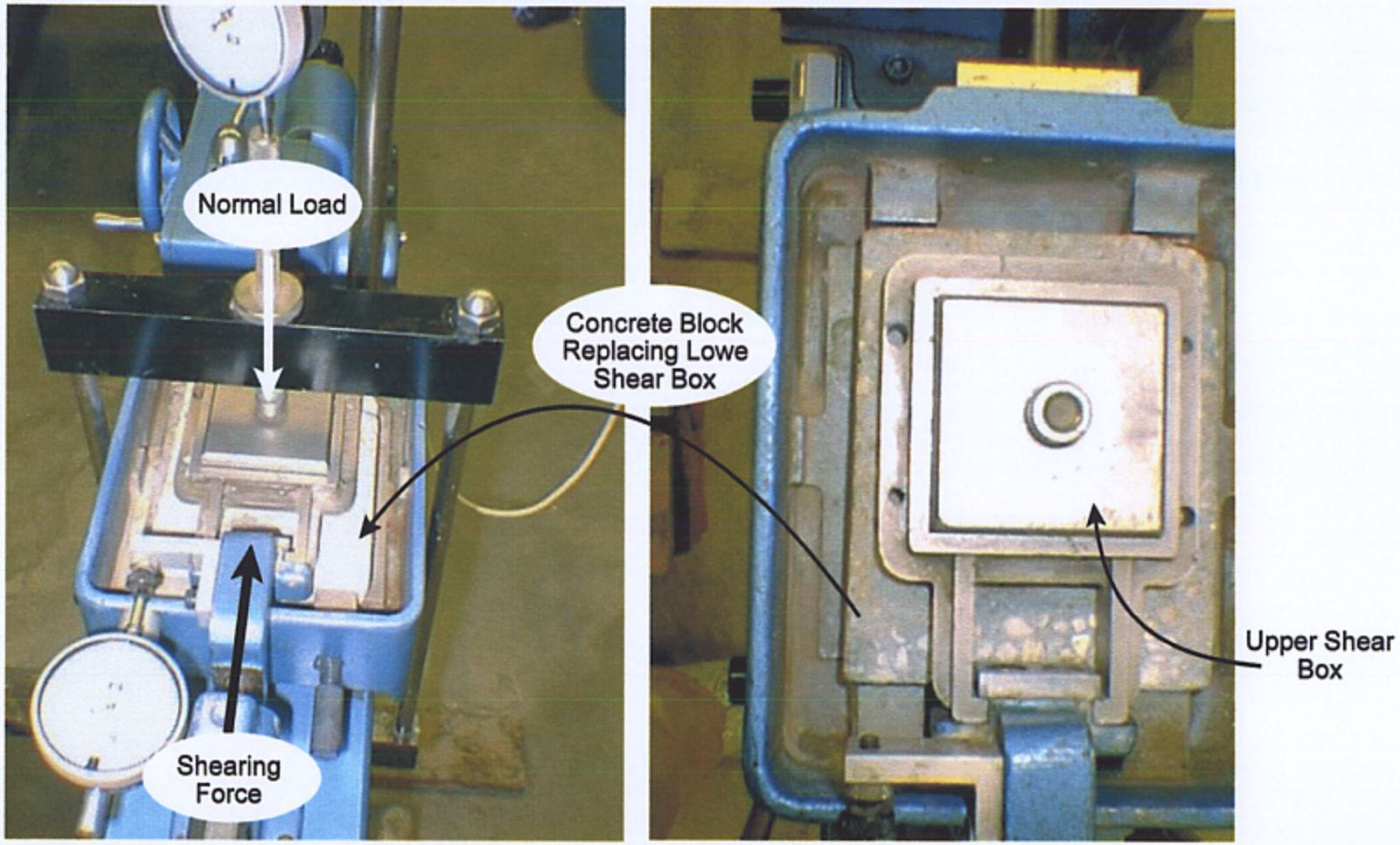

Figure 2.15 Direct Shear Apparatus with the Concrete Block.

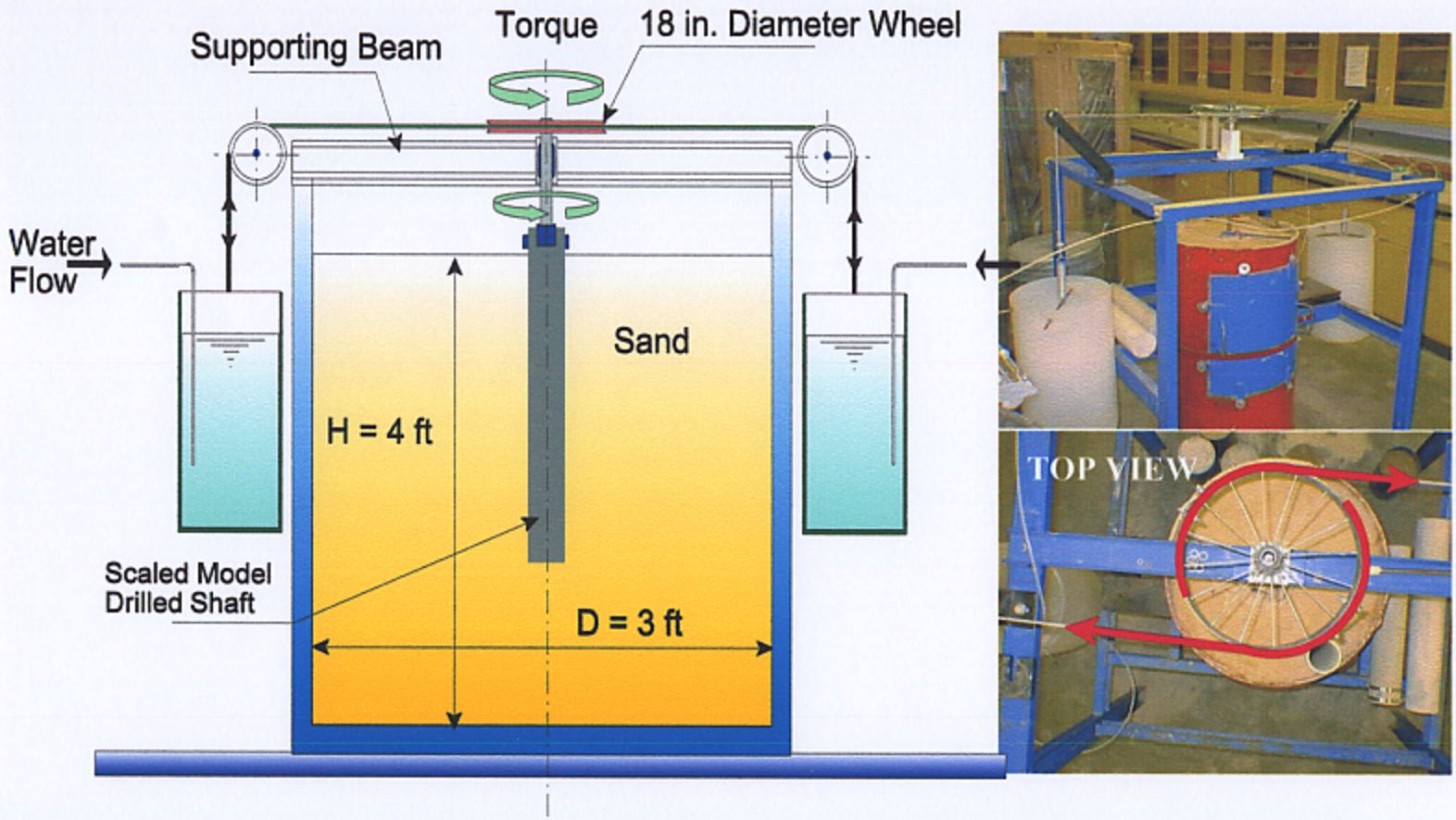

Figure 2.16 Scaled Model Torsional Testing Apparatus

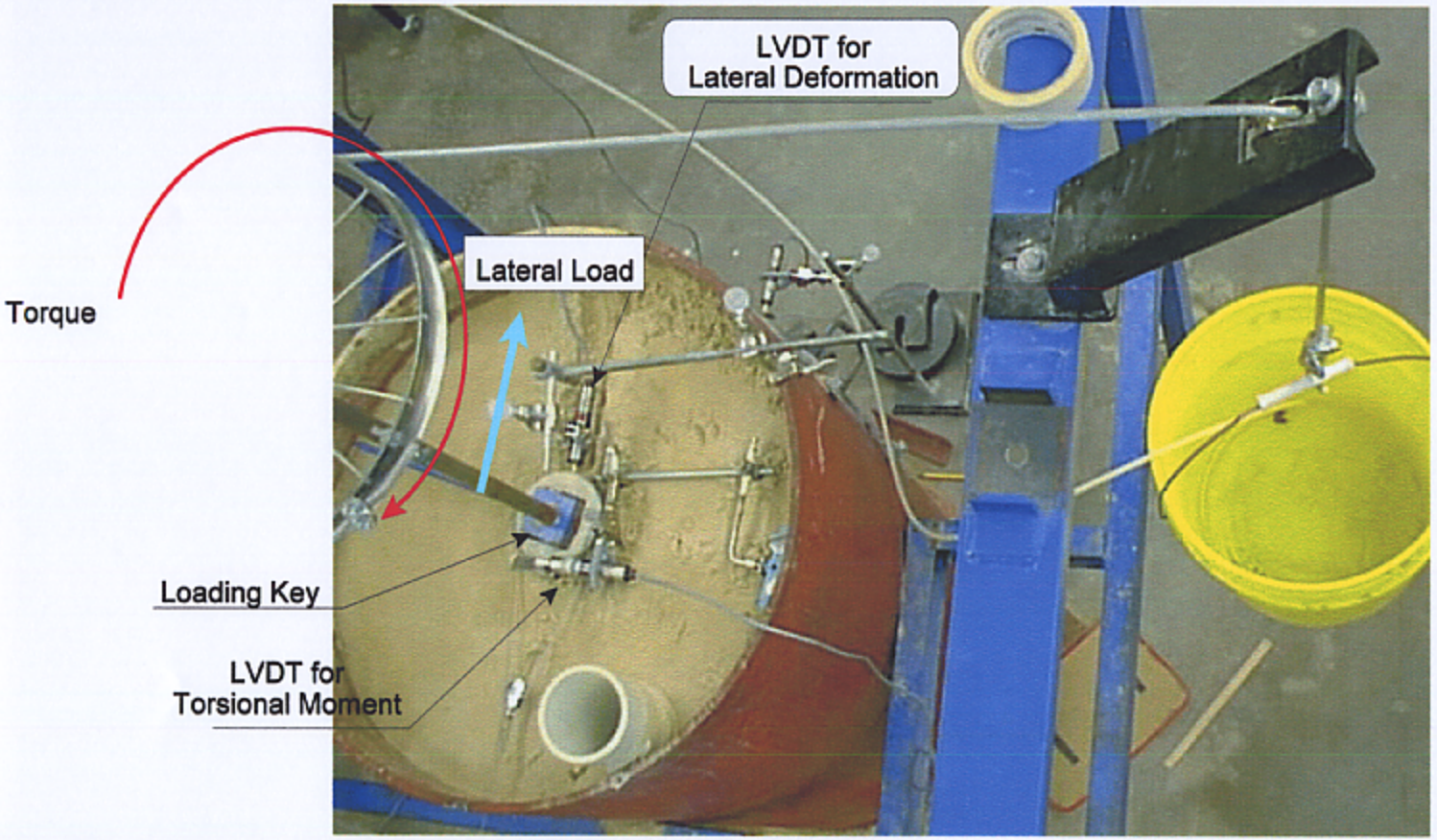

Figure 2.17 Torsional Testing Setup with Lateral Load and Torque Application

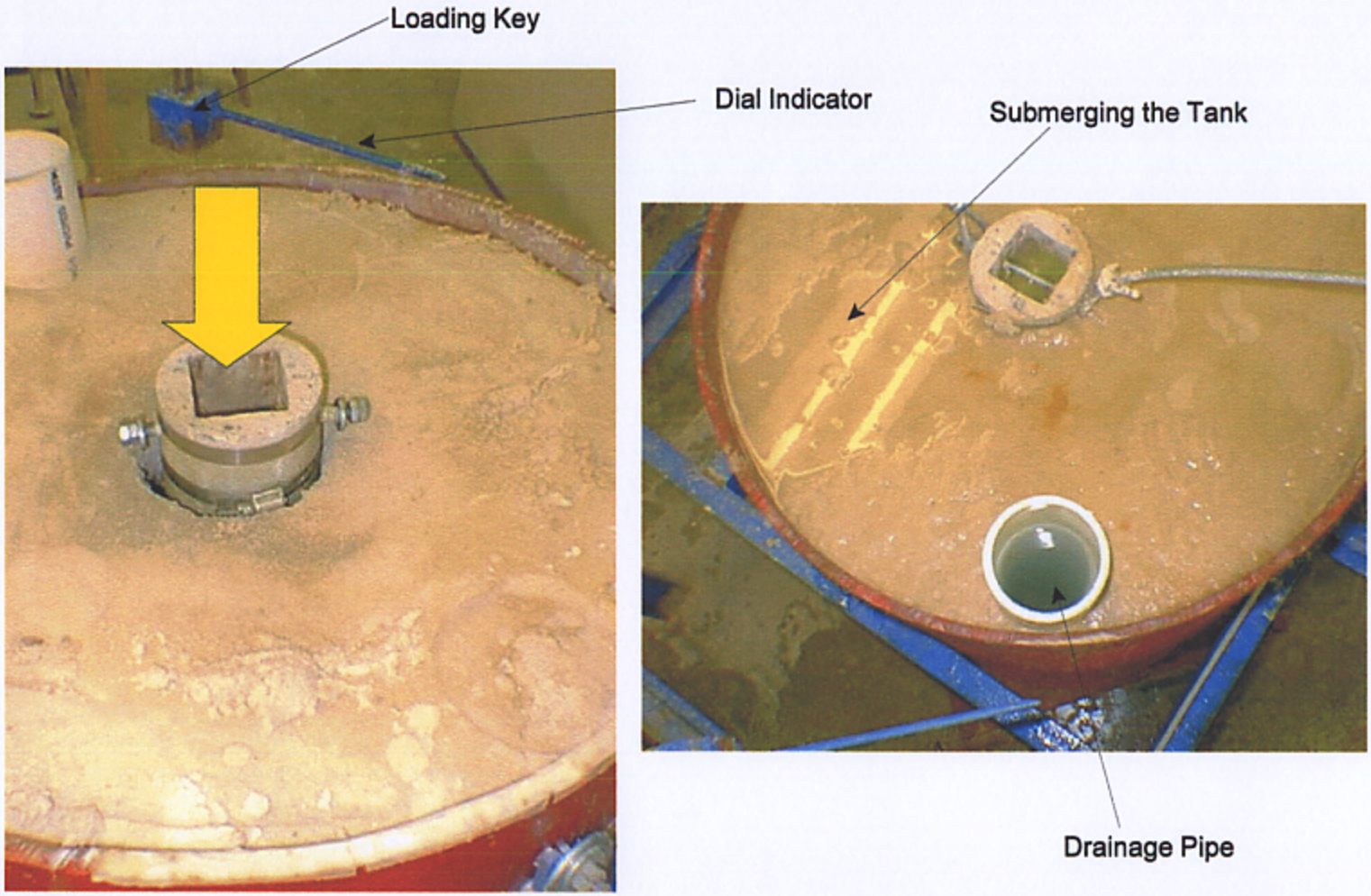

Figure 2.18 Consolidating the Soil To Provide Contact with the Shaft

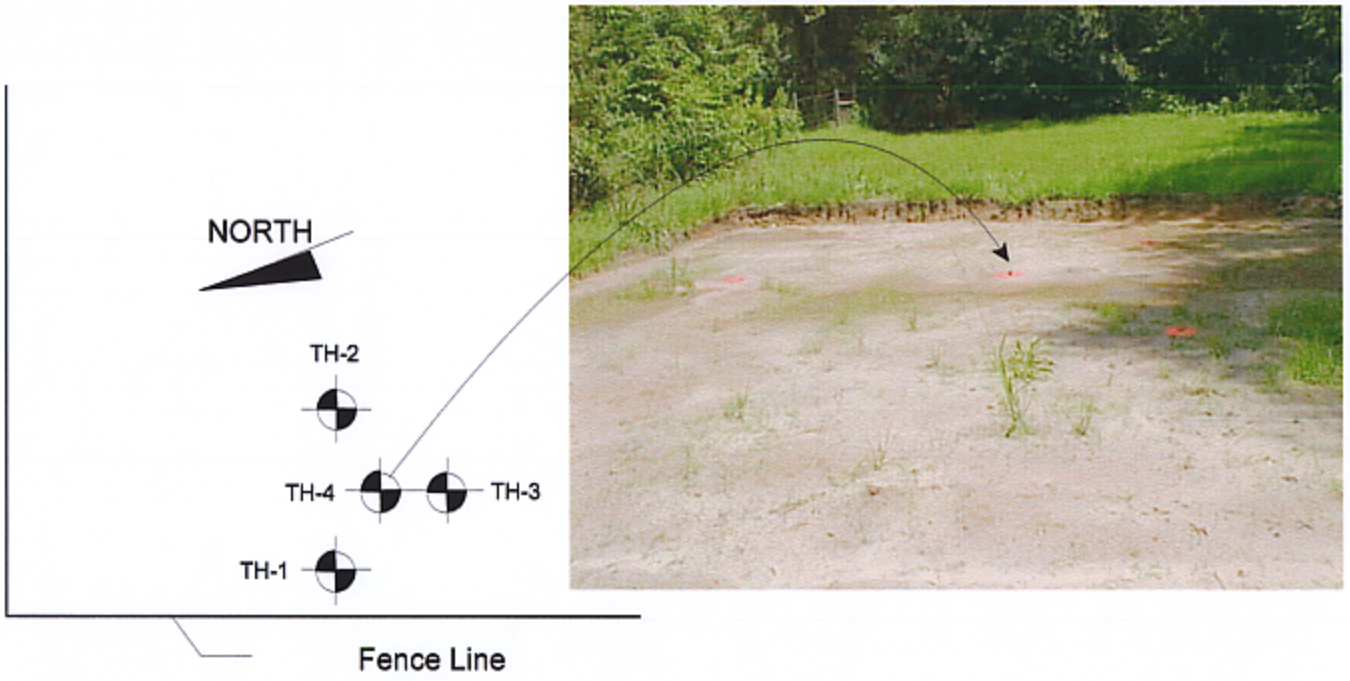

Figure 2.19 Site Location and Drilled Shaft Configuration for Field Testing

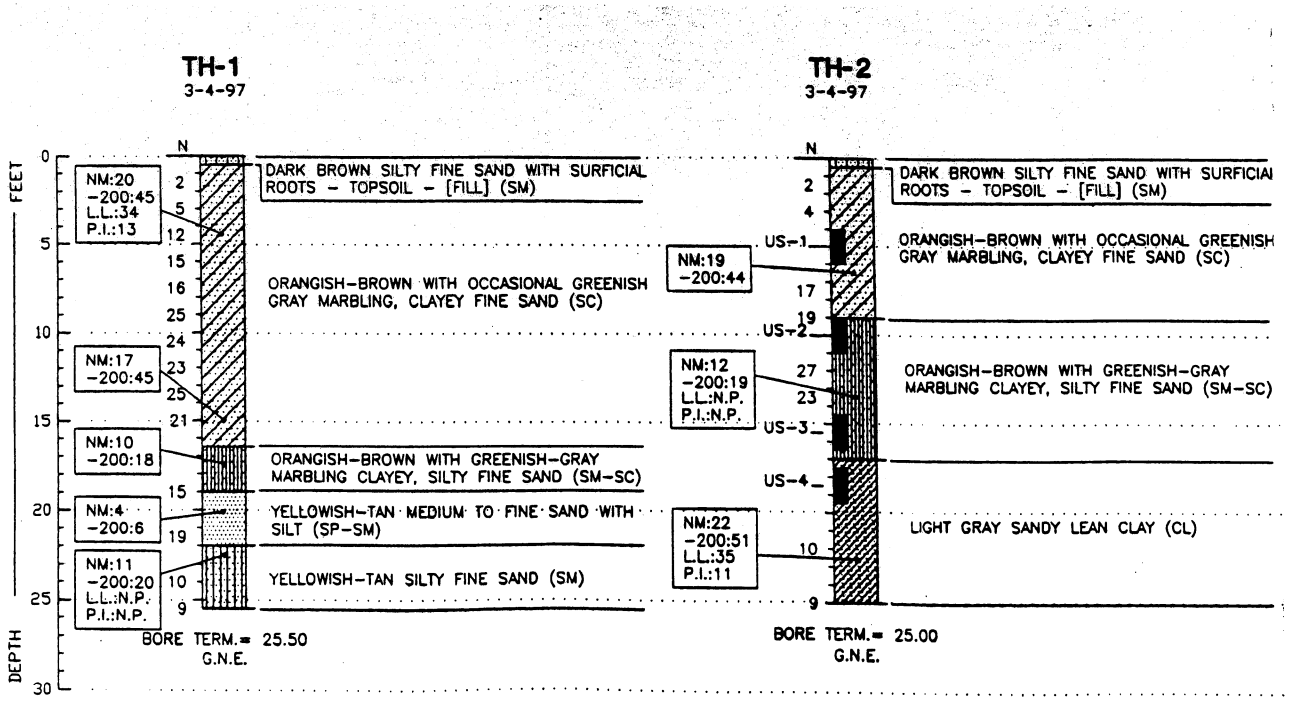

Figure 2.20 Soil Configuration at the Site

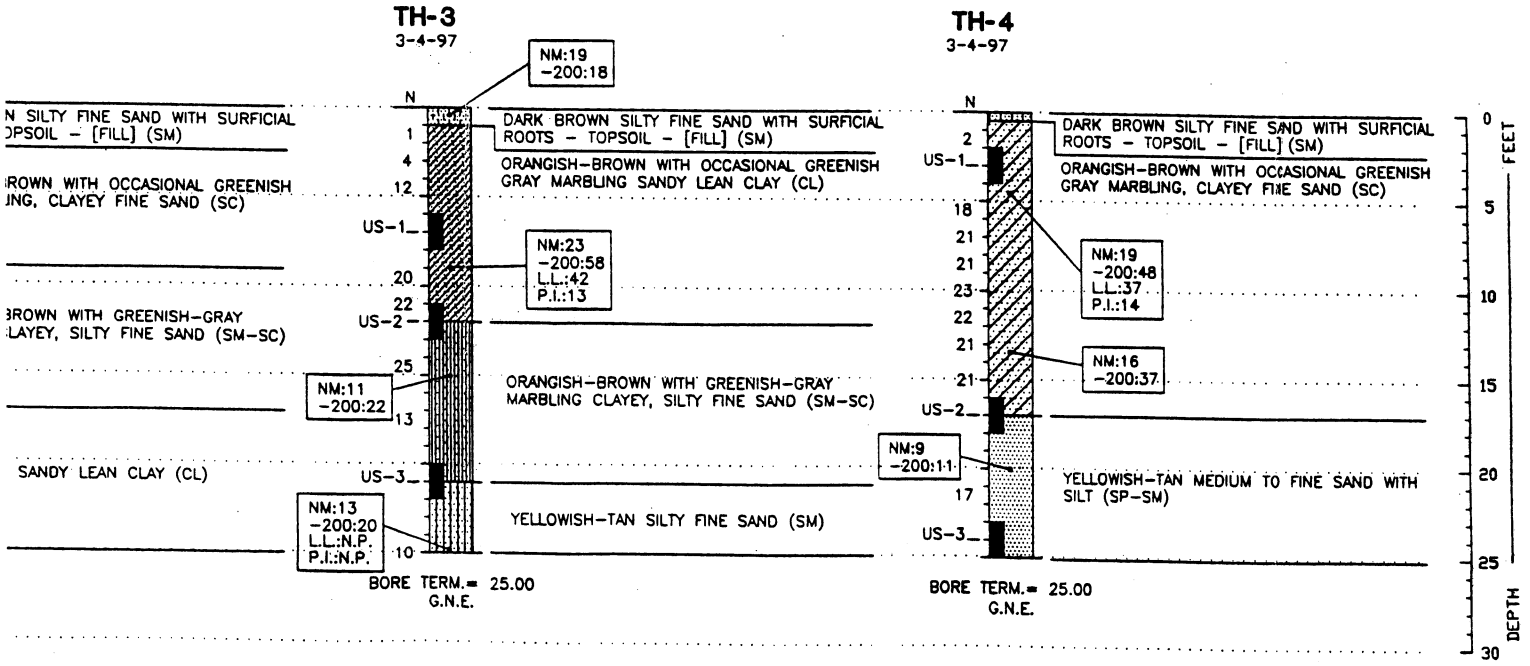

Figure 2.21 Soil Configuration at the Site

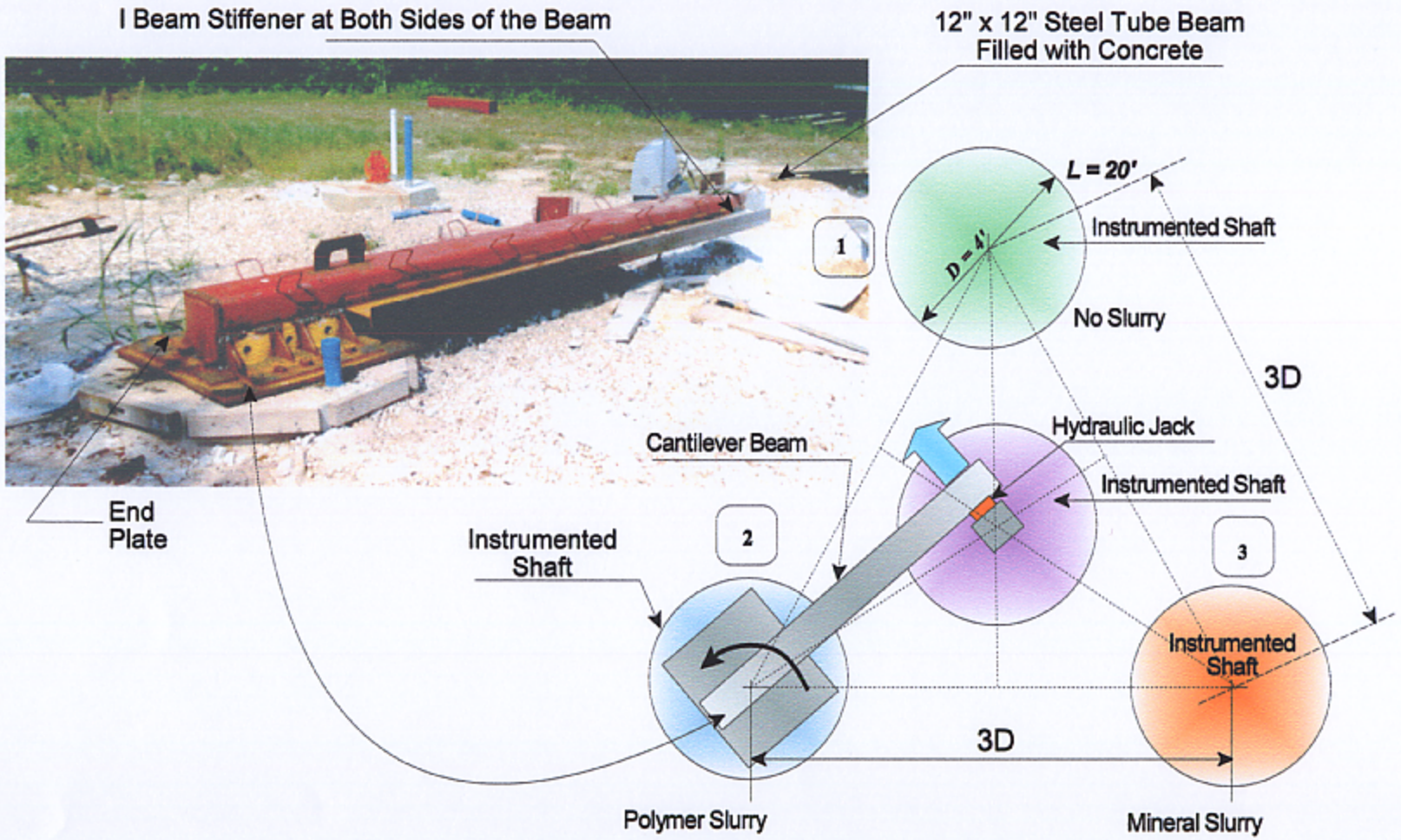

Figure 2.22 Field Test Arrangement

CHAPTER 3

FINITE ELEMENT ANALYSIS

3.1 Finite Element Analysis

To have a thorough insight at the behavior of the drilled shaft under combined loading conditions it was decided to develop a numerical simulation using the finite element analysis and to compare measurements obtained from field testing with those from the FEA modeling. Another advantage of using the numerical simulation in this study was the validation of the assumptions involved in the proposed analytical method for drilled shaft design.

Using the three dimensional FEA, it was possible to closely simulate the geometries, material properties, and loading conditions involved in the problem. The effect of method of construction on the drilled shaft behavior was simulated using different friction coefficients for both the mineral and the polymer slurries. The friction coefficients were obtained from the extensive laboratory tests on scaled models and direct shear testing.

The finite element analysis code used in this study is commercially known as ANSYS 5.3 and it can accommodate linear and nonlinear analysis with a wide range of choices for element and material libraries. Results from the FEA were transferred from the output data base of the program and analyzed using Excel spreadsheet add-in macros. Several macros were developed in this study to facilitate the reduction and plotting of an enormous amount of FEA data.

3.2 Three Dimensional FEA Modeling

The field tests carried out in this study were first analyzed using a three dimensional FEA modeling. The preliminary FEA analysis was conducted to assist in understanding the shaft behavior and to serve in setting the most economical and efficient instrumentation plan for the full scale drilled shafts. Accordingly it was decided to use two types of embedded gages to record the variation in the strain measurements during testing and to monitor the possibility of failure at the structural and foundation levels. The first and the second types of strain gages are descibed in the filed testing instrumentation section of chapter 4.

The second set of FEA analysis was performed after concluding the field testing and the results were used to compare with those obtained from the field measurements. In the second round of FEA analysis, few changes in the model were induced. These changes were mostly in the load application where a loading beam similar to the one used in the field was constructed and incremental loads were applied starting from 1,000 lb up to 50,000 lb. These increments were similar to those followed in the field tests **(Figures 3.1 to 3.5)**.

The locations of the strain gages along the shafts were similar in all the shafts **(Figure 3.5)**. However, with respect to the circumference of the shaft the locations slightly varied from shaft to another. This variation necessitated the analysis of all the nodes along each shaft model. In addition to exactly locating the relevant nodes, the analysis of all the nodes along the depth and the circumference of the shaft gave a full picture of the stress, strain, and deformation behavior of the shaft and the surrounding soil **(Figures 3.6 to 3.9)**.

3.2.1 Model Geometry of the Drilled Shaft

For the final analysis, additional modification was done on the soil surrounding the shaft. To closely simulate the variation in the soil strength with depth it was decided to build 10 soil layers with a thickness of 2 ft per layer. The supporting layer at the tip of the shaft was constructed from five major volumes with a diameter of 40 ft and depth of 20 ft **(Figure 3.1)**. The total number of volumes used in the 3D modeling were 56 volumes. Eight of these volumes were for the drilled shaft. The dimensions of the model were selected so that during load increment application, the influenced zones were away from the boundaries. Several trial and error models were constructed before the existing geometry was selected.

3.2.2 Three Dimensional Finite Element Meshing

After building the solid model, volumes that belong to the soil were glued togther. The same was done for the drilled shaft volumes. The discontinuity between the shaft and the soil was then used to establish the contact elements which represented the friction between the two media **(Figure 3.2)**. Before the meshing process each volume was assigned the pertain material properties. The lines in each volume were divided using predetermined divisions. The purpose was to generate a uniform mesh with consistent dimensions where nodal results can be selected and compared with a great accuracy with the filed measurements **(Figure 3.3)**. Additionally, having predetermined aspect ratios in the elements would eliminate any type of stress concentration in the model **(Figure 3.4)**. Before the meshing process, the pertain elements were selected and attributes of each volume were assigned.

Three types of elements were chosen for the 3D model. These elements include (1) solid 45 element, (2) contact 49 element, and (3) beam element. The contact elements were assigned the

proper real constants, with normal contact stiffness of 1,000,000 psi, sticking contact stiffness of 100,000 psi, penetration tolerance of 0.01, and static/dynamic friction ration of 1. In the selection of the contact stiffness and the sticking stiffness several trial and error runs were needed to establish the proper values.

The solid model was chosen to have a mapped mesh. This selection was necessary to eliminate any tetrahedral element generation. All the produced elements in the model were of solid six sides. Contact elements were generated with double-overlay elements. Such element generation would assume the soil be the target surface for the first overlay and then the process is reversed where the shaft would be considered as a target surface which would produce the second overlay. This meshing technique is always recommended when there is no distinct target surface like the soil and the shaft where at certain zones the target surface may change its setting along the length of the shaft. Additionally, using the double-overlay elements would minimize the penetration between the contacts. Reducing the penetration, however, could be accomplished through the penetration tolerance in the real constants of the contact elements but the reduction of the magnitude of this parameter might jeopardize the conversion process in the solution stage. Thus it was necessary to establish the double-overlay elements around the shaft model.

A detailed description of the elements used in this model is as follows:

1- Solid45 3-D Structural Element

SOLID45 is used for the three-dimensional modeling of solid structures. The element is defined by eight nodes having three degrees of freedom at each node: translations in the nodal x, y, and z directions. The element has plasticity, creep, swelling, stress stiffening, large deflection, and large strain capabilities.

Input Data

The geometry, node locations, and the coordinate system for this element are shown in Figure 3.10. The element is defined by eight nodes and the orthotropic material properties. Orthotropic material directions correspond to the element coordinate directions. Table 3.1 illustrates the input data for SOLID 45 elements.

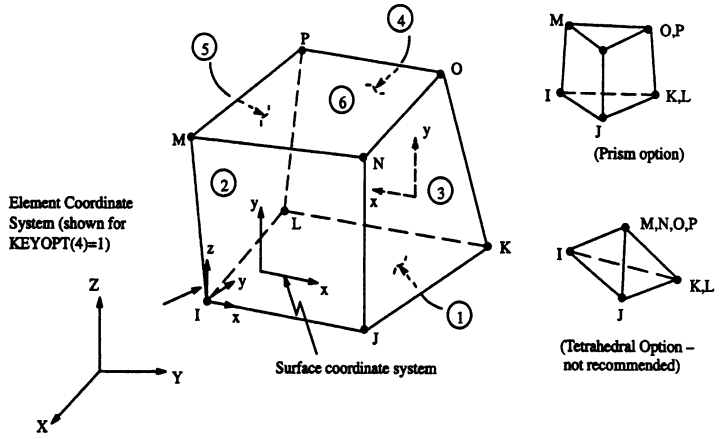

Figure 3.10 SOLID 45 3-D Structural Solid Element Used in the Study

Table 3.1 SOLID45 Input Summary

Label	**Explanation**
Nodes:	*I, J, K, L, M, N, 0, P*
Degrees of Freedom:	*UX, UY, UZ*
Real Constants:	*None*
Material Properties:	*EX, EY, EZ, ALPX, ALPY, ALPZ, NUXY, NUYZ, NUXZ, DENS, GXY, GYZ, GXZ, DAMP*
Surface Loads:	*Pressures: face I (J-I-L-K), face 2 (I-J-N-M), face 3 (J-K-O-N), face 4 (K-L-P-O), face 5 (L-I-M-P), face 6 (M-N-O-P)*
Special Features:	*Plasticity, Creep, Swelling, Stress stiffening. Large deflection. Large strain. Birth and death*

Output Data

The solution output associated with the element is in two forms: (1) nodal displacements included in the overall nodal solution, and (2) additional element output as shown in **Table 3.2**. Several output data items are illustrated in **Figure 3.11**. The element stress directions are parallel to the element coordinate system. The surface stress outputs are in the surface coordinate systems and are available for any face (KEYOPT(6)). The coordinate systems for faces UNM and KLPO are shown in Figure 3.4. The other surface coordinate systems follow similar orientations as indicated by the pressure face node description.

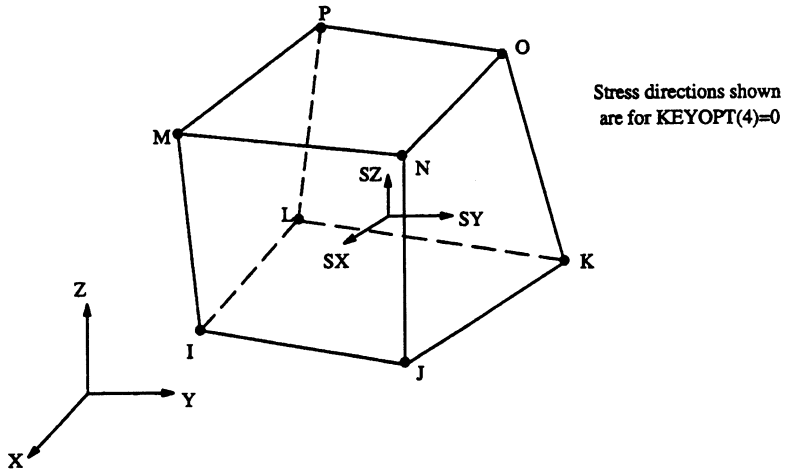

Figure 3.11 SOLID 45 Stress Output

Table 3.2 SOLID45 Element Output Explanations

Lable	Explanation
EL	*Element number*
NODES	*Nodes -1, J, K, L, M, N, 0, P*
MAT	*Material number*
VOL	*Volume*
XC,YC,ZC	*Global X,Y,Z location*
PRES	*PI at nodes J, I, L, K; P2 at I, J, N, M; P3 at J, K, 0, N; P4 at K, L, P, 0; P5 at L, I, M, P; P6 at M, N, 0, P*
TEMP	*T(l), T(J), T(K), T(L), T(M), T(N), T(0), T(P)*
FLUE	*FL(1), FL(J), FL(K), FL(L), FL(M), FL(N), FL(0), FL(P)*
SINT	*Stress intensity*
SEQV	*Equivalent stress*
EPEL(X, Y, —XZ)	*Elastic strains (X, Y, Z, XY, YZ, XZ)*

EPEL(1,2,3)	*Principal elastic strains*
S(X, Y, Z,—XZ)	*Stresses (X, Y, Z, XY, YZ, XZ)*
S(l,2,3)	*Principal stresses*
Nonlinear solution (printed only if the element has a nonlinear material):	
EPPL	*Average plastic strains (X, Y, Z, XY, YZ, XZ)*
EPEQ	*Average equivalent plastic strain*
SRAT	*Ratio of trial stress to stress on yield surface*
SEPL	*Average equivalent stress from stress-strain curve*
HPRES	*Hydrostatic pressure (postdata only)*
EPCR	*Average creep strains (X, Y, Z, XY, YZ, XZ)*
EPSW	*Average swelling strain*

CONTAC49 3D Point to Surface

Contact Element

CONTAC49 may be used to represent contact and sliding between two surfaces in three dimensions. The element has five nodes with three degrees of freedom at each node: translations in the nodal x, y, and z directions. Contact occurs when the contact node penetrates the target base. Elastic Coulomb friction and rigid Coulomb friction are allowed, where sliding is along the target base. Other contact elements, such as CONTAC12, CONTAC26, CONTAC40, CONTAC48, CONTAC52, etc. are also available.

Input Data

The geometry and node locations are shown in **Figure 3.12**. The element geometry is a pyramid with the base being a quadrilateral, vertices being nodes on one of the surfaces (called the target surface), and the opposing vertex being a node on the other surface (called the contact surface). A degenerate form of the element is allowed which takes the shape of a tetrahedron when the base is a triangle. The base on the target surface is called a target base, and the nodes defining the target base are called target nodes. The node on the contact surface that completes the pyramid is called

a contact node. A geometry display of this element shows the target base and the contact node (as a star). Nodes I, J, K and L define the target base, and node M is the contact node. The first surface tangent vector is taken to be the unit vector that is tangent to the target base and pointing from I to J. The surface normal vector is defined to be the unit vector that is perpendicular to the target base and pointing out from the target surface. The second surface tangent vector is taken as the cross product of the surface normal vector and the first surface tangent vector. Thus the first surface tangent vector, second surface tangent vector, surface normal vector are a right-handed element coordinate system. Nodes I, J, K and L should be specified so that the cross product of vectors U and JK points outward from the free surface at node J (as shown in Figure 3.7). Initially, node M may be far removed from the target base, may be coplanar with the target base, or may have penetrated the target base. Contact occurs only when the normal projection (to the target line) of node M lies on the target base. The normal contact stiffness, KN, is used in the penalty function method to determine contact forces. KN has units of force/length. KN corresponds to a penalty stiffness that acts in the direction of the target surface normal. Its use enforces displacement compatibility by limiting the penetration of the target base by the contact node. A large value of KN is usually needed to enforce compatibility if the penalty function method (KEYOPT(2)=0) is selected. A lower KN value can be used with the penalty function plus Lagrange multiplier method (KEYOPT(2)=1). The absolute tolerance applied in the direction of the surface normal, TOLN, is used to determine if penetration compatibility is satisfied when the penalty function plus Lagrange multiplier method (KEYOPT(2)=1) is used. Contact compatibility is considered to be satisfied if the contact node is within TOLN clearance on either side of the target base. The value of TOLN must be positive and has units of L. If KEYOPT(3)==0, no friction is considered between the surfaces and none of the remaining real constant input parameters are needed. The sticking contact stiffness, KT, has units

of force/length. KT is only used if elastic Coulomb friction behavior is sought (KEYOPT(3)=1). It enforces the sticking component of contact friction and corresponds to a stiffness in a direction tangential to the target base. KT defaults to KN/100. The ratio of static to dynamic coefficients of friction, FACT, has default and minimum values of 1.0. It is used when KEYOPT(3) = 1. The coefficient of friction, MU, is needed when KEYOPT(3) = I or 2. It may be specified as a function of temperature. This is the only use of temperatures in the element. The dynamic coefficient of friction uses MU directly while the static coefficient of friction is FACT*MU. Real constant TOLS is used to add a small tolerance that will internally increase the area of the target (nodes I to L). Units for TOLS are percent (1.0 implies a 1.0% increase in the target area). TOLS is useful for problems where contact nodes (M) are likely to lie on the edge of targets (as at symmetry planes or for models generated in a node-to-node contact pattern). In these situations, the contact node may repeatedly "slip" off one target and on to another target or completely out of contact, resulting in convergence difficulties from oscillations. A small value of TOLS will usually prevent this situation from occurring.

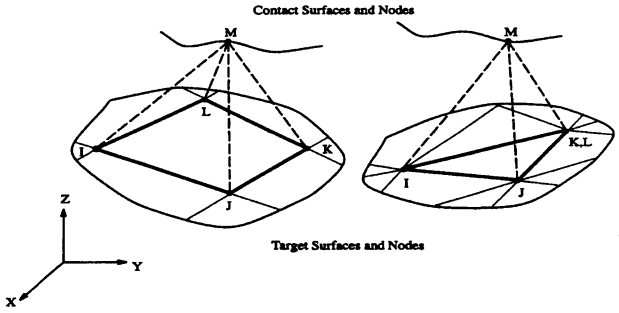

Figure 3.12 CONTACT 49 3-D Point to Surface Contact Element

Output Data

The solution output associated with the element is in two forms: (1) nodal displacements included in the overall nodal solution, and (2) additional element output (only if STAT = I or 2) as shown in **Table 3.3**.

Table 3.3 CONTAC49 Element Output Explanations

Label	Explanation
EL	*Element number*
NODES	*Nodes I, J, K, L and M*
XC,YC,ZC	*Center X, Y, Z location (postdata only)*
TEMP	*T(I), T(J), T(K), T(L), T(M)*
STAT.OLDST	*New and old contact statuses*
	1 Closed and sticking
	2 Closed and sliding
	3 Open but near contact
	4 Open and not near contact
NORM	*Surface normal vector components (X, Y, Z)*
FNTOT	*Total normal force*
FNPF	*Penalty function component of normal force*
GAP	*Gap size or penetration Total normal force*
AREA	*Area of target base*
LOCI,LOC2	*Dimensionless location of contactor node M on the target base:*
	(-1 to+1) if on quad surface, (0 to+1) if on tri surface
FSI	*Tangential force in element direction I (elastic or sliding)*
FS2	*Tangential force in element direction 2 (elastic or sliding)*
FSLIM	*Friction limit force*
MU	*Coefficient of friction*
ANGLE	*Principal angle of friction forces*

Material Properties

The solid model was divided into different volumes and each volume was assigned the pertain material properties. Volumes for the drilled shaft elements were assigned the concrete material properties, and for the soil volumes, the Drucker and Prager Capped yield model was used.

Concrete material model

The concrete material model predicts the failure of brittle materials. Both cracking and crushing

failure modes are accounted for. TB, CONCR accesses this material model, which is available with the reinforced concrete element SOLID65. The criterion for failure of concrete due to a multiaxial stress state can be expressed in the form

$$F/f_c - S \geq 0 \qquad (3.1)$$

where: F = a function (to be discussed) of the principal stress state (σ_{xp}, σ_{yp}, σ_{zp}) failure surface expressed in terms of principal stresses and five input parameters f_t, f_c, f_{cb}. f_1 and f_2 defined in **Table 3.4**

f_c = uniaxial crushing strength

σ_{xp}, σ_{yp}, σ_{zp} = principal stresses in principal directions xp, yp, and zp

If equation (3.1) is not satisfied, there is no attendant cracking or crushing. Otherwise, the material will crack if any principal stress is tensile while crushing will occur if all principal stresses are compressive. A total of five input parameters (each of which can be temperature dependent) are needed to define the failure surface. These are presented in **Table 3.4**.

Table 3.4 Concrete Material Table (Input on TBDATA Commands with TB,CONCR)

Label	Description	Constant
f_t	Ultimate uniaxial tensile strength	3
f_c	Ultimate uniaxial compressive strength	4
f_{cb}	Ultimate biaxial compressive strength	5
σ_h^a	Ambient hydrostatic stress state	6
f_1	Ultimate compressive strength for a state of biaxial compression superimposed on hydrostatic stress state σ_h^a	7
f_2	Ultimate compressive strength for a state of uniaxial compression superimposed on hydrostatic stress state σ_h^a	8

However, the failure surface can be specified with a minimum of two constants, f_t and f_c. The other three constants default to (William and Wamke, 1975):

$$f_{cb} = 1.2\, f_c \tag{3.2}$$

$$f_1 = 1.45\, f_c \tag{3.3}$$

$$f_2 = 1.725\, f_c \tag{3.4}$$

However, these default values are valid only for stress states where the condition

$$\sigma_h \leq \sqrt{3}\, f_c \tag{3.5}$$

$$(\sigma_h = \text{hydrostatic stress state} = 1/3\ (\sigma_{xp} + \sigma_{yp} + \sigma_{zp}) \tag{3.6}$$

is satisfied.

Drucker-Prager (DP) Model

This option uses the Drucker-Prager yield criterion with either an associated or nonassociated flow rule. The yield surface does not change with progressive yielding, hence there is no hardening rule and the material is elastic- perfectly plastic **(Figure 3.13)**. The equivalent stress for Drucker-Prager is

$$\sigma_e = 3\beta\sigma_m + \left[\frac{1}{2}\{s\}^T\{s\}\right]^{\frac{1}{2}} \tag{3.7}$$

where:

σ_m = the mean or hydrostatic stress $= \frac{1}{3}(\sigma_x + \sigma_y + \sigma_z)$

$\{s\}$ = the deviatoric stress

β = material constant

This is a modification of the von Mises yield criterion with $\{a\} = \{0\}$ that accounts for the influence of the hydrostatic stress component: the higher the hydrostatic stress (confinement pressure) the higher the yield strength. β is a material constant which is given as

$$\beta = \frac{2\sin\phi}{\sqrt{3}\ (3 - \sin\phi)} \tag{3.8}$$

where: ϕ = the input angle of internal friction

The material yield parameter is defined as

$$\sigma_y = \frac{6c\ \cos\phi}{\sqrt{3}\ (3 - \sin\phi)} \tag{3.9}$$

where: c = the input cohesion value

The yield criterion (equation (4.1-4)) is then

$$F = 3\beta\sigma_m + \left[\frac{1}{2}\{s\}^T\{s\}\right]^{\frac{1}{2}} - \sigma_y = 0 \tag{3.10}$$

This yield surface is a circular cone with the material parameters (equations (3.8) and (3.9)) chosen such that it corresponds to the outer aspices of the hexagonal Mohr-Coulomb yield surface. Figure 3.13

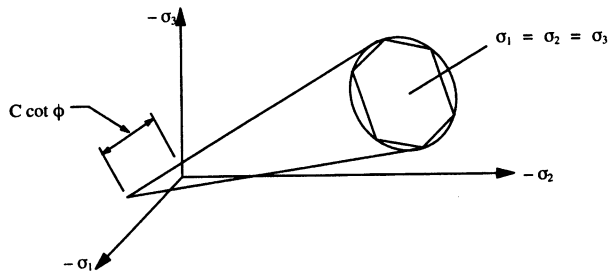

Figure 3.13 Drucker - Prager and Mohr - Coulomb Yield Surface

$\left\{\frac{\partial F}{\partial \sigma}\right\}$ is readily computed as

$$\left\{\frac{\partial F}{\partial \sigma}\right\} = \beta \lfloor 1 \quad 1 \quad 1 \quad 0 \quad 0 \quad 0 \rfloor^T + \frac{1}{\left[\frac{1}{2}\{s\}^T\{s\}\right]^{\frac{1}{2}}} \{s\} \tag{3.11}$$

$\{\delta Q/\delta \sigma\}$ is similar, however β is evaluated using φ_f (the input "dilatancy" constant). When $\varphi_f = \varphi$, the flow rule is associated and plastic straining occurs normal to the yield surface and there will less volumetric expansion and if φ_f is zero, there will be no volumetric expansion.

The equivalent stress parameter (output quantity SEPL) is defined as

$$\hat{\sigma}_e^{pl} = \sqrt{3}\ (\sigma_y - 3\beta\sigma_m) \tag{3.12}$$

The equivalent stress parameter is interpreted as the von Mises equivalent stress at yield at the current hydrostatic stress level. Therefore for any integration point undergoing yielding (stress ratio SRAT > 1), σ_e^{pl} (SEPL) should be close to the actual von Mises equivalent stress (SIGE) at the converged solution.

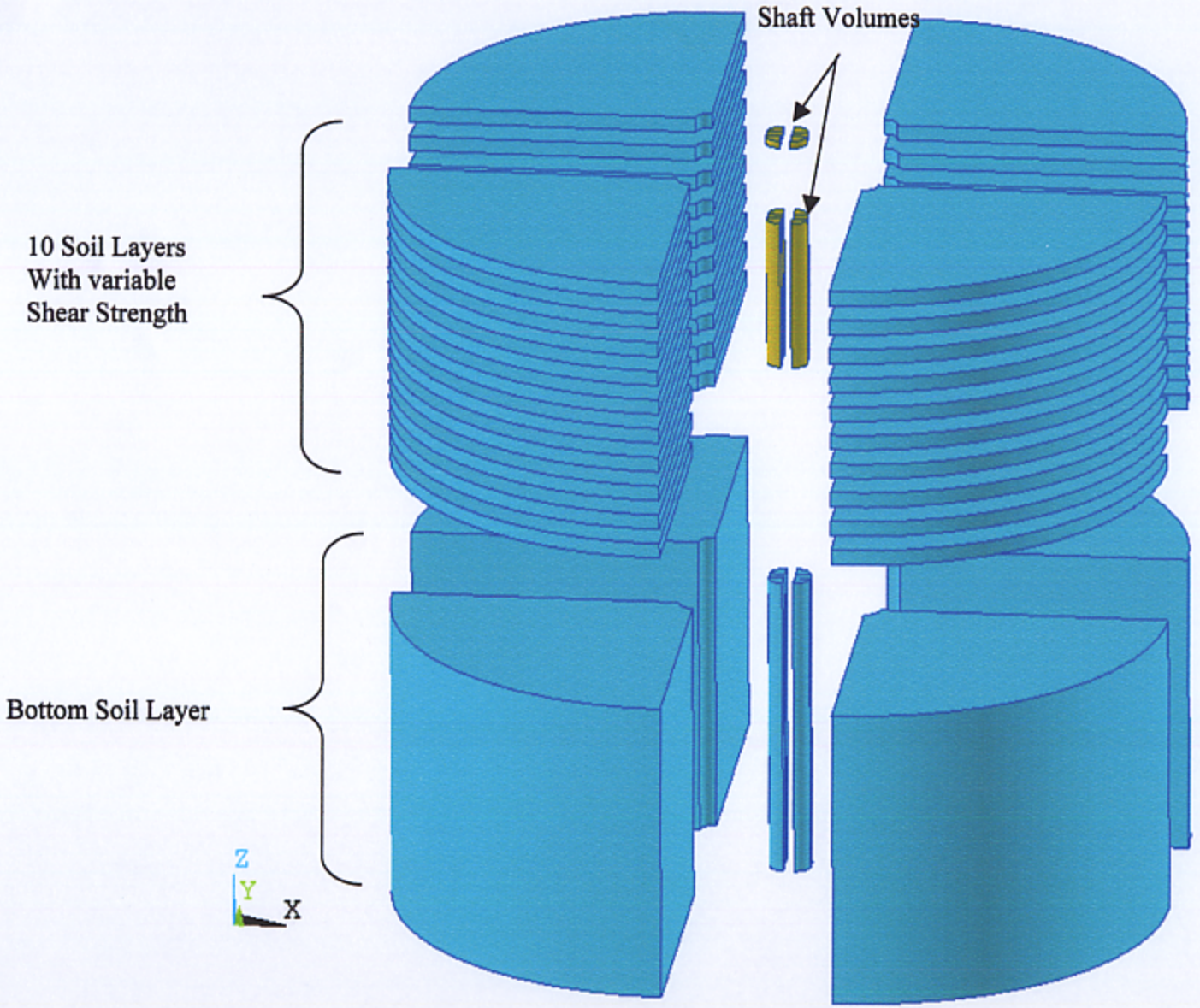

Figure 3.1 Geometry Composition (56 volumes) of the of the Drilled Shaft 3D Solid Model

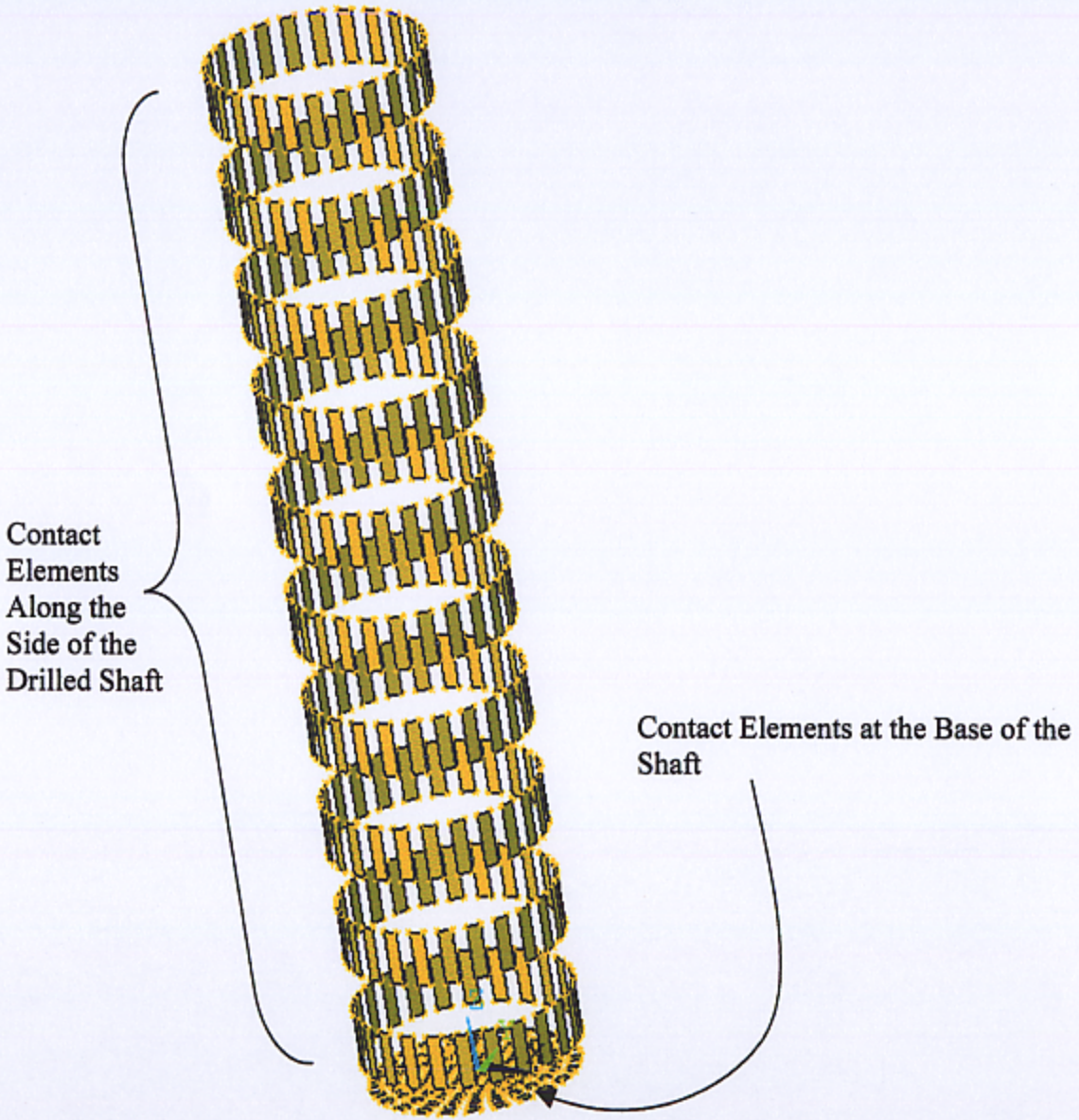

Figure 3.2 Double Overlay Element Generation Technique for the Contact Element Along the Drilled Shaft

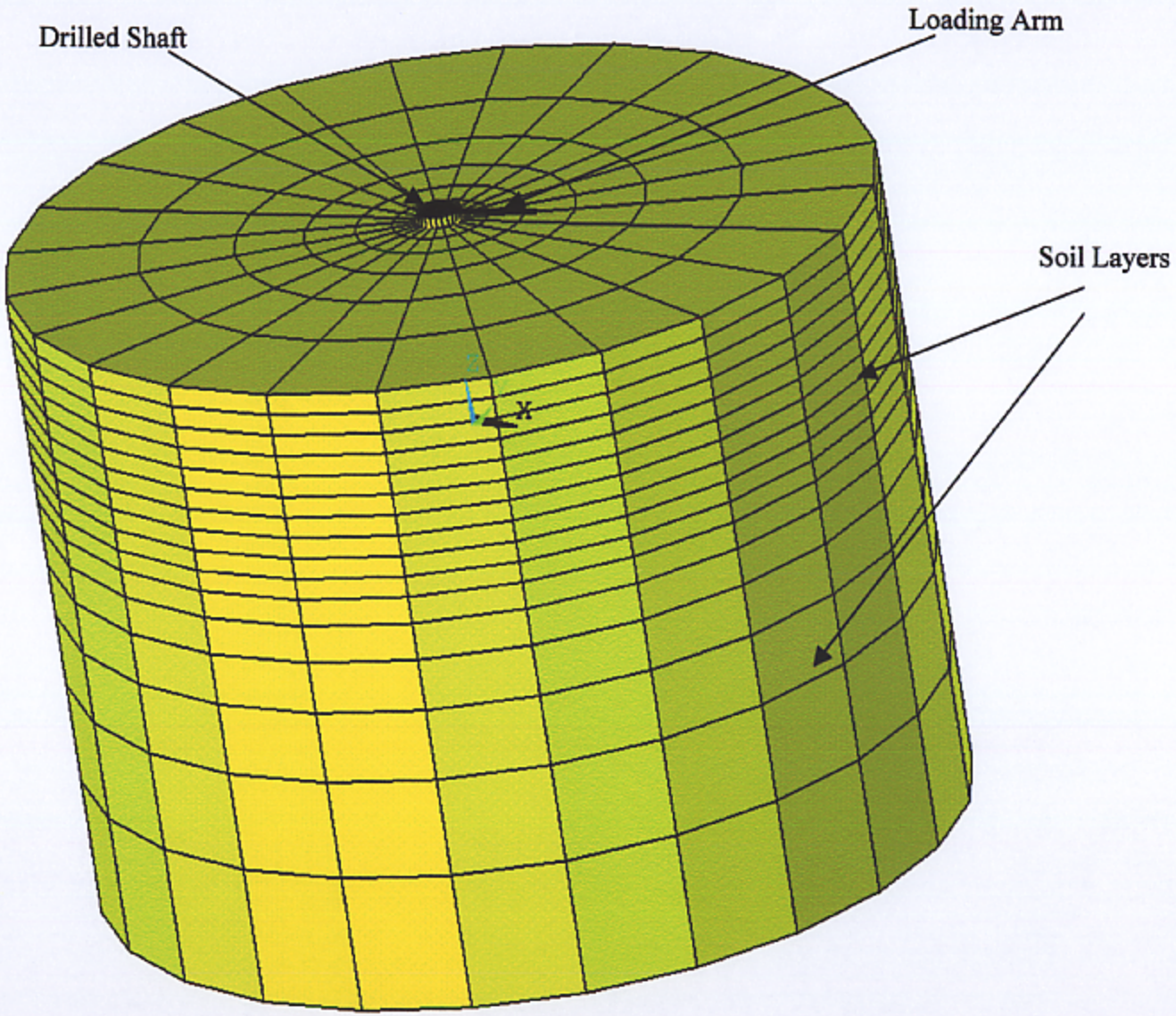

Figure 3.3 Mapped Meshing of the 3D Solid Model

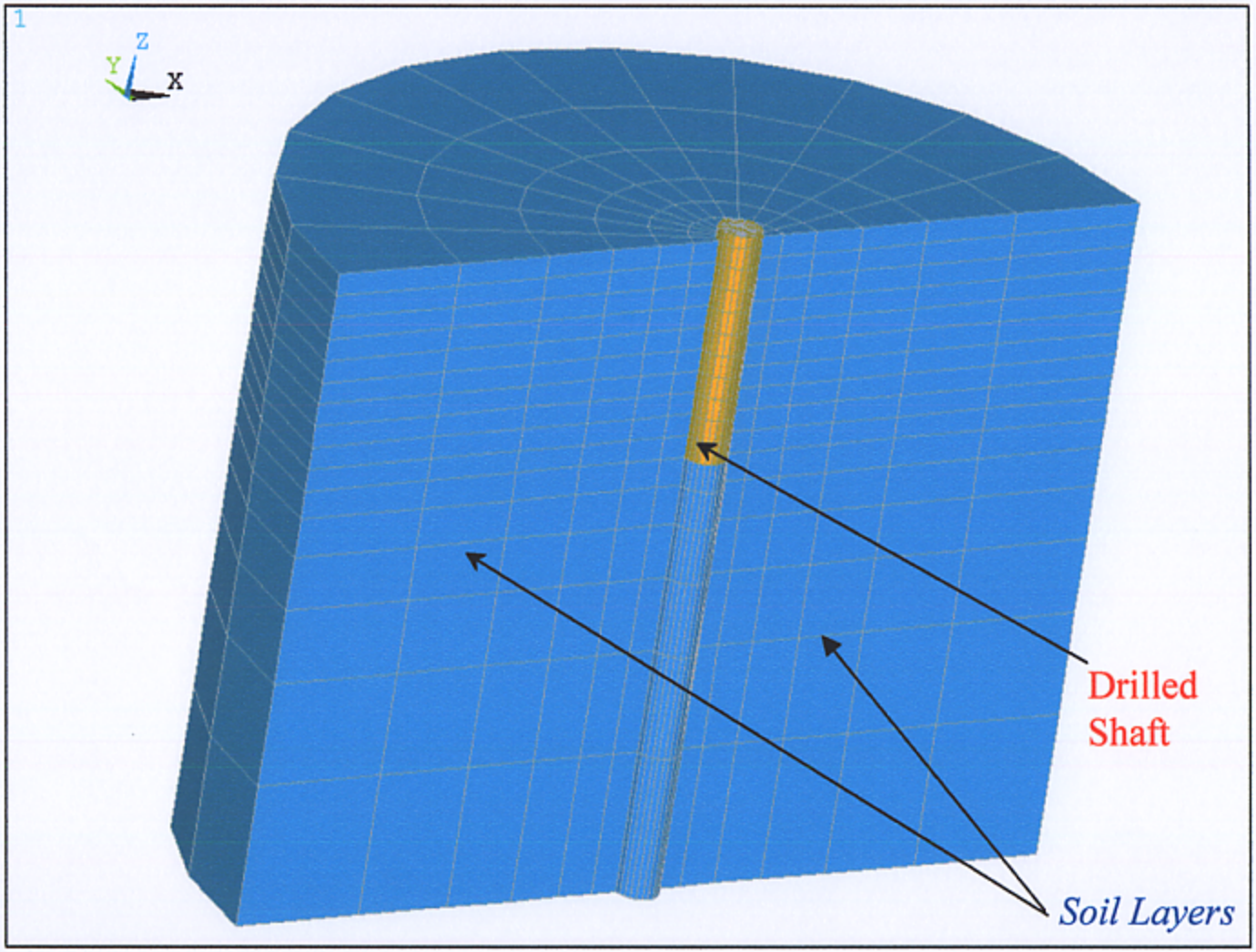

Figure 3.4 Cross Section Showing the 3D Finite Element Modeling of the Drilled Shaft and the Surrounding Soil Layers.

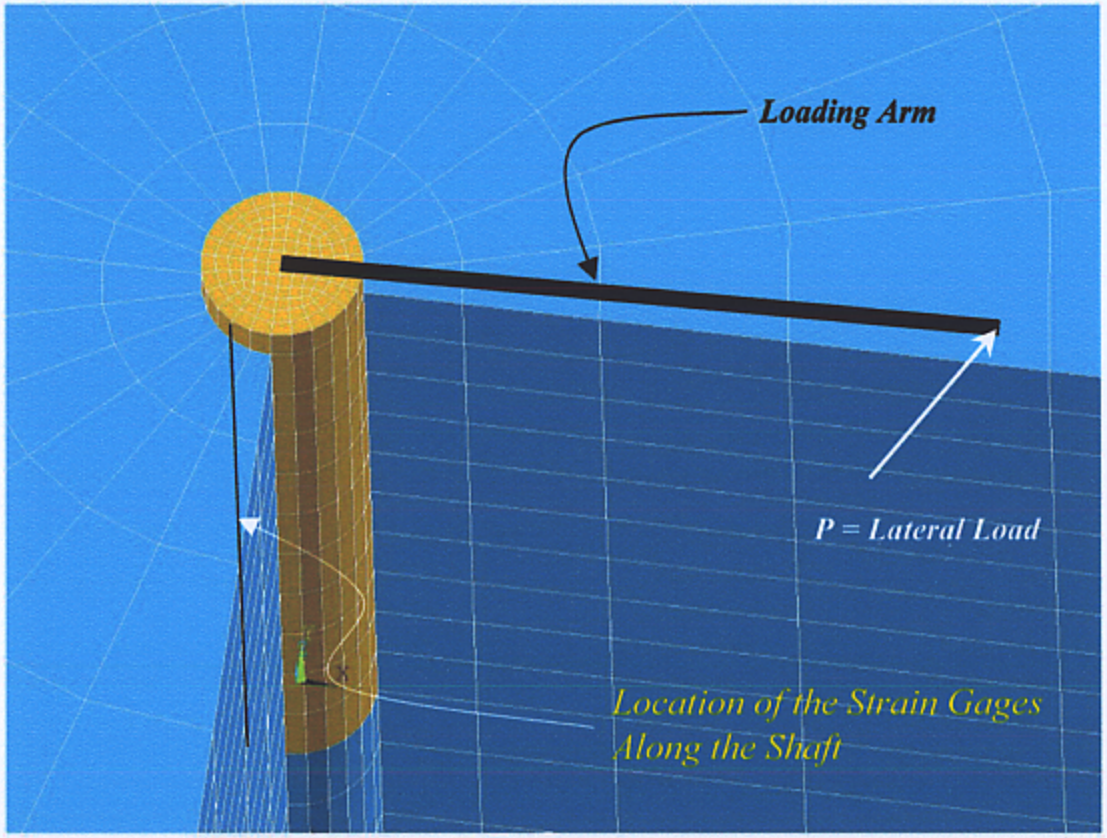

Figure 3.5 Corresponding Locations of the Strain Readings as Compared to the Full Scale Shaft

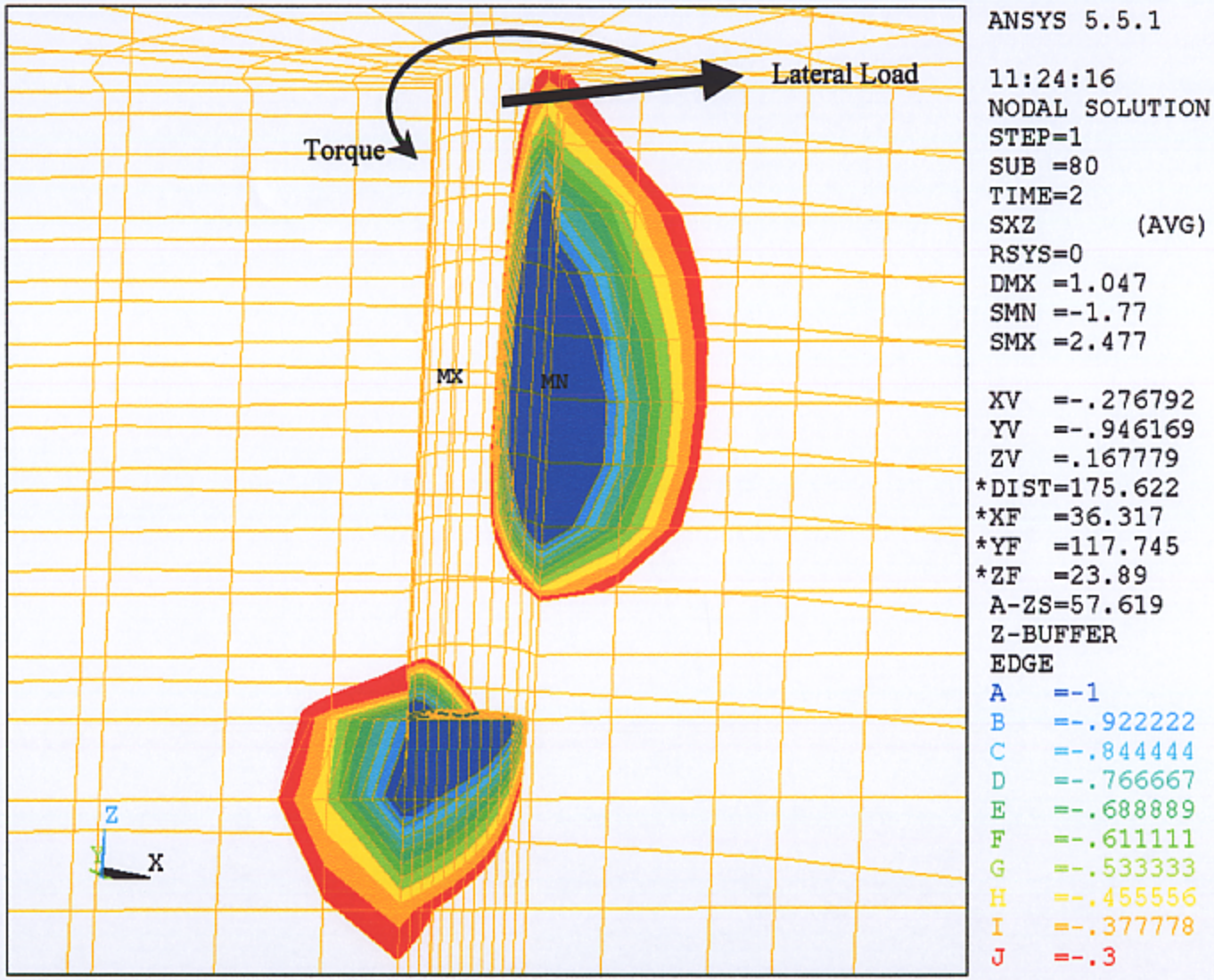

Figure 3.6 Shear Stresses Along A Drilled Shaft Subjected to Combined Loading Conditions

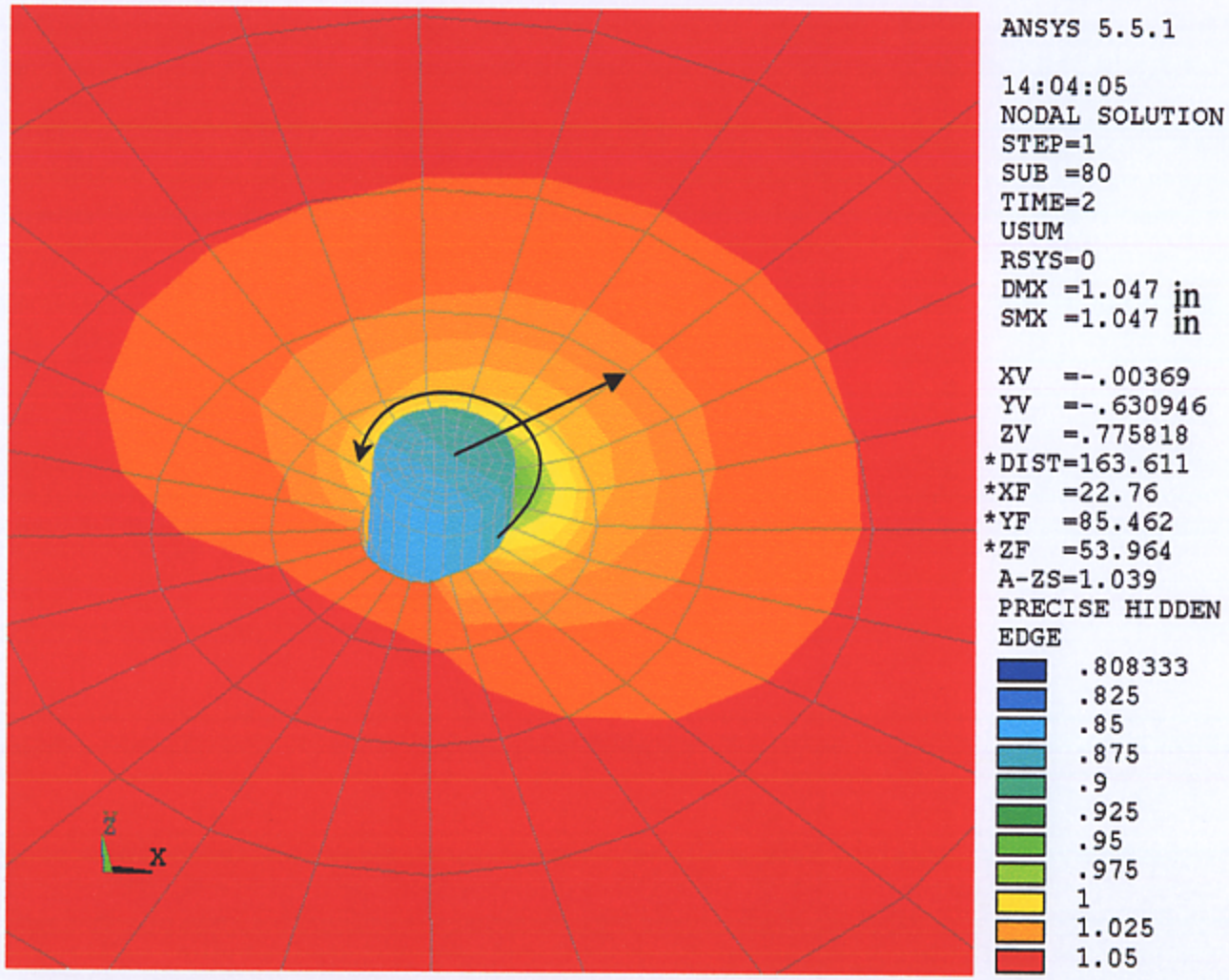

Figure 3.7 Lateral and Tensional Deformation at the Head of a Drilled Shaft Subjected to Combined Loading Conditions

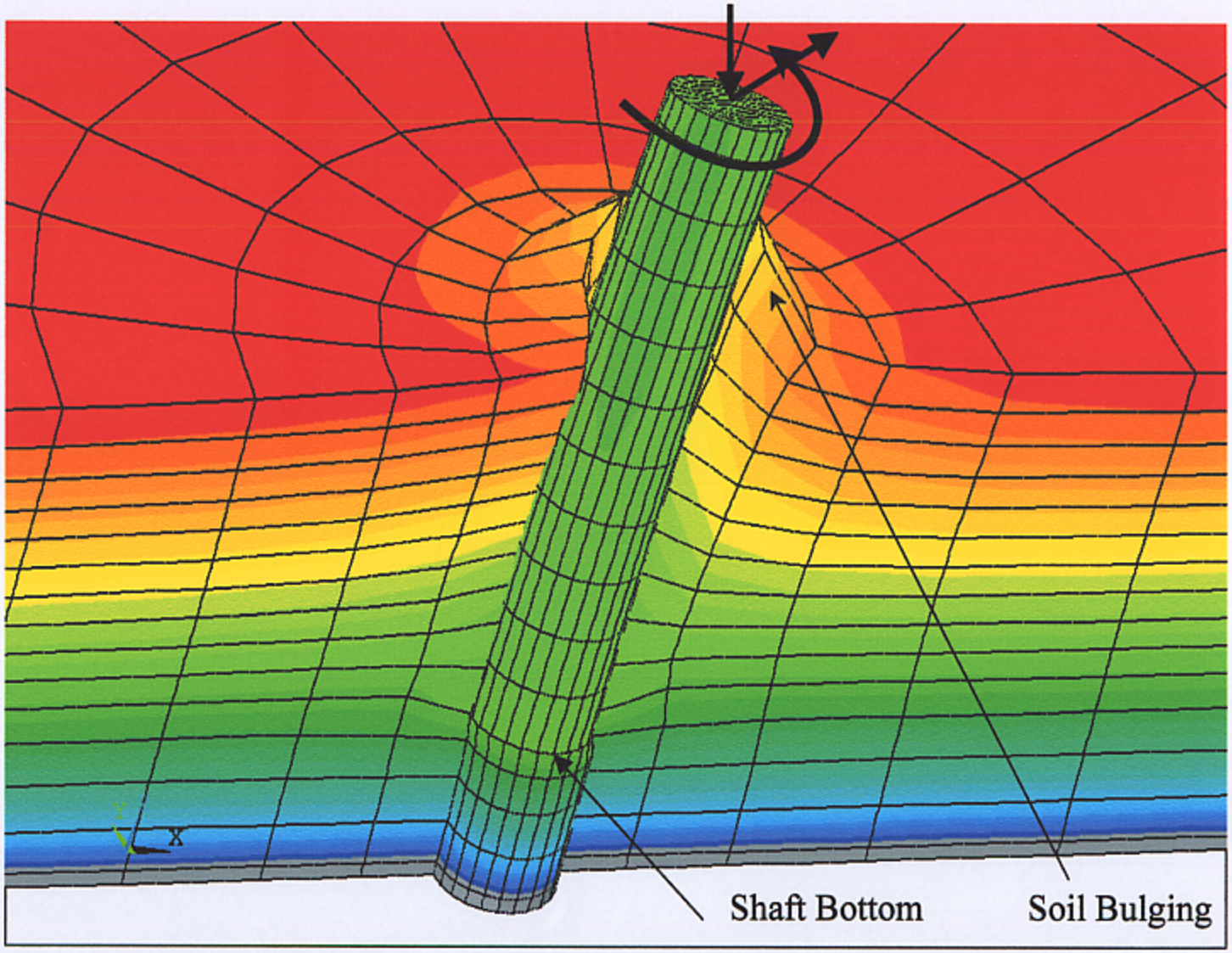

Figure 3.8 Lateral and Tensional Deformation at the Head of a Drilled Shaft Subjected to Combined Loading Conditions; Magnified x 500.

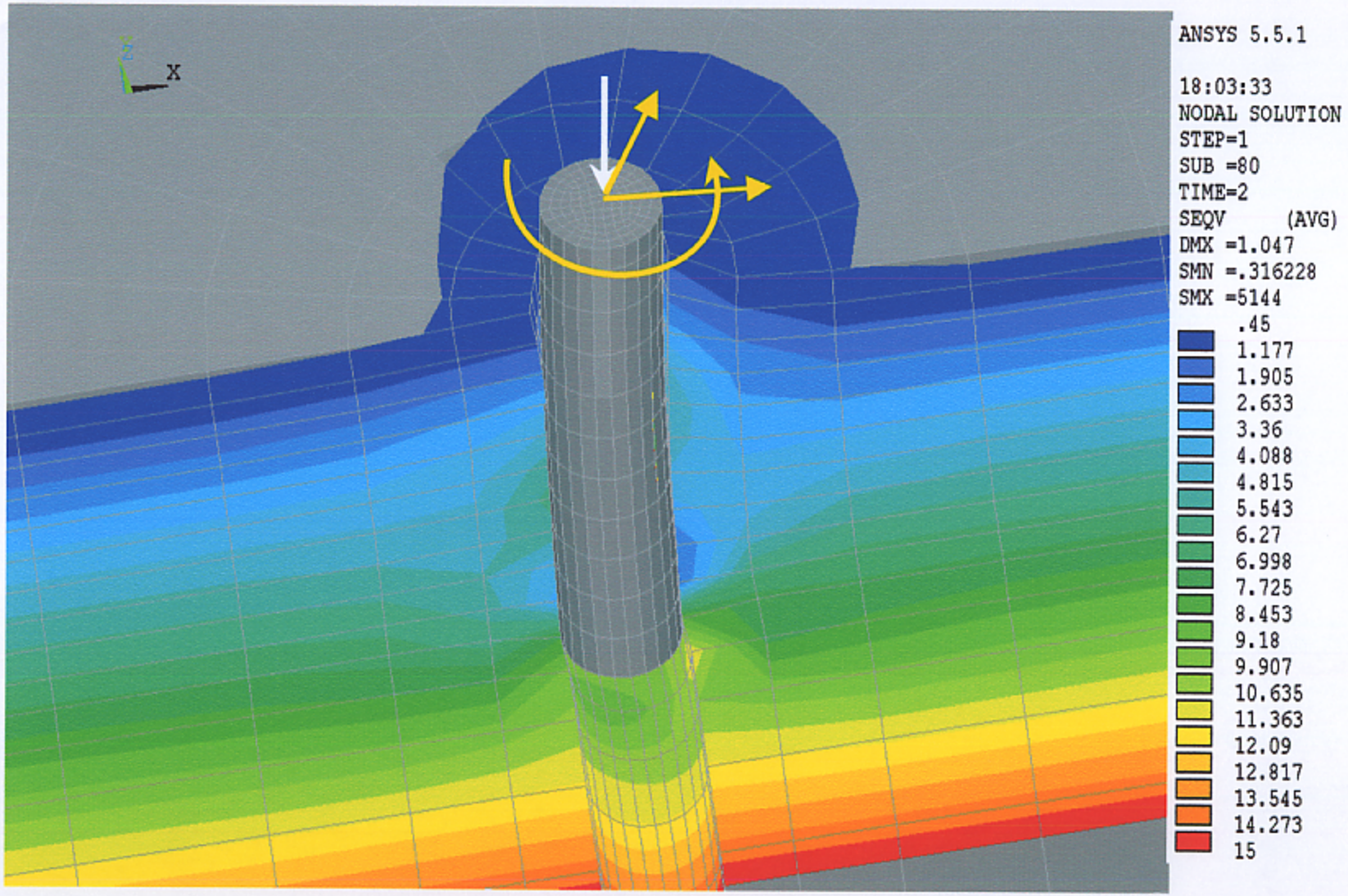

Figure 3.9 Soil Stresses Along a Drilled Shaft Subjected to Combined Loading Conditions; Magnified X200.

CHAPTER 4

RESULTS AND DISCUSSION

4.1 Introduction

Results obtained from this study were categorized into groups where each group was analyzed separately and then related to the others. An example for such categorization was the direct shear test results which were analyzed and compared with those obtained from the laboratory scaled model testing. Also, the one dimensional slurry penetration tests were compared with penetration from the scaled models. The direct shear test results were used to input the required frictional parameters for the Druker - Prager yield criterion in the finite element analysis. Also, it was possible to predict the fluid loss from the field tests using the method obtained from the one dimensional penetration tests. From the laboratory tests and the full scale field tests results along with the finite element analysis it was possible to develop a closed form solution method from which the ultimate capacity of the drilled shaft could be estimated.

4.1 Penetration Test Results

As it was described in chapter 2 the slurry penetration tests were performed using a non-standardized testing setup. A special setup was devised in the laboratory to determine the amount of penetration of both mineral and polymer slurries under various hydrostatic pressures. Increasing the pressure on the slurry corresponded the increase in the depth of the slurry in the borehole. Also, the device can measure and record the buildup of the filter cake at different slurry concentrations

and pressures. Using this testing setup it was possible to obtain soil samples to determine the effect of slurry penetration of the frictional resistance of the soil and the soil-shaft interaction.

Although the build up of the mineral composition along the walls of a shaft boring reduces the fluid loss with time, it was found that soil samples obtained from underneath a thick filter cake exhibited lower frictional resistance than those obtained from thin filter cakes. So the advantage of minimizing the filter cake may be offset by the reduction of the frictional resistance. On the other hand, polymer slurries did not possess such behavior. However, it was found that increasing the polymer slurry concentrations would certainly reduce the fluid loss. Also, polymer slurries if not fully mixed, gelatin formations may develop and cling to the borings walls which are just as unfavorable to frictional capacities as are the filter cake formations. A field test on a full scale shaft demonstrated such phenomena. Because of this concern, it is necessary to subject the drilled shaft borehole filled with polymer slurry to the same treatment of the mineral slurry and this is by shaving the shaft wall and removing any slurry accumulation along the borehole depth. Removing the penetrated slurry from the surrounding soil may not be feasible, but reducing the amount of penetration could be attained. Therefore to maximize the efficiency of the slurry, three features have to be considered simultaneously. The characteristics of an acceptable slurry are listed in Table 4.1.

Table 4.1 Required Features for Slurry Application in Drilled Shaft Construction

Slurry Characteristics	Mineral Slurry	Polymer Slurry
1- Viscous Fluid	a- To minimize fluid loss (High mineral concentration)	a- To minimize fluid loss (high polymer concentration)
2- High density Fluid	a- To produce large hydrostatic pressure on the side walls (High mineral concentration)	a- To produce large hydrostatic pressure on the side walls (High polymer concentration)

3- Replaceable Fluid	a- To minimize the filter cake buildup (low mineral concentration)	a- To speed pumping out the slurry from the borehole (low polymer concentration) b- To minimize gelatin formation and accumulation in the borehole (low polymer concentration)

It is obvious that for certain features slurry fluid should be with low mineral or polymer concentrations and for other features it is required to increase the concentrations. Such disparity can be minimized by using specifications shown in Table 4.2

Table 4.2 Slurry Specification for Construction in Fine Sands with Sodium Bentonite or Attapulgite (Florida Department of Transportation, 2000).

Item to be measured	Range of Results at 68 °F	Test Method
Density	64 to 73 lb/ft3 (in fresh water) 66 to 75 lb/ft3 (in salt water)	Mud density balance: FM 8-RP13B-1
Viscosity	28 to 40 seconds	Marsh Cone Method: FM 8 -RP13B -2
pH	8 to 11	Electric pH meter or pH indicator paper strips: FM 8-RP13B-4
Sand Content	4% or less	FM 8-RP 13B-3

One of the major properties that affect the behavior of both mineral and polymer slurries is the viscosity of the soil-water mix. The most common methods to determine the slurry viscosity is the Marsh funnel test. Although its simple and it has been approved by many state highway agencies as a mean of measuring the slurry viscosity, the Marsh funnel test has been the subject of disagreement between researchers and practitioners. For researchers, the Marsh funnel testing methodology is highly empirical. Results form the Marsh funnel test relate indirectly to the viscosity of the slurry in which the viscosity is measured as sec/quarter. Therefore, the Marsh Funnel

measurements indicate index values of the fluid viscosity in the sense that viscosity measurements can not be obtained at different parameters such as strain rate and or temperature. Shortcomings of this test are listed in literature. On the other hand, contractors still favor this approach for measuring slurry viscosity over other methods such as Fann viscometer because of its simplicity the field experience that was accumulated through years of practice.

To keep the balance between the demands of both sides, another technique was followed in this study where the slurry viscosity was measured by using the Zahn cup. The methodology of this test is similar to the March funnel except that the obtained measurements are recorded in terms of kinematic viscosity. The advantage of the Zahn cup method is that small samples were needed for testing which enable the study of the variation in the viscosity along the depth of a column of slurry. Results for this method correlated very well with those obtained from the Marsh funnel test. Therefore, it has been concluded that although the Fann viscometer provides better values for the plastic viscosity of the slurry, the simplicity and the practicality of the Marsh funnel or the Zahn cup tests should not be discarded. With caution and better correlations these tests can provide acceptable measurements for the slurry viscosity.

4.1.1 Mineral Slurry Penetration

Results from the slurry penetration tests signified the differences between mineral and polymer slurries in the mechanism of fluid infiltration in cohesionless soils. The particulate nature of mineral slurries is the major factor that make the differences between the two groups of slurries. Even for the same particulate slurries, there were some variations in the way of which Bentonite and Attapulgite slurries penetrate the soil and forming filter cakes.

In general it was found that the trends of slurry penetration were almost comparable. The rate of penetration (cm/sec) started very high and then after a certain period of time, the rate decreased to a constant steady state level. A typical mineral slurry penetration from the one dimensional flow test is shown in **Figure 4.1**. In this figure the Bentonite slurry was dyed with red color and the attapulgite was given a green color. In general it was found that the rate of penetration was higher for the Attapulgite than the Bentonite slurry and the rate of filter cake build up was higher in the Attapulgite than the Bentonite slurry.

Also it was found that thixotropy effect is more pronounced in bentonite than in attapulgite slurry. Thixotropy is a phenomenon in which a mineral slurry gains strength with time. Although it was not quantified in this investigation but its effect was noticeable in both bentonite and attapulgite slurries. Samples from attapulgite filter cake exhibited lower plasticity than those from the bentonite filter cake. Samples for attapulgite could not maintain their consistency upon removing them from the pressure chamber to the direct shear box **(Figure 4.2).** However, it has been noticed that, for the same concentration and immediately after slurry preparation, attapulgite slurry tends to agglomerate in a faster rate than the bentonite slurry which results in a slower flow through the Zahn cup indicating higher viscosity than bentonite slurry. The same phenomena was noticed in the penetration test with the scaled borehole **(Figure 4.3)**.

In the mineral slurries, the amount of penetration of the bentonite slurry was in general less than the attapulgite. For example, at concentration rate of 0.5 ppg the rate of penetration in the attapulgite slurry was 20% more than the bentonite **(Figure 4.4)**. Also differences in the rates of penetrations of 18% to 25% were recorded.

The formation of the filter cake in attapulgite slurry was more pronounced than in the case of bentonite slurry. That is because the filtration of the water in the slurry is faster in the attapulgite than in the bentonite slurry. It has been found that attapulgite clay has less tendency to hold the water in the slurry mix and this was the cause of the faster flow of water through the soil sample. In the case of bentonite slurry the formation of a thin layer of filter cake was sufficient to prevent the slurry from further filtration, where for the attapulgite the formation of the filter cake did not prevent the filtration of the water through the soil sample (**Figures 4.5 to 4.6 and Appendix A**). Similar results were reported by Larsen (1955). In his study, Larsen presented a detailed comparison in the yield and water loss between various types of clay minerals (**Table 4. 3**). For attapulgite clay the water loss was about 10 times higher than the bentonite slurry and filter cake permeability was about 30 higher.

Table 4.3 Properties of Different Clay Minerals (Larsen 1955)

Clay Mineral	Yield, bbl 15 cP mud/ton (fresh water)	Solids in filter cake, (% by weight)	API water loss at 15 cP	Filter cake Permeability, microdarcies	pH
Hectorite, CA	160	6.5	7	0.85	8.6
Na-Mont, WY	125	10	11	1.8	8.2
Ca-Mont, CA	71	16	15	2.1	8.7
Ca-Mont, TX	18	50	11	1.5	7.5
Illite, IL	13	67	57	38	7.4
Kaolinite, GA	14	70	190	285	7
Attapulgite, GA	105	23	105	68	7.1
Hallosite, CA	17	60	35	15	7.7

The results presented above were supported by the scaled borehole tests. These tests were conducted

in the laboratory to visually observe the pattern of slurry penetration and to simulate the field conditions. In this regard, it should be noted, that the similarity between the laboratory and the field conditions in the scaled borehole tests may not be close enough to draw a conclusion. Some variations between the laboratory and field conditions did exist, among them are (1) scaling effect including particle sizes and body forces, (2) boundary conditions effect, and (3) the degree of saturation and capillary effect on the rate of slurry penetration and filter cake formation. Despite these variations, the scaled borehole tests portrayed the mechanisms of the slurry penetration and the filter cake formation.

For lower dosages of bentonite and attapulgite (0.1 to 0.3 ppg) the differences in the penetration rate were significant compared to higher dosages. In the attapulgite slurry, the filter cake was formed and the water continued to filter through the soil, where for bentonite, no filter cake was formed and the slurry fully penetrated the soil. Unlike the bentonite slurries mixes, the attapulgite slurries never failed to develop a filter cake. The average filter cake formation for the attapulgite slurry was approximately 3/4 in. thick. However, even with this thickness, the attapulgite slurry penetration into the soil persisted. This slurry behavior may not be favored if the formation of the filter cake could not cease the fluid loss. However the advantage of the attapulgite slurry appeared latter when the shearing behavior of the affected soil was investigated. Additionally, the formation of thick layers of filter cake in attapulgite slurry indicated less penetration of the clay particles inside the soil voids leaving only the water in the slurry to saturate the surrounding soil. Also, because of the thixotropy effect, it was more difficult to shave the side walls from the bentonite buildup in the scaled model tests.

3	5	0.636	14.54	0.331	0.812	0.669	1.4
4	8	0.634	14.35	0.465	0.941	0.63	1.8
5	8	0.654	14.35	0.454	0.933	0.669	1.2
6	8	0.637	14.35	0.422	0.981	0.551	1.8
7	10	0.641	18.16	0.503	0.994	0.709	1.98
8	10	0.639	18.16	0.535	0.814	0.866	1.48
9	10	0.653	18.16	0.498	0.965	0.669	1.98
Average				**0.44**		**0.68**	**1.61**

Bentonite Test Results

Test #	Pressure (psi)	Void Ratio	Slurry Concentration (#g Water/g Clay)	Penetration Rate (in/sec)	R-squared	Filter Cake Thickness (in)	Shear Strength (psi)
1	5	0.636	14.54	0.289	0.879	0.08	1.01
2	5	0.648	14.54	0.268	0.963	0.039	1.2
3	5	0.64	14.54	0.216	0.936	0.08	1
4	8	0.634	14.35	0.322	0.883	0.04	1.1
5	8	0.629	14.35	0.34	0.96	0.04	1
6	8	0.619	14.35	0.315	0.944	0.08	1.3
7	8	0.621	14.35	0.42	0.945	0.04	1.08
8	8	0.628	14.35	0.356	0.906	0.04	1.28
9	8	0.619	14.35	0.334	0.946	0	1.56
10	10	0.639	18.16	0.595	0.927	0.04	1.5
11	10	0.638	18.16	0.41	0.923	0.04	1.63
12	10	0.632	18.16	0.329	0.985	0.04	1.8
Average				**0.35**		**0.05**	**1.29**

An attempt was made to fit the slurry penetration results in a relationship that can describe the magnitude of penetration vs. time. Accordingly, it was found that this relationship can best be depicted by using the following equation **(Figures 4.8 and Appendix A)**:

$$Y = \alpha T^{\beta} \tag{4.1}$$

Where

Y = slurry penetration (in.)

α and β = factors depend on slurry type and magnitude of hydrostatic pressure (psi)

T = time in sec.

Tables 4.5 and 4.6 present values for the α and β factor that were obtained from the data analysis

of the laboratory test results.

Table 4.5 Values of α and β for Attapulgite Slurry

Pressure (psi)												
Parameters	5	5	5	8	8	8	10	10	10			
α	0.020	0.010	0.004	0.031	0.021	0.037	0.048	0.022	0.033			
β	0.583	0.640	0.699	0.533	0.566	0.513	0.469	0.625	0.546			

Table 4.6 Values of α and β for Bentonite Slurry

Pressure (psi)												
Parameters	5	5	5	8	8	8	10	10	10	8	8	8
α	0.01030	0.032	0.033	0.202	0.054	0.039	0.018	0.175	0.085	0.083	0.068	0.162
β	0.68461	0.511	0.501	0.176	0.325	0.468	0.749	0.163	0.335	0.217	0.348	0.139

4.1.2 Polymer Slurry Penetration

For polymer slurries, the PHPA exhibited more tendency to penetrate the sand at concentration levels higher than 0.02 ppg **(Figures 4.9 to 4.10, Appendix A)** than KB SlurryPro. At concentrations less than 0.01 ppg, the two polymer slurries showed the same behavior in the rate of penetration. The variation in the penetration rate between the two slurries was not expected. However, such behavior could be resulted due the method of preparation for both slurries. During the preparation of the KB SlurryPro (Powder form) it was noticed that large gelatin clumps could easily be formed if the slurry was not properly mixed. As the dry granular polymer material begins to absorb water, the clumps swelled and increased in size. Accordingly, the rate of penetration slightly varied between the two slurries.

In general, such variation may not be significant to draw differences in penetration behavior of the two polymer slurries.

The type of SuperMud polymer used for the penetration testing was of the partially hydrolized polymer material. This type did not cause any gelatin clumping in the slurry during preparation and,

hence, the rate pf penetration was slightly higher than the KB slurry. If properly prepared the penetration of the two slurries would depend on the soil void ratio (e), slurry viscosity (μ), and the hydrostatic pressure (σ_0). In most cases the SuperMud slurry fully penetrated through the test mediums, but in tests showed only partial penetration. Generally, it was found that the penetration rate was greatly influenced by the viscosity vales (μ). Tabulated results of the polymer slurry penetration tests are given in Table 4.7.

Table 4.7 Penetration of Ploymer Slurries

KB SlurryPro Test Results

Test #	Pressure (psi)	Void Ratio	Slurry Concentration (# g polymer/1L of water)	Penetration Rate (in/sec)	R-squared	Shear Strength t (psi)
1	5	0.628	1	0.412	0.947	1.65
2	5	0.624	1.5	0.338	0.939	1.95
3	5	0.64	2	0.257	0.964	2
4	8	0.629	1	0.435	0.944	1.9
5	8	0.627	1.5	0.347	0.811	2.1
6	8	0.62	2	0.283	0.844	2.24
7	10	0.61	1	0.478	0.951	1.7
8	10	0.614	1.5	0.369	0.955	1.89
9	10	0.61	2	0.342	0.959	2.22

SuperMud Test Results

Test #	Pressure (psi)	Void Ratio	Slurry Concentration (# mL water/mL polymer)	Penetration Rate (in/sec)	R-squared	Shear Strength τ (psi)
1	5	0.676	200	0.119	0.798	2.2
2	5	0.698	400	0.156	0.891	1.8
3	5	0.671	800	0.192	0.882	1.8
4	8	0.699	200	0.183	0.909	2.01
5	8	0.695	400	0.193	0.548	1.64
6	8	0.67	800	0.282	0.724	1.64
7	10	0.654	200	0.178	0.736	1.8
8	12	0.648	200	0.221	0.965	1.92
9	12	0.643	400	0.389	0.913	1.8
10	12	0.637	800	0.532	0.994	1.72

4.2 Direct Shear Test Results:

Several undisturbed samples were obtained from the soil layer underneath the filter cake. A mold that has a sharp edge and the same dimensions as of the direct shear box was used to extract these samples. The extraction process was done immediately before starting the direct shear test. A set of tests was conducted on dry sand sample. Results from this set were used as a control data to compare with samples affect by the slurry penetration.

For the purpose of this study, the direct shear test was modified to test frictional behavior of the soil-concrete interface. **Figures 4.11 to 18** presents the results of this part of the direct shear tests.

Also, similar tests were conducted on soil samples using the conventional direct shear test to determine the angle of internal friction of the dry slurry inundate soil. **Figures 4.14** shows the variation in the frictional angles for soil samples obtained from the slurry penetration device and those tested under the dry condition. The drop in the friction resistance was dramatic for samples penetrated with mineral slurries. Polymer slurry samples exhibited larger friction resistance. However, slurry concentration was the main factor behind the reduction in the angle of friction of the soil. The higher the polymer concentration the lower the frictional resistance.

4.3 Torsional Test on Scaled Model Shafts

To have a better understanding of the torsional resistance of drilled shaft under combined loads, it was decided to conduct a series of tests on a scaled model shaft. As it was described in **Chapter 2**, these tests necessitated the development of a testing setup that could accommodate various combinations of loads. Using this setup, it was possible to apply simple torsional loads on a scaled

model shaft (1' = 1") as well as vertical, and horizontal loads. In the analysis and design of torsional resistance of drilled shafts, the FDOT methods assume simple torsional loads on the shafts. The effect of adding vertical and lateral loads on the torsional capacity could be inferred by using the device developed in this study.

When conducting the torsional test using the developed setup it was possible to separate the side friction from the base friction. One set of tests were conducted where the side friction was eliminated. This was done by enlarging the borehole so that the shaft surface was separated from surrounding soil. For this type of testing only the simple torque was applied.

To eliminate the base friction, two circular plates with diameter equal to shaft diameter were placed a the bottom of the shaft. The two plated were lubricated to minimize the friction between them. This arrangement made the torsional resistance to be at the sides only. As for the base friction test, the shaft was subjected to simple torque.

The torsional tests were performed on dry and saturated cohesionless soil. Mineral and polymer slurries were also used in testing the torsional capacity. The following sections present y the results of the scaled model torsional tests.

As can be seen from **Figure 4.19 and Appendix A,** the torsional resistance of the scaled model was the highest for the dry soil condition. When the mineral slurries were used it was found that the rotation resistance was dropped by about 65 to 50 percent for the bentonite and attapulgite slurries, respectively. The polymer slurries exhibited 20 to 30 percent reduction in the torsional resistance.

These limited laboratory test results conformed with those obtained from the conventional direct shear tests.

The large reduction in the frictional resistance for the mineral slurries was due to the filter cake development around the borehole. Even when this layer was removed before testing, the presence of mineral slurries in the adjacent soil may have contributed to the weak interaction between the soil-shaft material and soil-soil friction.

Cleaning the boreholes from polymer slurries was much easier as compared with the mineral slurries. This was because of the very thin film of polymer slurry that adhered to the side walls and the timeless efforts spent to trim it.

In the dry soil, an additional tests were conducted to determine the residual frictional resistance that remained in the shaft after completing the torsional testing. The shaft was rotated back to its original position and another round of torsional loads were applied. In this situation the soil stresses have been relieved and accordingly the frictional capacity was reduced by 70 to 77%.

For tests conducted on based on the side resistance only, the reductions obtained in the torsional capacities were similar to those obtained from the full resistance (side and base). The base resistance tests showed a very small contribution for the shaft base on the over whole capacity of the shaft **(Figure 4.20)**.

4.4 Combined Loading Conditions

The torsional tests on scaled drilled model were repeated with the addition of lateral loads. Adding 20 lb lateral load on the shaft increased the torsional capacity by about two folds. When the lateral load was increased to 80 lb the torsional resistance was increased by 2.2 times. This was an indication that increasing the lateral load may not necessary improve the capacity. However, the addition of 20 lb lateral load was enough to develop the maximum capacity in the shaft and increasing this lateral load by 4 time increased the torsional capacity by 20% only **(Figures 4.21 to 25 and Appendix A).**

4.5 Full Scale Field Tests

Three full scale field tests were conducted on 4 ft diameter x 20 ft depth drilled shafts. The arrangement of the field tests were described in detail in chapter 2. The full scale shafts were subjected to torsional as well as lateral loads. The load application was done through a 10 ft steel arm. Measurements of strain values inside the shaft and rotational displacements were recorded along with the load increase **(Figures 26 to 33).**

The first field test was performed on the dry shaft. This test designation came because of the method of construction of the shaft where no slurries were used to stabilized the borehole. The other two boreholes were stabilized with mineral and polymers slurries.

The dry shaft demonstrated the largest capacity among the other shafts. The shaft was gradually loaded up to failure. It was not possible to induce a significant rotation in this shaft. The resistance to the applied torsional loads was so high that the structure of the shaft experienced the failure.

Upon continuous loading, it was noticed that at 490,000 ft-lb torsional load, a large structural crack was suddenly developed followed by a drastic drop in the reading of the load cell. Before that there was no appreciable rotational movement for the shaft. The largest rotation was recorded for the steel arm, but this was because of the cantilever action deflection. The maximum load recorded (490,000 ft-lb) was assigned as the ultimate capacity of the dry shaft **(Figures 4.26 to 4.28)**.

For the shaft constructed using bentonite slurry, the rotational displacement was very noticeable. At torsional loads of 180,000 ft.lb. Additionally, the soil movement around the shaft head was distinguishable. The laser beams readings and the strain gages inside the shaft confirmed the rotation of the shaft. An excessive rotational displacements were recorded from the laser beams when the electronic strain gages did not indicate any large strains in the structure. The load application continued until no more increase in the loading could be recorded. At that stage, the shaft experienced a large rotational displacement at 280,000 ft.lb **(Figure 4.29)**.

The third shaft was constructed using polymer slurry. This shaft showed more resistance than the bentonite shaft. At 280,000 ft.lb the performance of the shaft was similar to the dry one. Considering that the dry shaft was structurally failed, it was decided to remove the soil around the shaft up to a depth of 5 ft below the ground surface. Releasing the 5ft of lateral pressure left the shaft with 15 ft embedment length. After removing the surrounding soil, the load application gradually increased until a noticeable crack was developed at the shaft head indicating a structural failure. The laser beam movements did not show any large rotational displacements as for the bentonite shaft. The maximum load reached during this test was 420,000 ft.lb **(Figure 4.30)**. This was about 70,000 ft.lb less that the dry shaft and about 140,000 ft.lb more than the bentonite shaft.

These tests indicated that the method of construction did make the difference in the torsional capacity, especially when all the three shafts were constructed at the same time and at the same place. Accordingly, it can be conclude that the dry shaft produced the largest capacity followed by the shaft constructed using polymer slurry and lowest capacity was for the bentonite method. After eight months from construction it was noticed that the filter cake from the bentonite slurry still existed around the shaft. Using a sharp toll it was possible to peel the filter cake even at depth of 6 ft below the ground. This observation indicated the effect of the filter cake formation of the side friction of the shaft. Similar observation was noticed in the polymer shaft. Some polymer accumulations were seen of the shaft after eight month for the end of construction.

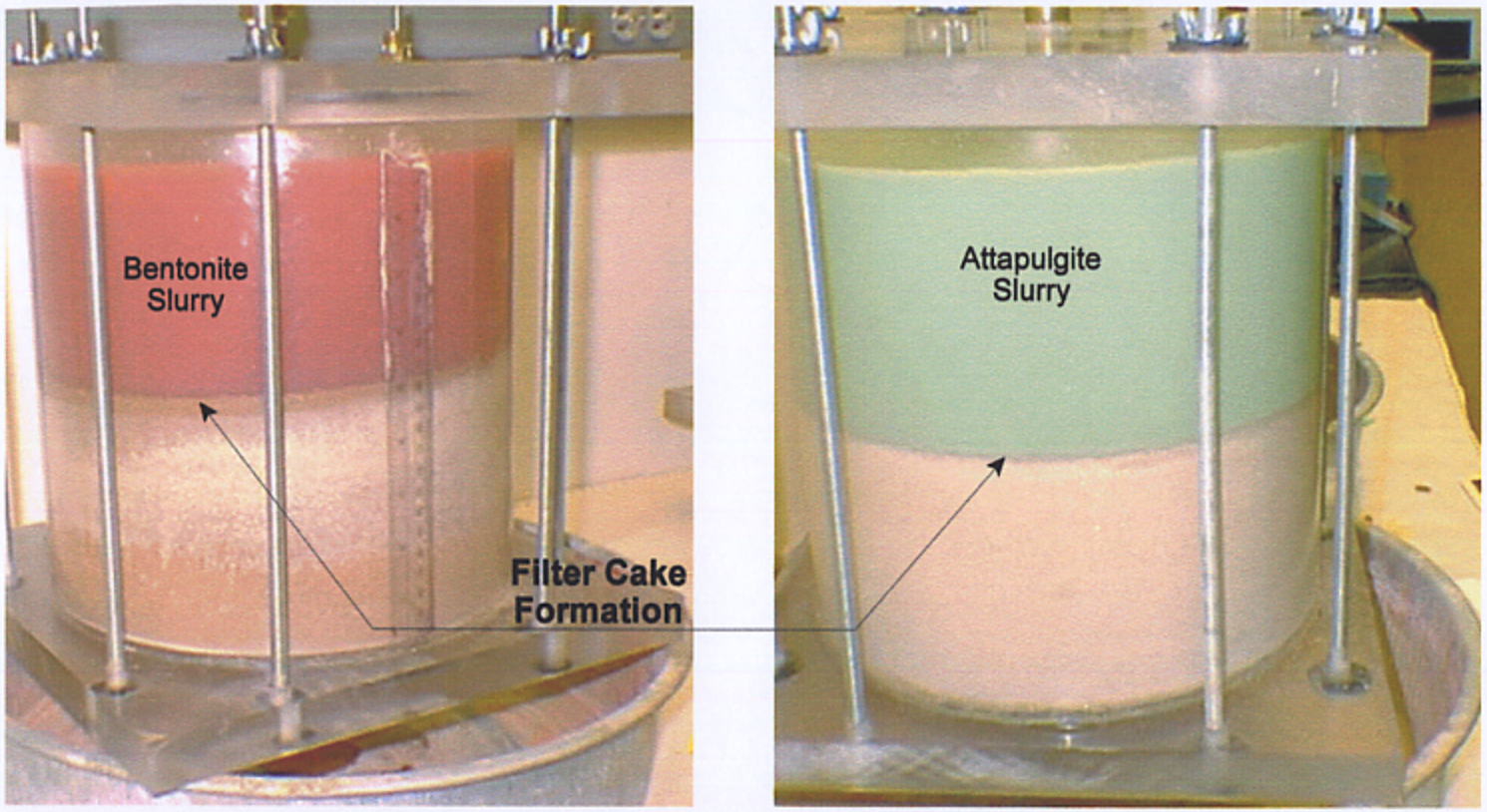

Figure 4.1 Fluid Loss in Bentonite and Attapulgite Slurries at the Same Concentration and Hydrostatic Pressure

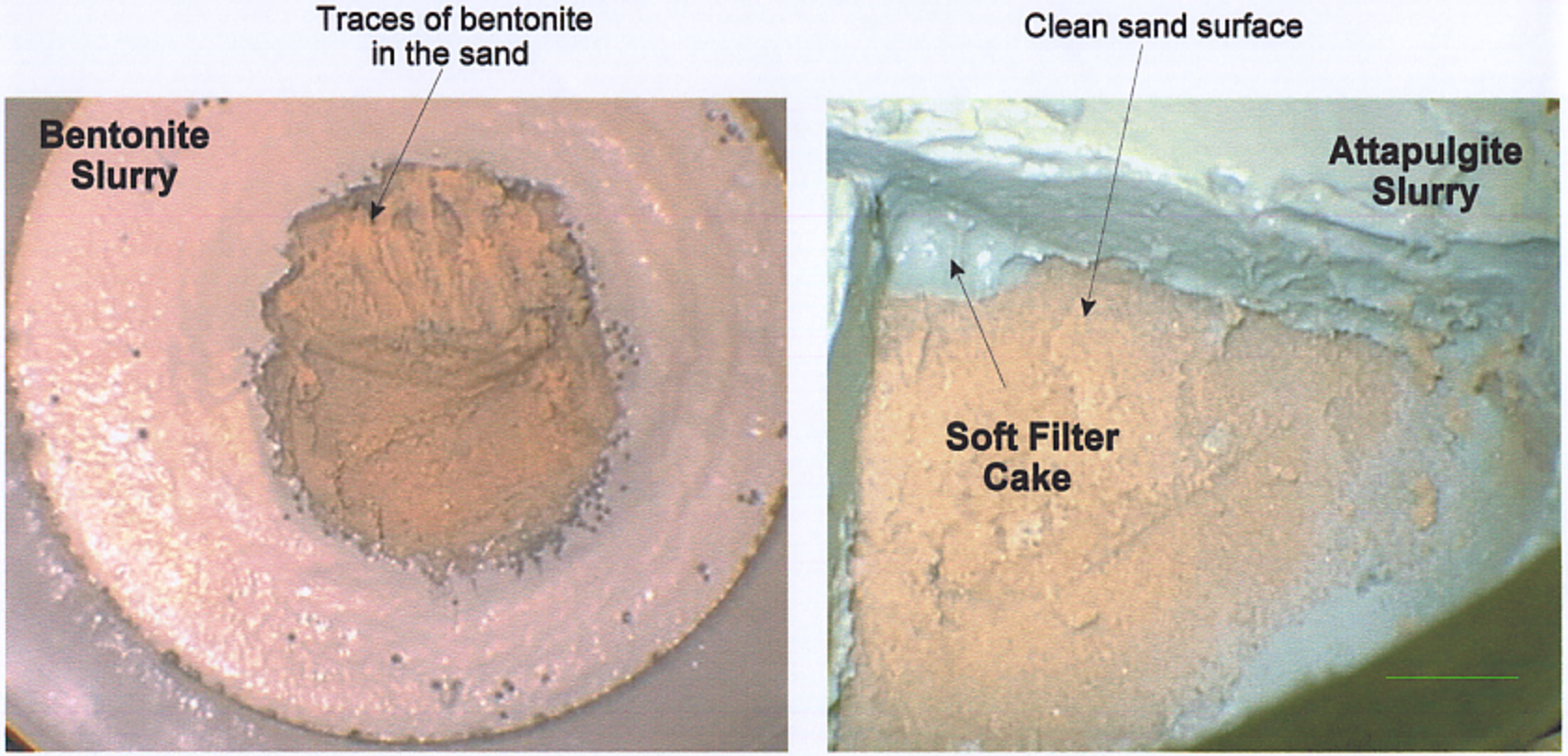

Figure 4.2 Filter Cake Formation in the One Dimensional Flow Test

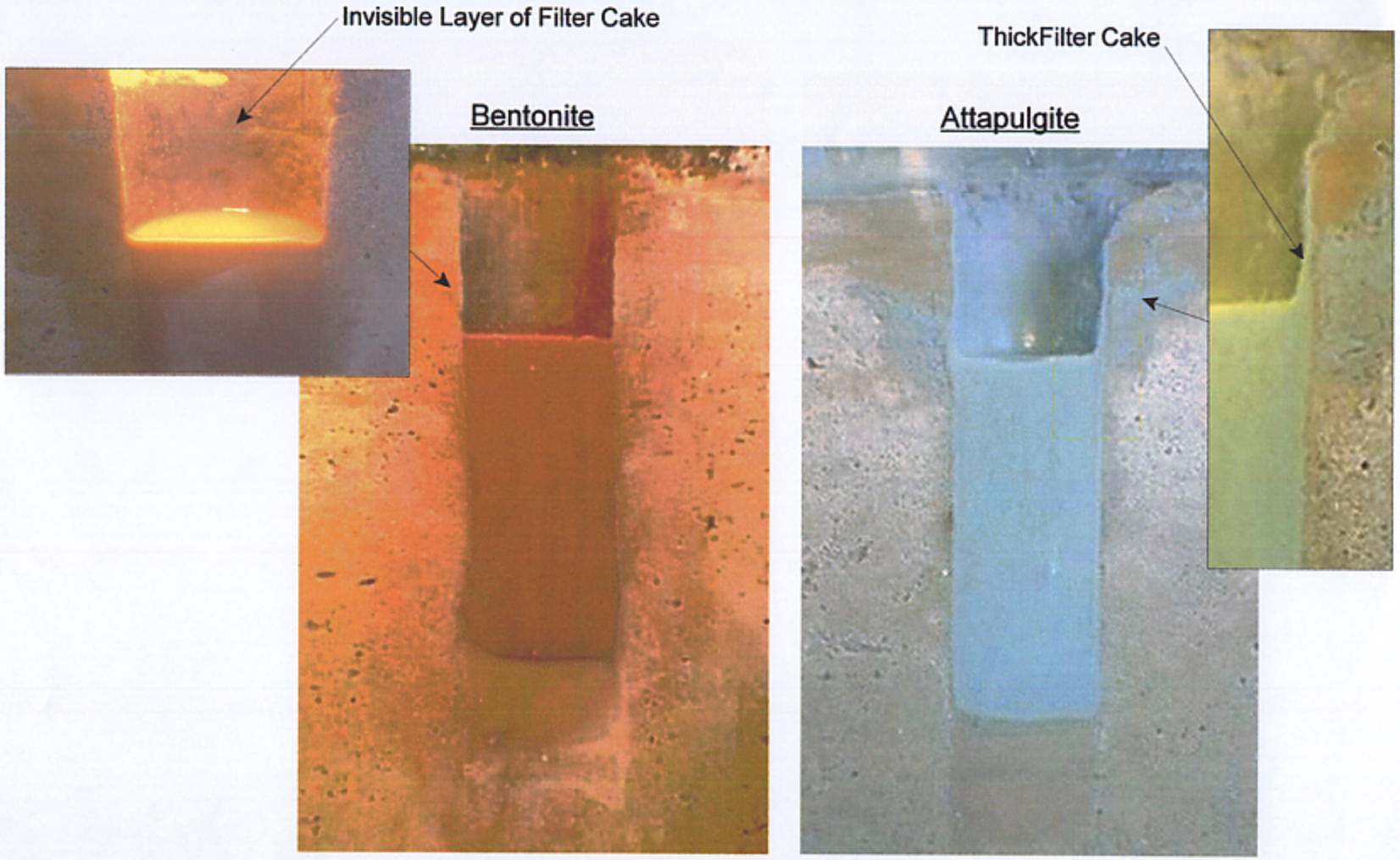

Figure 4.3 Build up of Filter Cake in the Borehole Tests

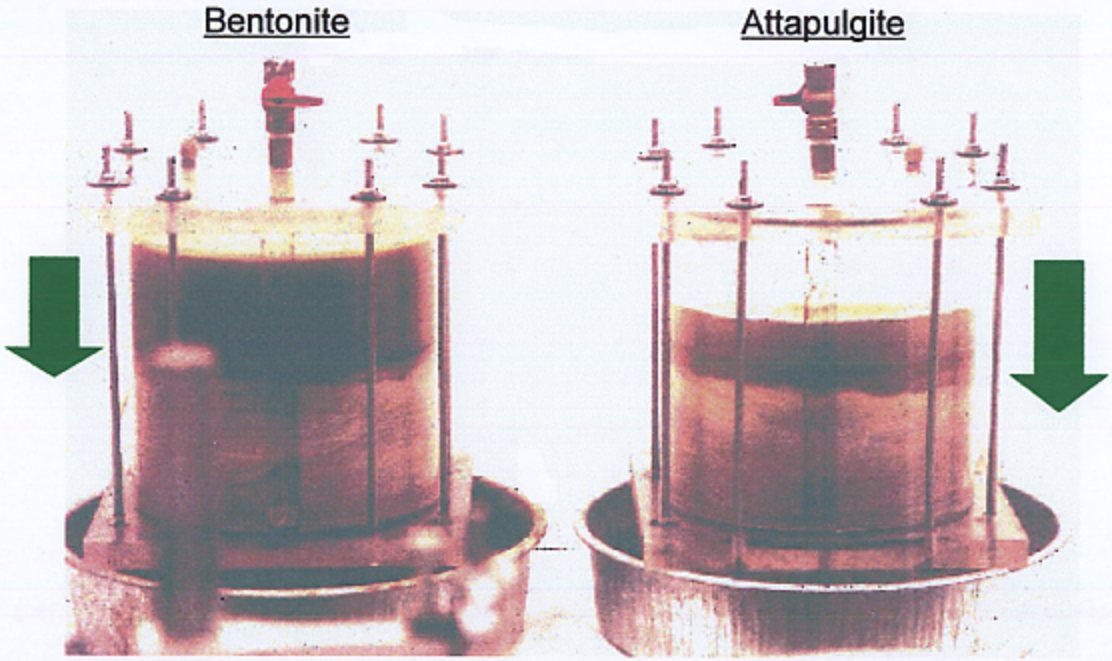

Figure 4.4 Rate of Penetration in Bentonite and Attapulgite Slurries at Concentration = 0.5ppg.

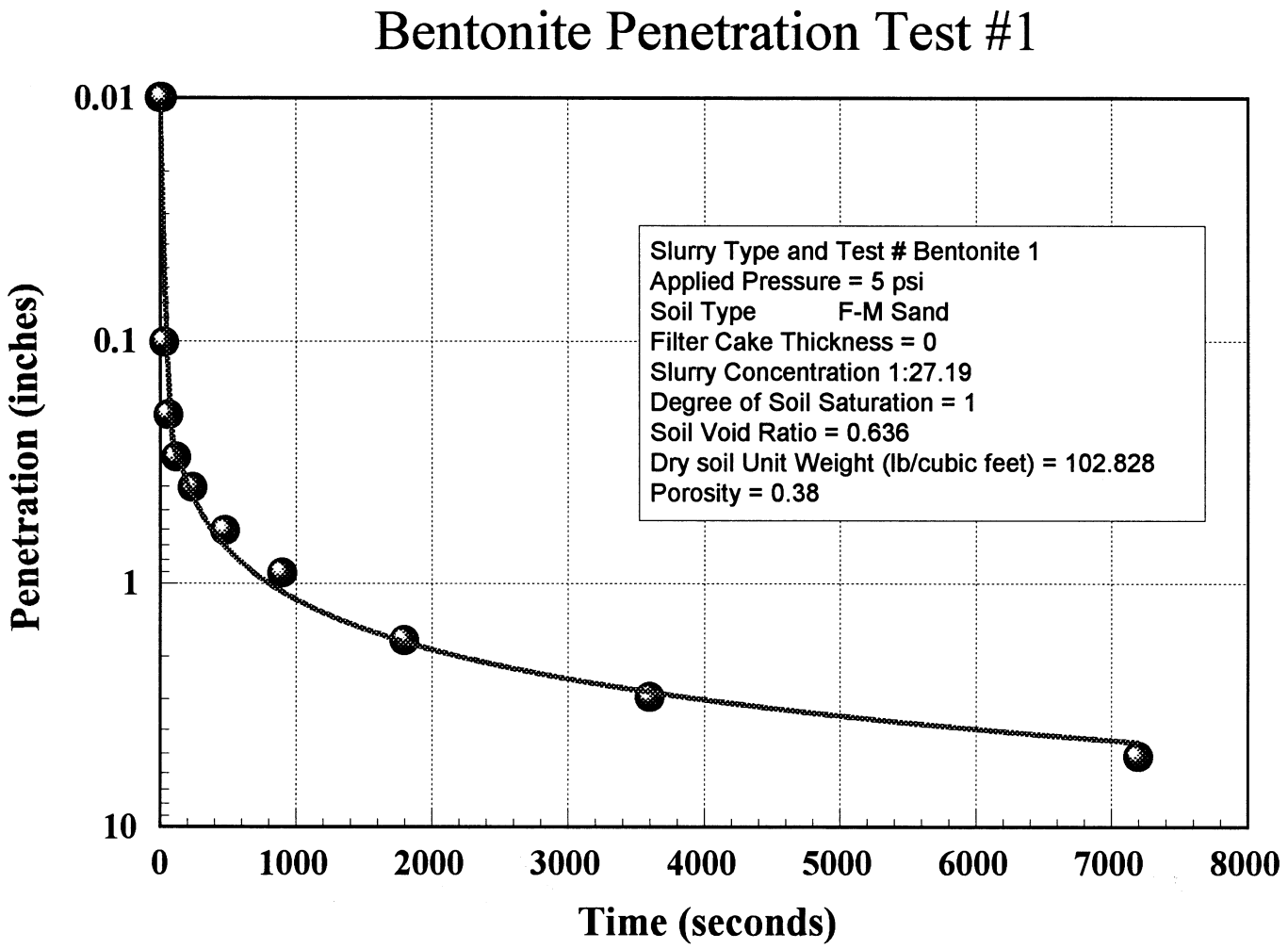

Figure 4.5 Bentonite Slurry Penetration in Sandy Soil Under Hydrostatic Pressure = 5 psi.

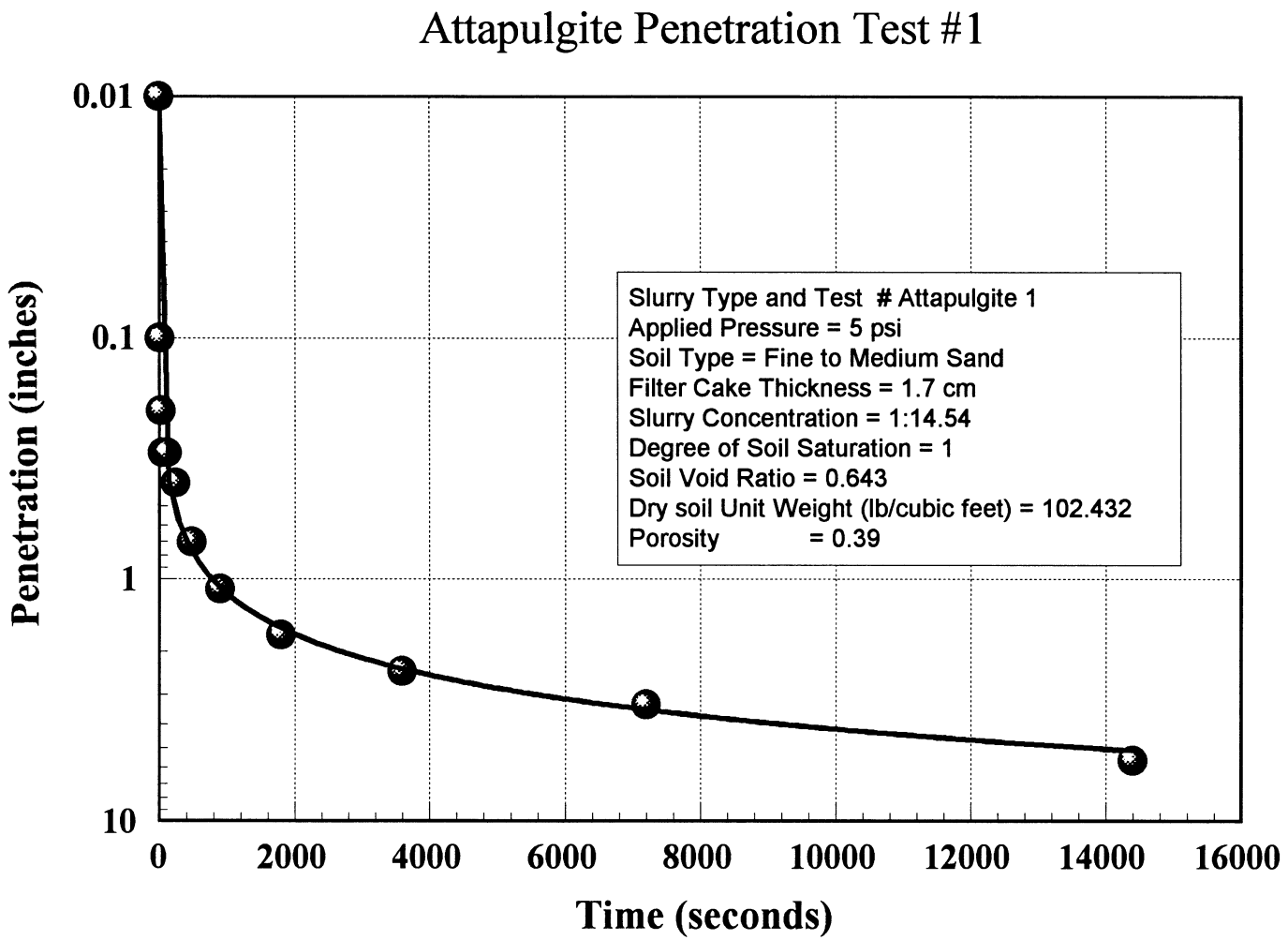

Figure 4.6 Attapulgite Slurry Penetration Under Hydrostatic Pressure = 5 psi.

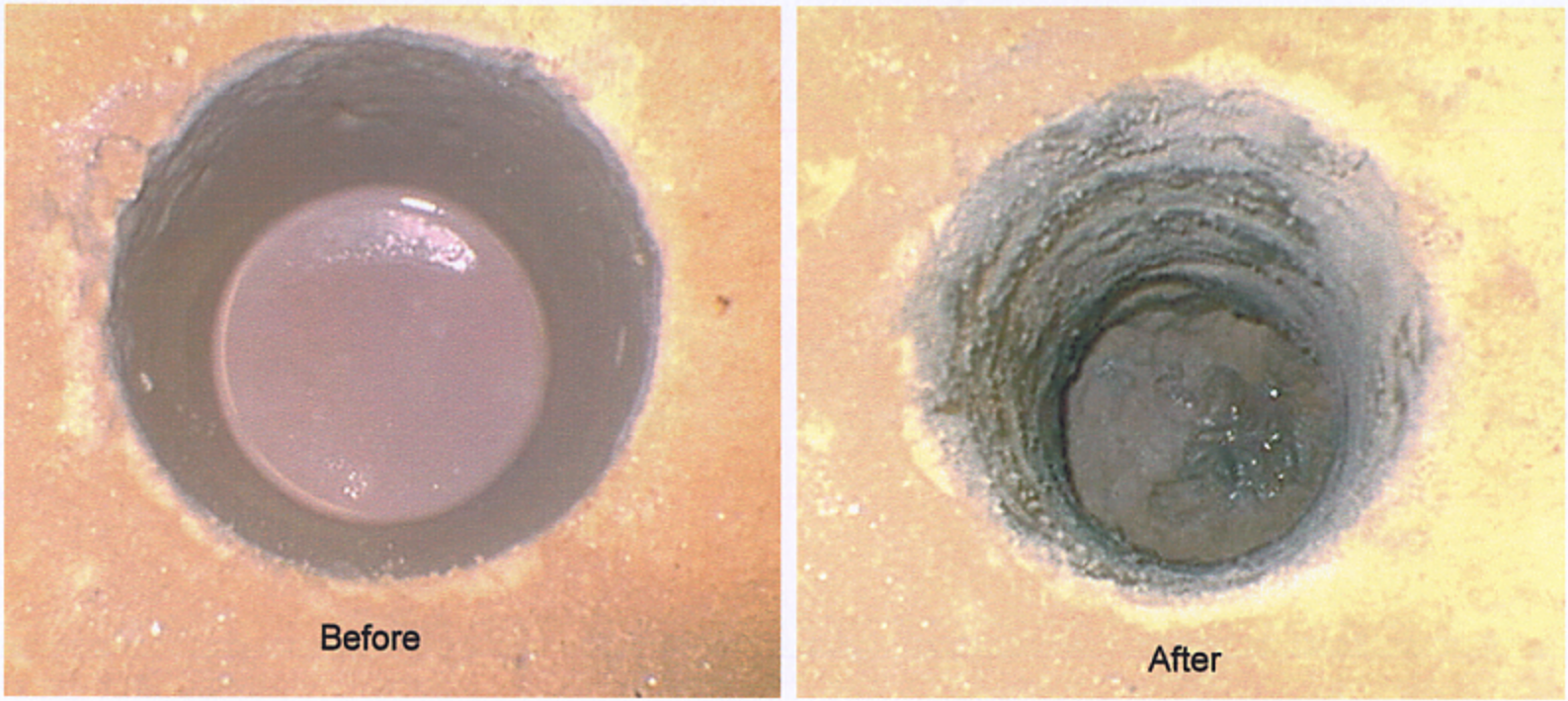

Figure 4.7 Bentonite Traces along the Borehole Side Walls Before and After Cleaning

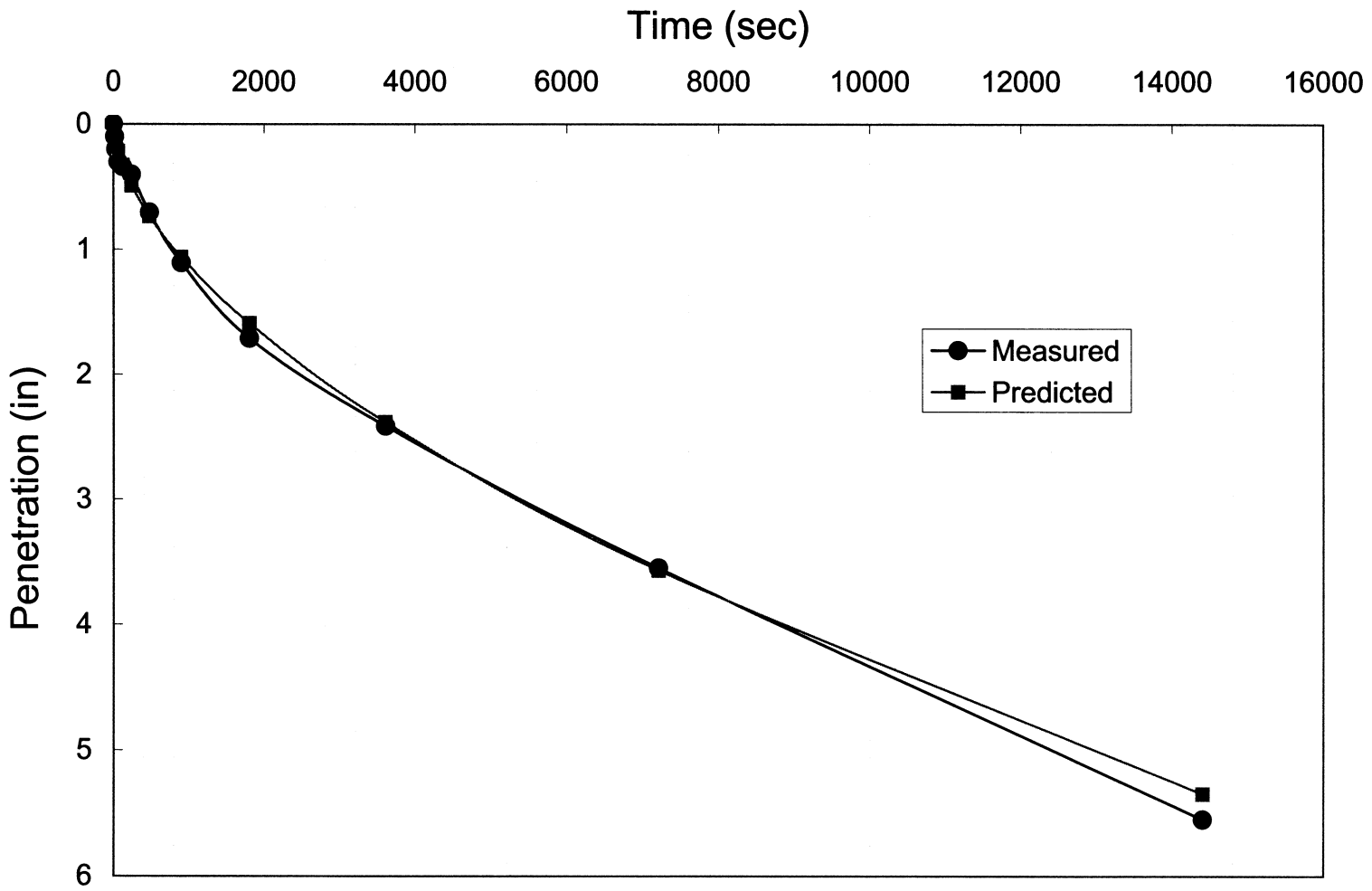

Figure 4.8 Attapulgite Slurry Penetration in Cohesionless Soil Under Pressure = 5 psi

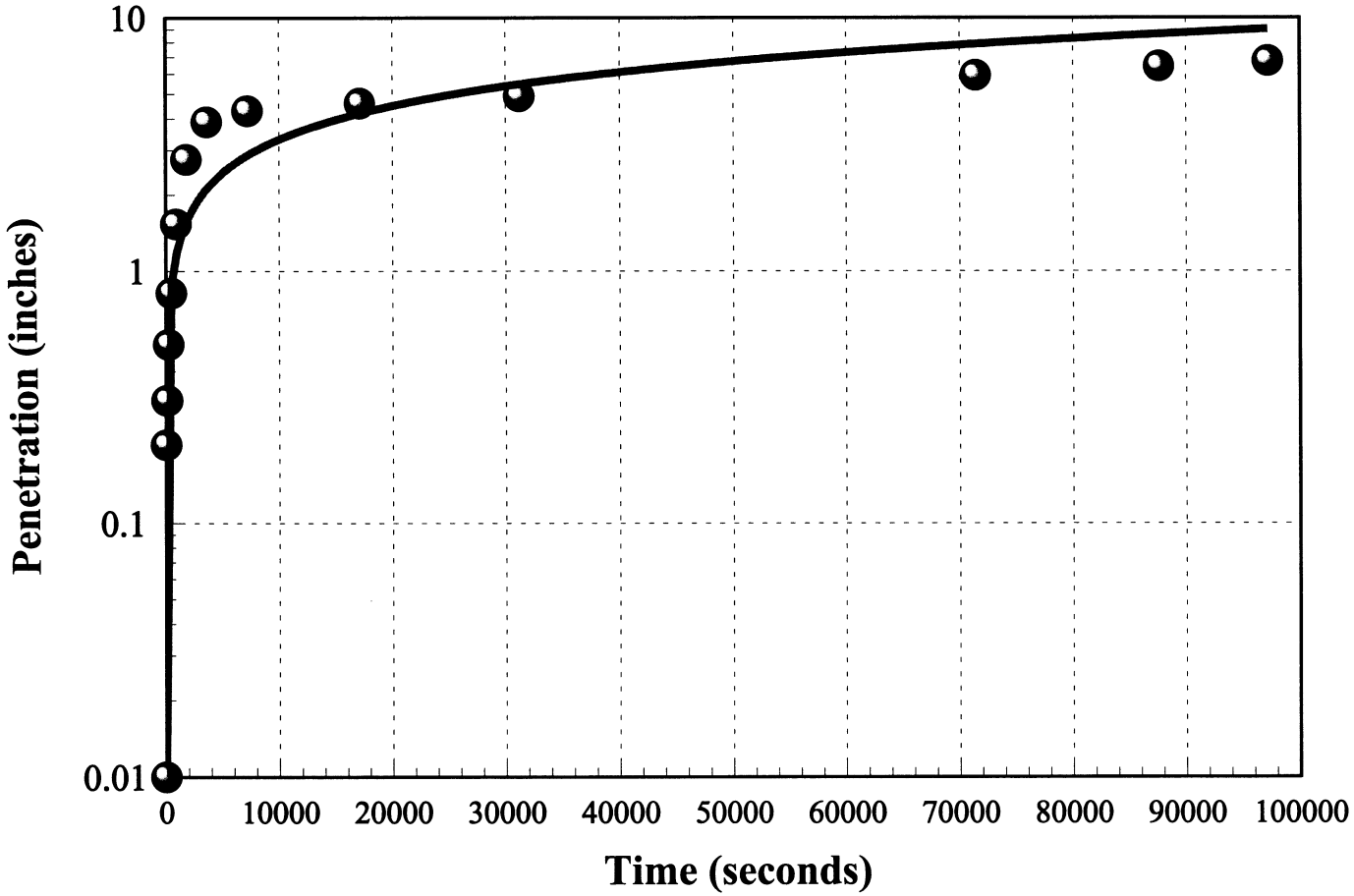

Figure 4.9 KB SlurryPro Penetration Test # 1at 5psi and Void Ratio 0.628, Polymer Concentration = 1g to 1L.

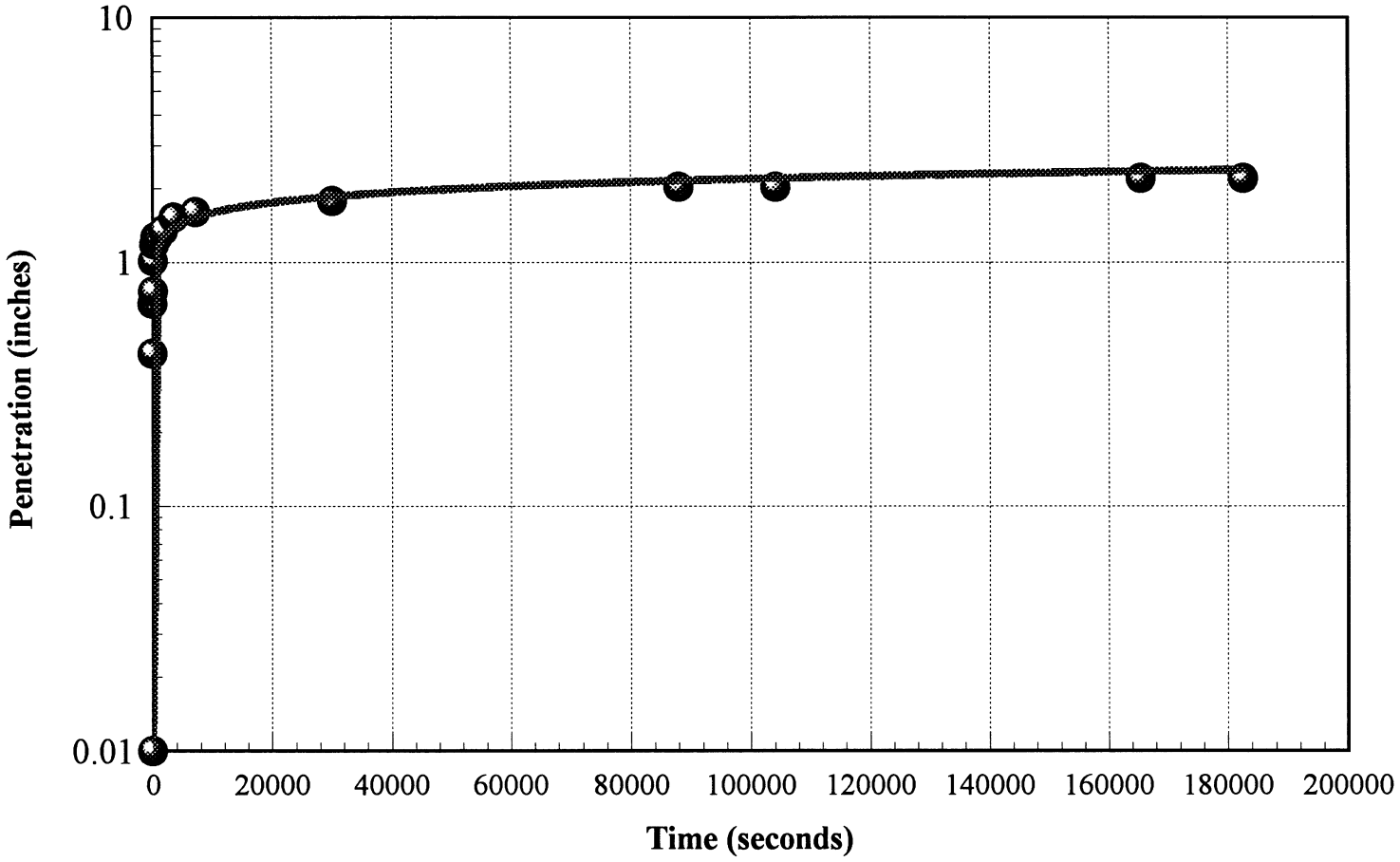

Figur 4.10 PDS Slurry Penetration Test # 1 at pressure = 5 psi, Void Ratio = 0.876 and polymer Concentration = 1:200.

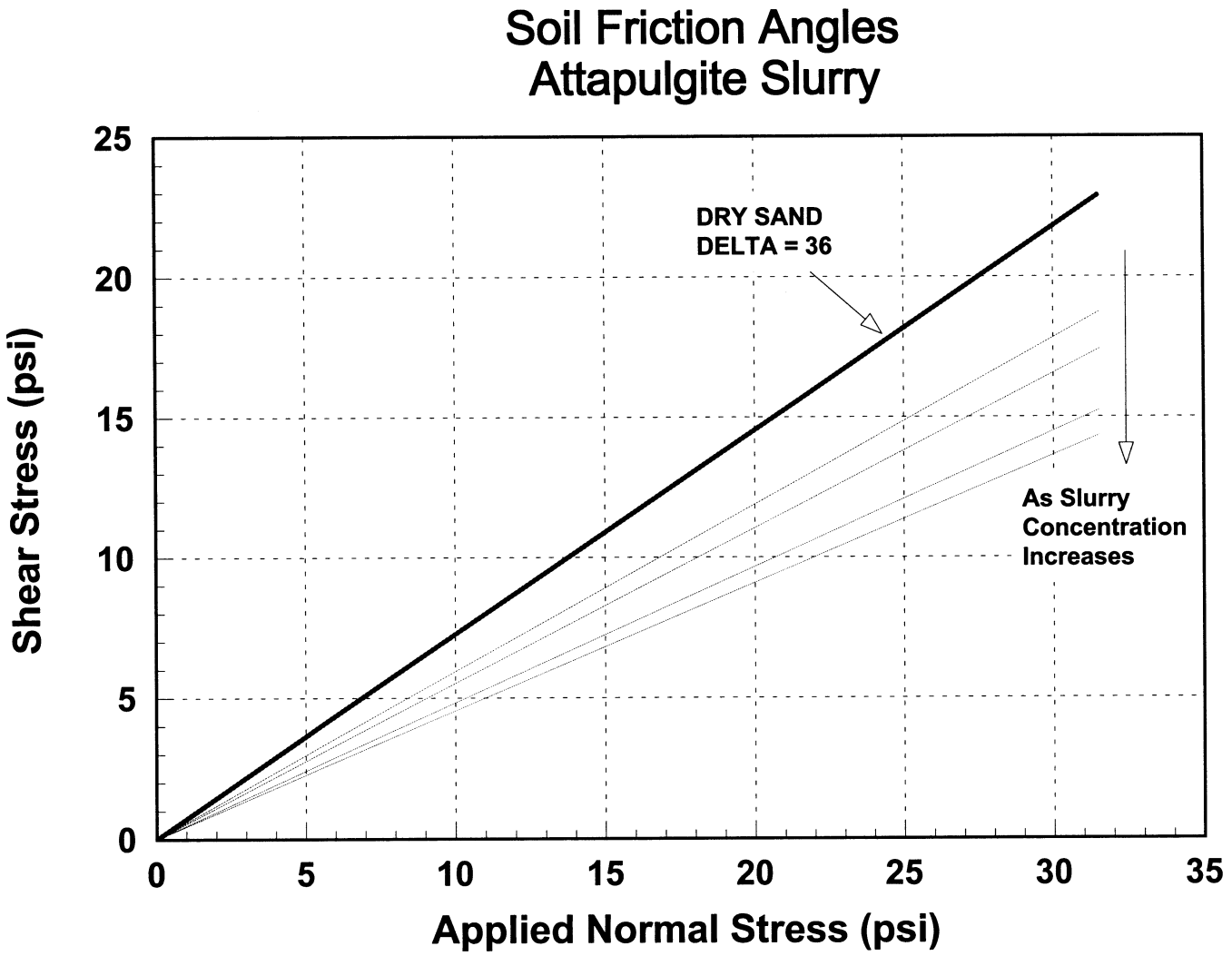

Figure 4.11 Friction angles for soil-soil samples penetrated with attapulgite slurry

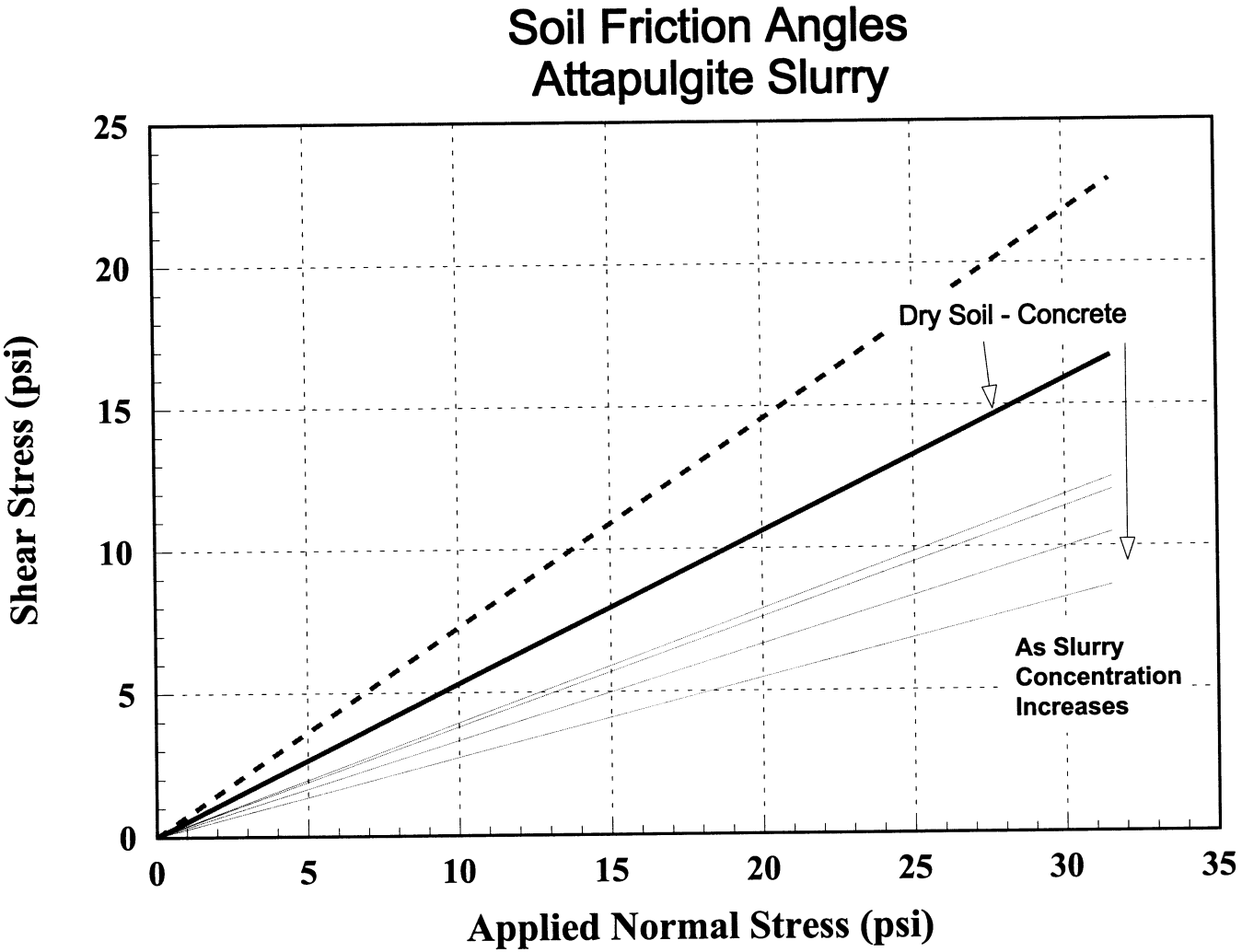

Figure 4.12 Friction angles for soil - concrete samples penetrated with attapulgite slurry

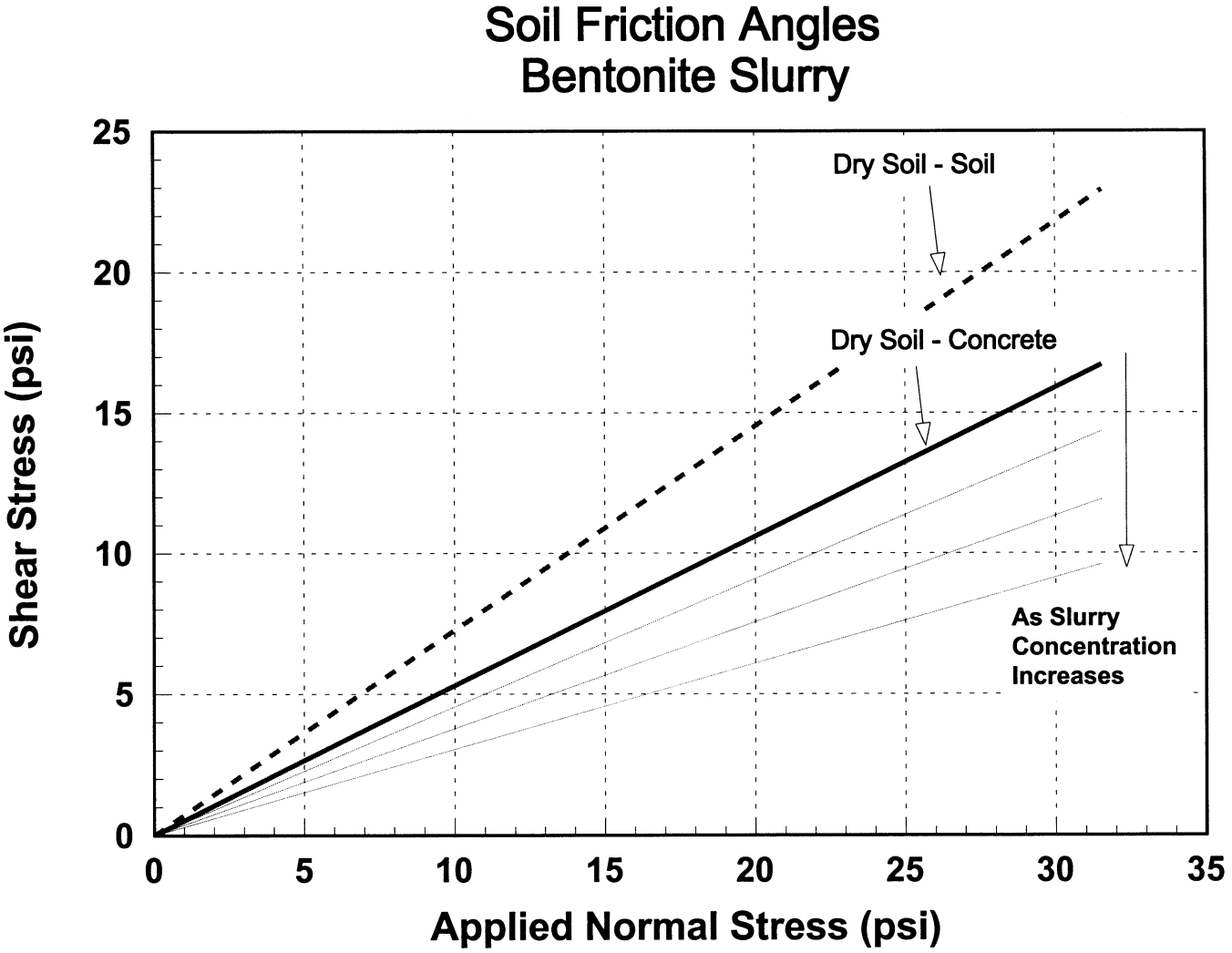

Figure 4.13 Friction angles for soil - concrete samples penetrated with bentonite slurry

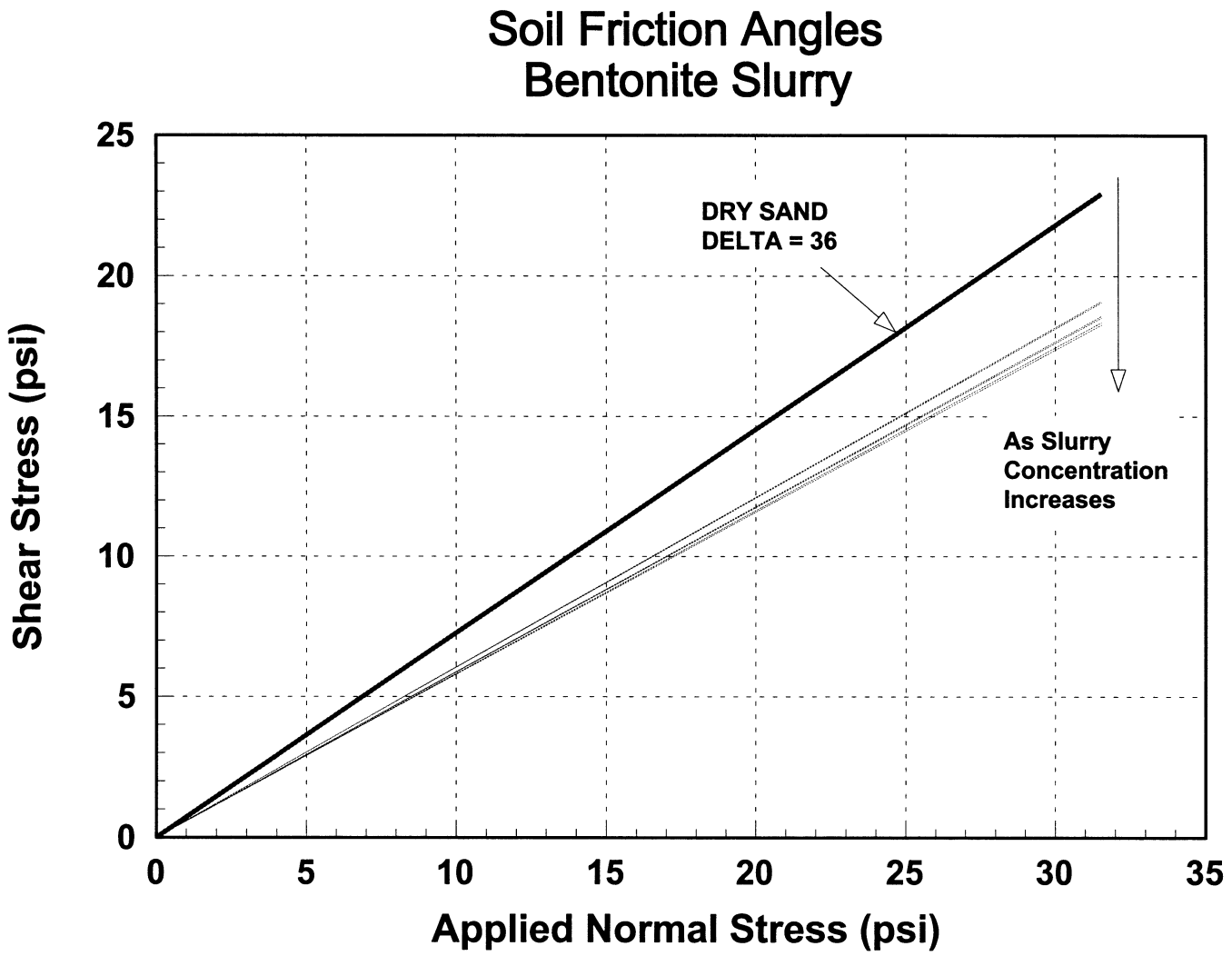

Figure 4.14 Friction angles for soil - soil samples penetrated with bentonite slurry

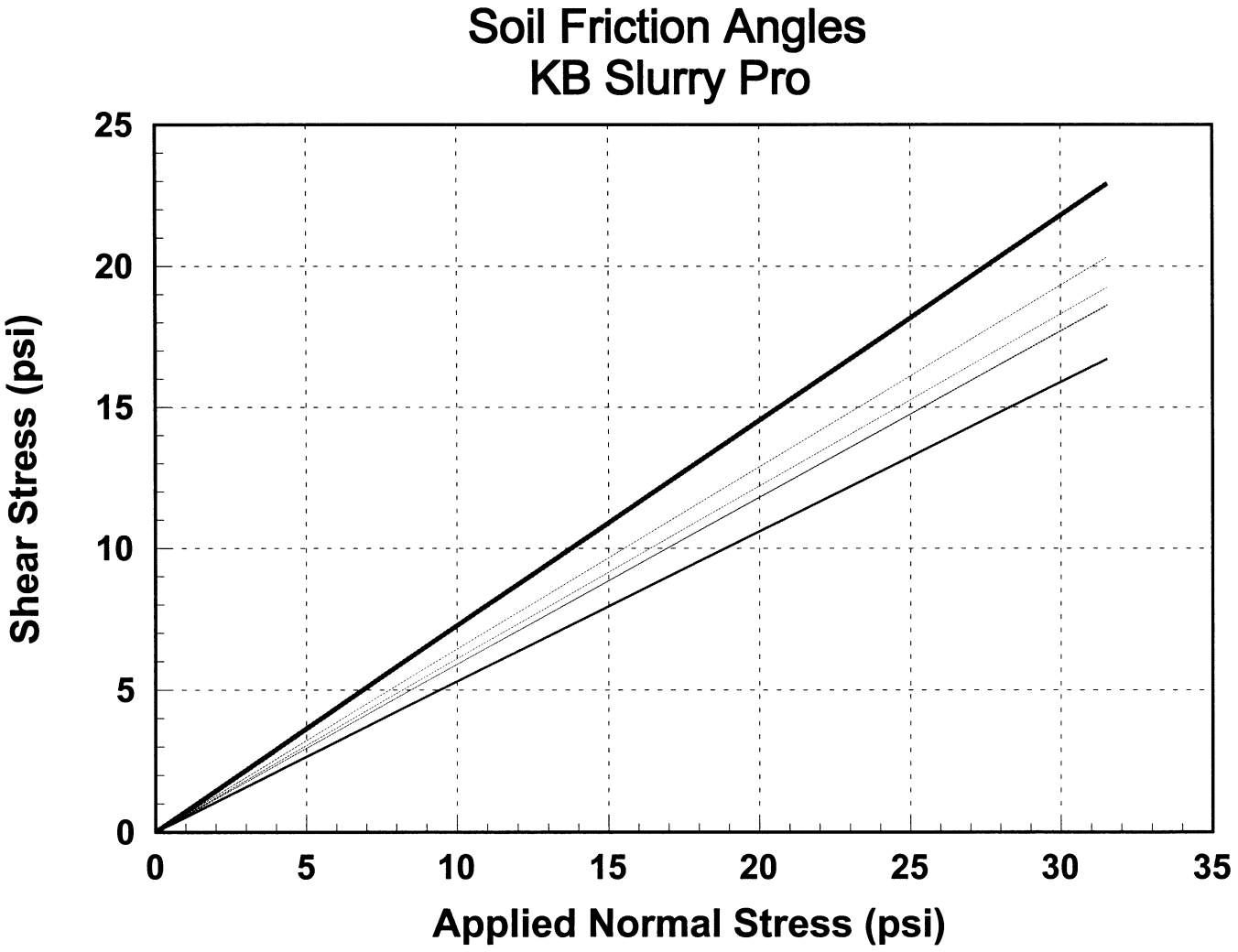

Figure 4.15 Friction angles for soil - Soil samples penetrated with bentonite slurry

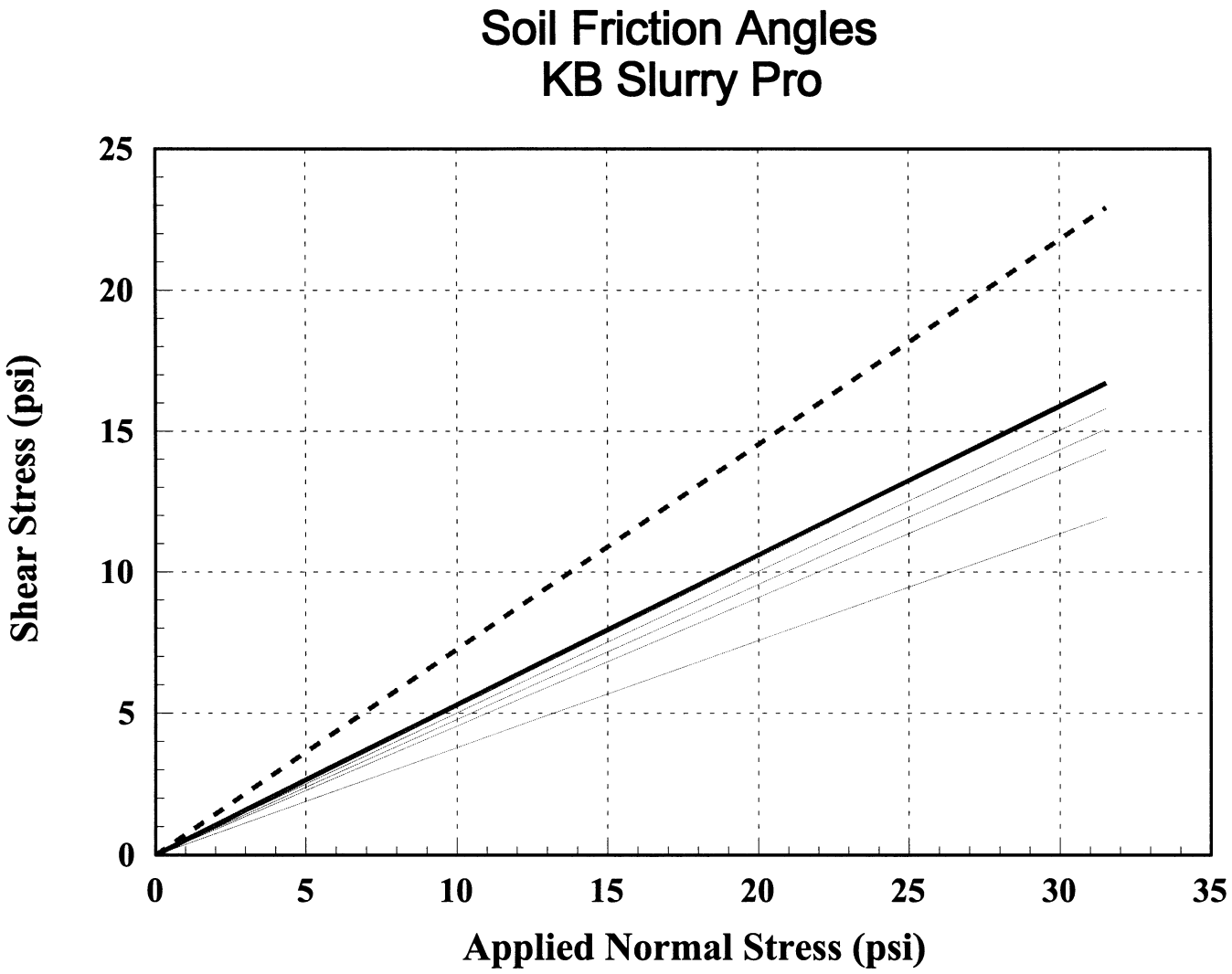

Figure 4.16 Friction angles for soil - concrete samples penetrated with bentonite slurry

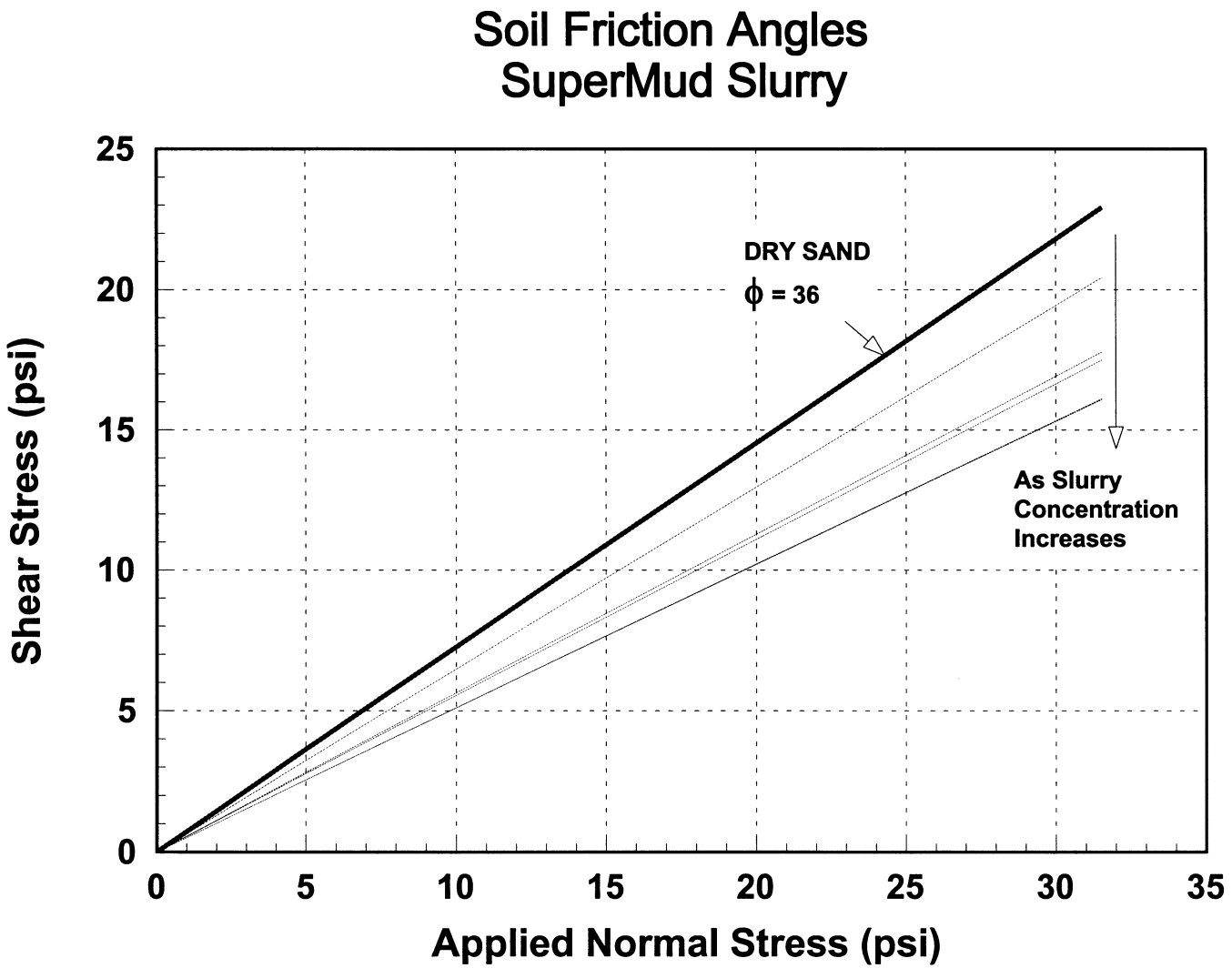

Figure 4.417 Friction angles for soil - soil samples penetrated with bentonite slurry

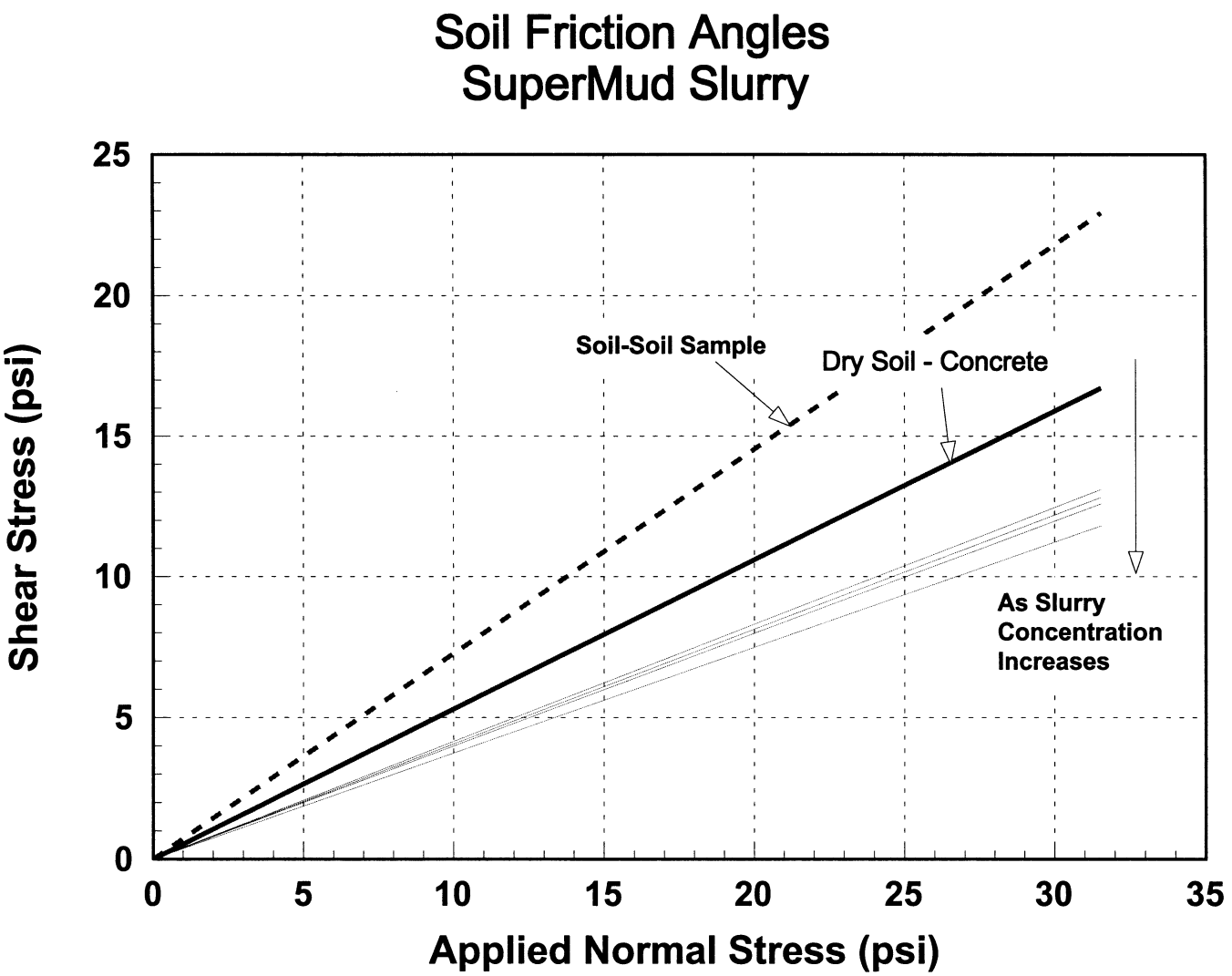

Figure 4.18 Friction angles for soil - concrete samples penetrated with bentonite slurry

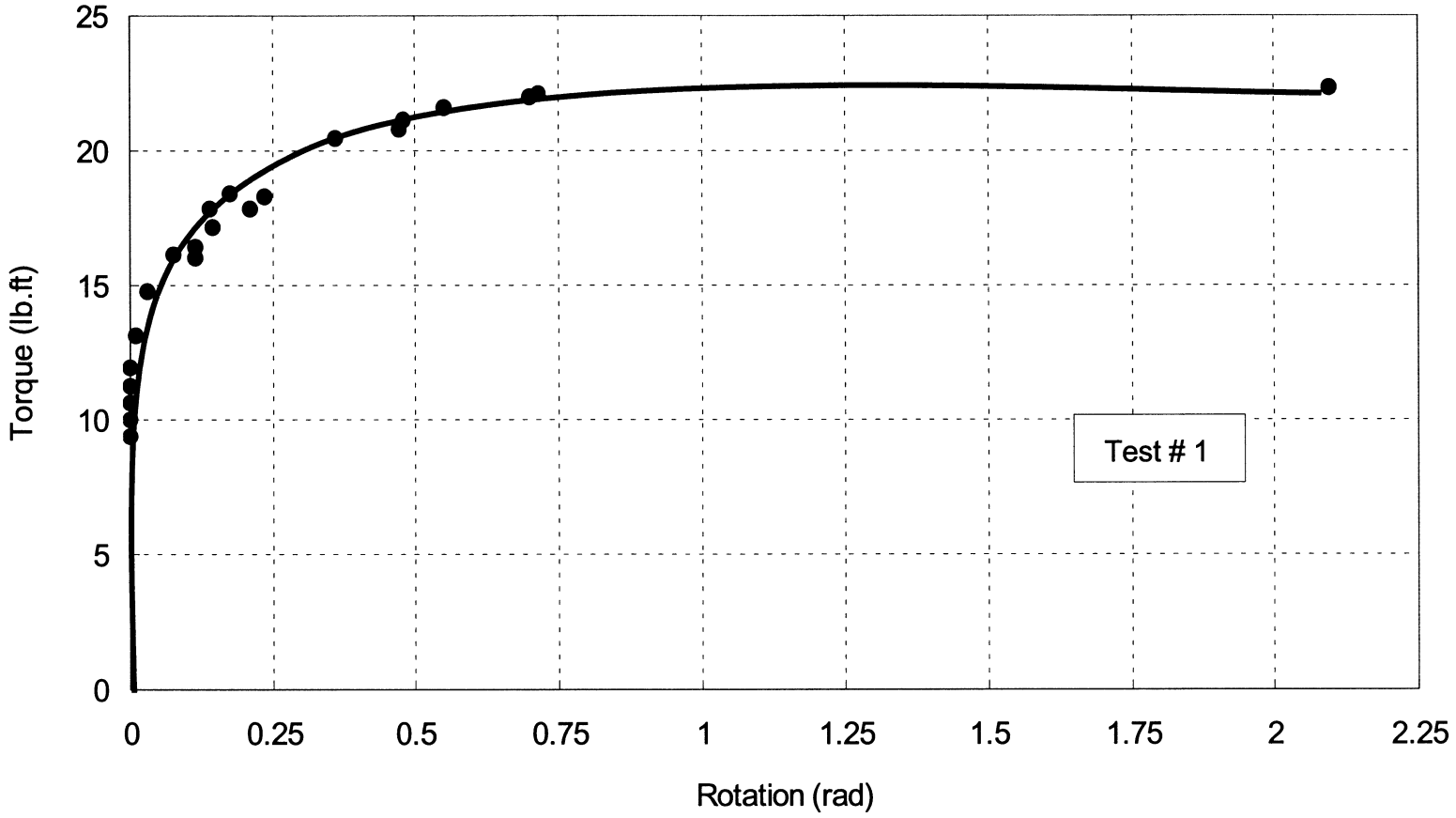

Figure 4.19. Simple Torsional Test on Scaled Model Shaft

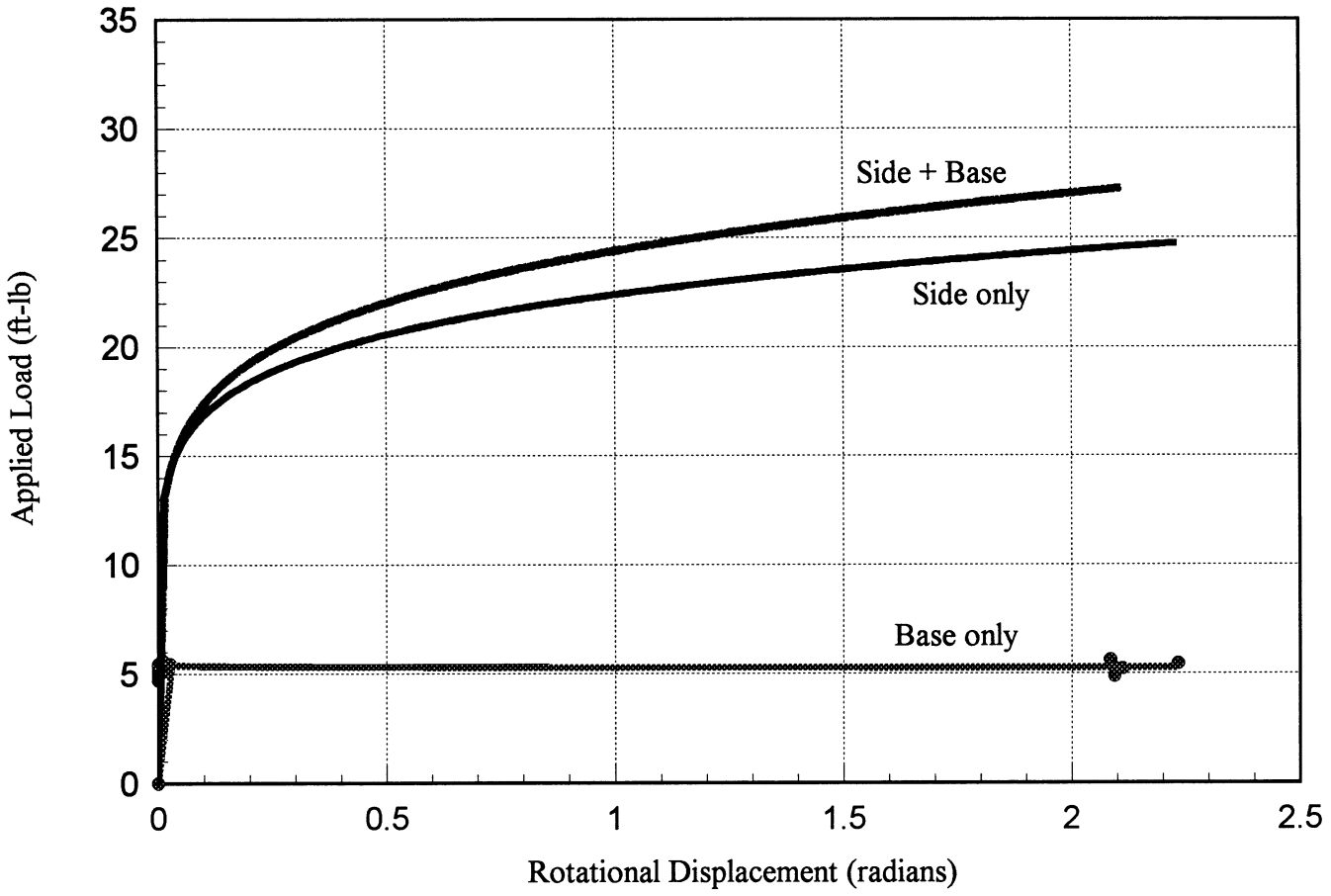

Figure 4.20 Comparison between Total, Side, and Base Friction Trends on Scaled Model Shaft

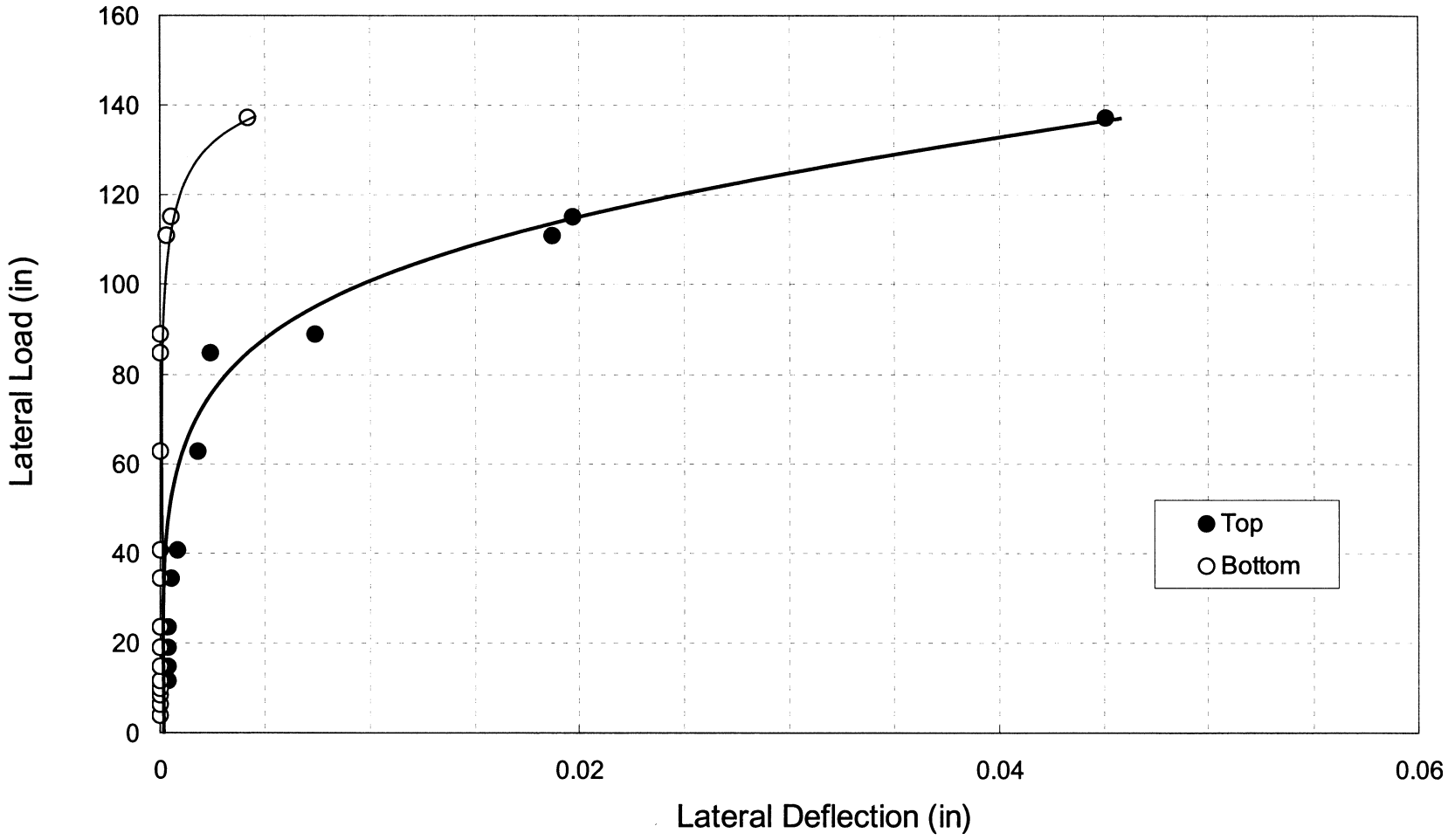

Figure 4.21 Test # 1 for Lateral Load vs. Lateral Deformation of Scaled Shaft

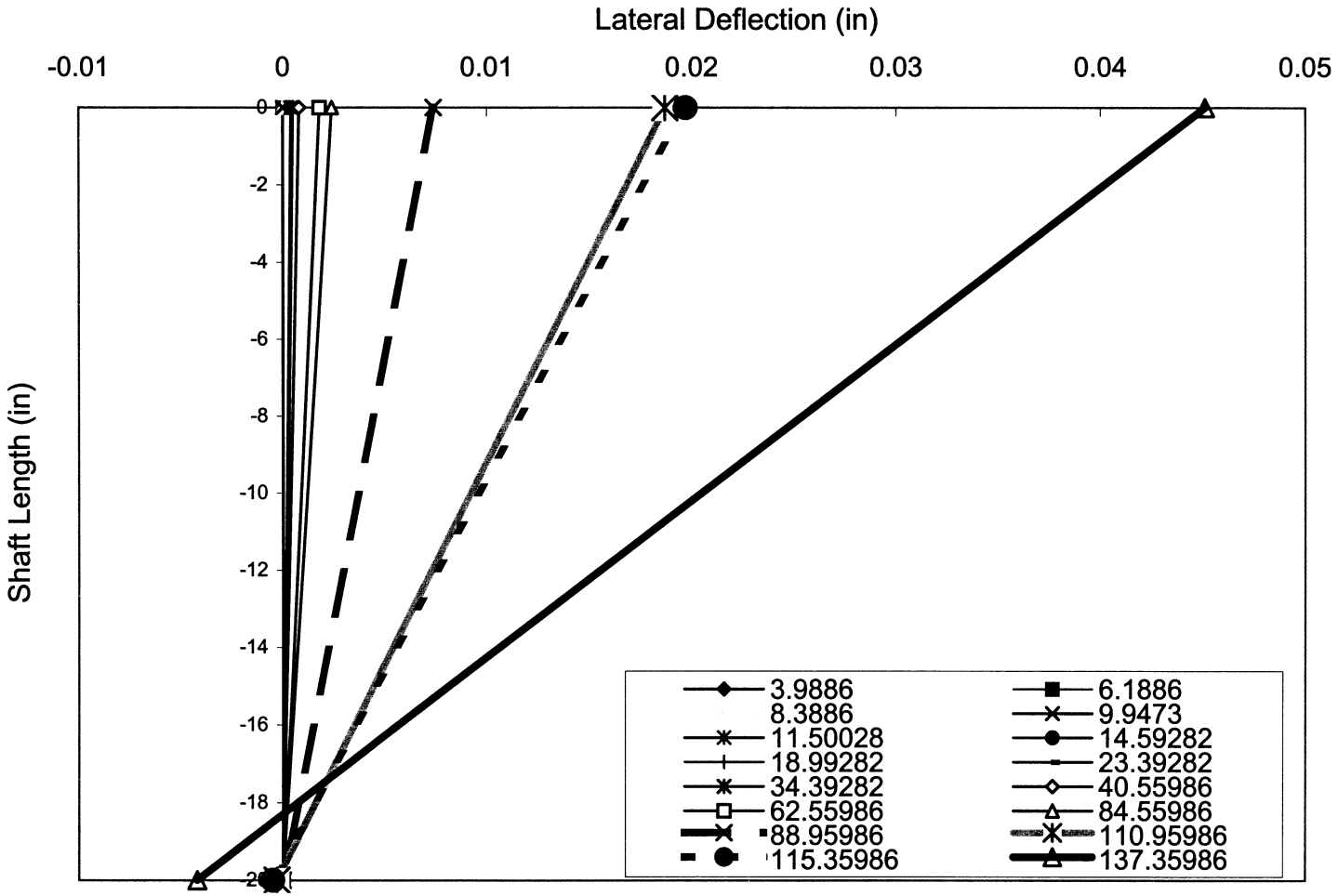

Figure 4.22. Test # 1 for Lateral Load vs. Lateral Deformation of Scaled Shaft

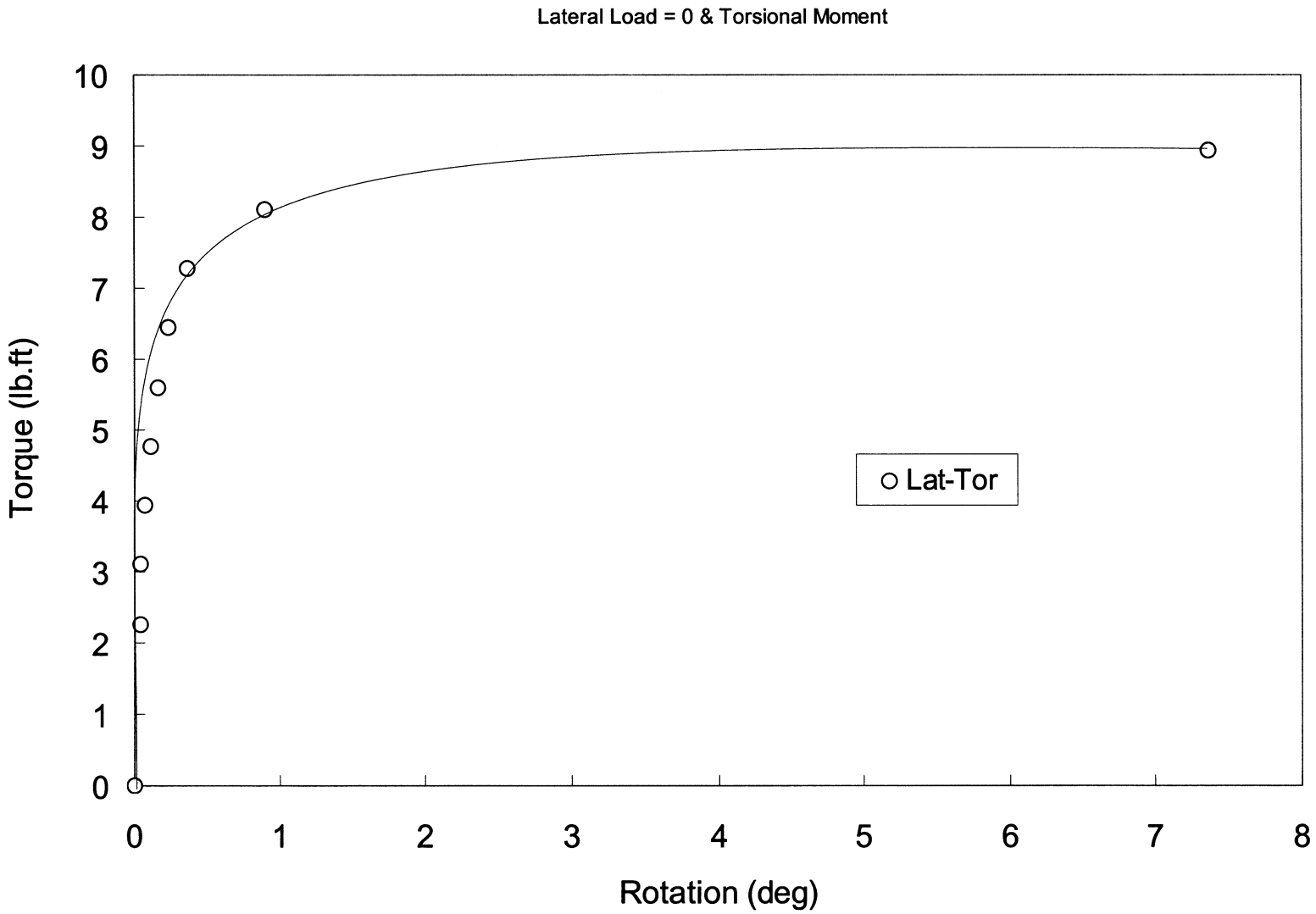

Figure 4.23 Test # 8 for Lateral Load & Moment

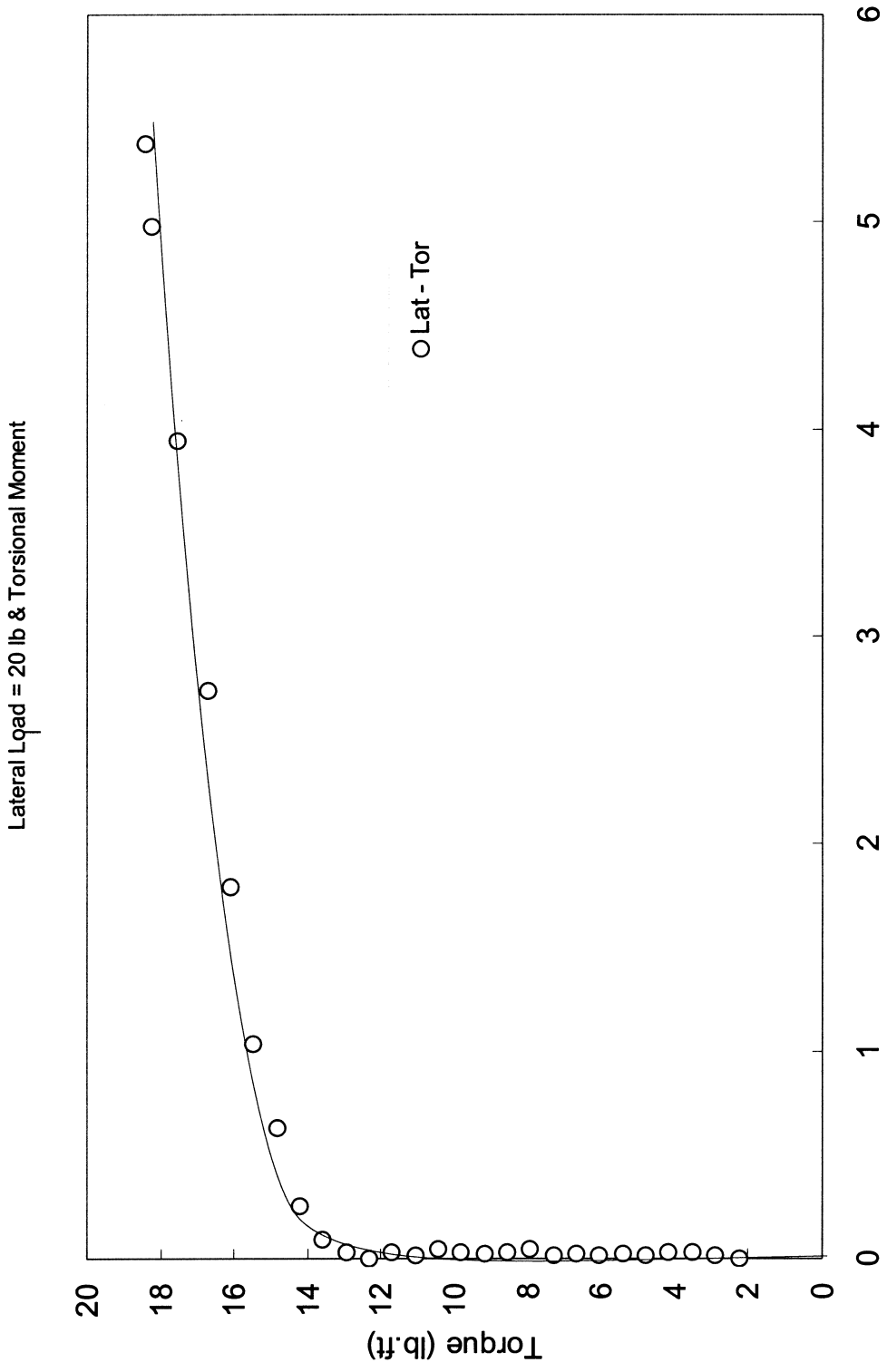

Figure 4.24 Test # 8 for Lateral Load & Moment

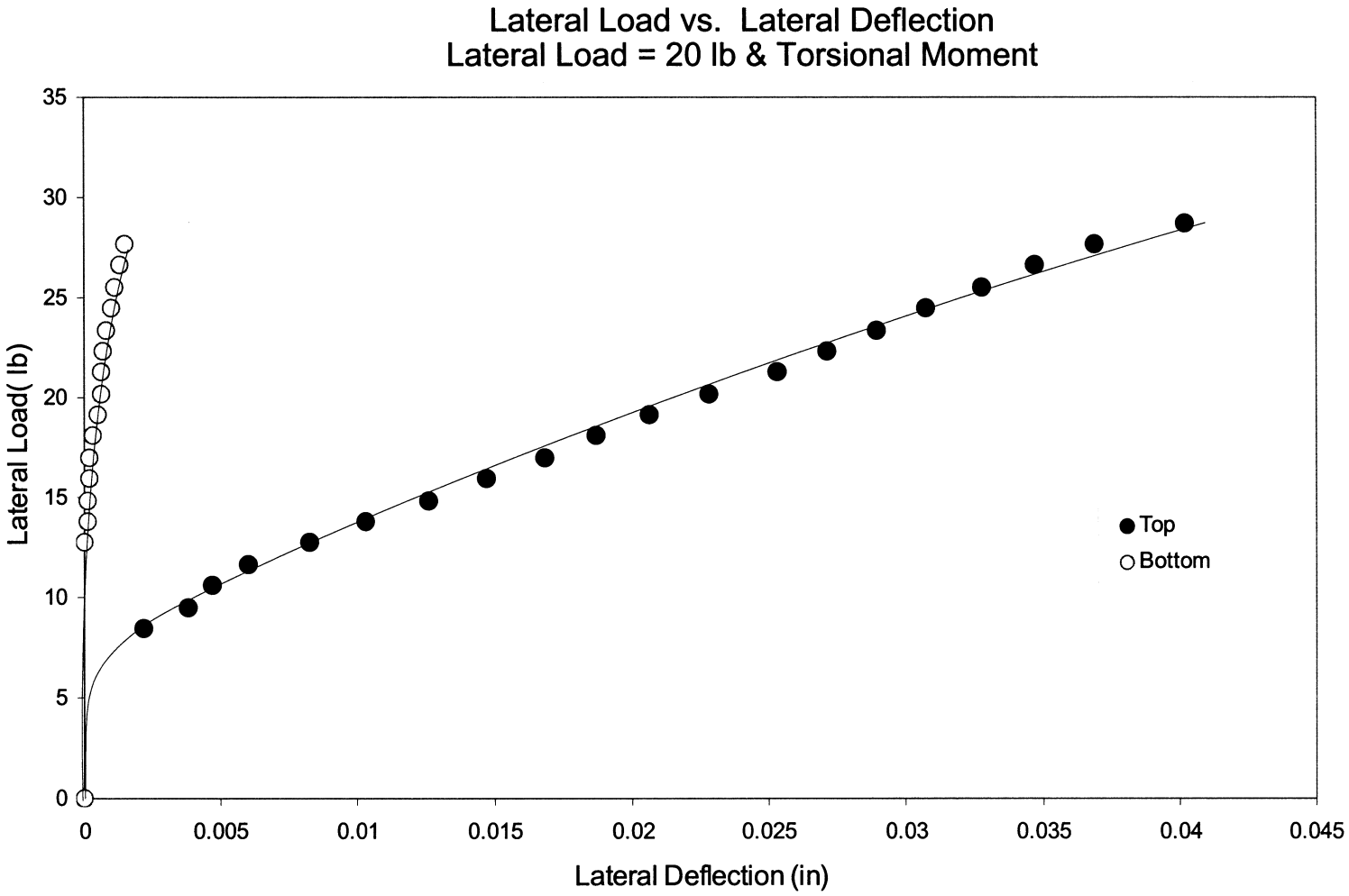

Figure 4.25 Test # 8 for Torsional and Lateral Load Test

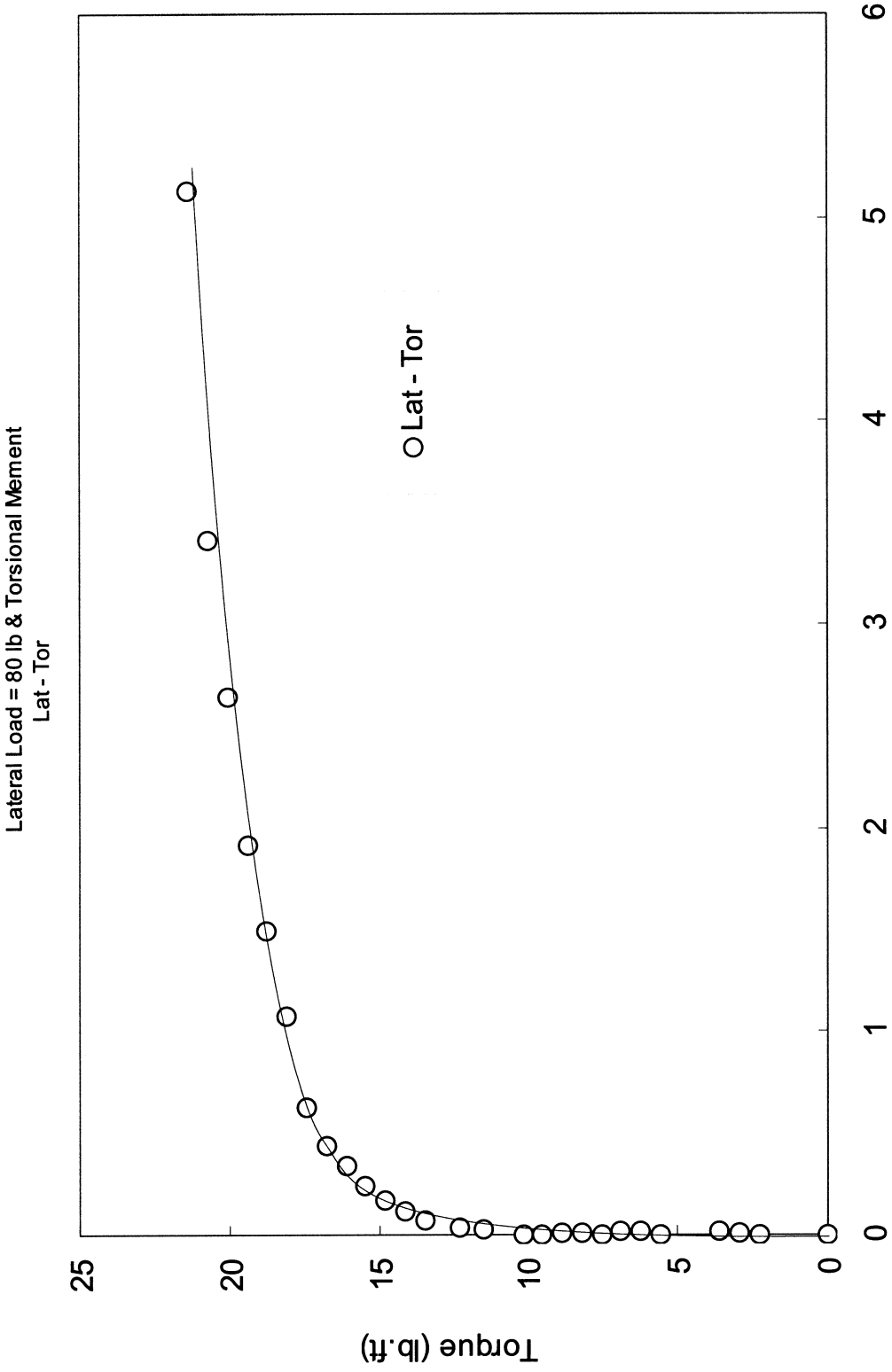

Figure 4.26 Test # 8 for Lateral Load & Moment

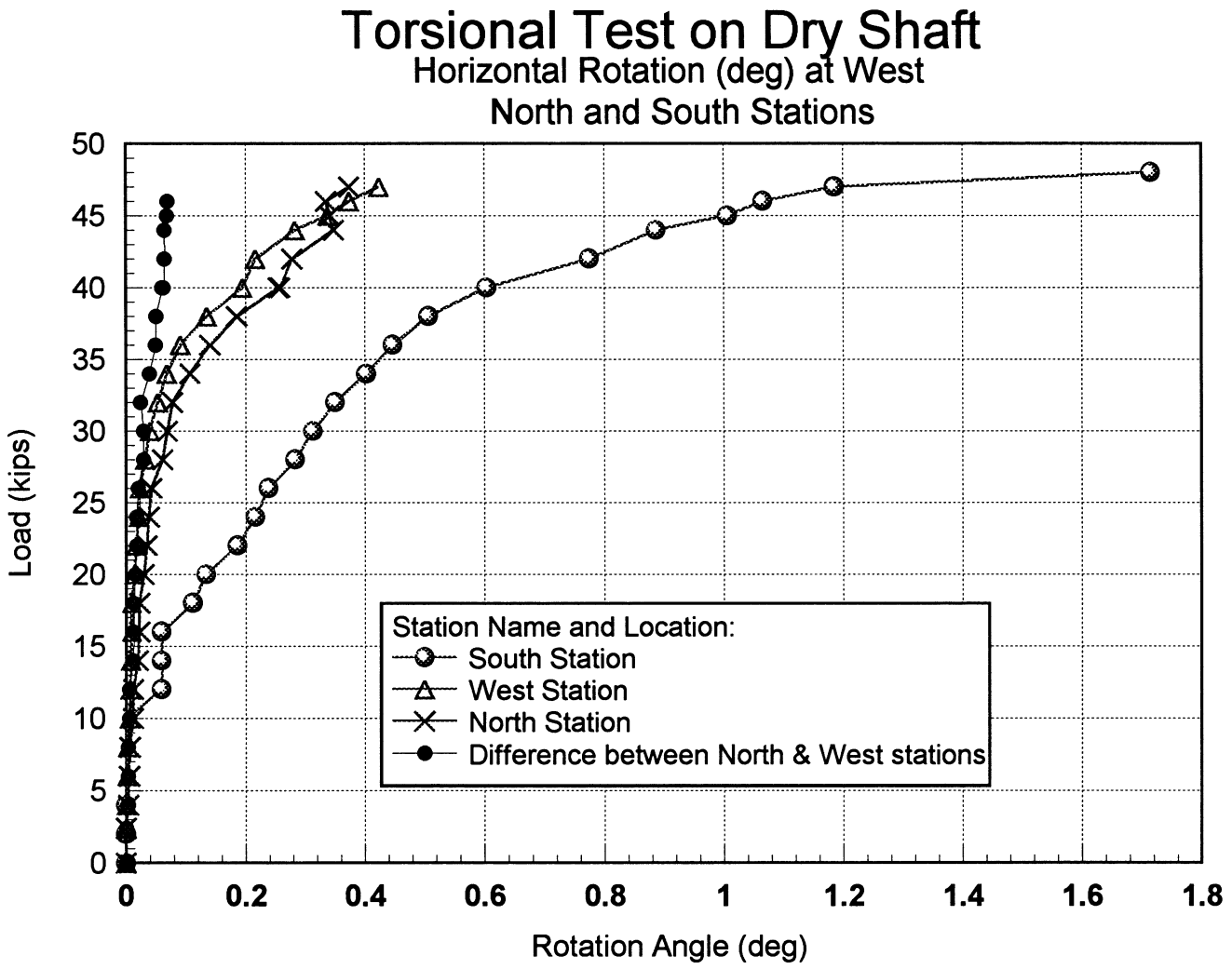

Figure 4.27 Field Test # 1 of Full Scale Drilled Shaft , Dry Borehole

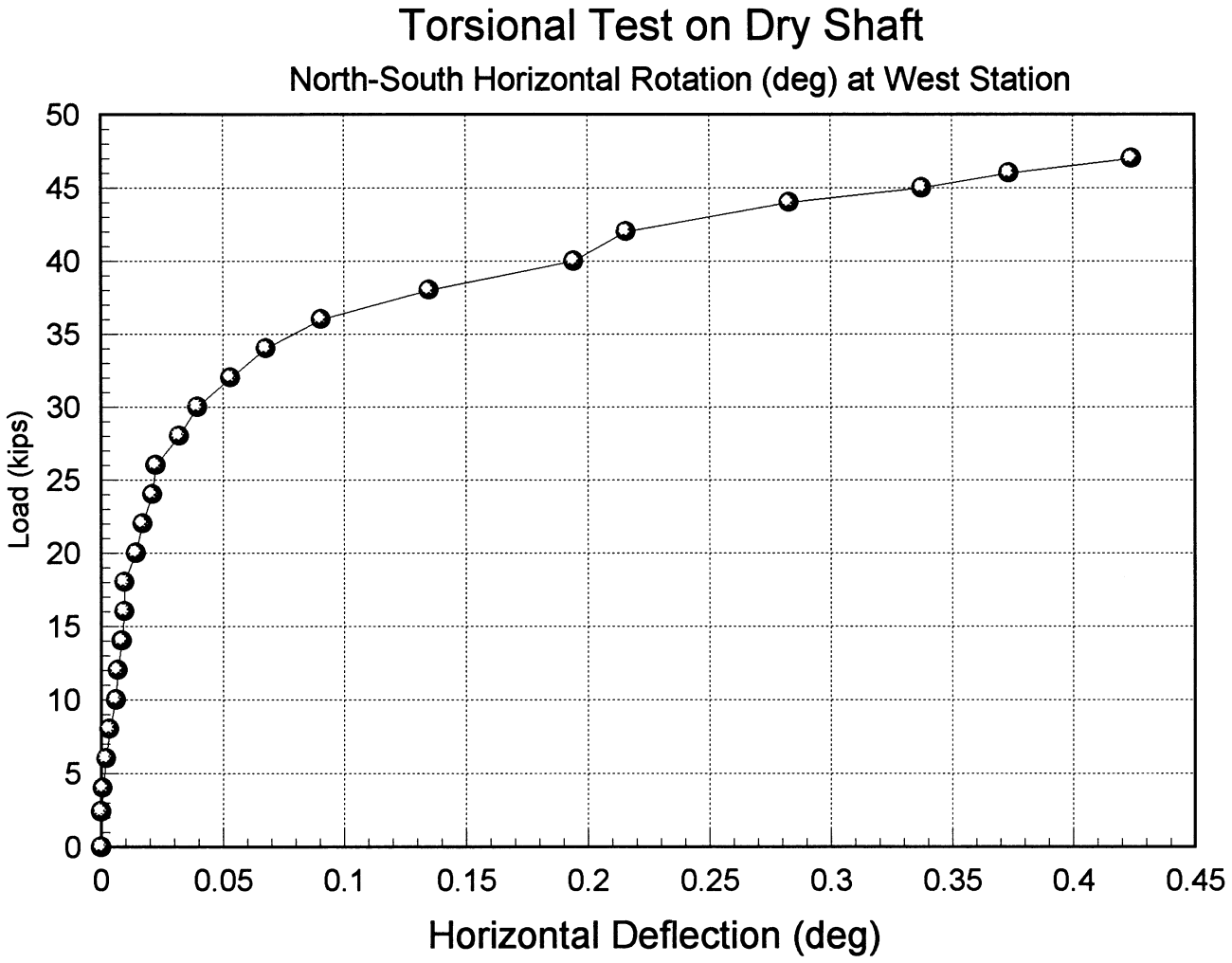

Figure 4.28 Field Test # 1 of Full Scale Drilled Shaft , Dry Borehole

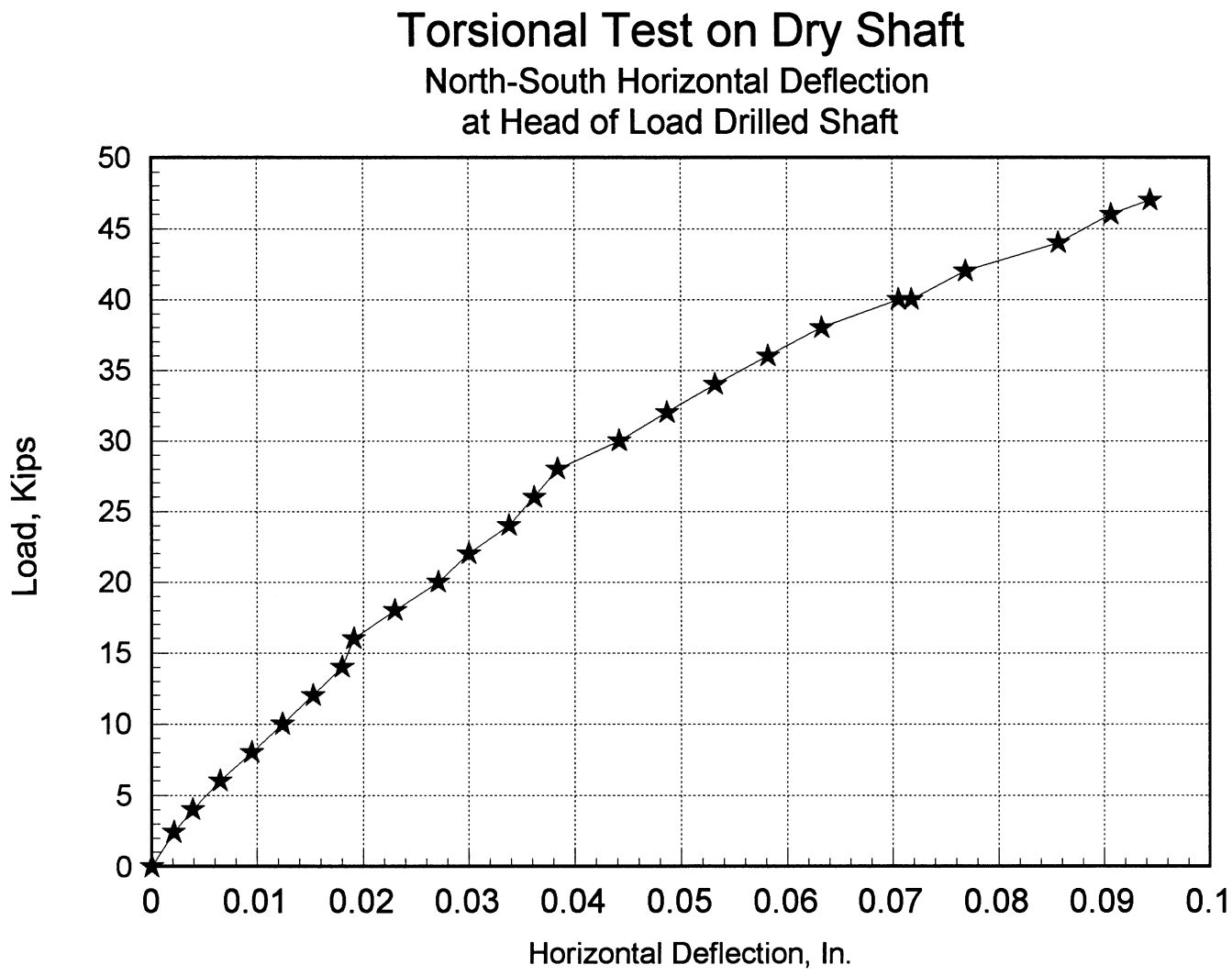

Figure 4.29 Field Test # 1 of Full Scale Drilled Shaft , Dry Borehole

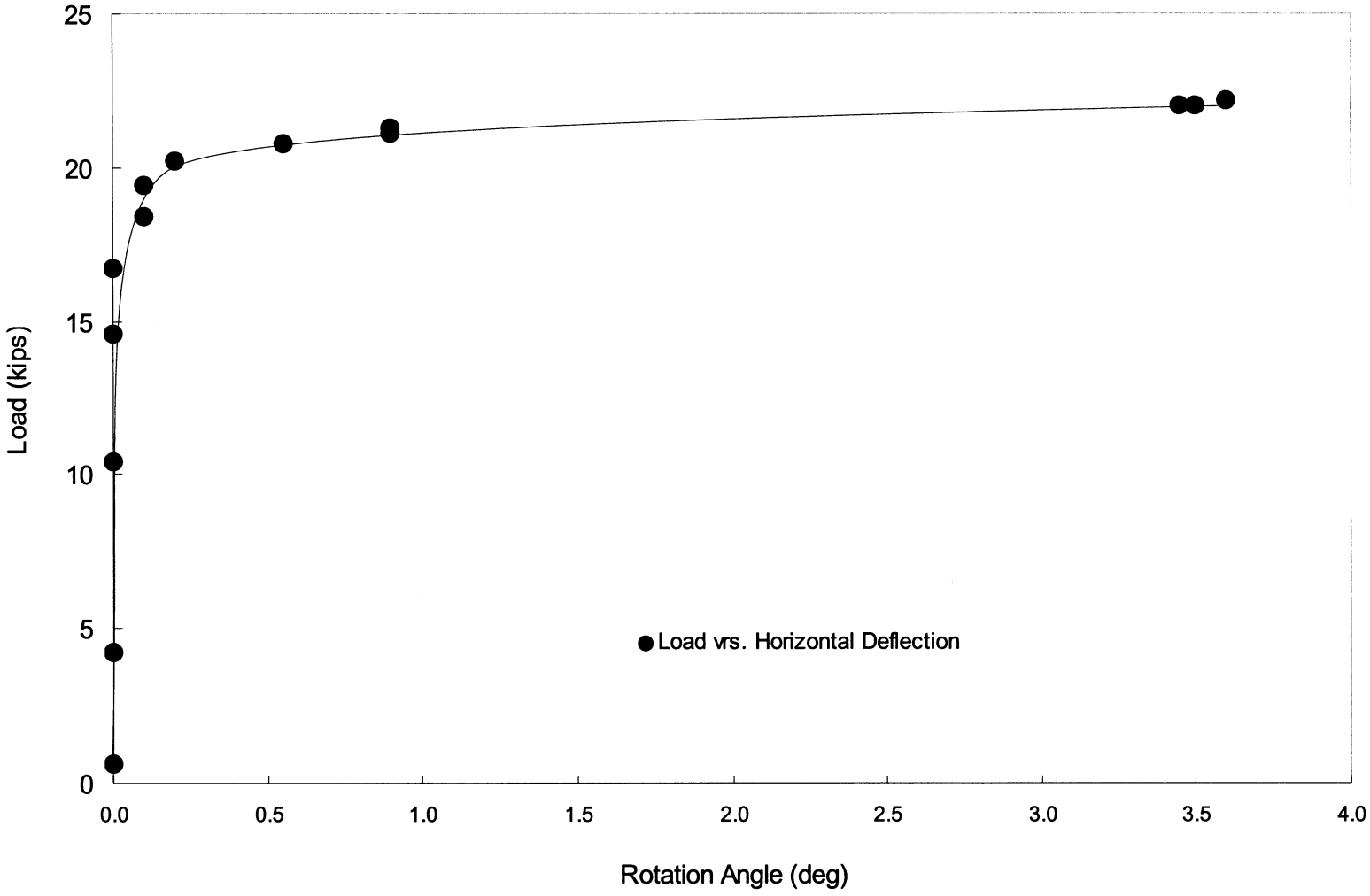

Figure 4.30 Field Test # 2 of Full Scaled Drilled Shaft, Bentonite Slurry Borehole, South Side.

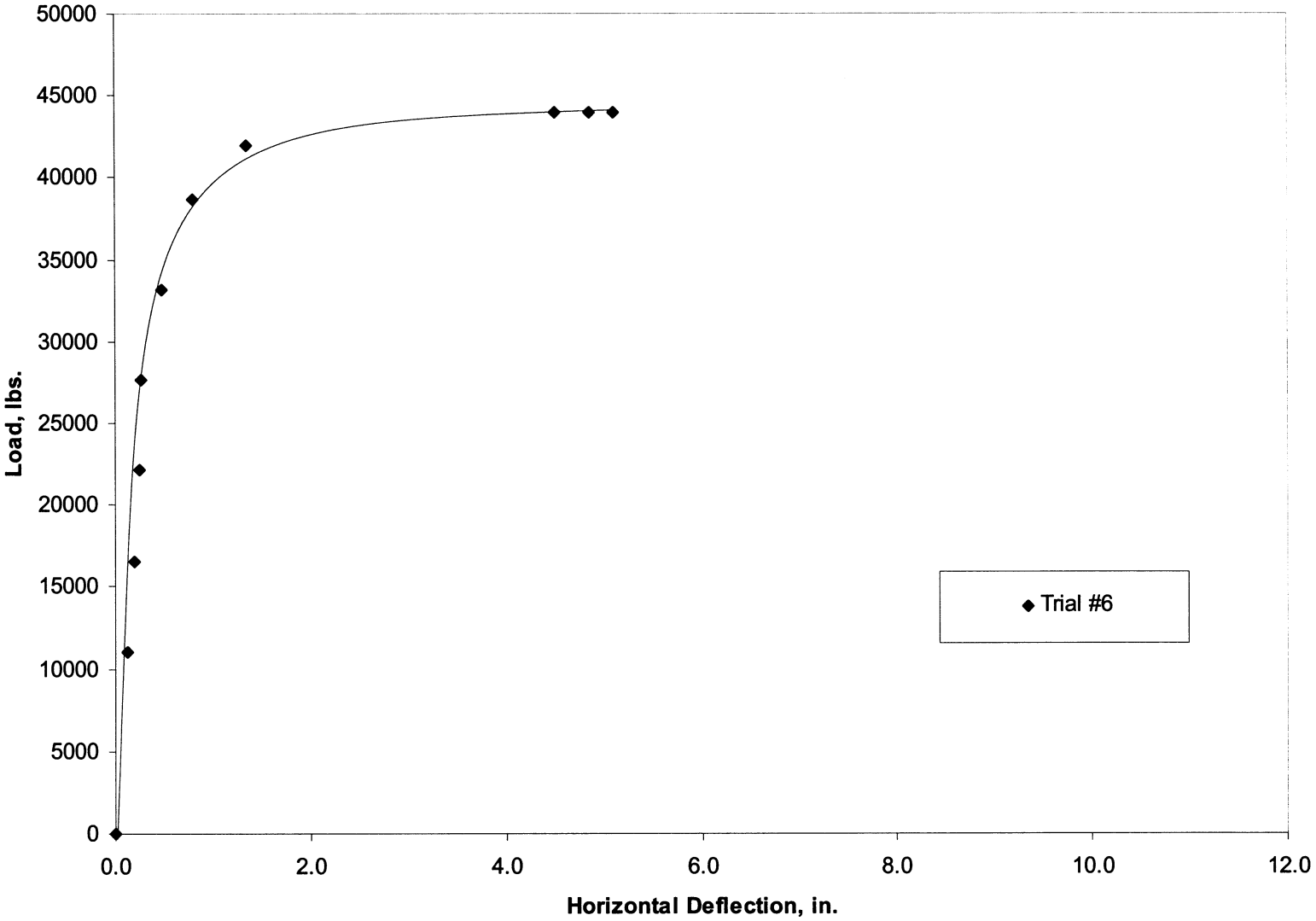

Figure 4.31 Field Test # 3 of Full Scaled Drilled Shaft, Polymer Slurry Borehole, South Side.

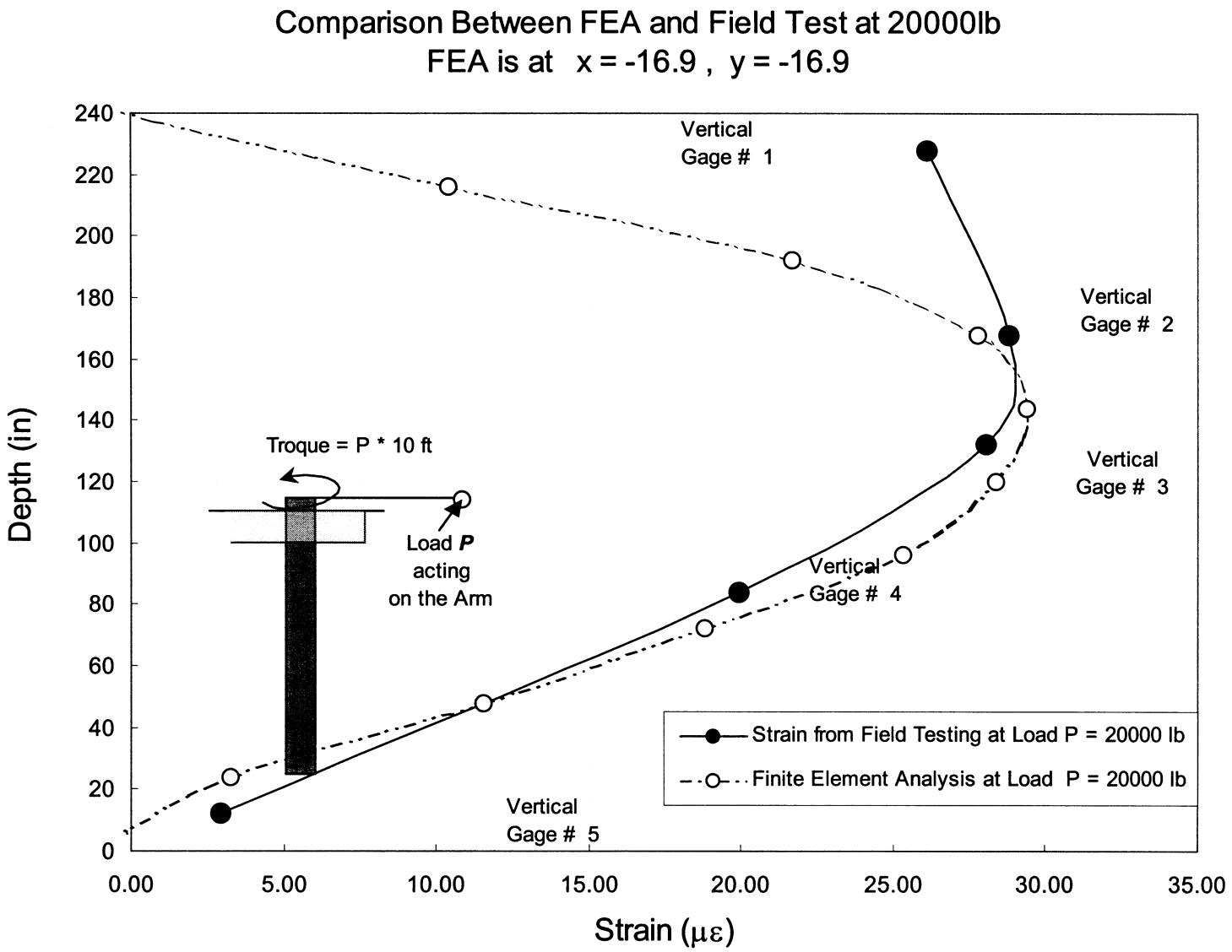

Figure 4.32 Comparison of Strain Measurements of Test # 1 with the FEA Results

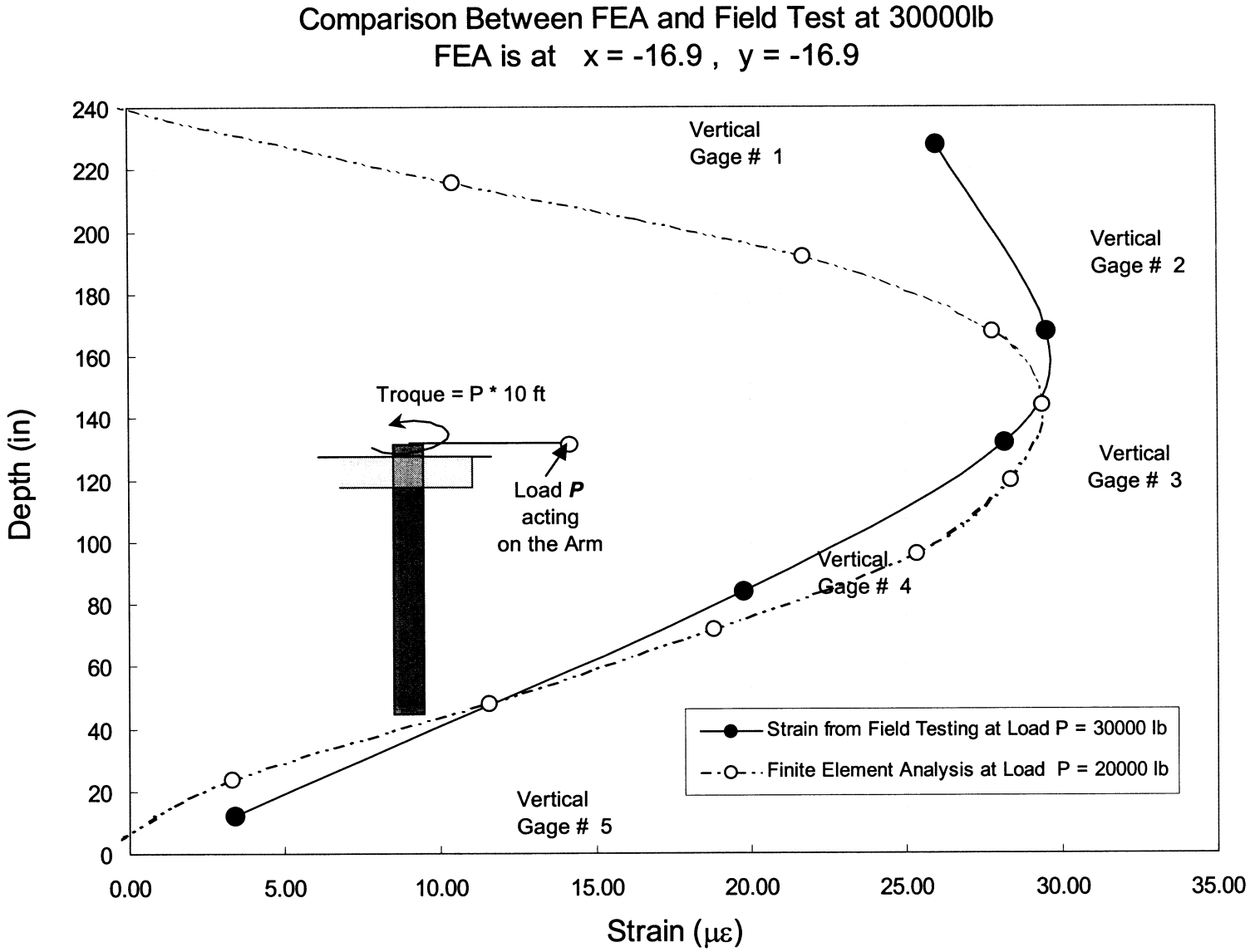

Figure 4.33 Comparison of Strain Measurements of Test # 1 with the FEA Results

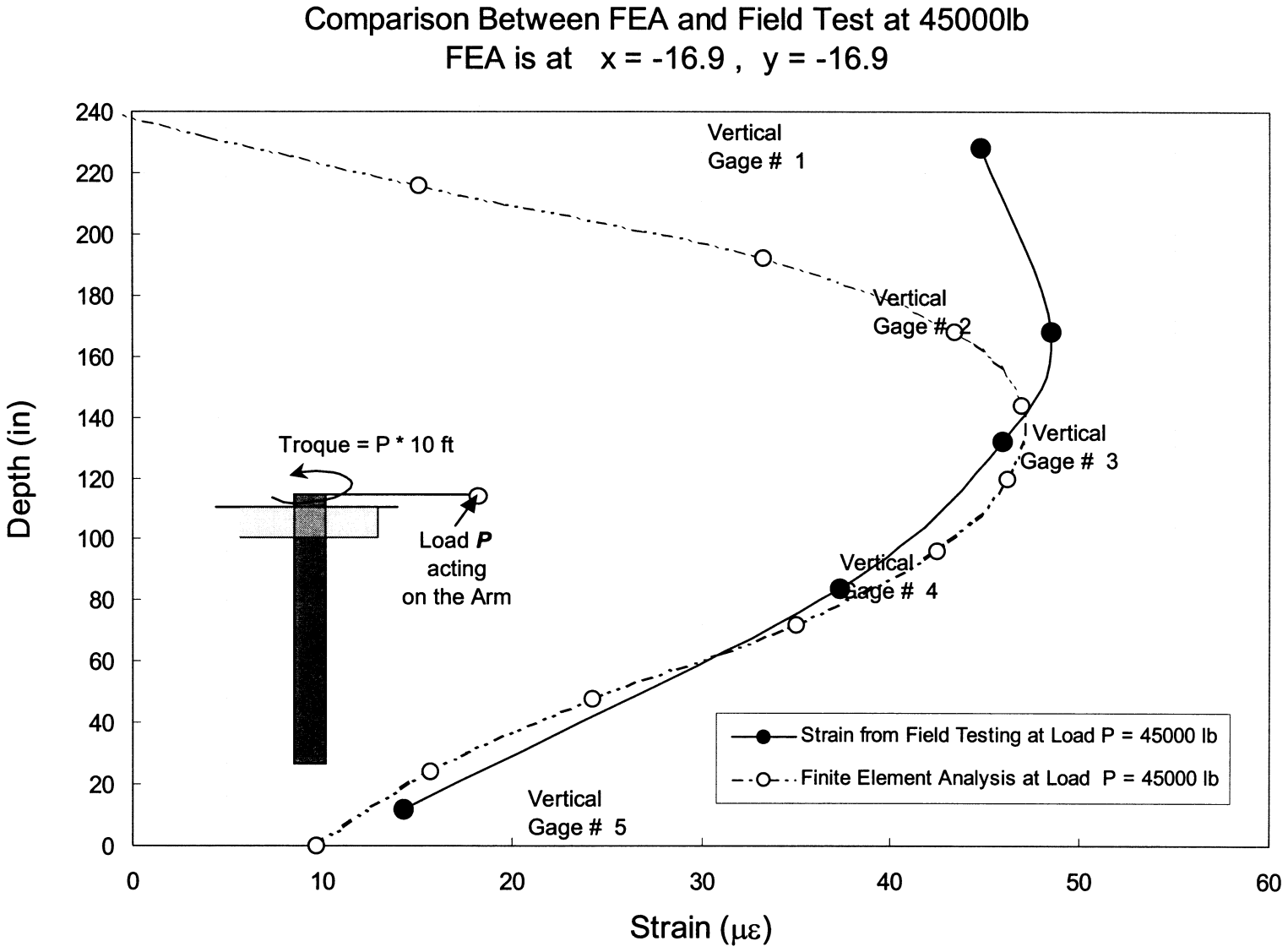

Figure 4.34 Comparison of Strain Measurements of Test # 1 with the FEA Results

CHAPTER 5

METHOD FOR ANALYSIS OF DRILLED SHAFT CAPACITY UNDER TORSIONAL LOADING

5.1 Methodology

In most situations, the design of drilled shafts to resist lateral loads is based on acceptable lateral deflection rather than the ultimate lateral capacity. The two generally used approaches of calculating lateral deflections are:

1. Subgrade reaction approach (Reese and Matlock, 1956, Matlock and Reese 1960)
2. Elastic continuum approach (Poulos, 1971a and b)

Subgrade Reaction Approach: This approach treats a laterally loaded drilled shaft as a beam on elastic foundation. It is assumed that the beam is supported by a **Winkler** soil model according to which the elastic soil medium is replaced by a series of infinitely closely spaced independent and elastic springs (Figure 5.1).

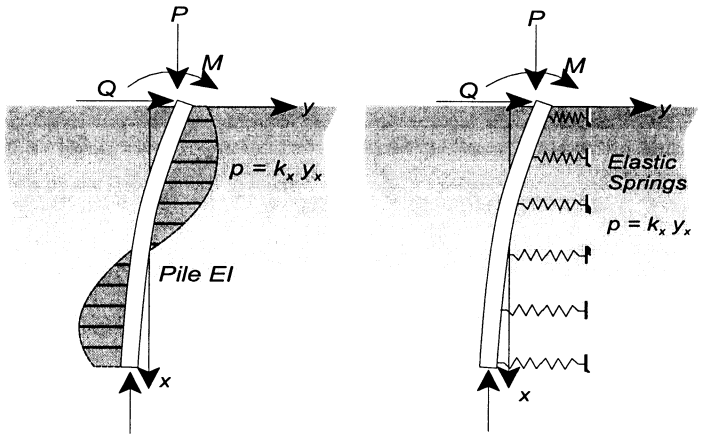

Figure 5.1 Approximation of soil reaction due to lateral loading

The stiffness of these springs k_h (also called the modulus of horizontal subgrade reaction) can be expressed as follows:

$$k_h = p / y \qquad \textbf{5.1}$$

where:

p = the soil reaction per unit length of drilled shaft

y = the drilled shaft deformation and k_h has the units of force length

Palmer and Thompson (1948) employed the following form to express the modulus of a horizontal subgrade reaction:

$$k_x = k_h (x / L)^n \qquad \textbf{5.2}$$

where

k_h = value of k at $x = L$ or tip of the drilled shaft
x = any point along drilled shaft depth
n = a coefficient equal to or greater than zero

The most commonly used value of n for sands and normally consolidated clays under long-term loading is unity. For overconsolidated clays ***n*** is taken zero. According to Davisson and Prakash (1963). a more appropriate value of ii will be 1.5 for sands and 0.15 for clays under undrained conditions.

For the value of $n = 1$, the variation of k_h with depth is expressed by the following relationship:

$$k_h = n_h . x \qquad \textbf{5.3}$$

where n_h is the constant of modulus of subgrade reaction. This applies to cohensionless soils and normally consolidated clays where these soils indicate increased strength with depth due to overburden pressures and the consolidation process of the deposition. Typical values are listed in **Table 5.1.**

TABLE 5.1a Estimated Values for k_h*

Soil Type	Values
Granular	n_h ranges from 1.5 to 2001b/in^3, is generally in the range from 10 to 1001b/in^3, and is approximately proportional to relative density
Normally loaded organic silt Peat Cohesive soils	 n_h ranges from 0.4 to 3.01b/in^3 n_h is approximately 0.21b/in^3 k_h is approximately 67 S_u , where S_u is the undrained shear strength of the soil

*After Davisson, 1970.
Note: The effects of group action and repeated loading are not included in these estimates.

TABLE 5.1b Recommended Values of $n_{,,}$ for Submerged Sand

Relative Density	Loose	Medium	Dense
1. Terzaghi (1955) Range of values of n_h (lb/in^3)	2.6-7.7	7.7-26	26-51
2. Reese et al. (1974)	(Static and Cyclic Loading)		

Relative Density	Loose	Medium	Dense
Recommended n_h (lb/in^3)	20	60	125

For the value of $n = 0$, the modulus will be constant with depth and this assumption is most appropriate for drilled shafts in overconsolidated clays.

The soil reaction vs. deflection relationship for real soils is nonlinear and Winkler's idealization would require modification. This can be done by using p - y curves approach. The behavior of a drilled shaft can thus be analyzed by using the equation of an elastic beam supported on an elastic foundation and is given by the following equation:

$$EI\,(d^4y/dx^4) + p = 0 \qquad \textbf{5.4}$$

where:

E = modulus of elasticity of drilled shaft
I = moment of inertia of drilled shaft section
p = soil reaction which is equal to (k_h y)

Equation (5.4) can be rewritten as follows:

$$(d^4y/dx^4) + (k_h\, y / EI) = 0 \qquad \textbf{5.5}$$

Solutions for equation (5.5) to determine deflection and maximum moments are given in literature for cohesionless and cohesive soils. The extension of these solutions to incorporate nonlinear soil behavior by using p-y curves are also described there.

p-y Curves

The heart of the p-y method is the definition of the lateral load-deflection relationships between the foundation and the soil. These are expressed in the form of p-y curves, where p is the lateral soil

resistance per unit length of the foundation (expressed in units of force per length), and y is the lateral deflection. Typical p-y curves are shown in **Figure 5.2.**

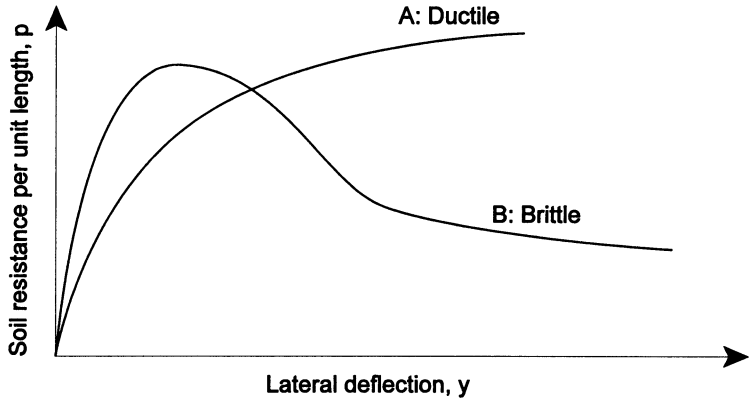

Figure 5.2 Typical p-y curves

The p-y relationship might first appear to be a nonlinear extension of the Winkler beam-on-elastic-foundation concept. However, there is an important difference between the two: The Winkler model considers only compressive forces between the foundation and the soil, whereas the lateral soil load acting on a deep foundation is the result of compression on the leading side, shear friction on the two adjacent sides, and possibly some small compression on the back side. These components are shown in **Figure 5.3.** Thus, it is misleading to think of the p-y curve as a compression phenomenon only (Briaud et al. 1983, and Smith, 1989).

The ultimate compression resistance will probably be much greater than the ultimate side shear resistance. However,- mobilization of the side shear requires much less deflection, so it may be an important part of the total resistance at the small deflections; generally associated with the working loads. There is a need for additional research to more fully understand this behavior.

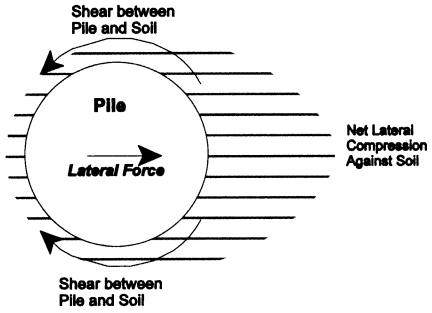

Figure 5.3a The soil resistance to lateral pile movement has both compression and shear components. The sum of them is the p in p-y curves (Smith, 1989).

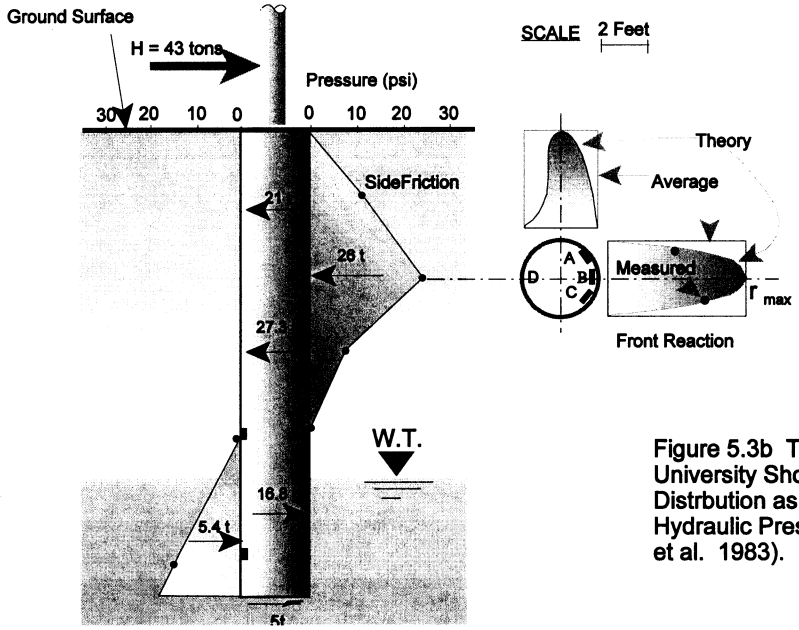

Figure 5.3b Test # 1 at Texas A & M University Showing Pressure Distrbution as Measured with the Hydraulic Pressure Cells Load (Briaud et al. 1983).

The p-y curve for a particular point on a foundation depends on many factors, including the following:

- *Soil type*
- *Type of loading (i.e., short term static, sustained static, repeated, or dynamic)*
- *Foundation diameter and cross-sectional shape*
- *Coefficient of friction between foundation and soil*
- *Depth below the ground surface*
- *Foundation construction methods*

The influence of these factors is not well established, so it has been necessary to develop p-y curves

empirically from full-scale load tests. Most of this data were obtained from 10 to 24 in (250-600 mm) diameter steel pipe piles. Reese (1984, 1986) many of the tests conducted thus far and provides recommended p-y`curves for analysis and design.

Some curves are ductile, as shown in curve A in **Figure 5.2**. These curves reach the maximum resistance, P_{max}, at a certain deflection, and then maintain this resistance at greater deflections. Other curves are brittle, as shown in curve B in Figure 5.2, and have a decreasing p at large deflections. Brittle curves can occur in some clays, especially if they are stiff or if the loading is repeated or dynamic. Soft clays under static loading and sands appear to have ductile curves. Brittle curves are potentially more troublesome because of their potential for producing large foundation movements.

There have been some efforts to develop p-y curves from in-situ pressuremeter or dilatometer tests (Baguelin et al. 1978; Briaud et al. 1983; and Robertson et al., 1989). Although these tests directly measure something similar to the compression component of lateral pile resistance, they do not address the side shear component. This may be at least a partial explanation of Baguelin's assessment that this approach produces pessimistic results. There also are scale effects to consider. Further research may improve the reliability of these methods.

In this study it was decided that the empirical p-y relationships for the cohesionless soils suggested by Reese (1984) may not be needed in this case, especially because these relationships were developed form lateral load testing. Therefore, the subgrade reaction approach has been followed is this study to estimate the lateral pressure distribution along a drilled shaft and Smith's suggestion

for the pressure distribution at each cross section has be utilized. In this case the lateral pressure distribution at each cross section was considered as a combination of active pressure (circular curve) and pressure due to the lateral load (sine curve). The combination of this two functions will produce the pressure distribution similar to **Figure 5.3a**.

Proposed Method

The following steps describe in detail the suggested method for determining the ultimate capacity of a mast arm drilled shaft under torsional and lateral loading conditions.

1- Calculate the load, moments from the mast arms (Figure 5.4)

2- Transfer the loads and moments to the drilled shaft (Figure 5.5)

3- Determine the resultant lateral force and overturning moment (Figure 5.6)

4- Using the subgrade reaction method determine the soil pressure along the shaft (Figure 5.7)

5- Distribute the lateral pressure around the shaft perimeter at specified depths (Figure 5.8)

6- Obtain the resultant pressure around the shaft perimeter at specified depths (Figure 5.9)

7- Set the threshold lateral pressure using Rankin's method along the shaft depth (Figure 5.10)

8- Integrate the net soil pressure along the shaft (Figure 5.11)

9- Determine the maximum torsional resistance using

$$\textit{Maximum Torsional Resistance } \tau = p_h \tan \delta \qquad 5.6$$

where:

p_h = Integrate the net soil pressure along the shaft (Step 8)

δ = soil-shaft angle of friction $\approx \varphi$ = soil angle of friction

The assumption of $\delta = \varphi$ may be valid especially for the dry boreholes and for the polymer slurries. It is recommended that a factor of 0.5 to 0.6 to be used when attapulgite or bentonite slurries are used.

1- Loading Conditions on Mast Arm Structure

* Mz= Over turning moment due to the weight of the arm

* Mx = overturning moment due to the wind effect
* Fz = Wind Force on the mast assembly
* Fx = 20% of Fz (AASHTO requirements)
* M_T = torsional moment due to wind effect

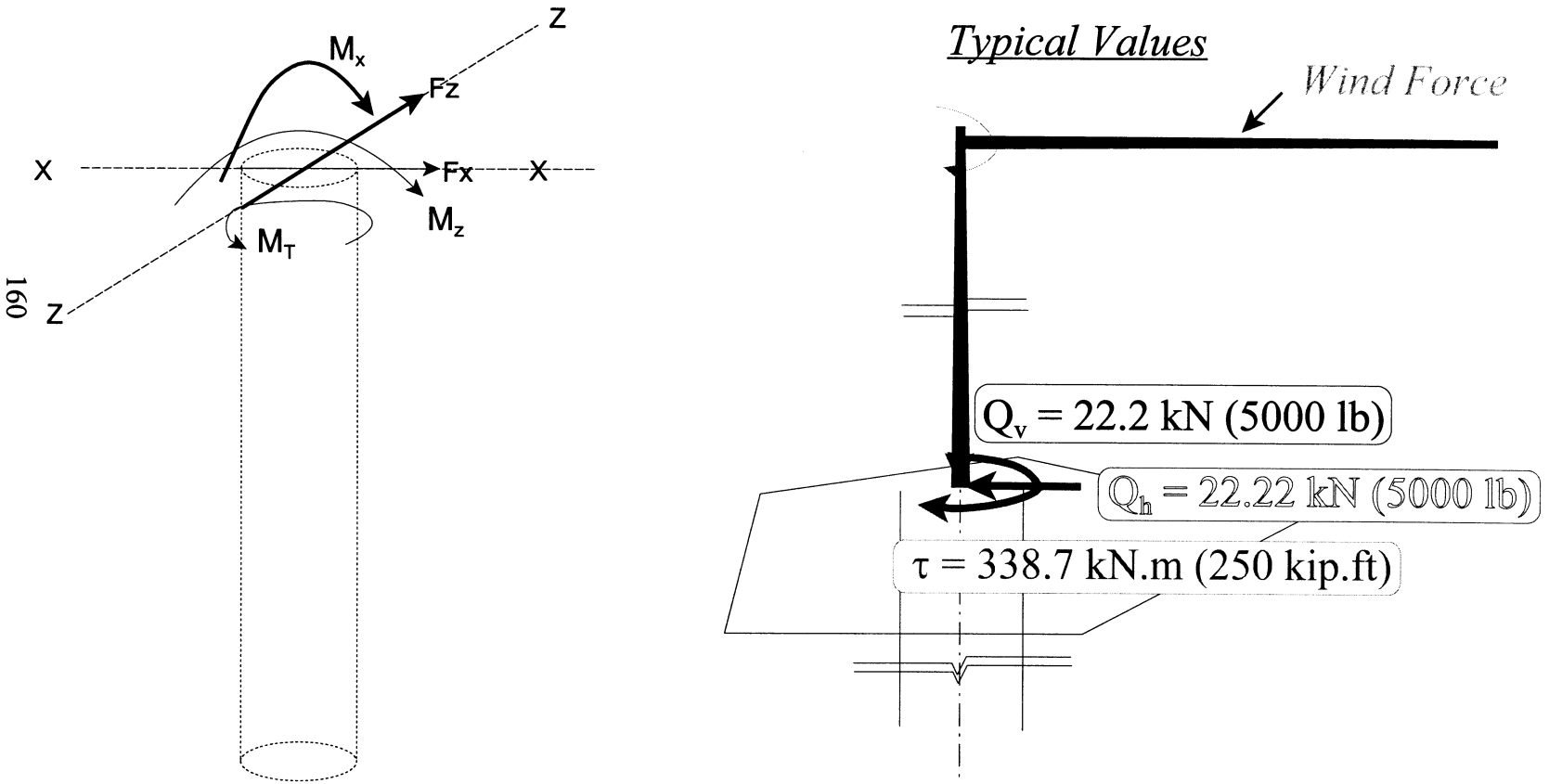

Figure 5.4 Loads and moments from the mast arms

2- APPLIED LOADS:

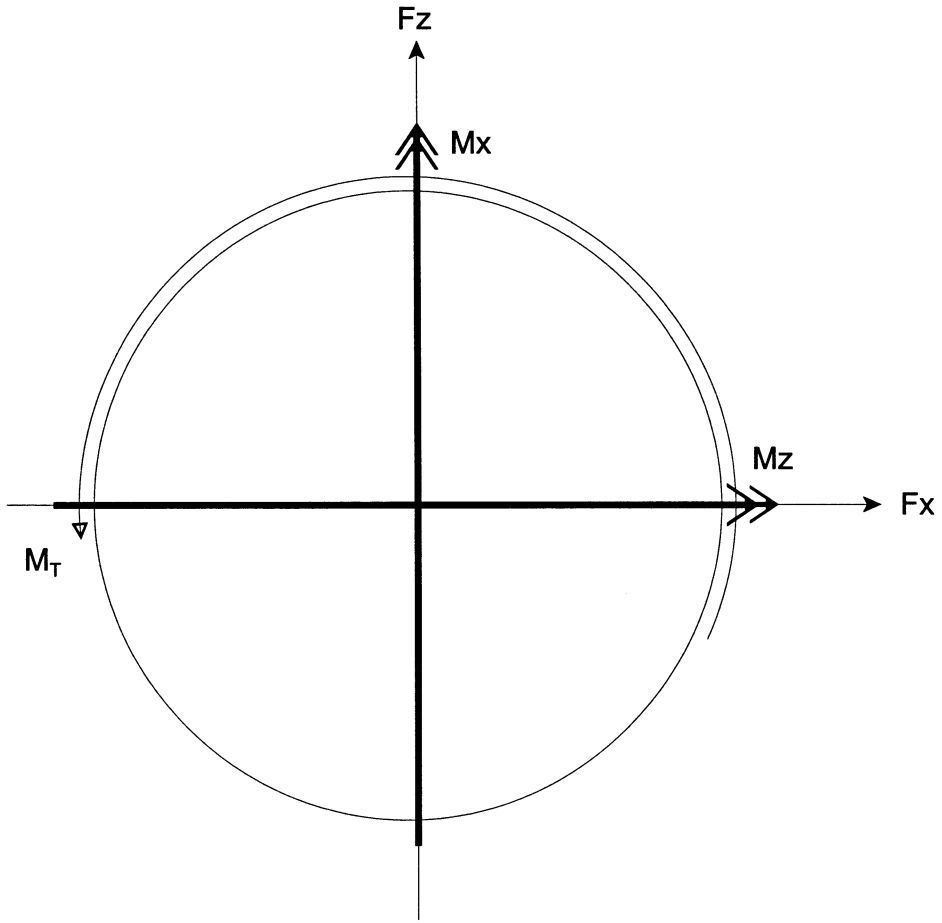

Figure 5.5 Distribution of the loads and moments from the mast arms on the drilled shaft axes

3- RESULTANTS OF THE APPLIED LOADS:

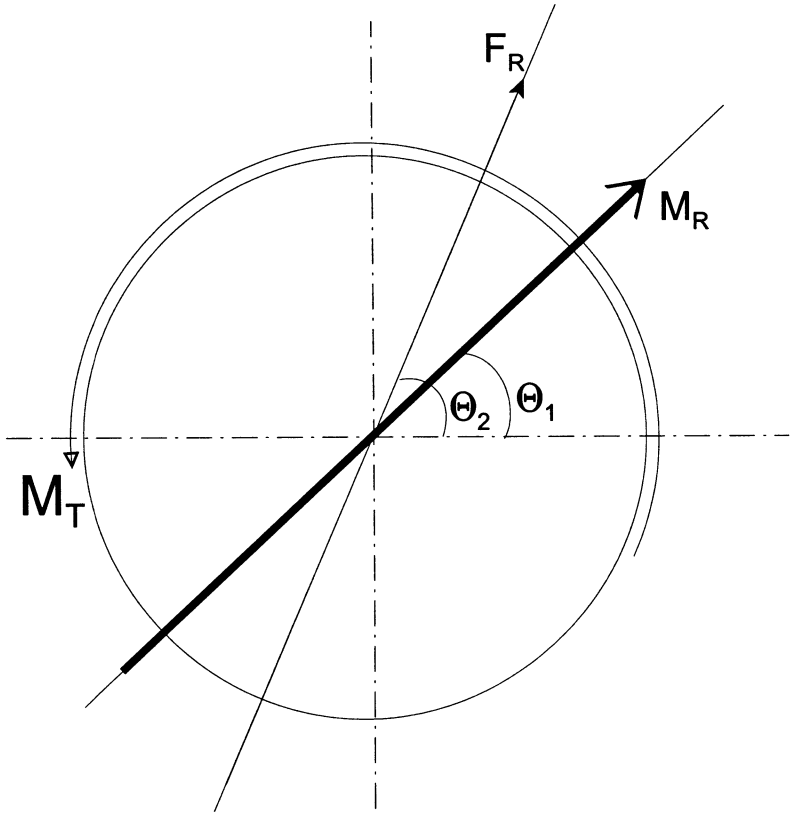

Figure 5.6 Resultant load and moment at the foundation level

4- SOIL PRESSURES FROM OUT OF PLANE LOADS:

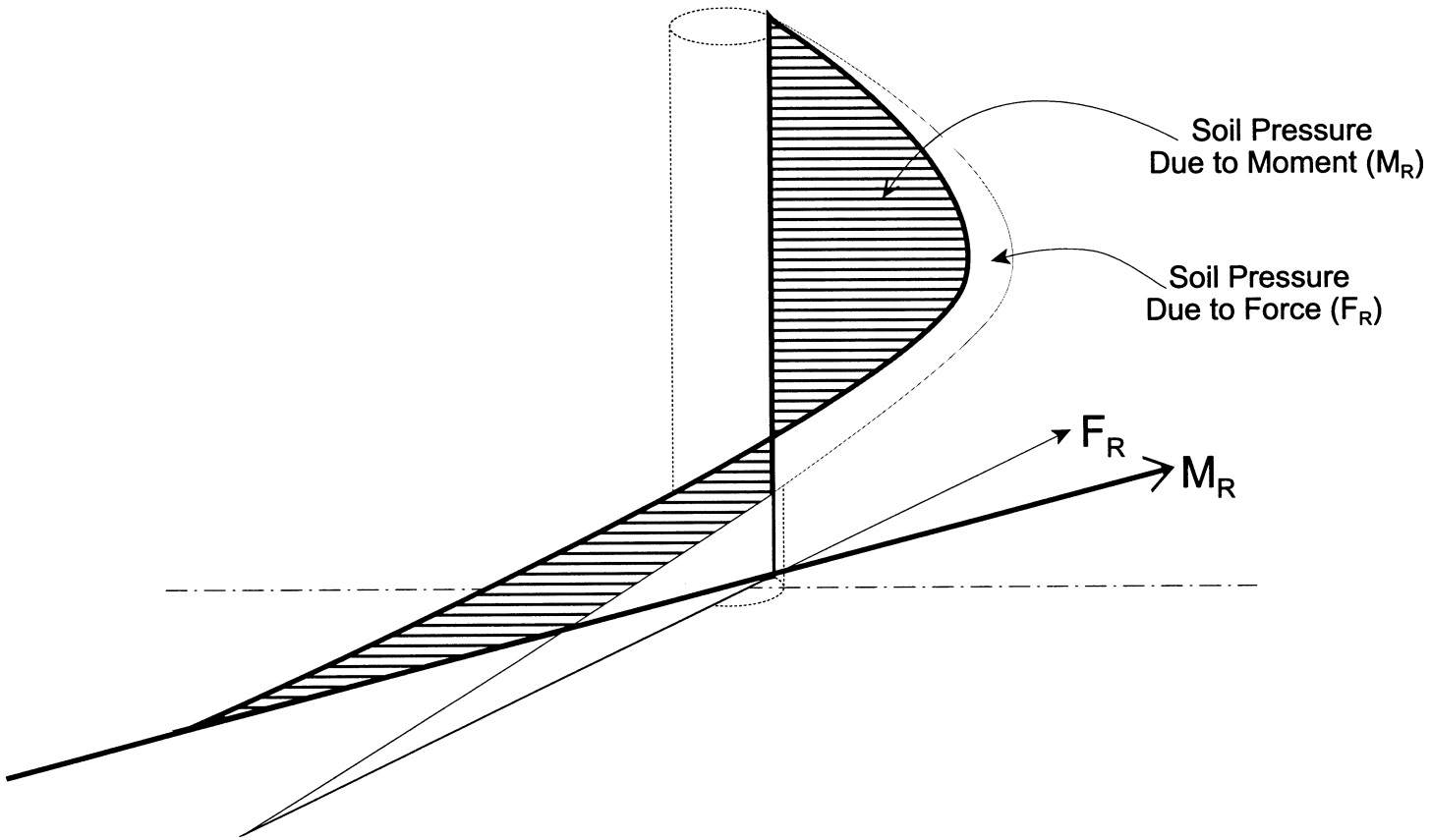

Figure 5.7 Distribution of the earth pressure due to the resultant load and moment using the subgrade reaction method

5- SOIL PRESSURES FROM OUT OF PLANE LOADS:

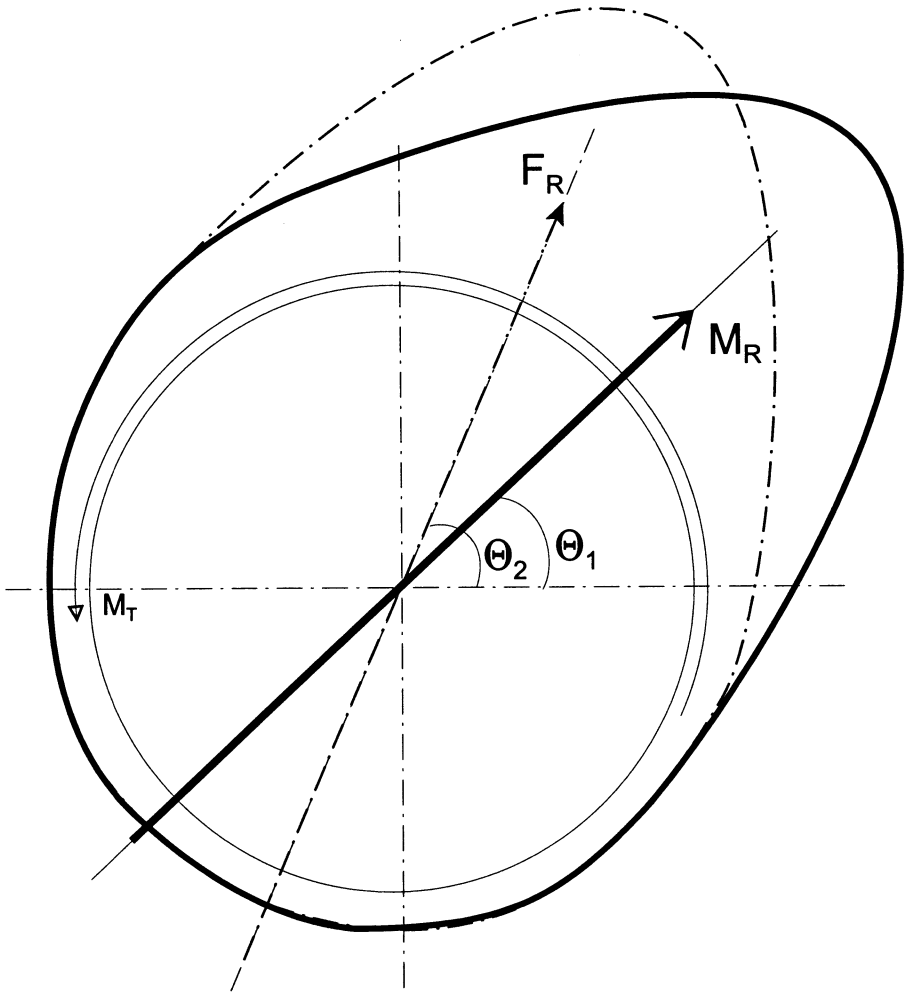

Figure 5.8 Distribution of the earth pressure due to the resultant load and moment at each depth along the shaft

6- OBTAINING RESULTANT SOIL PRESSURE:

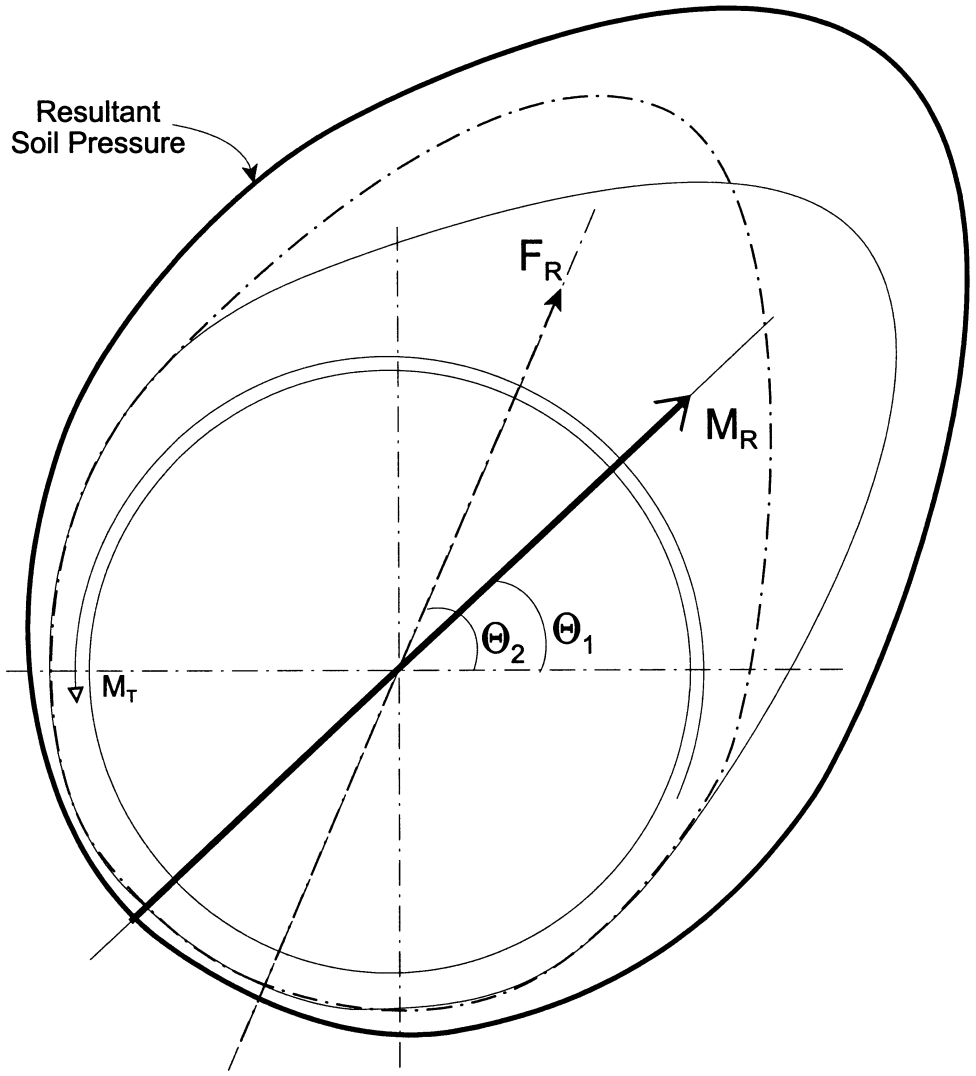

Figure 5.9 Resultant earth pressure at each depth along the shaft

7- MAXIMUM STRESSES ON THE SHAFT

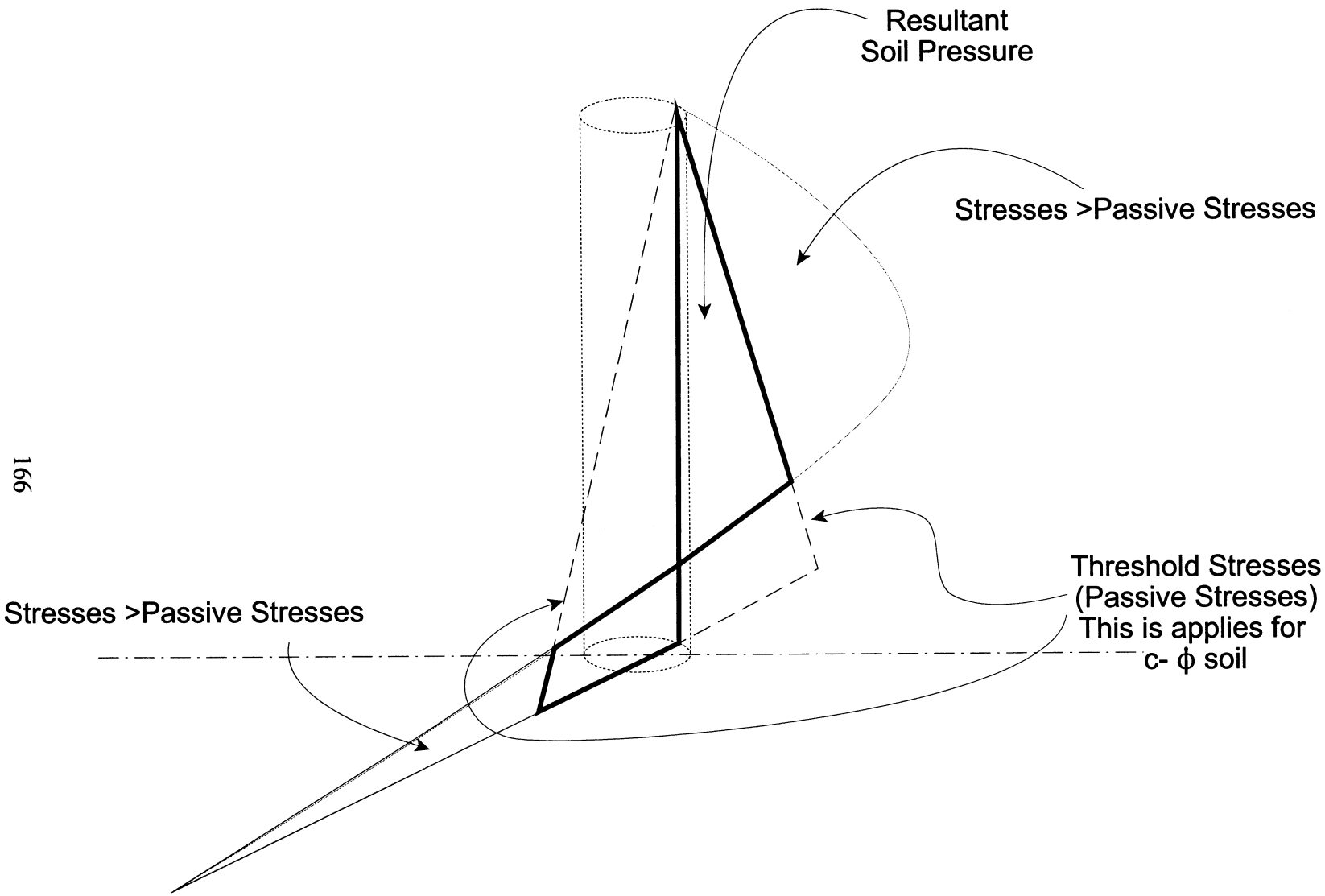

Figure 5.10 Setting the threshold pressure (Rankin's Pressure) at each depth along the shaft

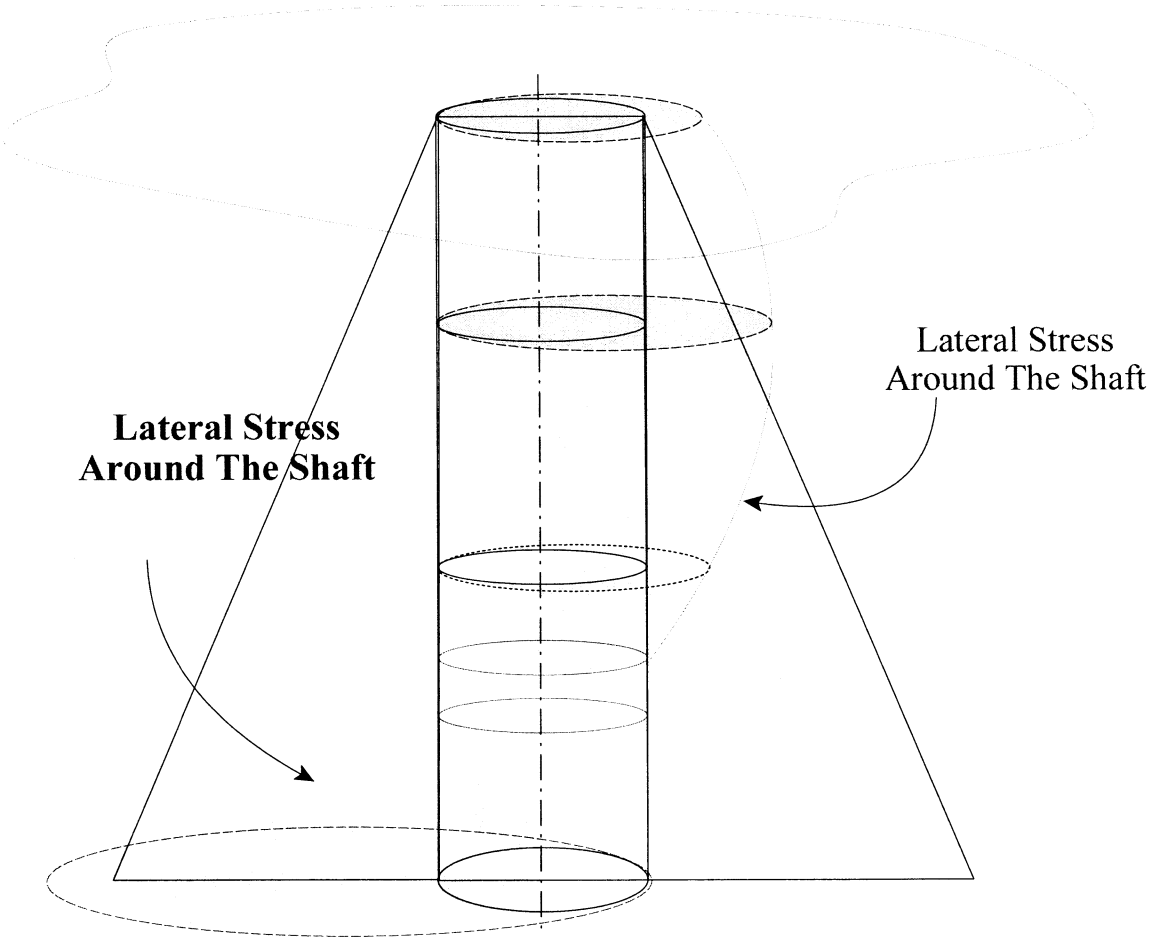

Figure 5.11 Final Pressure along the shaft

CHAPTER 6

CONCLUSION

Based on the results from this study, it can be concluded the following:

1- Including lateral loads is essential for determining the ultimate torsional capacity of mast arm drilled shaft

2- Using a simple torsional load underestimates the carrying capacity of the shaft

3- Method of construction is an important factor in estimating the load transfer perimeter of drilled shaft.

4- Lateral load of a magnitude equal to the applied torque increased the torsional capacity by about two folds.

5- Increasing the lateral load beyond the torque value may not appreciate the torsional capacity.

From the limited laboratory results it was found:

6- Reduction factors in the load transfer when mineral slurries are used can range from 0.35 to 0.5.

7- Attapulgite slurry has higher reduction factors.

8- Reduction factors in the load transfer when polymer slurries are used can range from 0.7 to 0.8. These values are for concentrations between 1:800 and 1:400.

9- The reduction factors may decrease if polymer concentration increased to 1 part polymer to 200 part water.

10- As for the mineral slurries high polymer concentration is helpful in reducing slurry penetration.

However, the difficulty of high concentrations (1:200) may arise during concrete placement in the boreholes.

11- Fluid loss in polymer slurries is higher than mineral slurries.

12- The effect of polymer slurry on the concrete material was on the positive side as compared with the bentonite slurry. Polymer slurry caused some itching in the concrete when a full scale shaft was exposed. Although it is not fully known, but other studies by Majano and O'Neill (1993) supported this behavior.

13- A drilled shaft constructed using bentonite slurry exhibited load capacity of about 50 percent as compared with the dry borehole shaft.

14- A drilled shaft constructed using polymer slurry performed as well as the dry hole shaft.

15- Using the suggested analytical method in this study, one can determine the ultimate capacity of a drilled shaft subjected to lateral and torsional loads. A comparison between all the FDOT methods and other methods using limit equilibrium approach for the lateral earth pressure is presented in **Table 6.1**. A close comparison of the factor of safety was found between the suggested method and District 5 method. However, as it was stated earlier in this study, the existing methods consider only the simple torsional load on the drilled shaft without including the lateral loads and the overturning moments. Such combined loads may significantly influence the torsional capacity of the drilled shaft if the magnitudes of these loads or the conditions of the surrounding soil/soil layers are different.

Table 6.1 Comparison between various methods

All results of these analyses are shown as summarized in the following table.

Mx = 187.35 kip.ft Vx = 1.83 kip Shaft Length = 20 ft Soil Unit weight = 110 lb/ft^3

Mz = 131.88 kip.ft Vz = 9.16 kip Shaft diameter = 4 ft Soil Friction = 30°

Torsional Moment , Mt = 300.11 kip.ft n_h = 60 lb/in^3 Soil-Shaft Friction = 30°

Case # 1 Case # 2

METHOD	SIDE RESISTANCE (Kips-ft) (Dry)	SIDE RESISTANCE (Kips-ft) (Submerged)	BASE RESISTANCE (Kips-ft)	TOTAL TORSIONAL RESISTANCE, T (Dry)	TOTAL TORSIONAL RESISTANCE, T (Submerged)	FS = T/Mt (Dry)	FS = T/Mt (Submerged)
STRUCTURAL DESIGN OFFICE METHOD (SDO)	159.614	69.069	28.053	187.667	97.123	0.625	0.323
DISTRICT 5 METHOD	319.226	138.138	20.04	339.266	158.178	1.13	0.527*
DISTRICT 7 METHOD	319.226	138.138	23.85	343.067	161.988	1.14	0.5399
DISTRICT 5 PROPOSED METHOD	492.009	212.944	31.80	523.899	212.976	1.74	0.71
NEW YORK DOT METHOD	351.026	169.938	-	351.026	169.938	1.17	0.566
PL – METHOD	319.276	138.138	31.80	351.026	169.938	1.17	0.566
BRINCH HANSEN'S METHOD	-	1665.44	30 ***	-	1695.44	-	5.6
BROMS METHOD	768.0	356	30 ***	798	380	2.66	1.26
P – Y CURVE METHOD (LPILE PROGRAM)	480	480	30 ***	510	510	1.7	1.7
MODULUS OF SUBGRADE REACTION APPROACH METHOD	715.415	496.40	30 ***	745.415	526.4	2.48	1.75
Dr. Tawfiq's Method	300	186	30 ***	330	216	1.1	0.72

* Because of high β-value.

** Because of high kq-value.

*** Base torsion resistance ≈ 10% of side torsion resistance.

Case # 1 = Dry Soil along the total length

Case # 2 = Submerged Soil along the total length

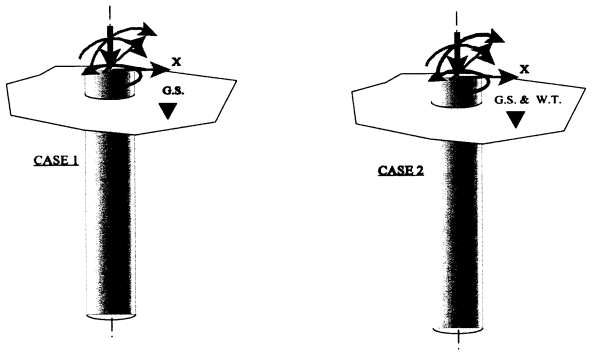

REFERENCES

Bowles, Joseph E., Foundation Analysis and Design, McGraw Hill, New York, 1988.

Das, Braja M., Principles of Foundation Engineering, PWS-Kent Publishing Company, Boston, Massachusetts, 1984.

Davisson M. T. and Prakash, S., "A Review of Soil Pile Behavior," Highway Research Record, No. 39, 1963, pp. 25-48.

Matlock, H. and Reese, L. C., "Foundation Analysis of Offshore Pile Support Structures," Proceedings Fifth International Conference on Soil Mechanics an Foundation Engineering, Paris, Vol. 2, 1961, pp. 91-97.

Matlock, H. and Reese, L. C., "Generalized Solutions for Laterally Loaded Piles, Transactions of the American Society of Civil Engineers, Vol. 127, 1962, part 1 pp. 1220-1247.

Palmer, L. A. and Thompson, J. B., "The Earth Pressure and Deflection Along the Embedded Lengths of Piles Subjected to Lateral Thrust," Proceedings Second International Conference on Soil Mechanics and Foundation Engineering, Rotterdam, Holland, Vol. V, 1948, pp. 156-161.

Poulos, H. G., "Behavior of Laterally Loaded Piles: I-Single Piles," J. Soil Mech. Found. Div., ASCE, Vol. 97, No. SM. 5, 1971a, pp. 711-731.

Poulos, H. G., "Behavior of Laterally Loaded Piles: II-Pile Groups," J. Soil Mech. Found. Div. ASCE, Vol. 97, No. SM, 1971b, pp. 733-751.

Poulos, H. G., "Analysis of Pile Groups Subjected to Vertical and Horizontal Loads," Aust. Geomechanics J., Vol., G4, No. 1, 1974, pp. 26-32.

Poulos, H. G. and Davis, E. H., Pile Foundation Analysis and Design. Wiley, New York, 1980.

Poulos, H. G. and Madhav, M. R., "Analysis of the Movement of Battered Piles," Proceedings 1st Australion-New Zealand Conference on Geomechanics, Melbourne, Australia, 1971, pp. 268-275.

Reese, L. C., O'Neill, M. W., and Smith, E., "Generalized Analysis of Pile Foundations," Proceedings J. Soil Mech. Found. Div., Vol. 96, No. SM1, 1970, pp. 235-250.

Reese, L. C. and Welch R. C., "Lateral Loading of Deep Foundations in Stiff Clay," J. Geotech. Eng. Div., ASCE, Vol. 101, No. GT 7, July 1975, pp. 633-649.

Reese, L. C. and Matlock, H., "Non-dimensional Solutions for Laterally Loaded Piles with Soil Modulus Assumed Proportional to Depth," Proceedings 8th Texas Conference on Soil Mechanics and Foundation Engineering, Austin, TX, 1956, pp. 1-41.

Smith, Trevor D. (1989), "Fact or Fiction: A Review of Soil Response to a Laterally Moving Pile",

Foundation Engineering: Current Principles and Practices, Vol. 1, p. 588 - 598.

MathCad

Working Example for the Proposed Method

DRILLED SHAFT UNDER TORSIONAL LOADING ANALYZED BY THE TAWFIQ-MTENGA METHOD

INPUT DATA

Load Acting on Shaft

Moment about the x-axis $M_x := 187.35 \cdot kip \cdot ft$ Shear in the x-axis direction: $V_x := 1.83 \cdot kip$

Moment about the z-axis $M_z := 131.88 \cdot kip \cdot ft$ Shear in the z-axis direction: $V_z := 9.16 \cdot kip$

Torsional Moment: $M_{tor} := 300.11 \cdot kip \cdot ft$

Shaft Geometry

Shaft Diameter: $D := 4 \cdot ft$ Radius (computed): $R := \frac{D}{2}$ $R = 2 \cdot ft$

Shaft Length: $L := 20 \cdot ft$ Water Table from top of shaft $H_w := 5 \cdot ft$

Soil and Shaft Material Properties

Soil Unit Weight: $\gamma := 110 \cdot \frac{lbf}{ft^3}$

Angle of Friction : $\phi := 30 \cdot deg$

Cohession Coefficient: $C := 0$

$Nh := 60 \cdot \frac{lbf}{in^3}$

Modulus of Elasticity of the Shaft Material: $E := 3600000 \cdot psi$

Mesh Size Control Along Length $n := 50$ Along Circumference $nang := 50$

CALCULATIONS

Resultant of the Bending Moment (x-z-plane) $M_R := \sqrt{\left(M_x^2 + M_z^2\right)}$ $M_R = 229 \cdot kip \cdot ft$

Resultant of the Shear Forces (x-z-plane): $V_R := \sqrt{\left(V_x^2 + V_z^2\right)}$ $V_R = 9 \cdot kip$

Orientation of moment resultant from the x-axi $\psi_m := \operatorname{atan}\left(\frac{M_z}{M_x}\right)$ $\psi_m = 35.143 \cdot \text{deg}$

Orientation of shear resultant from the x-axis $\psi_s := \operatorname{atan}\left(\frac{V_z}{V_x}\right)$ $\psi_s = 78.702 \cdot \text{deg}$

Soil Passive Pressure Coefficient $kp := \frac{1 + \sin(\phi)}{1 - \sin(\phi)}$ $kp = 3$

$I := \frac{\pi \cdot \left(\frac{D}{2}\right)^4}{4}$ $PS := E \cdot I$ $T := \left(\frac{PS}{Nh}\right)^{.2}$ $T = 2.777$ m

$Z := L \cdot \frac{1}{T}$ $Z = 2.195$ $Z_w := H_w \cdot \frac{1}{T}$ $Z_w = 0.549$

Ap and Bp values graphed (tabulated) for z-values of 1.0, 1.5, 2.0, 2.5, 3.0, 3.5, 4.0, 5.0 and 10.0. For any other z-value a 2nd order interpolation will have have to be implemented.

The Curve coeffecients for the know values (of Zm) are given by matrix A and B below .

The Interpolation process follows

$$Zm := \begin{bmatrix} 1 \\ 1.5 \\ 2 \\ 2.5 \\ 3 \\ 3.5 \\ 4 \\ 5 \\ 10 \end{bmatrix}$$

Find position of desired z-value relative to the known z-values (Zm)

$pos := if\left(Z < Zm_0, \text{"LW-Err"}, if\left(Z < Zm_1, 0, if\left(Z < Zm_2, 1, if\left(Z < Zm_3, 2, if\left(Z < Zm_4, 3, if\left(Z < Zm_5, 4, if\right.\right.\right.\right.\right.\right.$

$pos = 2$

Position :=
- k1 ← "Value Out of Lower Range" if pos="LW-Err"
- k3 ← "Value Out of Upper Range" if pos="UP-Err"
- if pos=7
  - k1 ← 6
  - k2 ← 7
  - k3 ← 8
  - zb1 ← Zm_6
  - zb2 ← Zm_7
  - zb3 ← Zm_8
- if pos≠7
  - k1 ← pos
  - k2 ← pos + 1
  - k3 ← pos + 2
  - zb1 ← Zm_{pos}
  - zb2 ← Zm_{pos+1}
  - zb3 ← Zm_{pos+2}
- [k1, k2, k3, zb1, zb2, zb3]

$$Position = \begin{bmatrix} 2 \\ 3 \\ 4 \\ 2 \\ 2.5 \\ 3 \end{bmatrix}$$

$k1 := Position_0$
$k2 := Position_1$
$k3 := Position_2$

$zb1 := Position_3$
$zb2 := Position_4$
$zb3 := Position_5$

Curve coefficients for Ap and Bp curves for z-values of 1.0, 1.5, 2.0, 2.5, 3.0, 3.5, 4.0, 5.0 and 10.0.
Appropriate values to interpolate to obtained Ap and Bp values for z-values between the above

$$A := \begin{bmatrix} 0 & 0 & 0 & 0 & 0 & 0 & 0 & 0 & 0 \\ -17.71 & -7.829 & -4.378 & -2.705 & -2.578 & -2.697 & -2.651 & -2.559 & -2.811 \\ 23.653 & 6.973 & 2.922 & 1.442 & 1.685 & 2.257 & 2.259 & 2.118 & 2.662 \\ 0 & 0 & 0 & 0 & -0.224 & -0.615 & -0.616 & -0.547 & -0.921 \\ 0 & 0 & 0 & 0 & 0 & 0.06 & 0.056 & 0.045 & 0.15 \\ 0 & 0 & 0 & 0 & 0 & 0 & 0 & 0 & -0.012 \\ 0 & 0 & 0 & 0 & 0 & 0 & 0 & 0 & 0.0003 \end{bmatrix}$$

$$B := \begin{bmatrix} 0 & 0 & 0 & 0 & 0 & 0 & 0 & 0 & 0 \\ -11.899 & -7.191 & -3.382 & -2.155 & -1.749 & -1.638 & -1.632 & -1.67 & -1.535 \\ -75.232 & 7.682 & 3.16 & 2.07 & 1.802 & 1.765 & 1.818 & 1.945 & 1.764 \\ 400.16 & -0.358 & -0.388 & -0.42 & -0.459 & -0.504 & -0.586 & -0.7344 & -0.693 \\ -679.91 & -0.262 & -0.164 & -0.104 & -0.0578 & -0.02 & 0.031 & 0.1056 & 0.1233 \\ 547.35 & 0.242 & 0.122 & 0.0713 & 0.0445 & 0.029 & 0.0145 & -0.0026 & -0.0102 \\ -168.6 & -0.051 & -0.0194 & -0.0094 & -0.0053 & -0.0034 & -0.0019 & -0.0004 & 0.0003 \end{bmatrix}$$

$j := 0 .. n$ $\qquad Z_{max} := Z$

$k1 = 2$ $\qquad k2 = 3$ $\qquad k3 = 4$

$$z_j := \frac{Z_{max}}{n} \cdot j$$

$$Ap1_j := \sum_{i=0}^{6} A_{i,k1} \cdot (z_j)^i \qquad Ap2_j := \sum_{i=0}^{6} A_{i,k2} \cdot (z_j)^i \qquad Ap3_j := \sum_{i=0}^{6} A_{i,k3} \cdot (z_j)^i$$

$$Bp1_j := \sum_{i=0}^{6} B_{i,k1} \cdot (z_j)^i \qquad Bp2_j := \sum_{i=0}^{6} B_{i,k2} \cdot (z_j)^i \qquad Bp3_j := \sum_{i=0}^{6} B_{i,k3} \cdot (z_j)^i$$

Interporlation to Particular Z-value

$$Ap_j := \frac{(Z - zb2)\cdot(Z - zb3)}{(zb1 - zb2)\cdot(zb1 - zb3)} \cdot Ap1_j + \left[\frac{(Z - zb1)\cdot(Z - zb3)}{(zb2 - zb1)\cdot(zb2 - zb3)} \cdot Ap2_j + \frac{(Z - zb2)\cdot(Z - zb1)}{(zb3 - zb2)\cdot(zb3 - zb1)} \cdot Ap \right.$$

$$Bp_j := \frac{(Z - zb2)\cdot(Z - zb3)}{(zb1 - zb2)\cdot(zb1 - zb3)}\cdot Bp1_j + \left[\frac{(Z - zb1)\cdot(Z - zb3)}{(zb2 - zb1)\cdot(zb2 - zb3)}\cdot Bp2_j + \frac{(Z - zb2)\cdot(Z - zb1)}{(zb3 - zb2)\cdot(zb3 - zb1)}\cdot Bp\right.$$

$zb1 = 2$ $zb2 = 2.5$ $zb3 = 3$ $Z = 2.195$

Variation of Ap Values (Pink Curve are interpolated Values for Specific z-value)

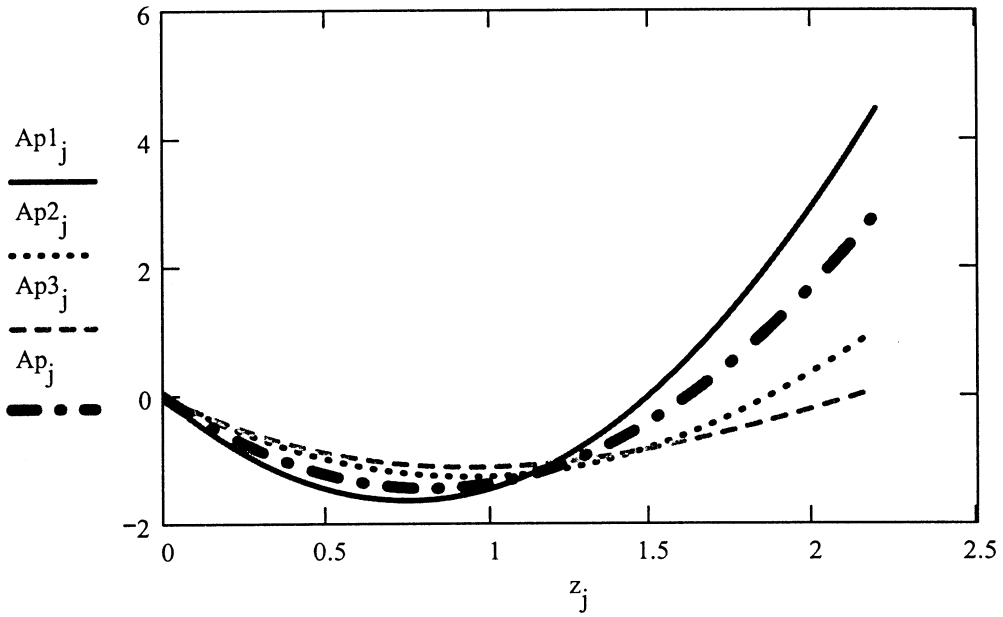

Variation of Bp Values (Pink Curve are interpolated Values for Specific z-value)

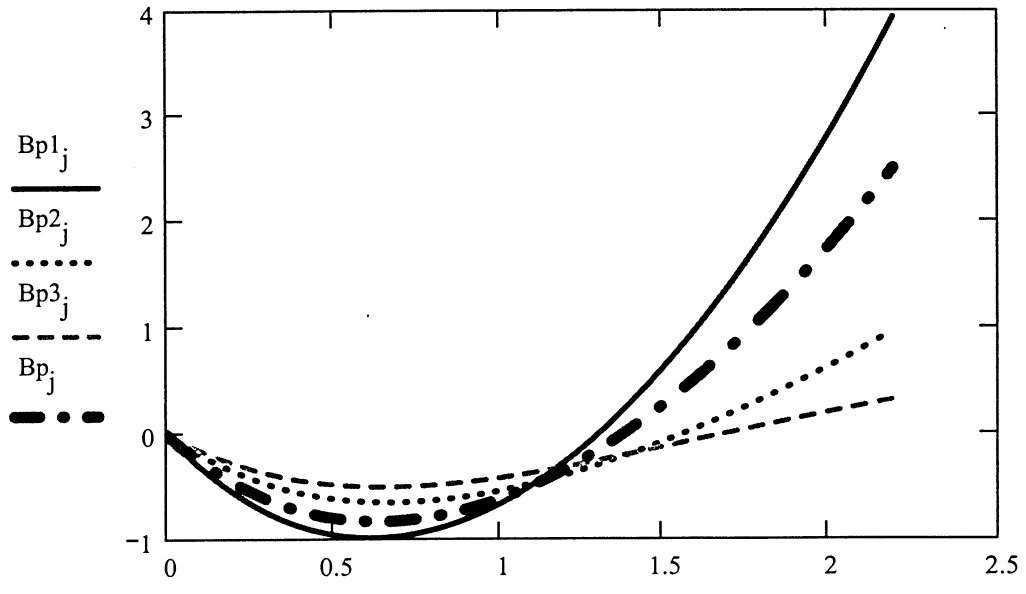

Computation of pressure on the soil created by the shear and bending moment

$$Pa_j := \frac{Ap_j \cdot V_R}{T \cdot ft} \qquad Pb_j := \frac{Bp_j \cdot M_R}{T^2 \cdot ft} \qquad \gamma_w := 62.5 \cdot \frac{lbf}{ft^3}$$

$$Px_j := Pa_j + Pb_j \qquad P_j := |Px_j| \qquad Pas_j := \frac{Ap_j \cdot V_R}{T \cdot ft} \qquad \gamma_{sb} := \gamma - \gamma_w$$

$$Ppassive_j := if\left[z_j \le Z_w, \gamma \cdot \left(z_j \cdot T \cdot kp\right), \gamma \cdot Z_w \cdot T \cdot kp + \gamma_{sb} \cdot \left(z_j - Z_w\right) \cdot T \cdot kp\right]$$

$$Pactive_j := if\left[z_j \le Z_w, \gamma \cdot \left(z_j \cdot T \cdot \frac{1}{kp}\right), \gamma \cdot Z_w \cdot T \cdot \frac{1}{kp} + \gamma_{sb} \cdot \left(z_j - Z_w\right) \cdot T \cdot \frac{1}{kp}\right]$$

$$Pp_j := if\left(|Px_j| > Ppassive_j, Ppassive_j, |Px_j|\right) \qquad Pbs_j := \frac{Bp_j \cdot M_R}{T^2 \cdot ft}$$

$$pm(\theta) := if(\sin(\theta) < 0, 0, \sin(\theta)) \qquad pv(\theta) := if\left(\sin\left(\theta - \psi_s + \psi_m\right) < 0, 0, \sin\left(\theta - \psi_s + \psi_m\right)\right)$$

$$pmv(\theta) := pm(\theta) + pv(\theta)$$

$$f(\theta, pk, pp) := \left[\begin{array}{l} m \leftarrow 0 \\ m \leftarrow \sin(\theta) \ \text{ if } \sin(\theta) > 0 \\ p \leftarrow |pk \cdot m| \\ pr \leftarrow pp \ \text{ if } p > pp \\ pr \leftarrow p \ \text{ if } p < pp \\ pr \end{array}\right] \qquad fa(\theta, pk) := \left[\begin{array}{l} m \leftarrow 1 \\ m \leftarrow 0 \ \text{ if } \sin(\theta) > 0 \\ p \leftarrow |pk \cdot m| \\ p \end{array}\right]$$

$$\Delta T_j := \int_0^{2 \cdot \pi} R^2 \cdot \frac{L}{n} \cdot \tan(\phi) \cdot f\left(\theta, P_j, Ppassive_j\right) d\theta \qquad Tq := \sum_{j=0}^{n} \Delta T_j \qquad Tq = 212 \cdot kip \cdot ft$$

$$\Delta Ta_j := \int_0^{2\cdot\pi} R^2 \cdot \frac{L}{n} \cdot \tan(\phi) \cdot fa\left(\theta, Pactive_j\right) d\theta \qquad Tqa := \sum_{j=0}^{n} \Delta Ta_j \qquad Tqa = 37 \cdot kip \cdot ft$$

$$T_{case1} := Tq + Tqa$$

$$\Delta 2T_j := \int_0^{2\cdot\pi} R^2 \cdot \frac{L}{n} \cdot \tan(\phi) \cdot \left(\left| Pa_j \right| \cdot pv(\theta) + \left| Pb_j \right| \cdot pm(\theta) \right) d\theta$$

$$Tq2 := \sum_{j=0}^{n} \Delta 2T_j \qquad Tq2 = 303 \cdot kip \cdot ft$$

$$\tau(\theta, pm, pv, pp) := \left[\begin{array}{l} m \leftarrow 0 \\ v \leftarrow 0 \\ m \leftarrow \sin(\theta) \text{ if } \sin(\theta) > 0 \\ v \leftarrow \sin\left(\theta - \psi_s + \psi_m\right) \text{ if } \sin\left(\theta - \psi_s + \psi_m\right) > 0 \\ p \leftarrow \left| pv \cdot v + pm \cdot m \right| \\ pr \leftarrow pp \text{ if } p > pp \\ pr \leftarrow p \text{ if } p < pp \\ pr \end{array} \right]$$

$$\tau a(\theta, pm) := \left[\begin{array}{l} m \leftarrow 1 \\ m \leftarrow 0 \text{ if } \sin(\theta) > 0 \\ m \leftarrow 0 \text{ if } \sin\left(\theta - \psi_s + \psi_m\right) > 0 \\ p \leftarrow pm \cdot m \\ p \end{array} \right]$$

$$\Delta 3T_j := \sum_{k=0}^{nang} R^2 \cdot \frac{2\cdot\pi}{nang} \cdot \frac{L}{n} \cdot \tan(\phi) \cdot \tau\left(\frac{2\cdot\pi}{nang} \cdot k, Pb_j, Pa_j, Ppassive_j\right)$$

$$Tq3 := \sum_{j=0}^{n} \sum_{k=0}^{nang} R^2 \cdot \frac{2\cdot\pi}{nang} \cdot \frac{L}{n} \cdot \tan(\phi) \cdot \tau\left(\frac{2\cdot\pi}{nang} \cdot k, Pb_j, Pa_j, Ppassive_j\right) \qquad Tq3 = 225 \cdot kip \cdot ft$$

$$\Delta 3Ta_j := \sum_{k=0}^{nang} R^2 \cdot \frac{2\cdot\pi}{nang} \cdot \frac{L}{n} \cdot \tan(\phi) \cdot \tau a\left(\frac{2\cdot\pi}{nang} \cdot k, Pactive_j\right)$$

$$Tqa3 := \sum_{j=0}^{n} \sum_{k=0}^{nang} R^2 \cdot \frac{2\cdot\pi}{nang} \cdot \frac{L}{n} \cdot \tan(\phi) \cdot \tau a\left(\frac{2\cdot\pi}{nang} \cdot k, Pactive_j\right) \qquad Tqa3 = 28 \cdot kip \cdot ft$$

$$T_{case2} := Tq3 + Tqa3$$

CALCULATIONS

TORSION CAPACITY OF DRILLED SHAFT

CASE 1: Torsional strength with stress limited to passive stress and without phase shift, active stress region included

$$T_{case1} = 249 \cdot kip \cdot ft$$

CASE 2: Torsional strength with stress limited to passive stress and with phase shift, active stress region included

$$T_{case2} = 253 \cdot kip \cdot ft$$

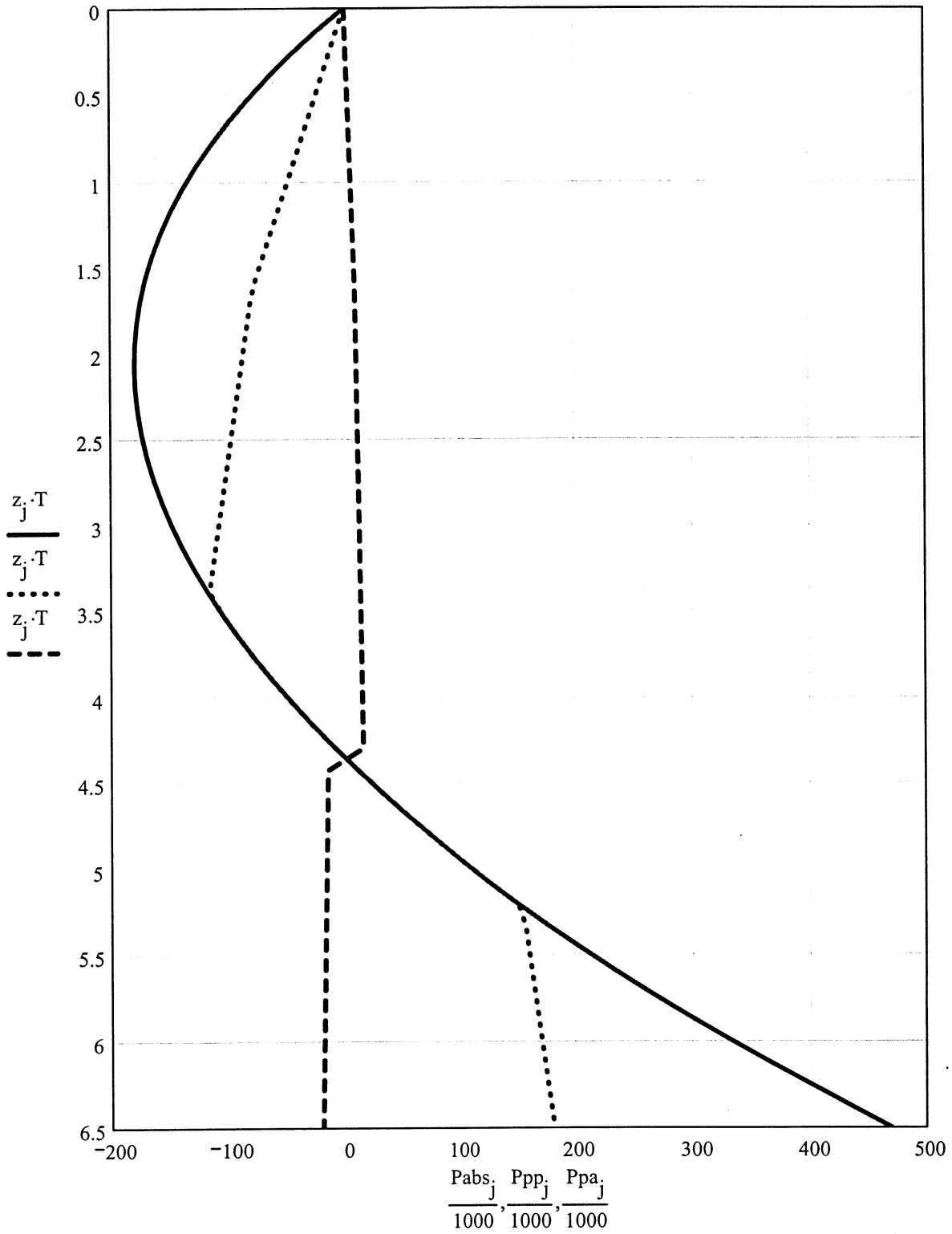

Variation of Stresses With Depth

$jk := 0 .. nang$

$$\alpha_{jk} := \frac{2 \cdot \pi}{nang} \cdot jk$$

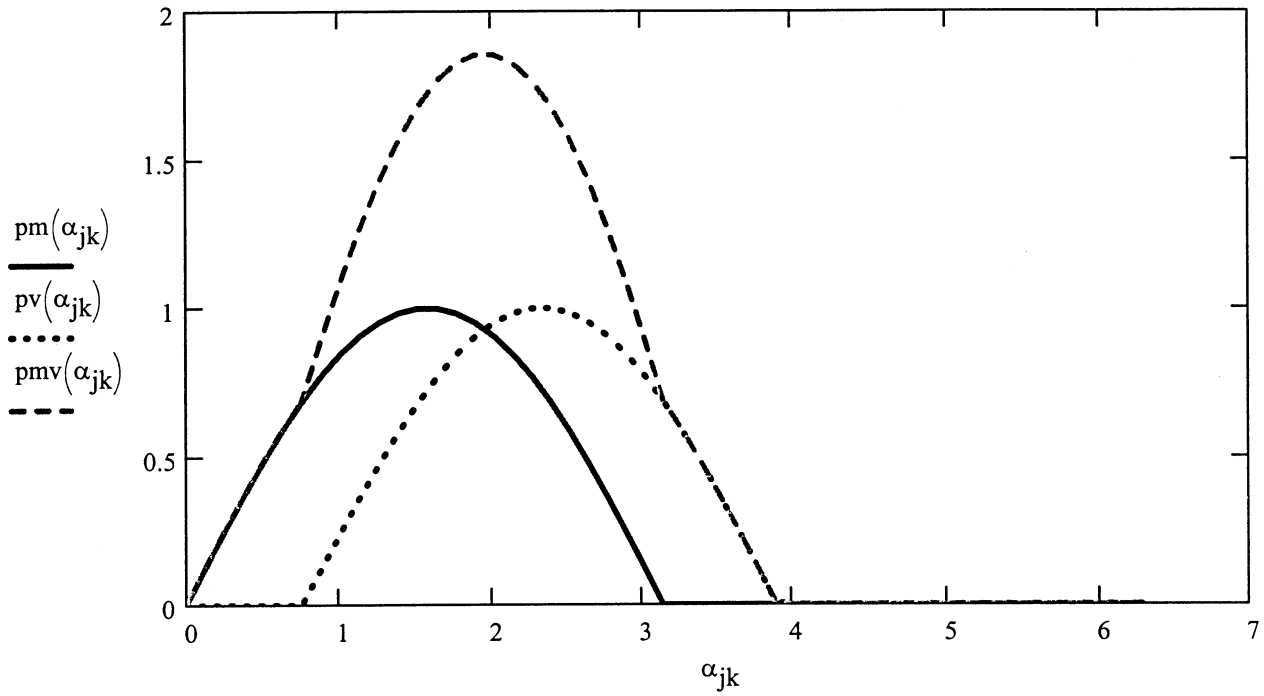

$N \equiv newton$ $kip \equiv 1000 \cdot lbf$

$KN \equiv 1000 \cdot newton$

APPENDIX A

Laboratory Test Results

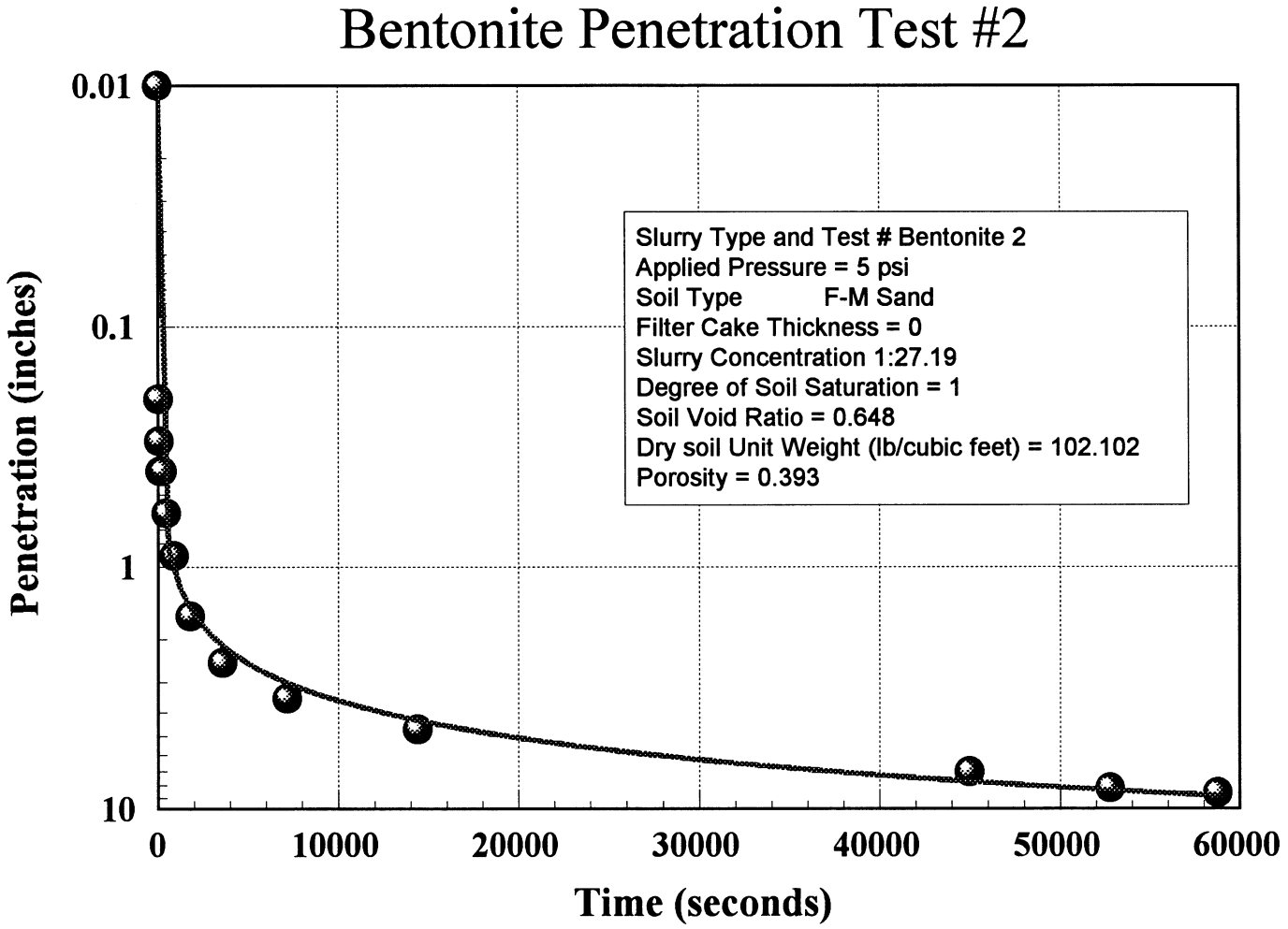

Figure 4.6 Bentonite Slurry Penetration in Sandy Soil Under Hydrostatic Pressure = 5 psi.

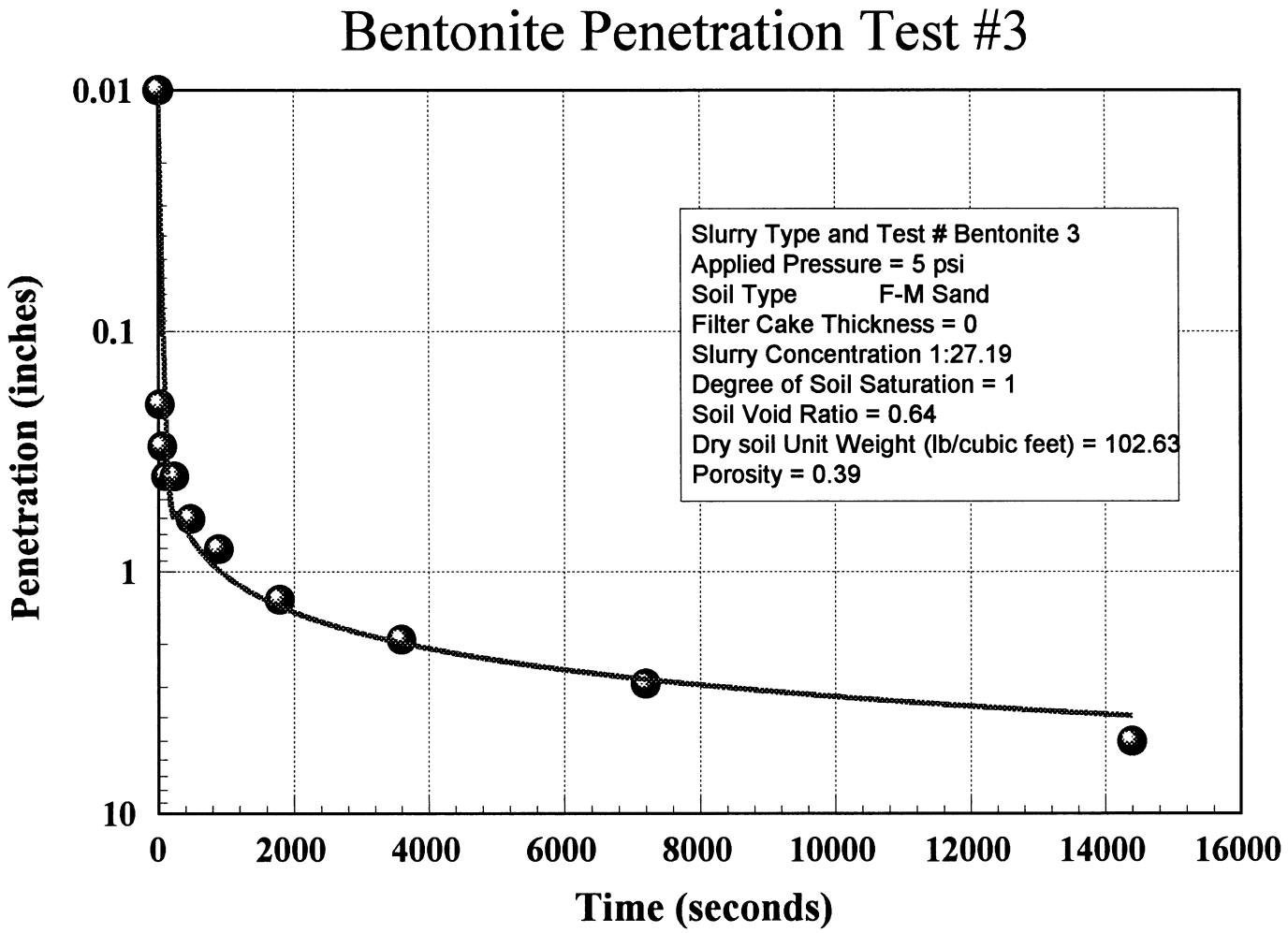

Figure 4.7 Bentonite Slurry Penetration in Sandy Soil Under Hydrostatic Pressure = 5 psi.

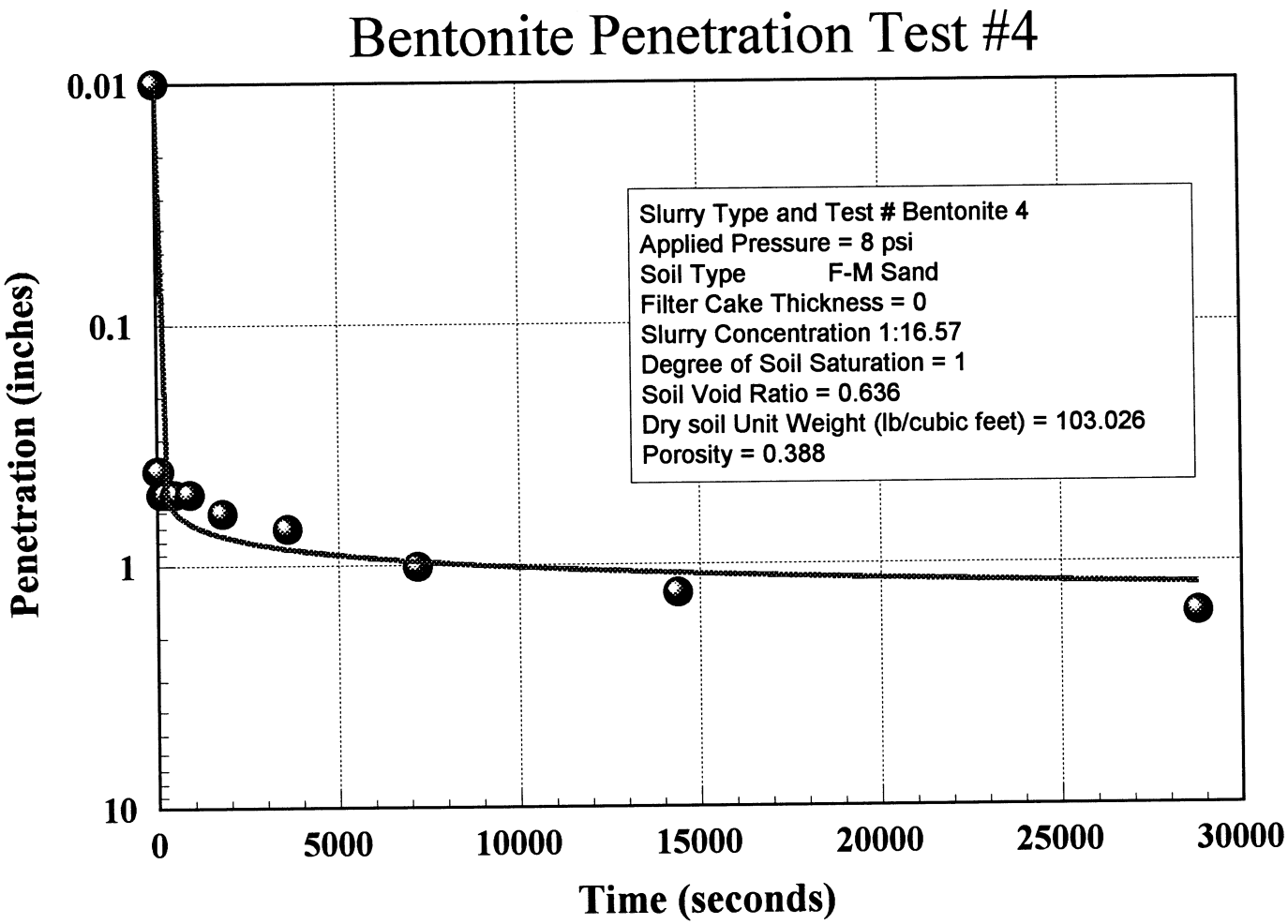

Figure 4.8 Bentonite Slurry Penetration in Sandy Soil Under Hydrostatic Pressure = 8 psi.

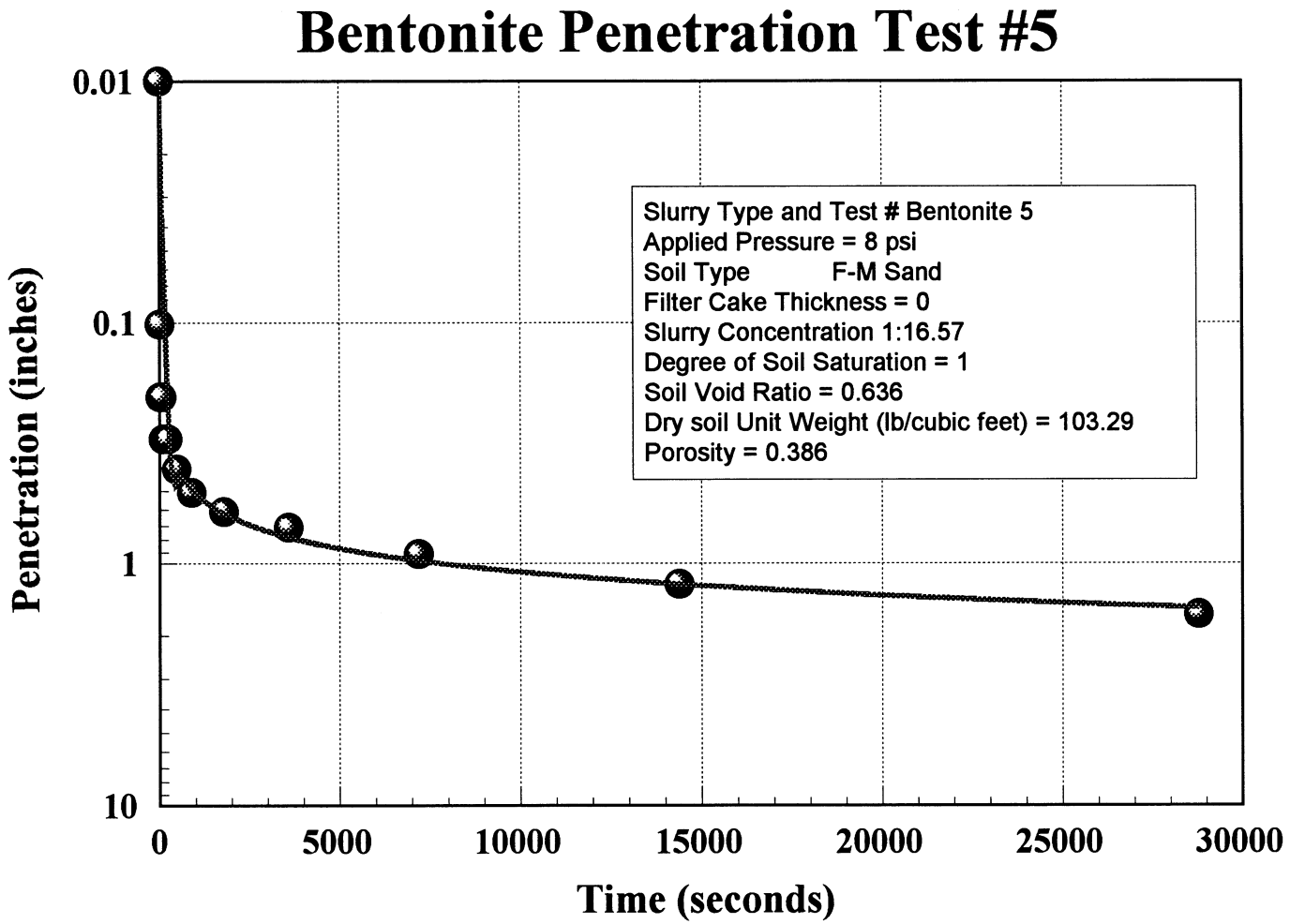

Figure 4.9 Bentonite Slurry Penetration in Sandy Soil Under Hydrostatic Pressure = 8 psi.

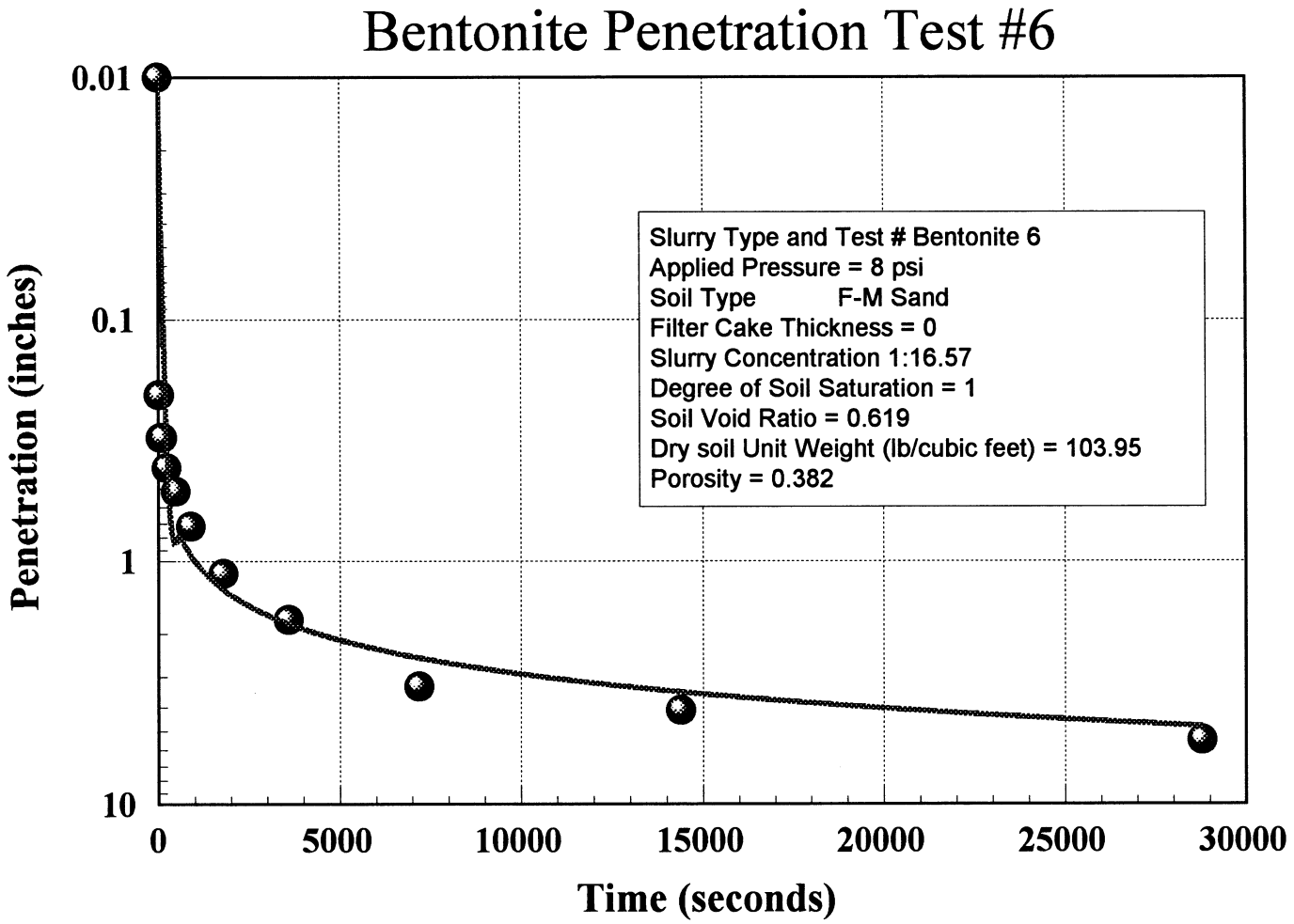

Figure 4.10 Bentonite Slurry Penetration in Sandy Soil Under Hydrostatic Pressure = 8 psi.

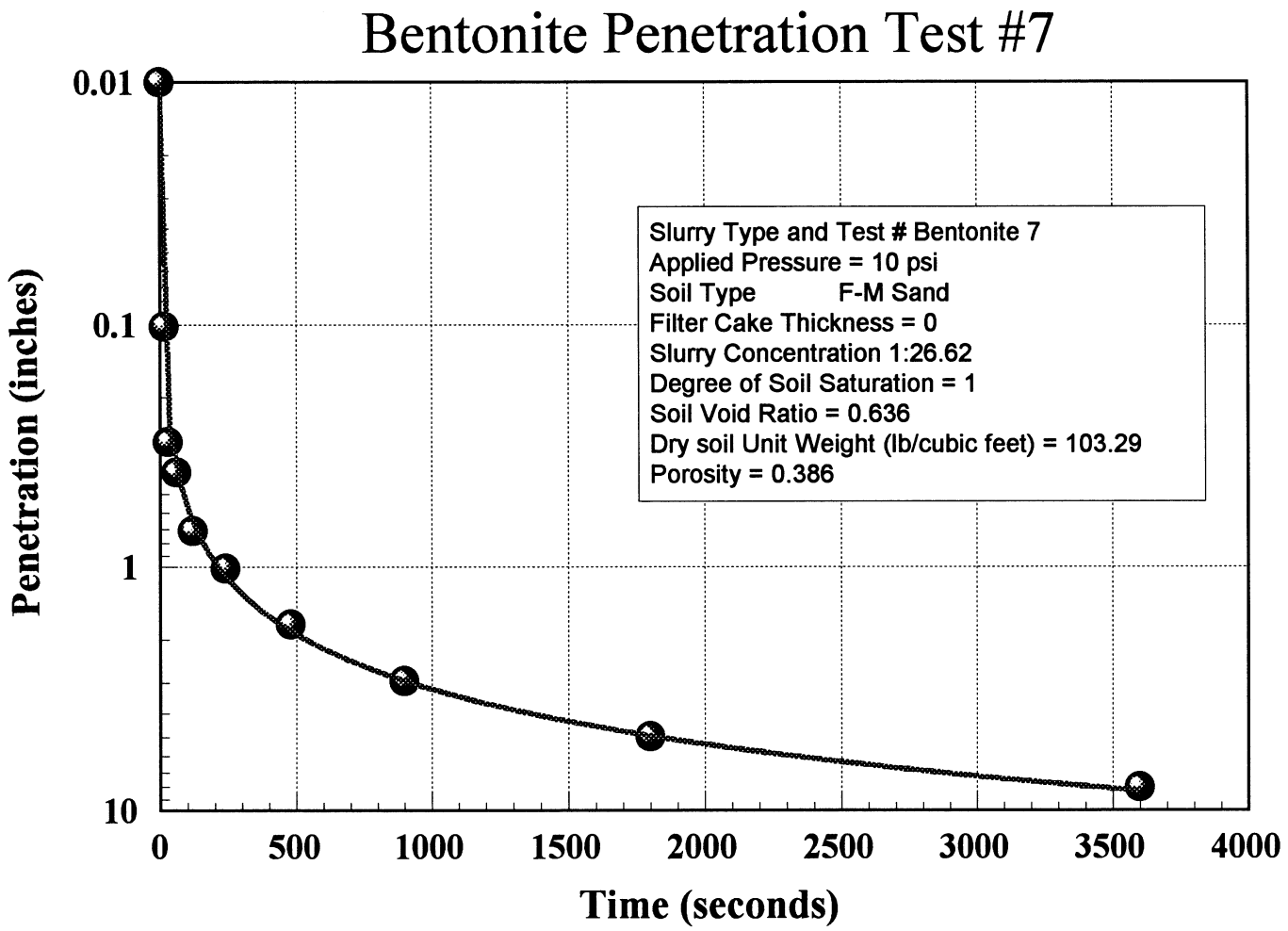

Figure 4.11 Bentonite Slurry Penetration in Sandy Soil Under Hydrostatic Pressure = 10 psi.

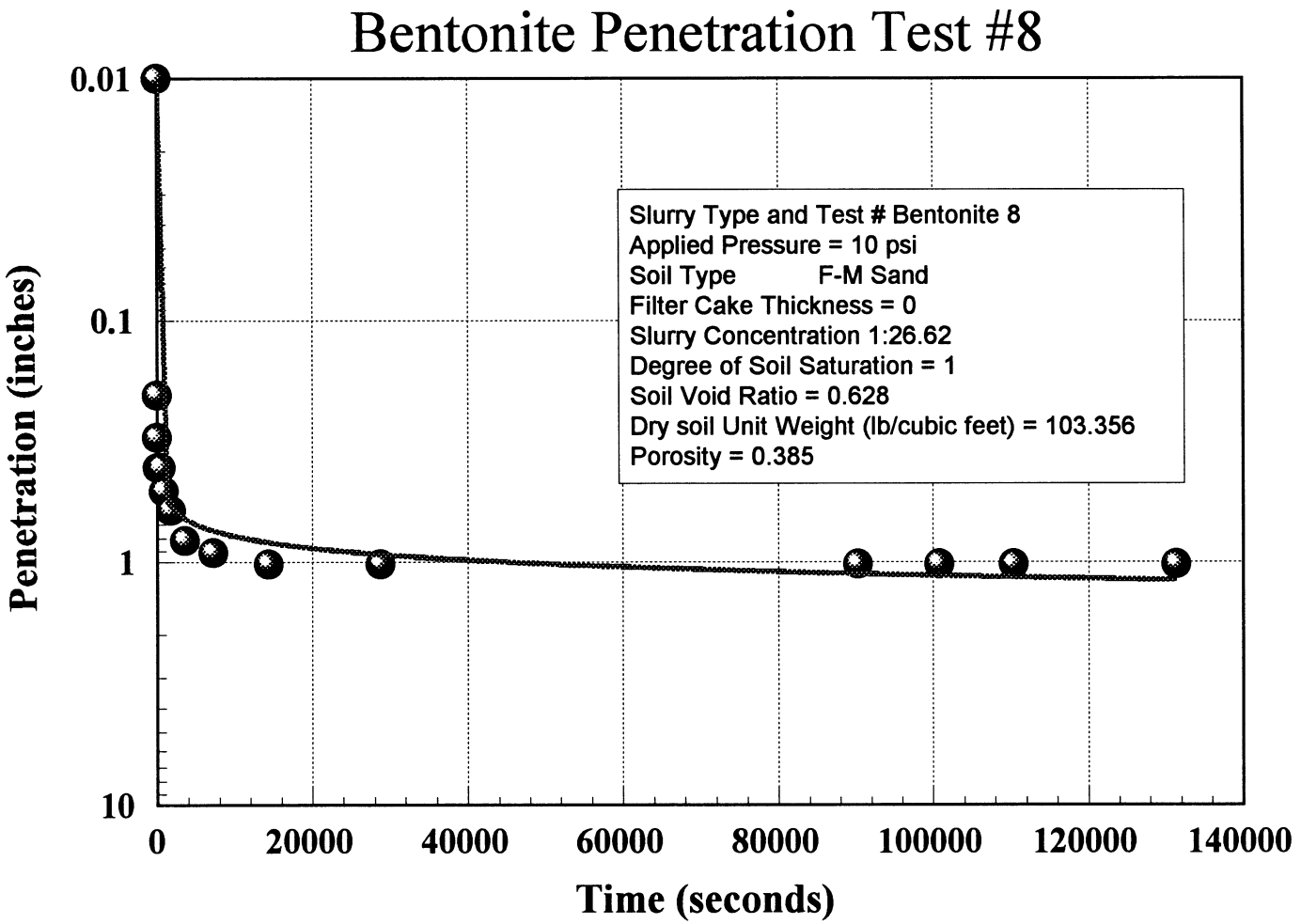

Figure 4.12 Bentonite Slurry Penetration in Sandy Soil Under Hydrostatic Pressure = 10 psi.

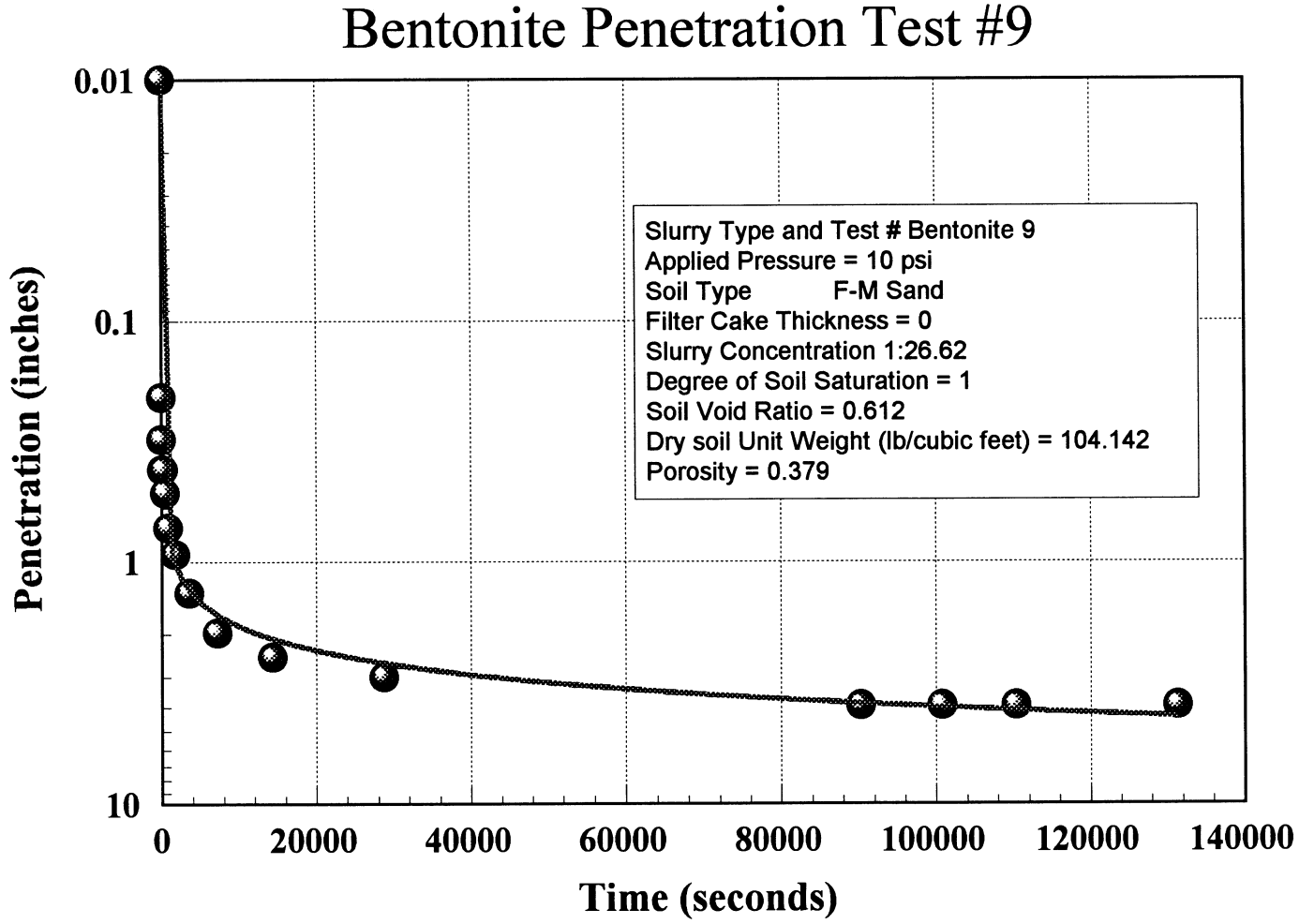

Figure 4.13 Bentonite Slurry Penetration in Sandy Soil Under Hydrostatic Pressure = 10 psi.

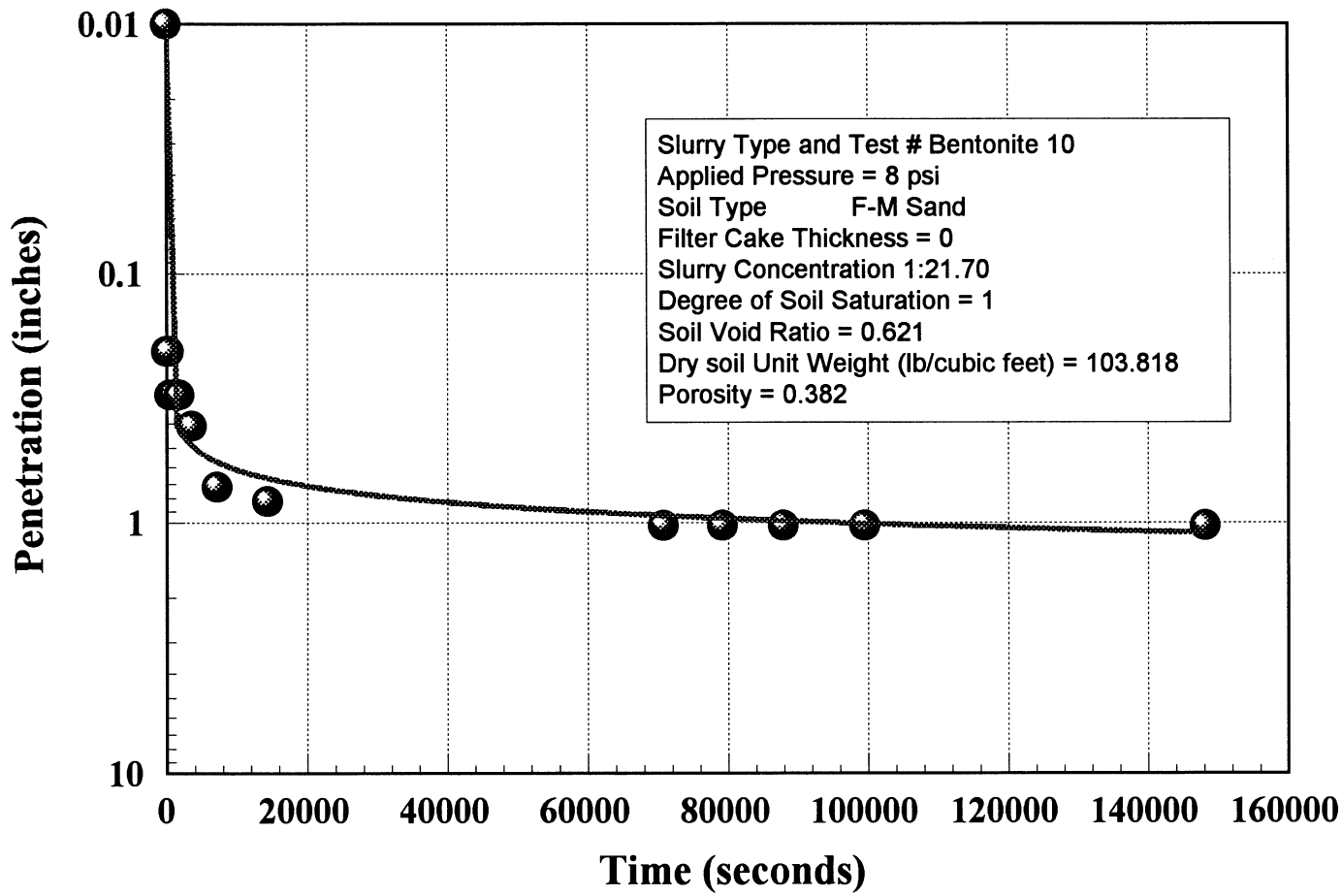

Figure 4.14 Bentonite Slurry Penetration in Sandy Soil Under Hydrostatic Pressure = 8 psi.

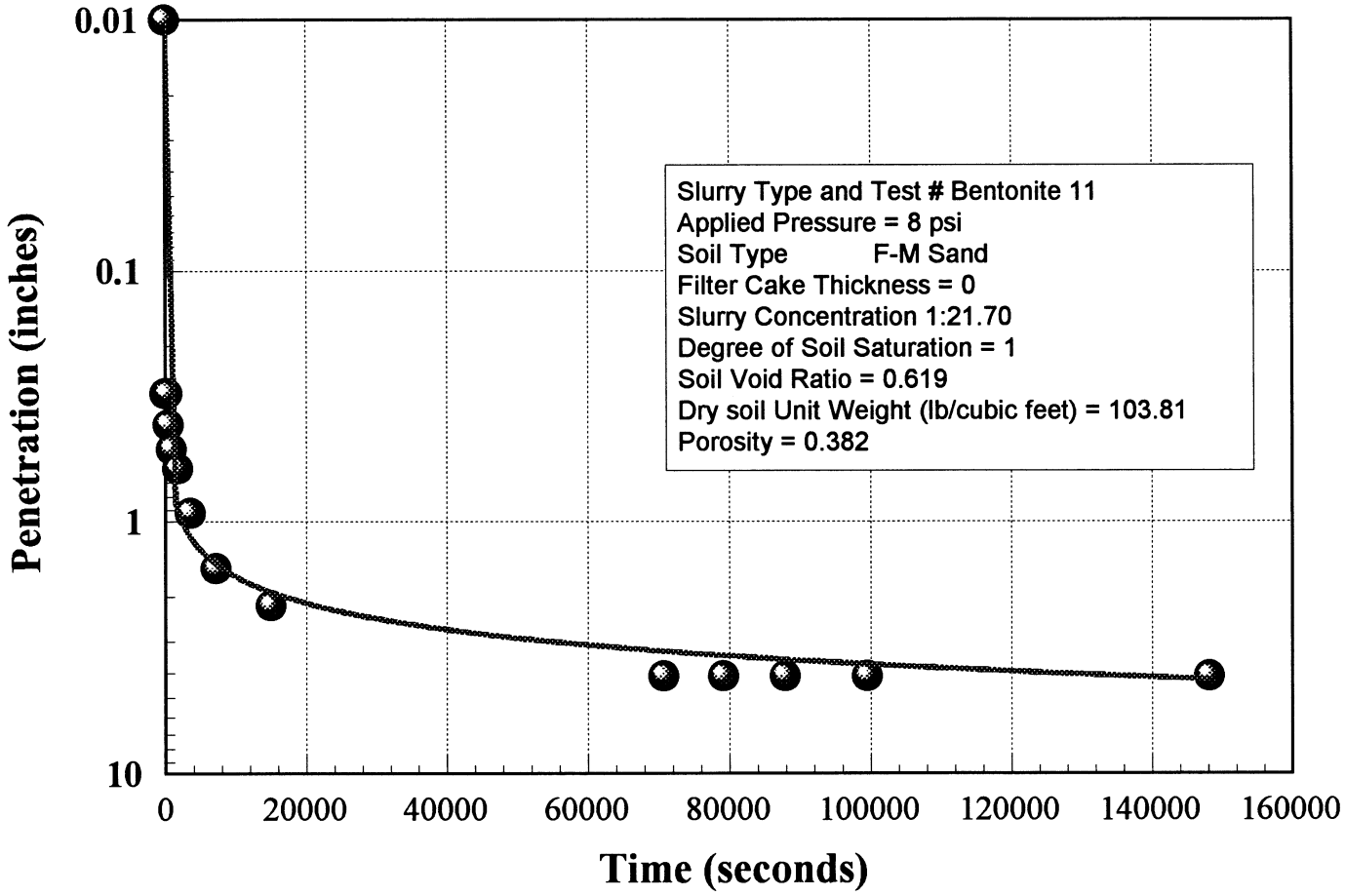

Figure 4.15 Bentonite Slurry Penetration in Sandy Soil Under Hydrostatic Pressure = 8 psi.

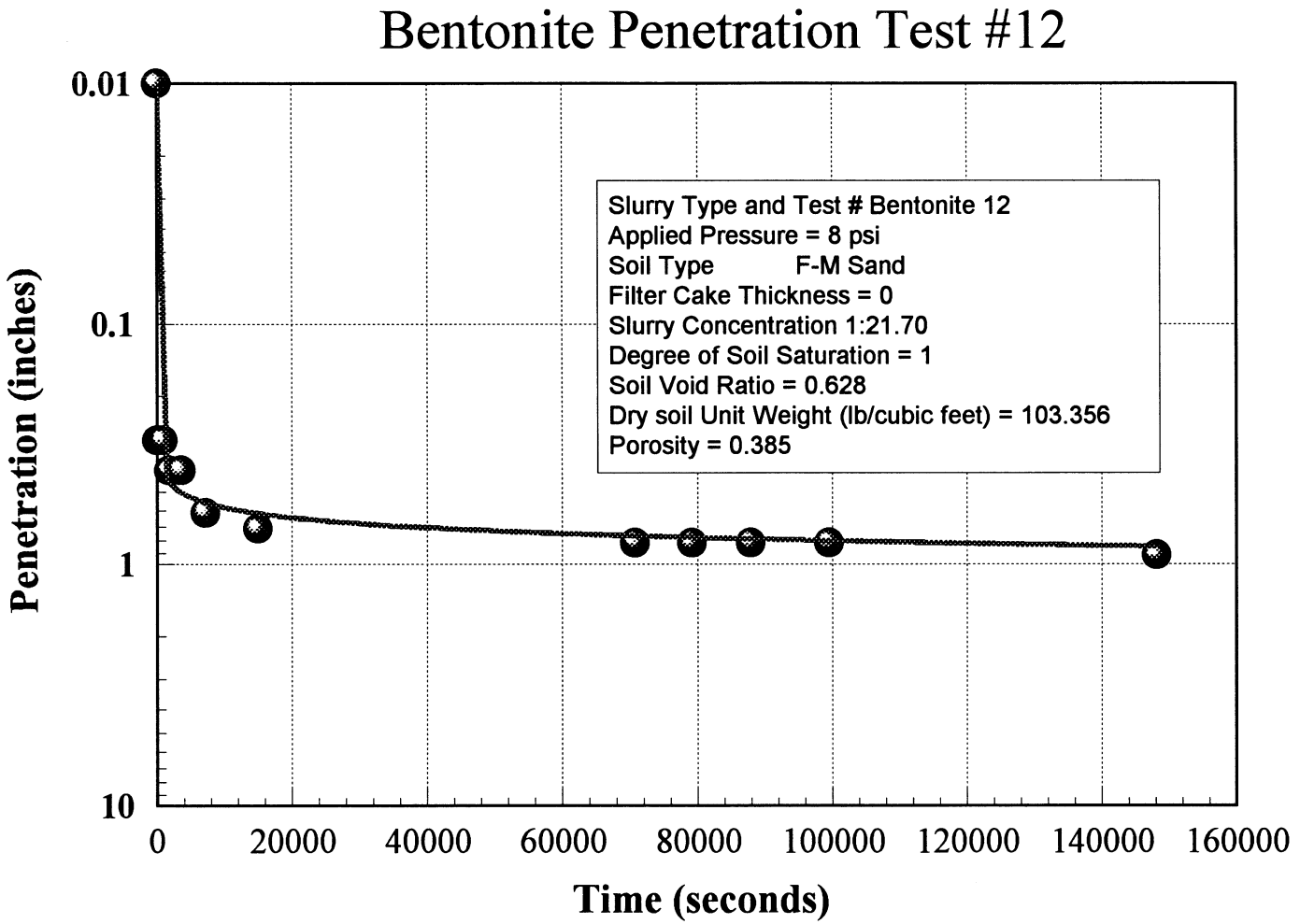

Figure 4.16 Bentonite Slurry Penetration in Sandy Soil Under Hydrostatic Pressure = 8 psi.

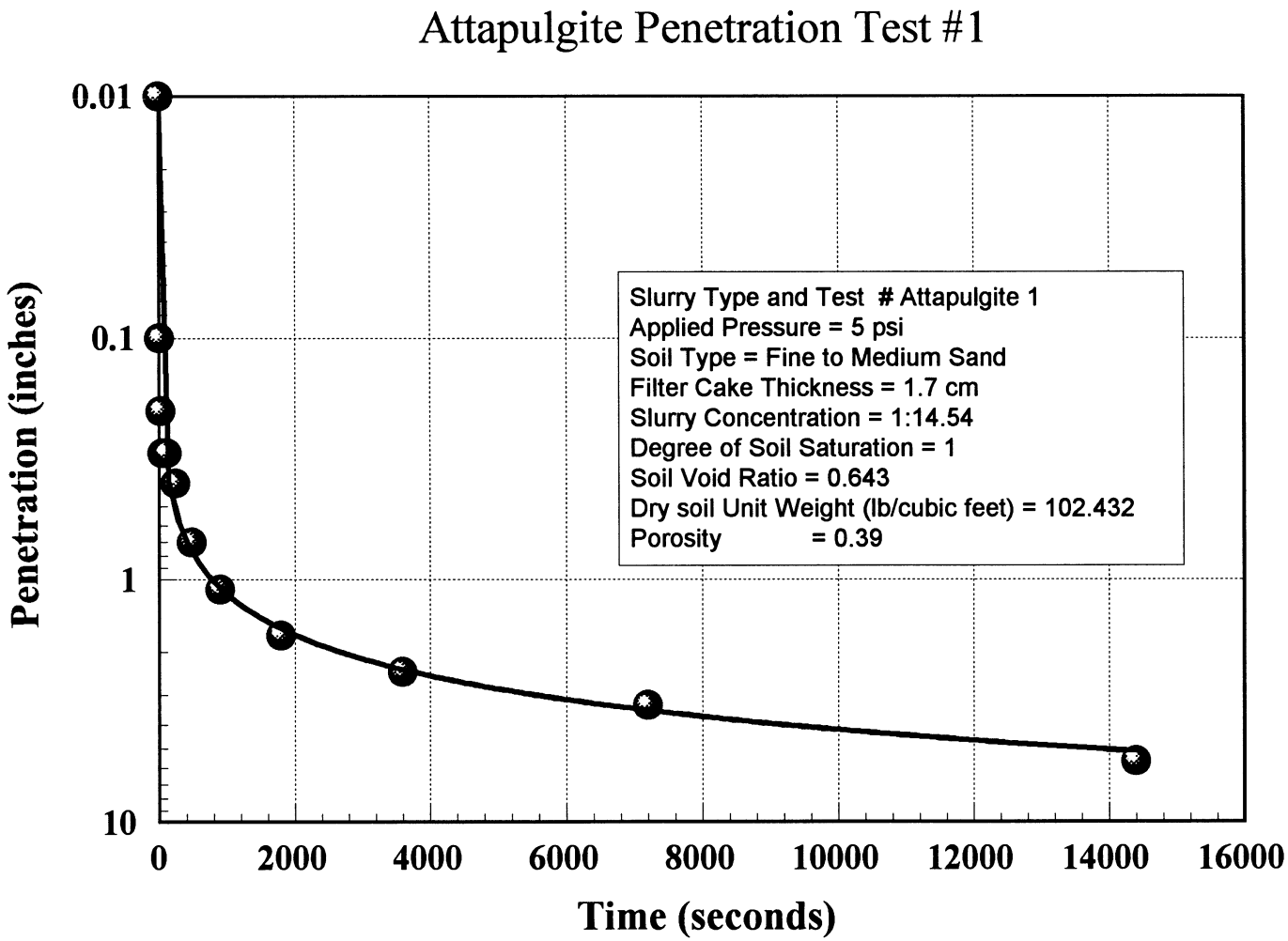

Figure 4.6 Attapulgite Slurry Penetration Under Hydrostatic Pressure = 5 psi.

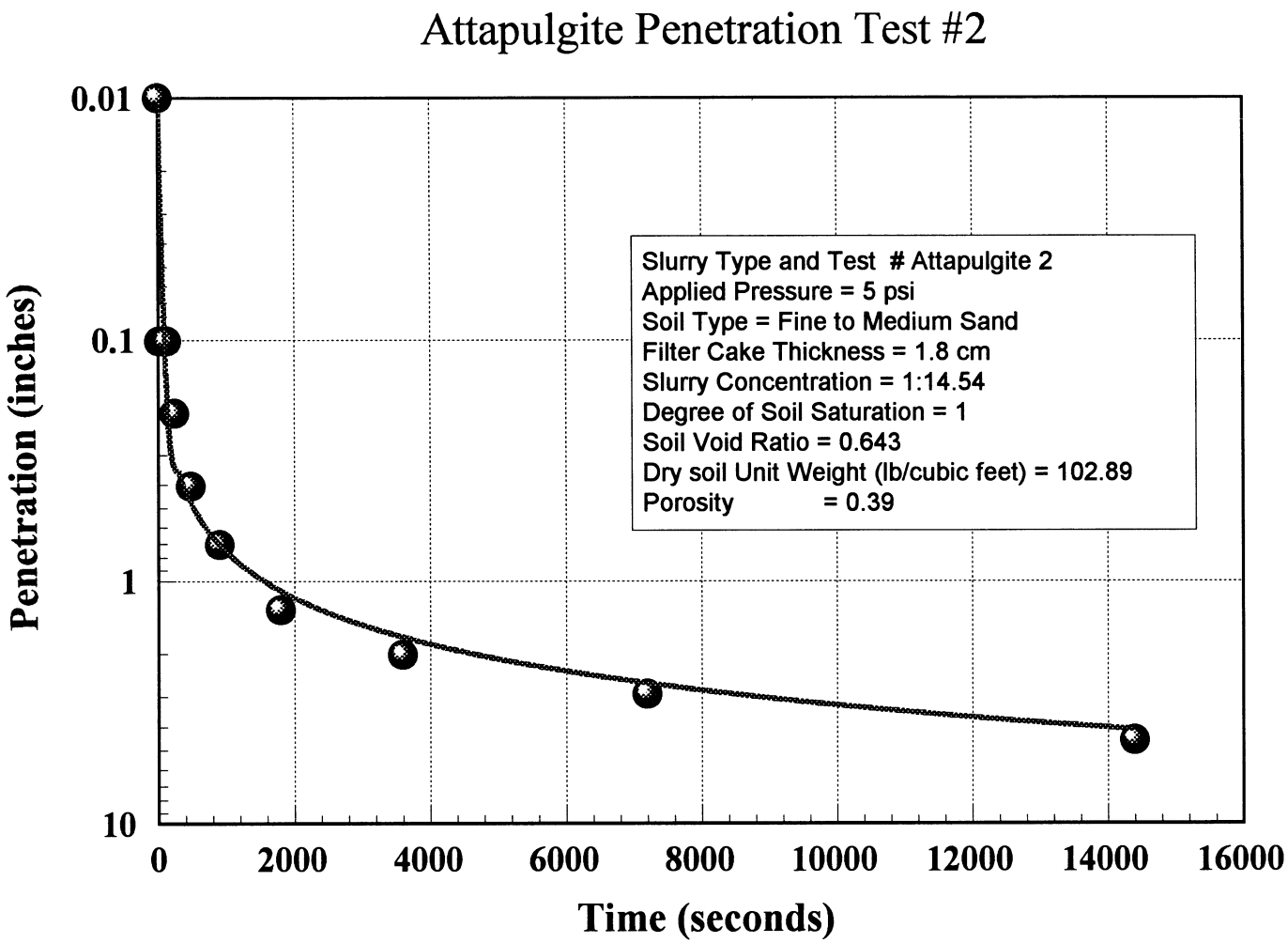

Figure 4.18 Attapulgite Slurry Penetration Under Hydrostatic Pressure = 5 psi.

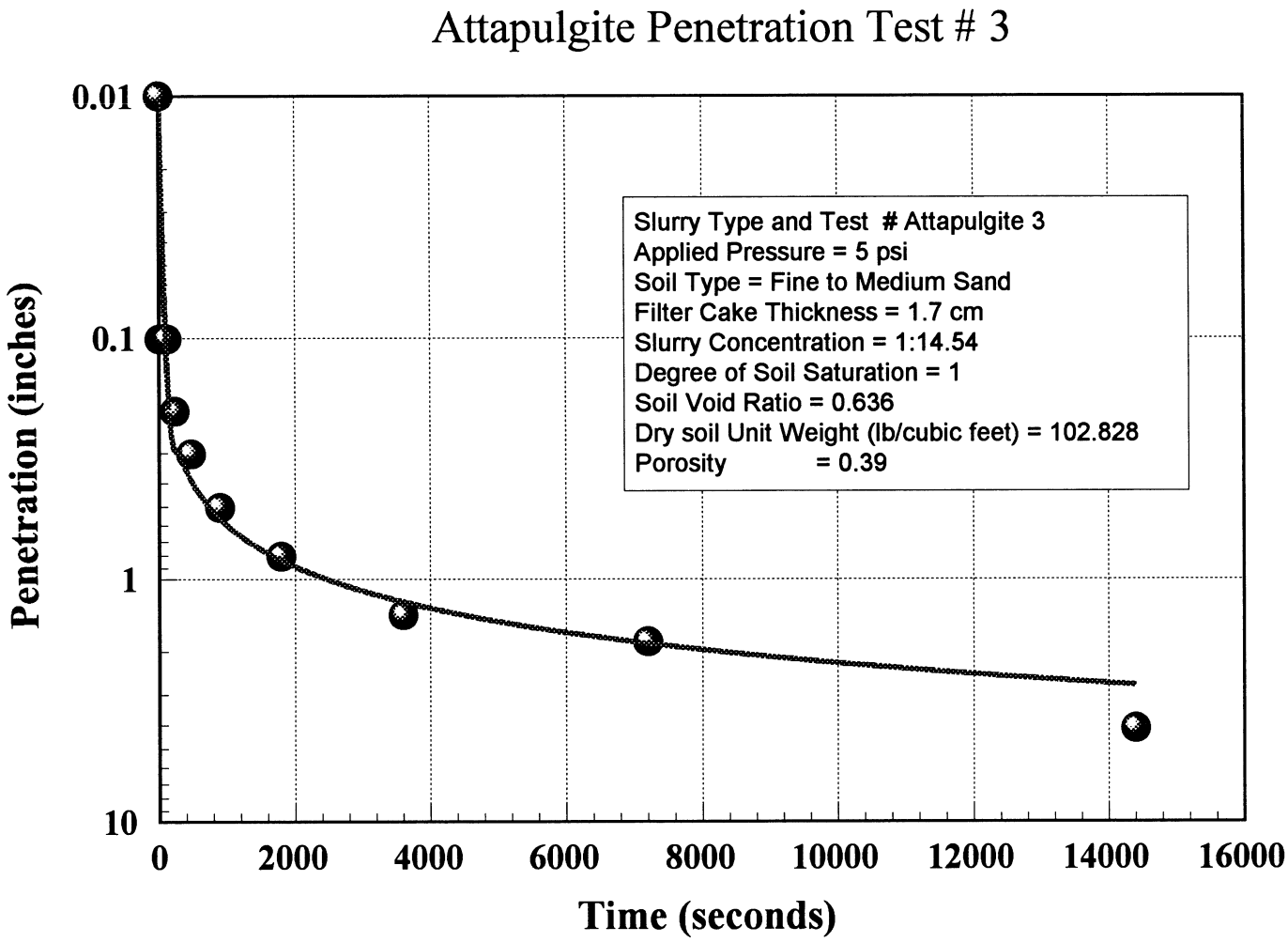

Figure 4.19 Attapulgite Slurry Penetration Under Hydrostatic Pressure = 5 psi.

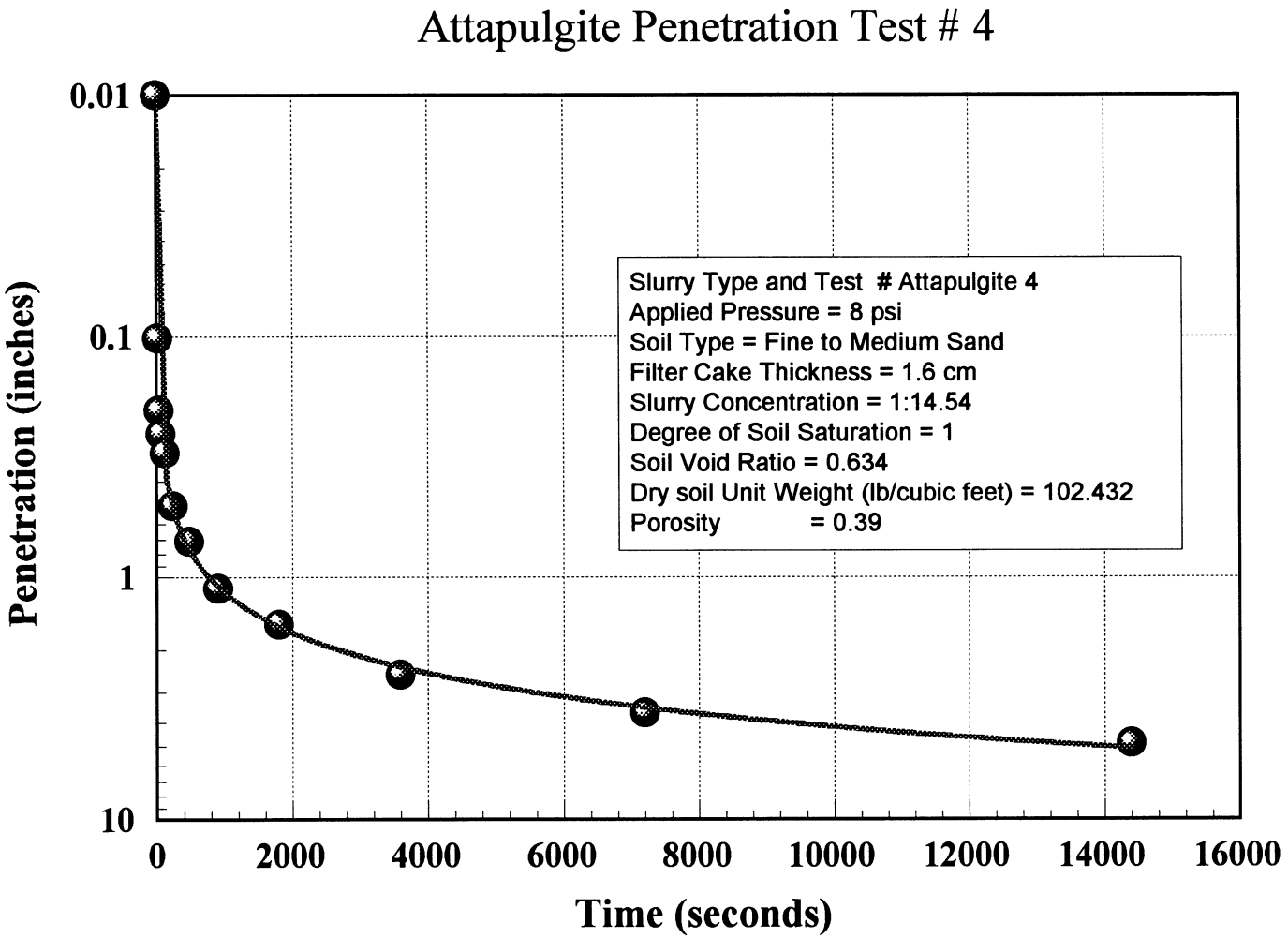

Figure 4.20 Attapulgite Slurry Penetration Under Hydrostatic Pressure = 8 psi.

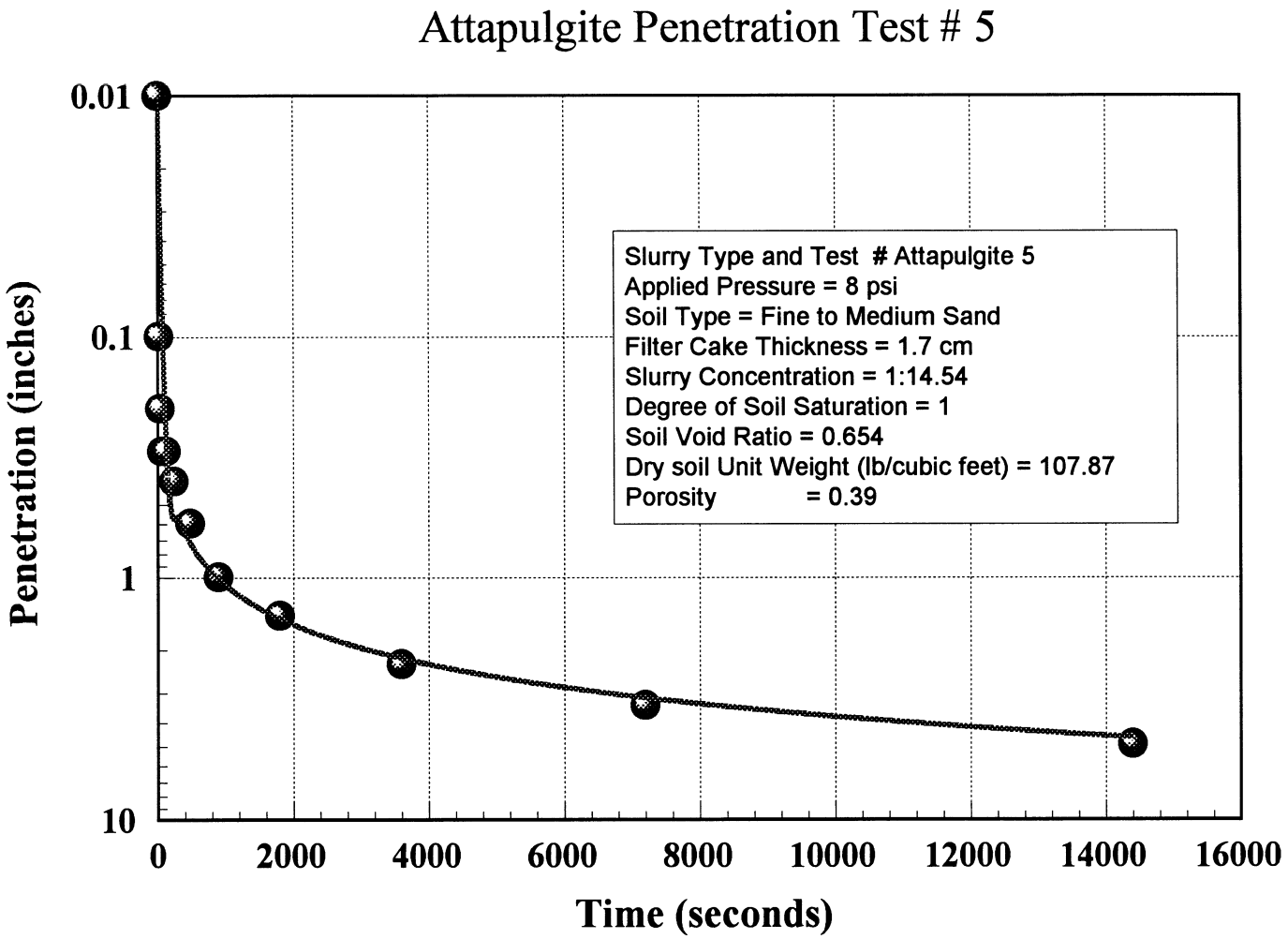

Figure 4.21 Attapulgite Slurry Penetration Under Hydrostatic Pressure = 8 psi.

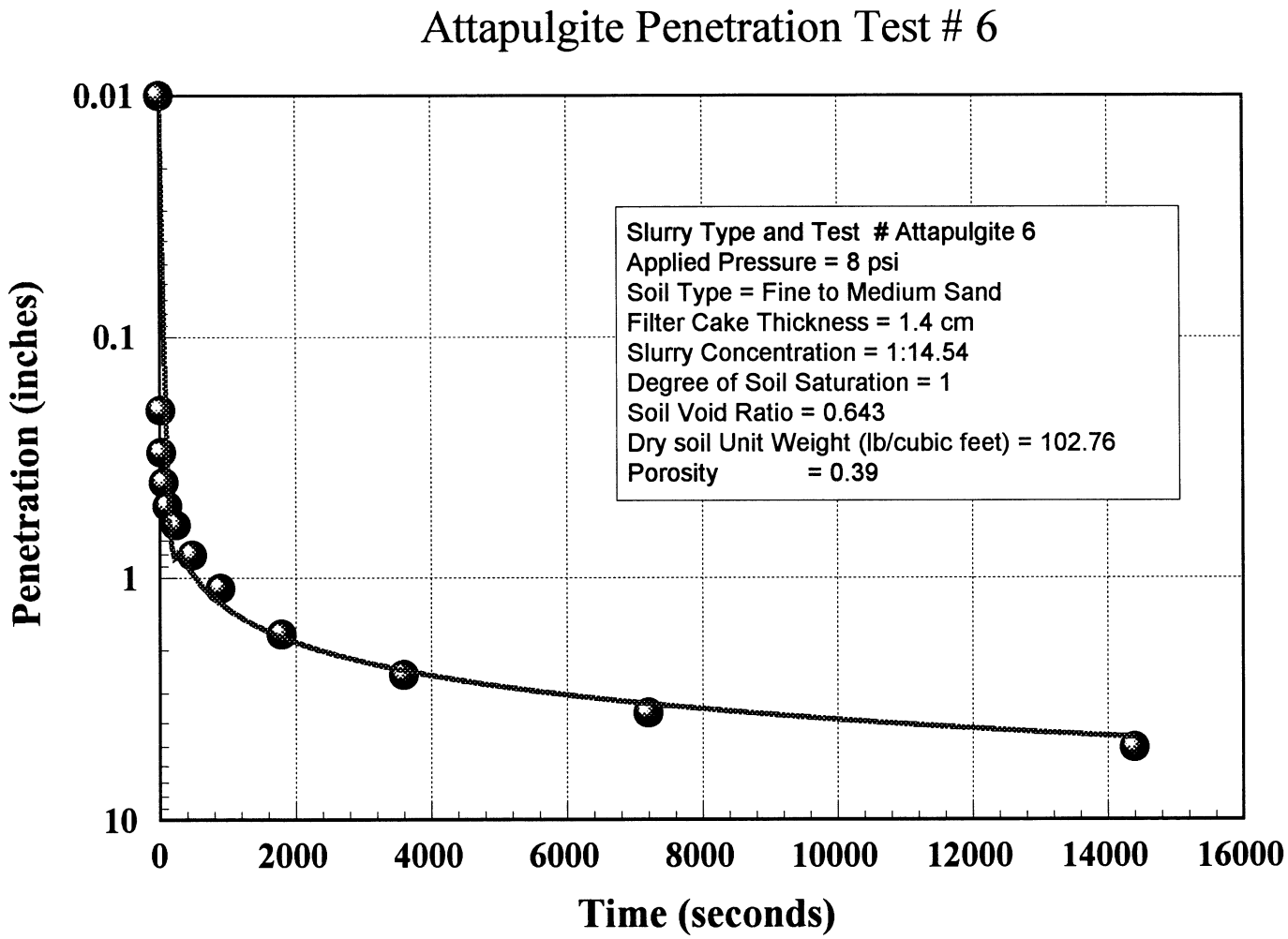

Figure 4.22 Attapulgite Slurry Penetration Under Hydrostatic Pressure = 8 psi.

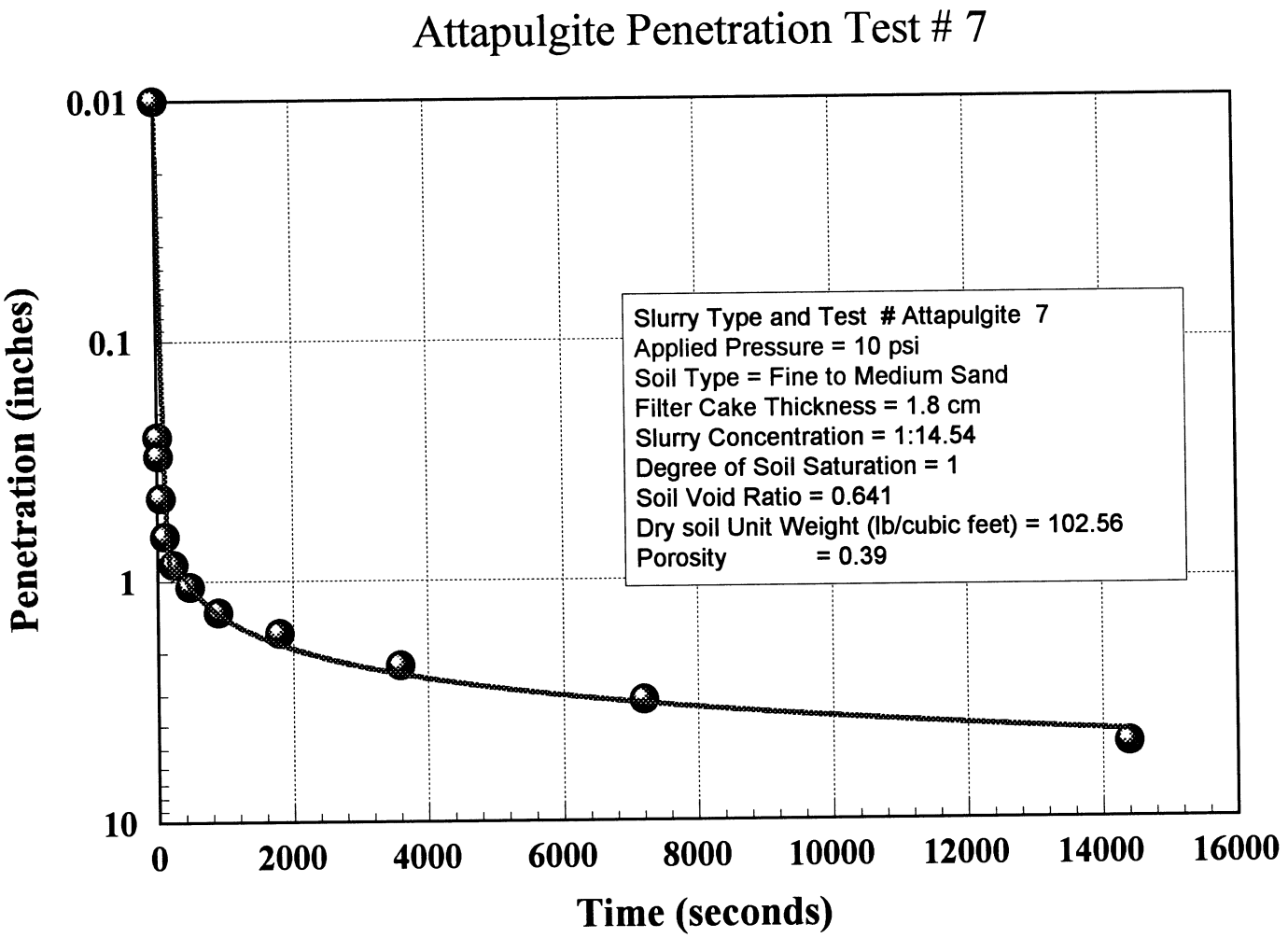

Figure 4.23 Attapulgite Slurry Penetration Under Hydrostatic Pressure = 10 psi.

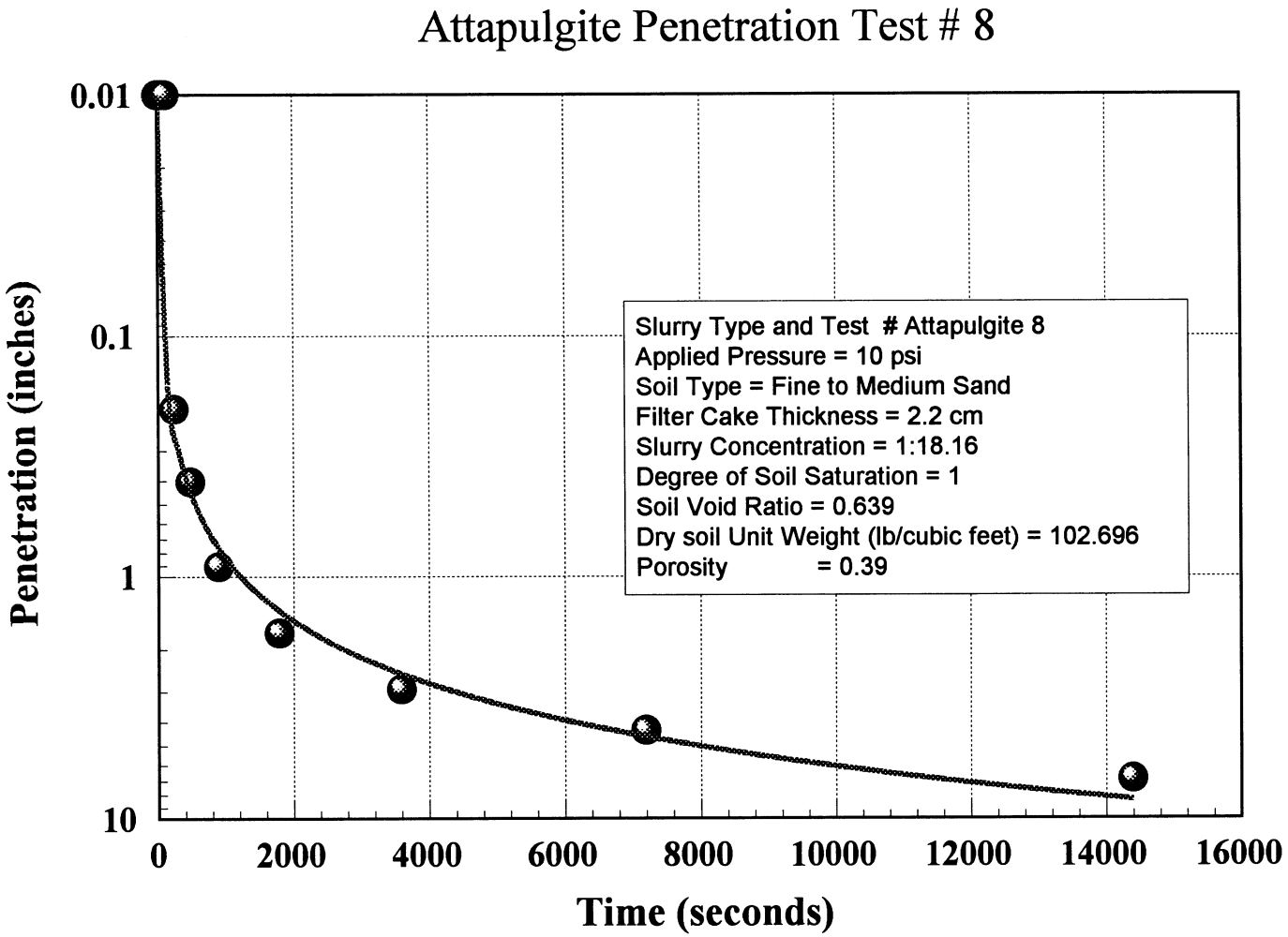

Figure 4.24 Attapulgite Slurry Penetration Under Hydrostatic Pressure = 10 psi.

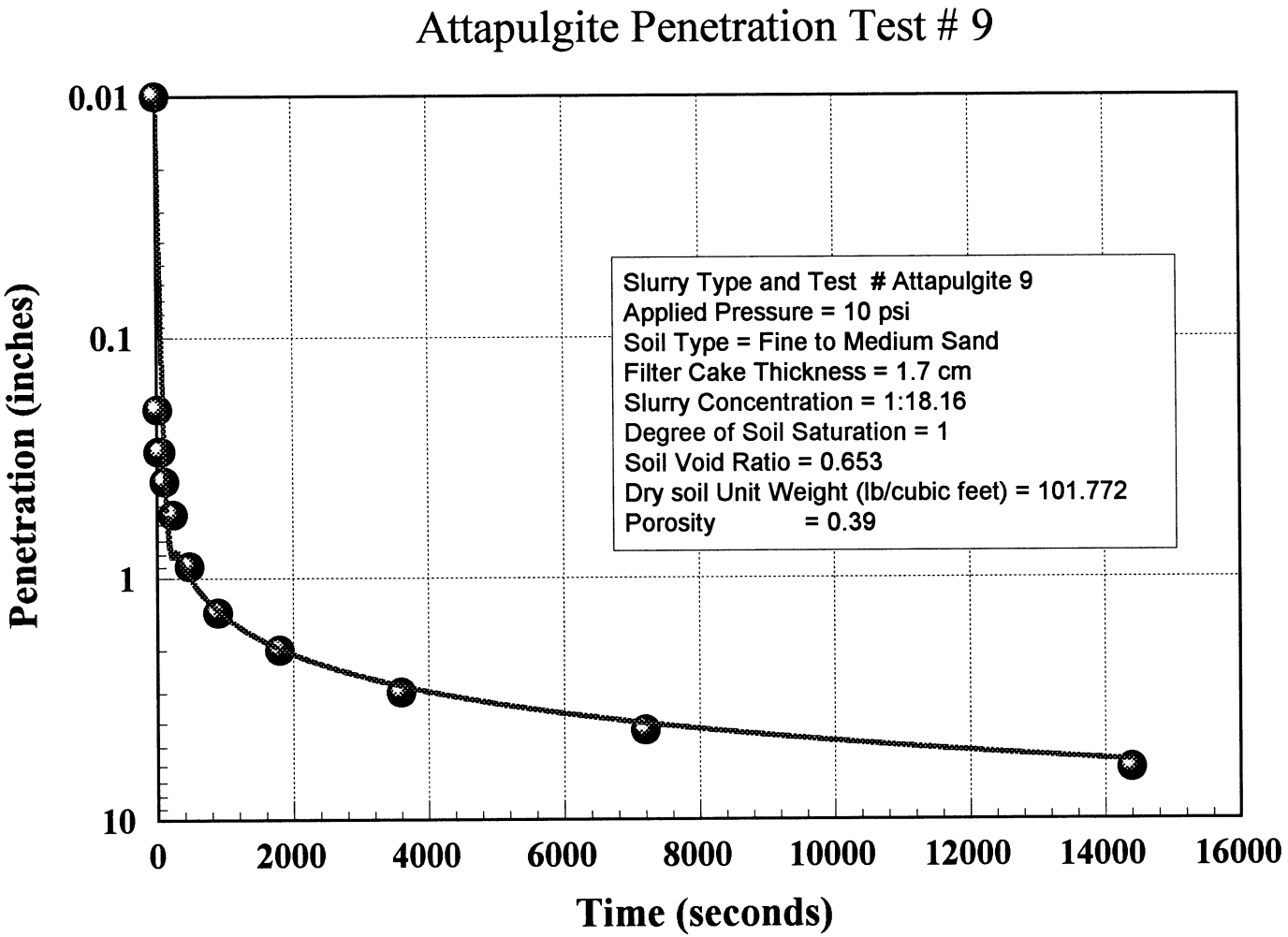

Figure 4.25 Attapulgite Slurry Penetration Under Hydrostatic Pressure = 10 psi.

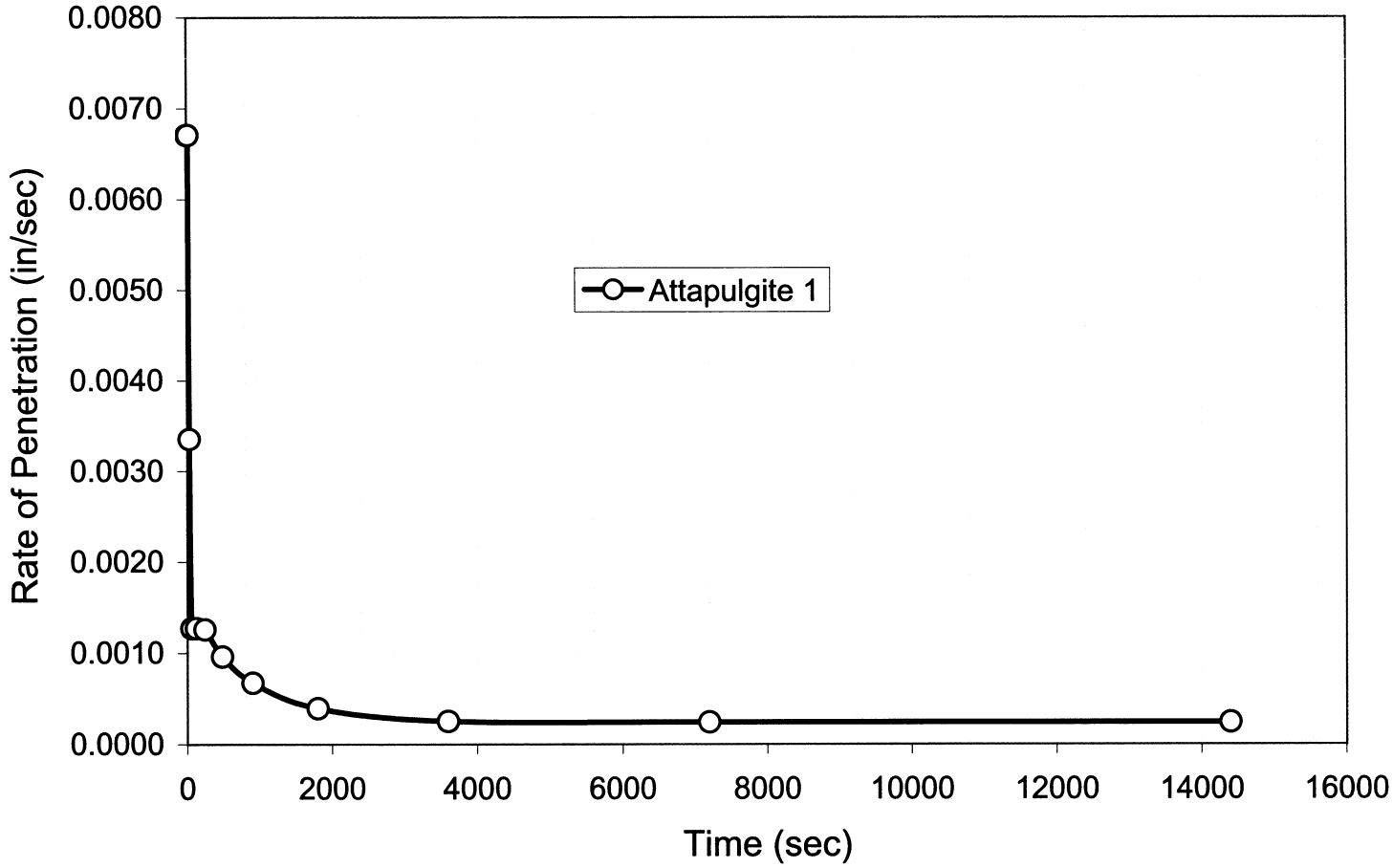

Figure 4.26 Attapulgite Slurry Penetration Rate in Cohesionless Soil Under Pressure = 5 psi

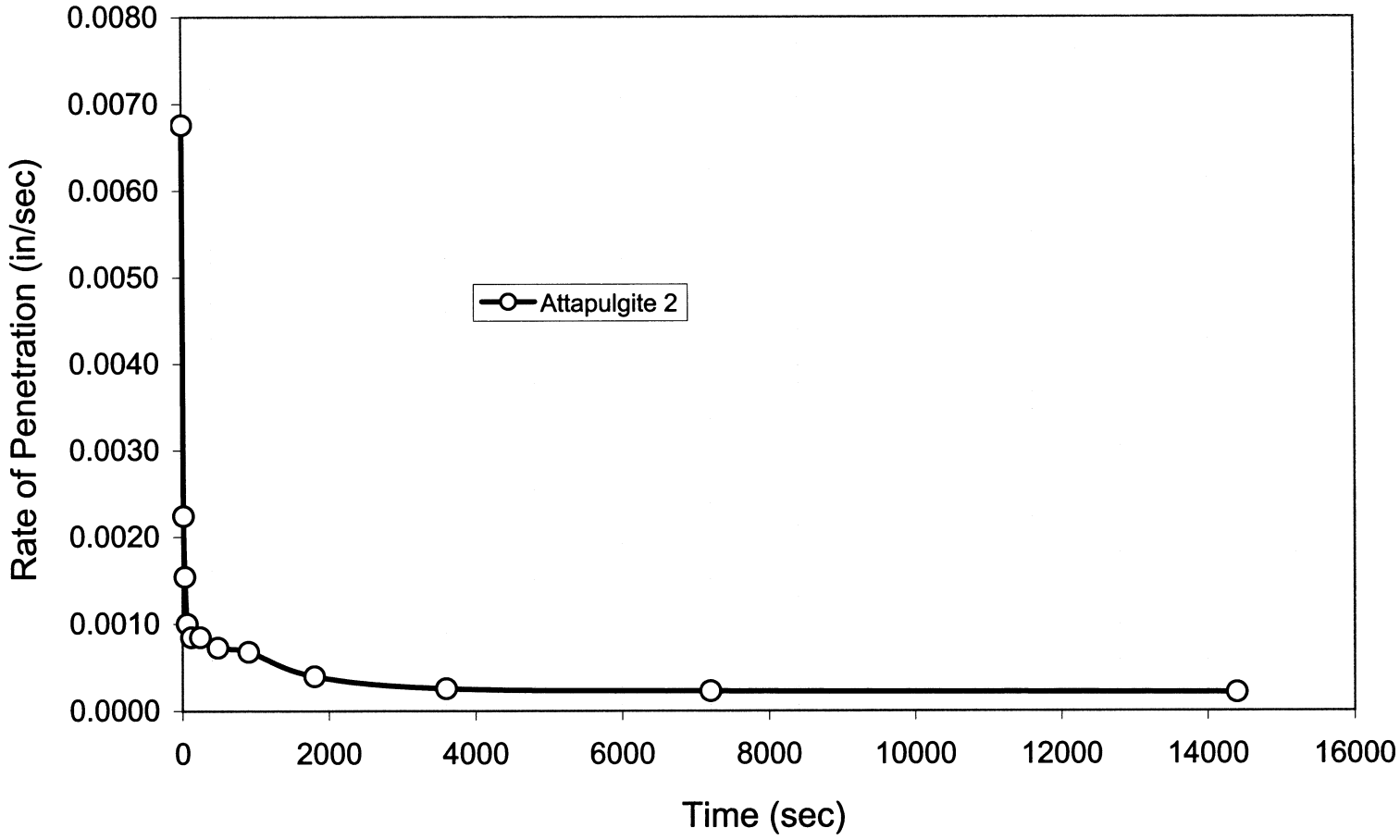

Figure 4.27 Attapulgite Slurry Penetration Rate in Cohesionless Soil Under Pressure = 5 psi

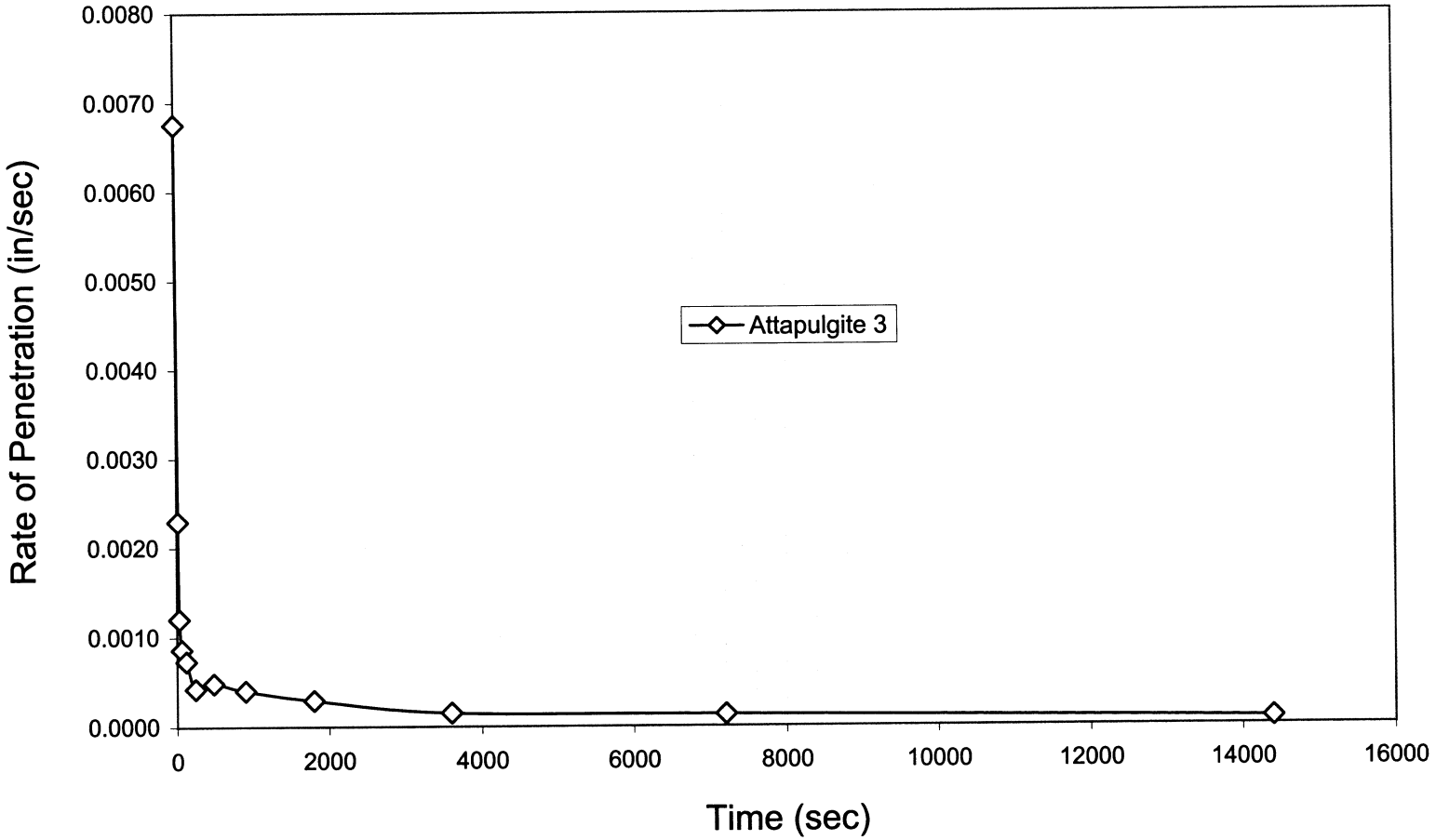

Figure 4.28 Attapulgite Slurry Penetration Rate in Cohesionless Soil Under Pressure = 5 psi

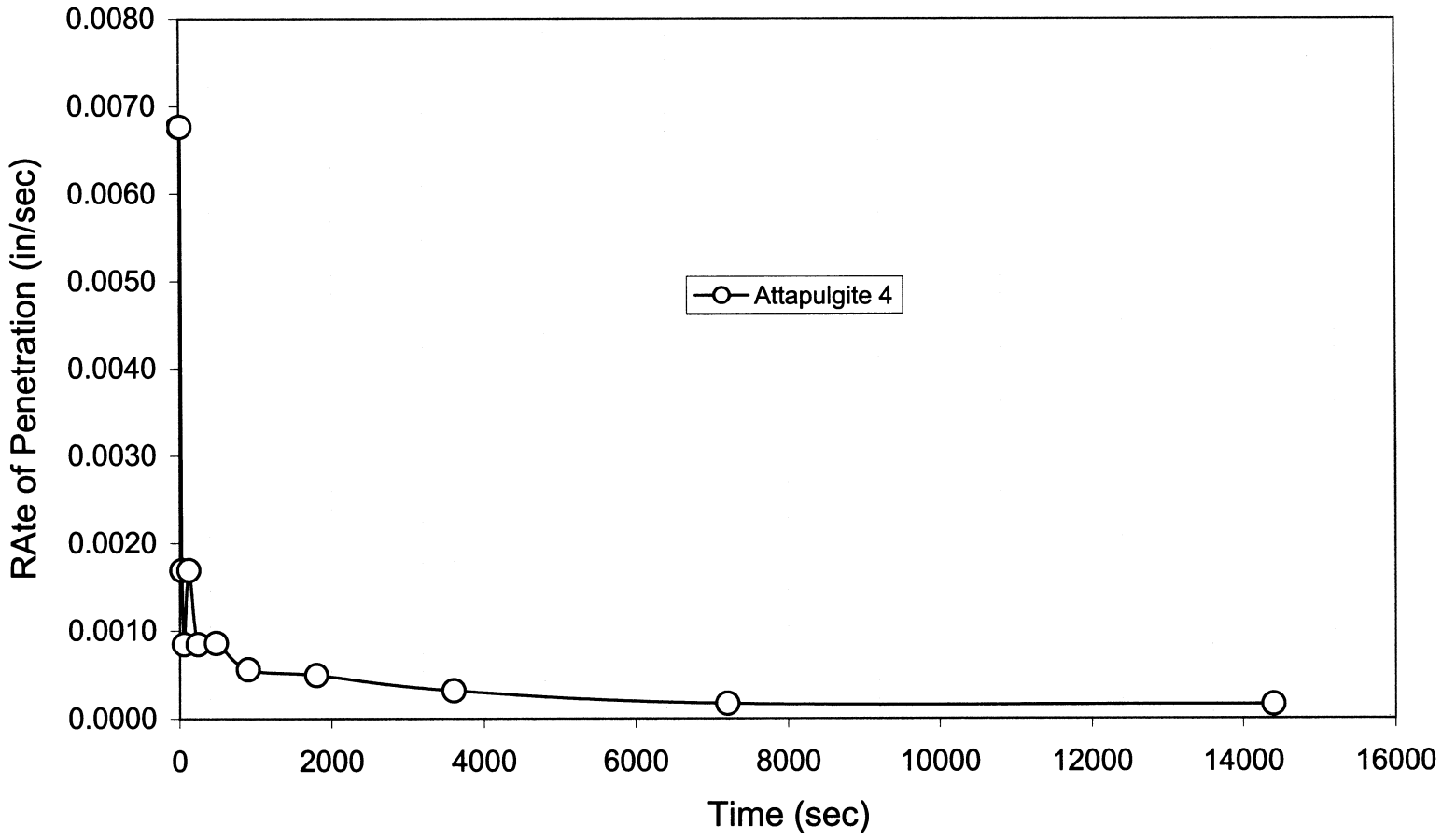

Figure 4.29 Attapulgite Slurry Penetration Rate in Cohesionless Soil Under Pressure = 8 psi

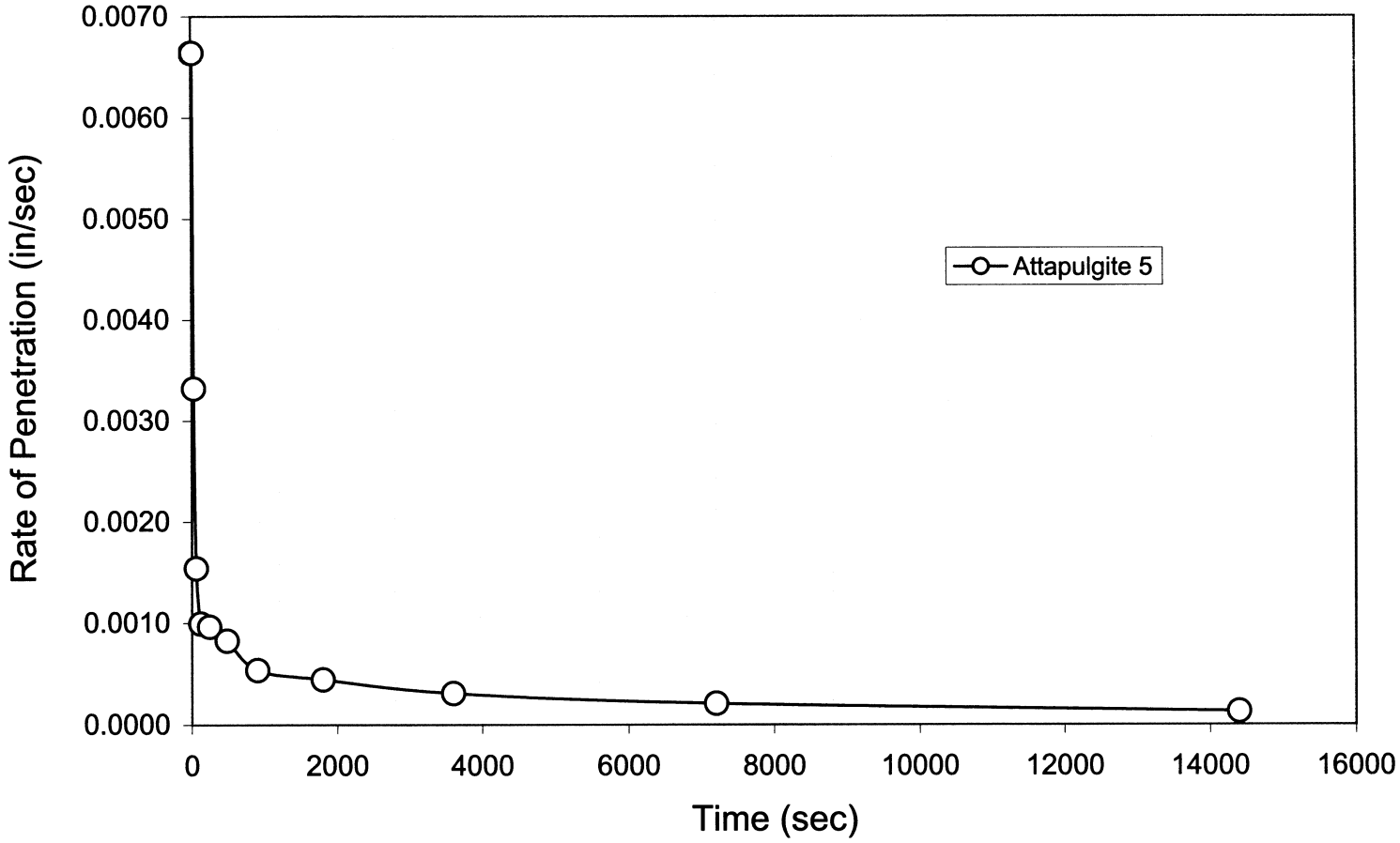

Figure 4.30 Attapulgite Slurry Penetration Rate in Cohesionless Soil Under Pressure = 8 psi

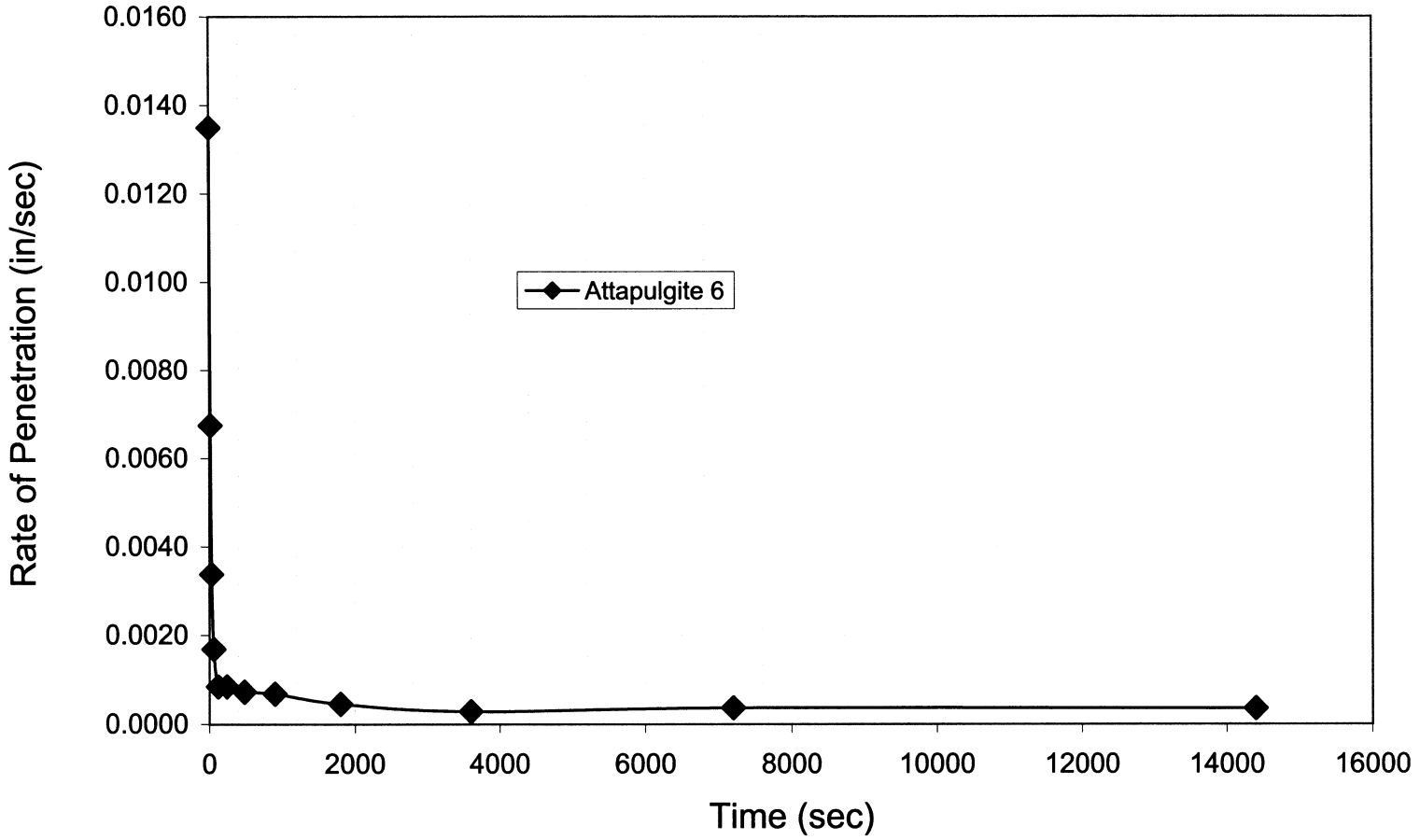

Figure 4.31 Attapulgite Slurry Penetration Rate in Cohesionless Soil Under Pressure = 8 psi

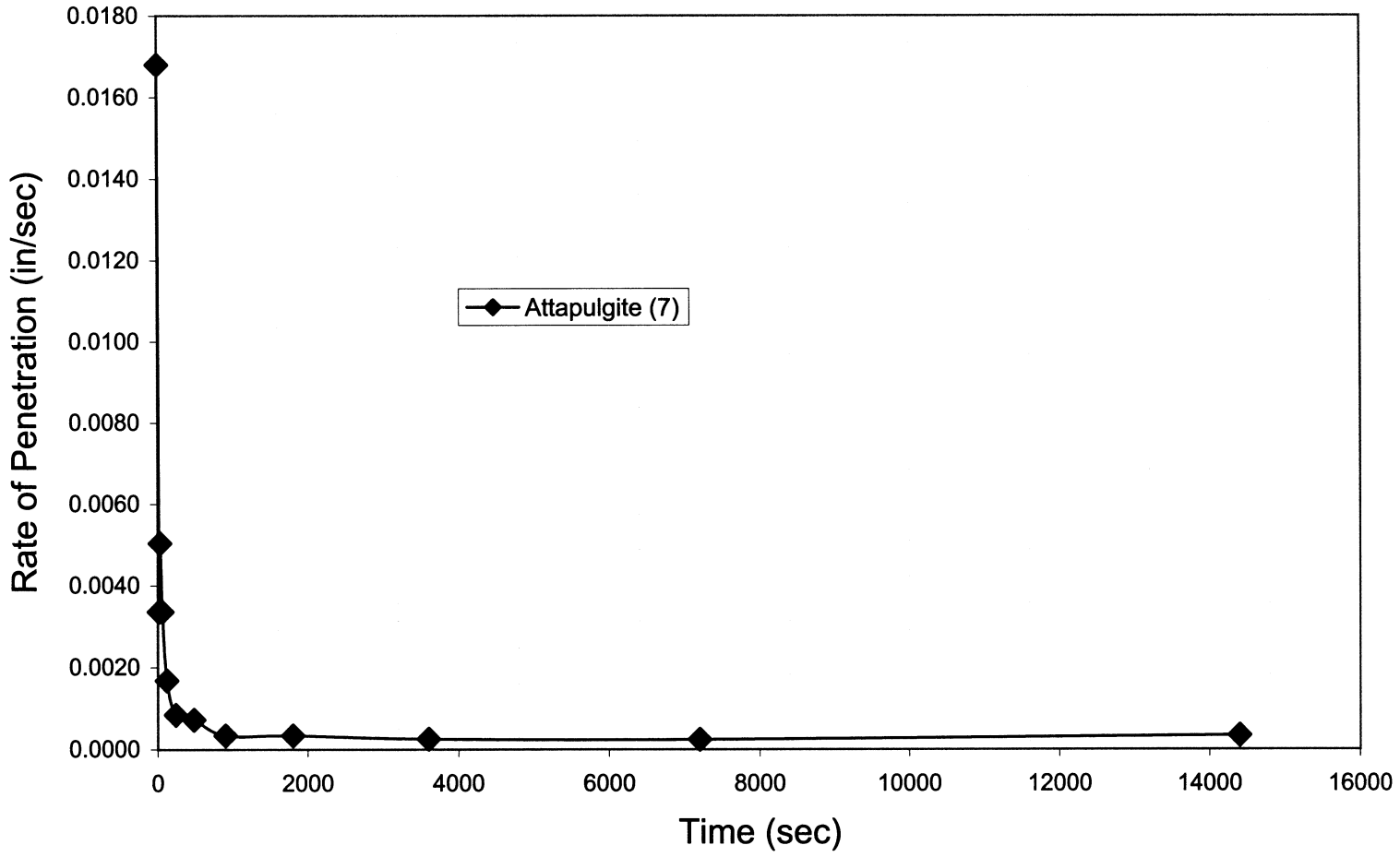

Figure 4.32 Attapulgite Slurry Penetration Rate in Cohesionless Soil Under Pressure = 10 psi

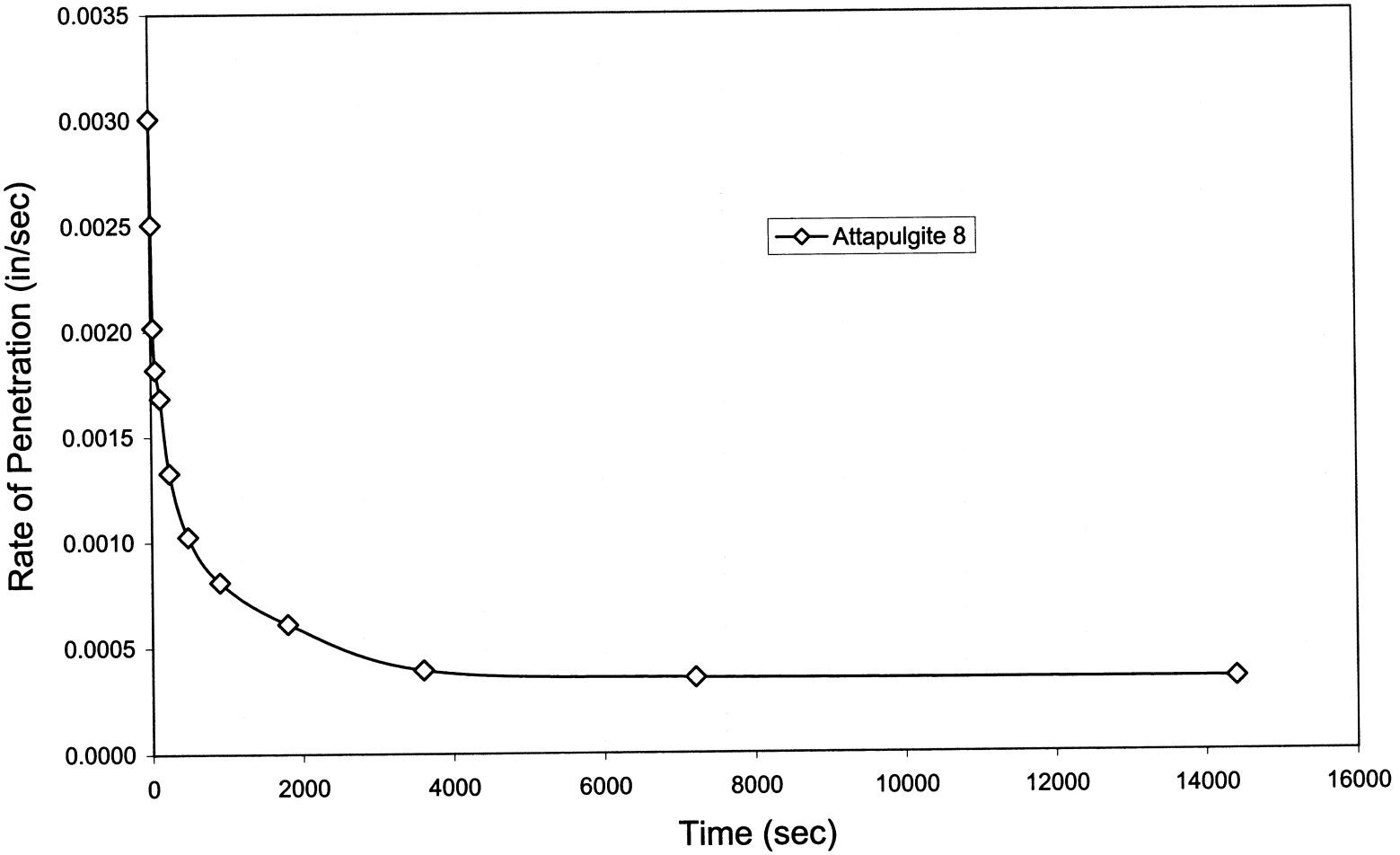

Figure 4.33 Attapulgite Slurry Penetration Rate in Cohesionless Soil Under Pressure = 10 psi

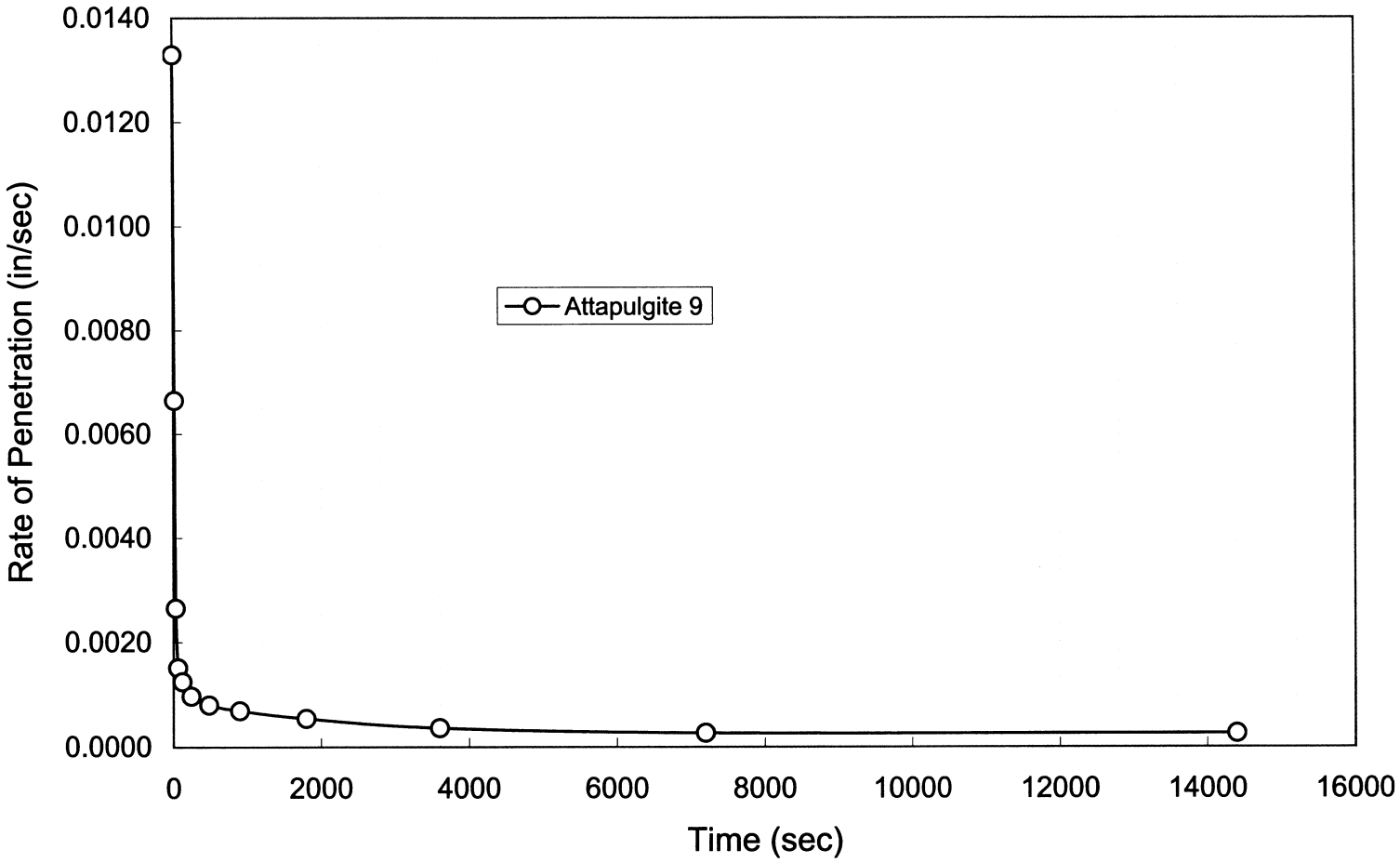

Figure 4.34 Attapulgite Slurry Penetration Rate in Cohesionless Soil Under Pressure = 10 psi

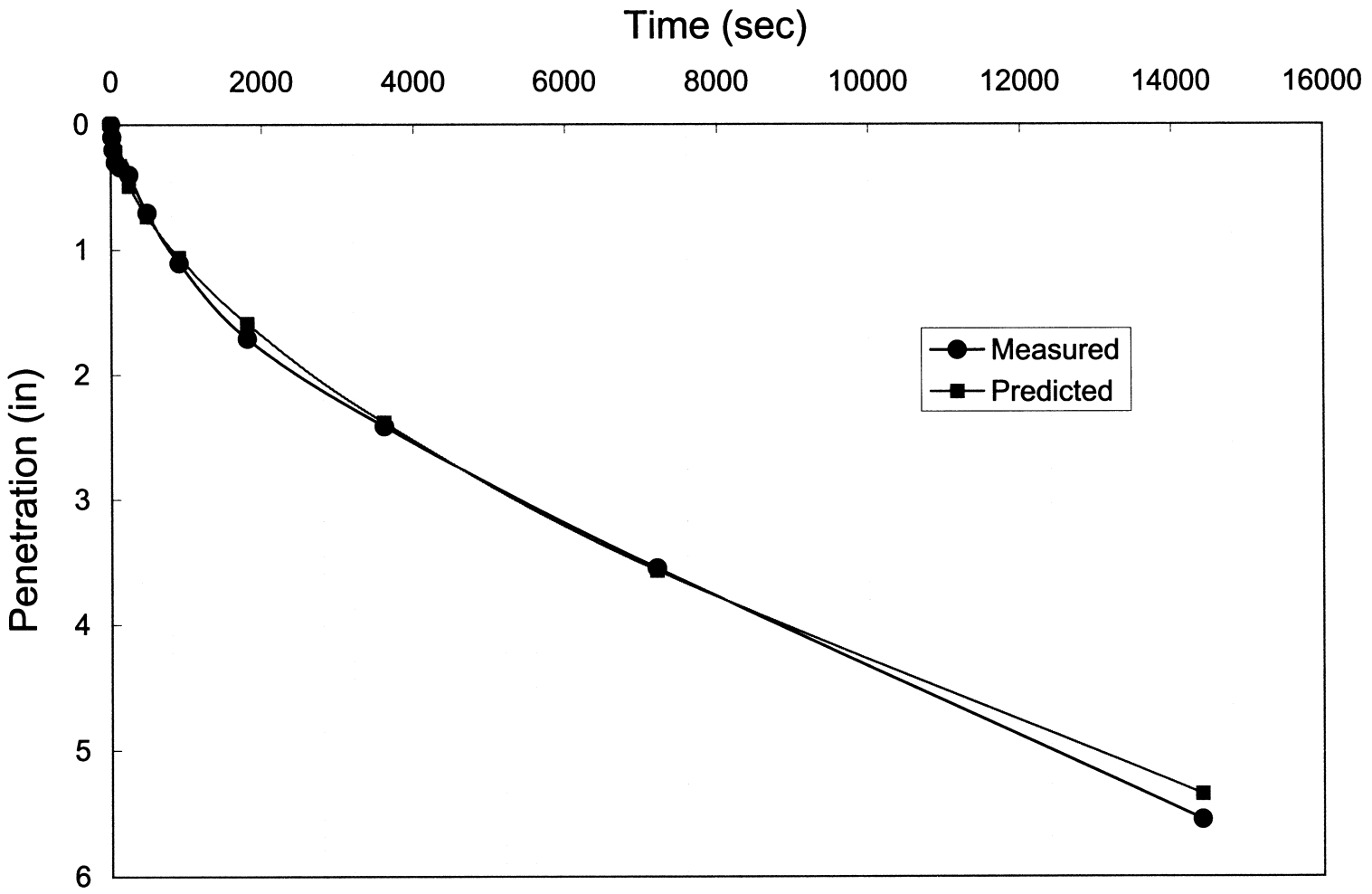

Figure 4.8 Attapulgite Slurry Penetration in Cohesionless Soil Under Pressure = 5 psi

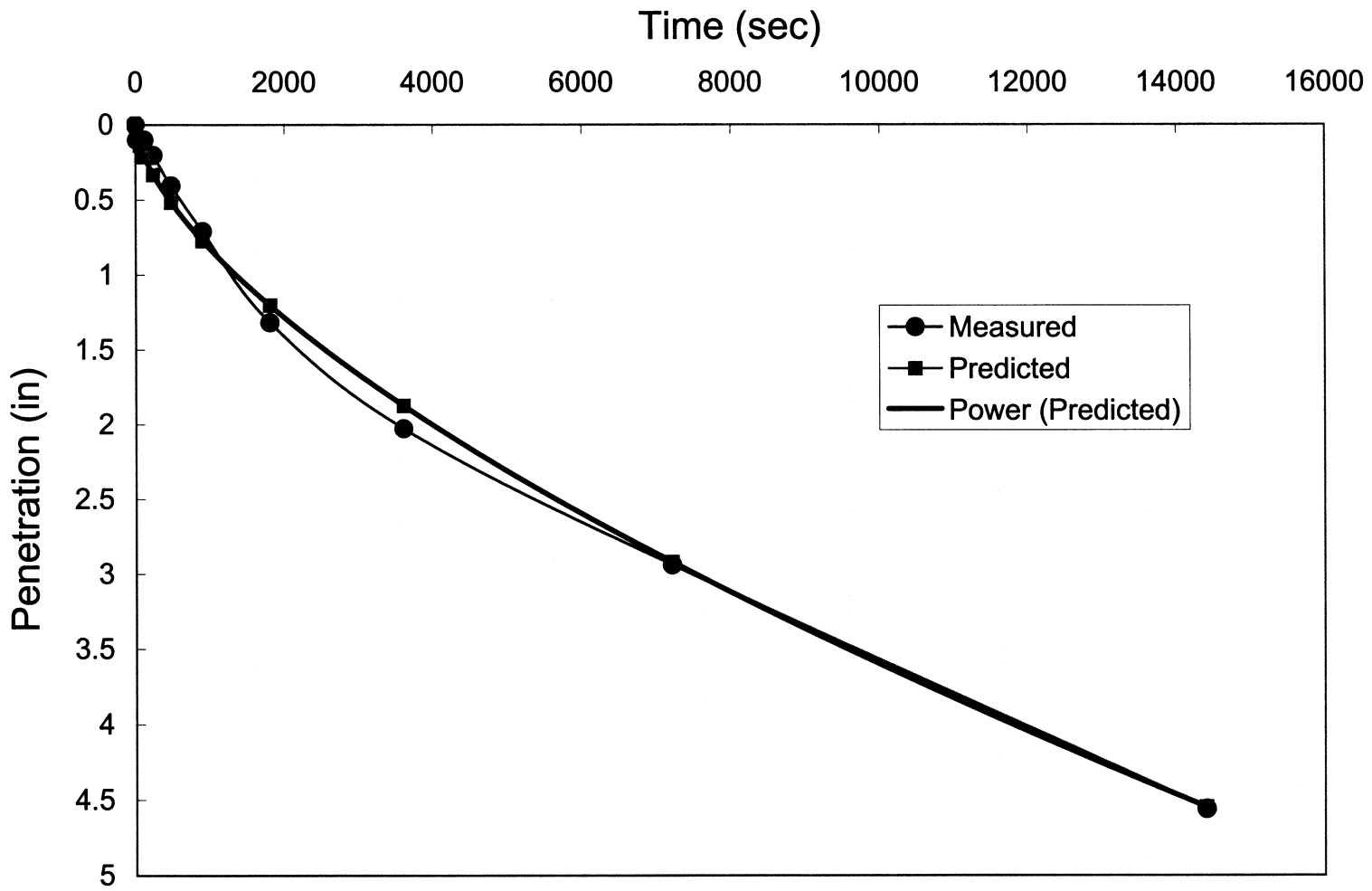

Figure 4.37 Attapulgite Slurry Penetration in Cohesionless Soil Under Pressure = 5 psi

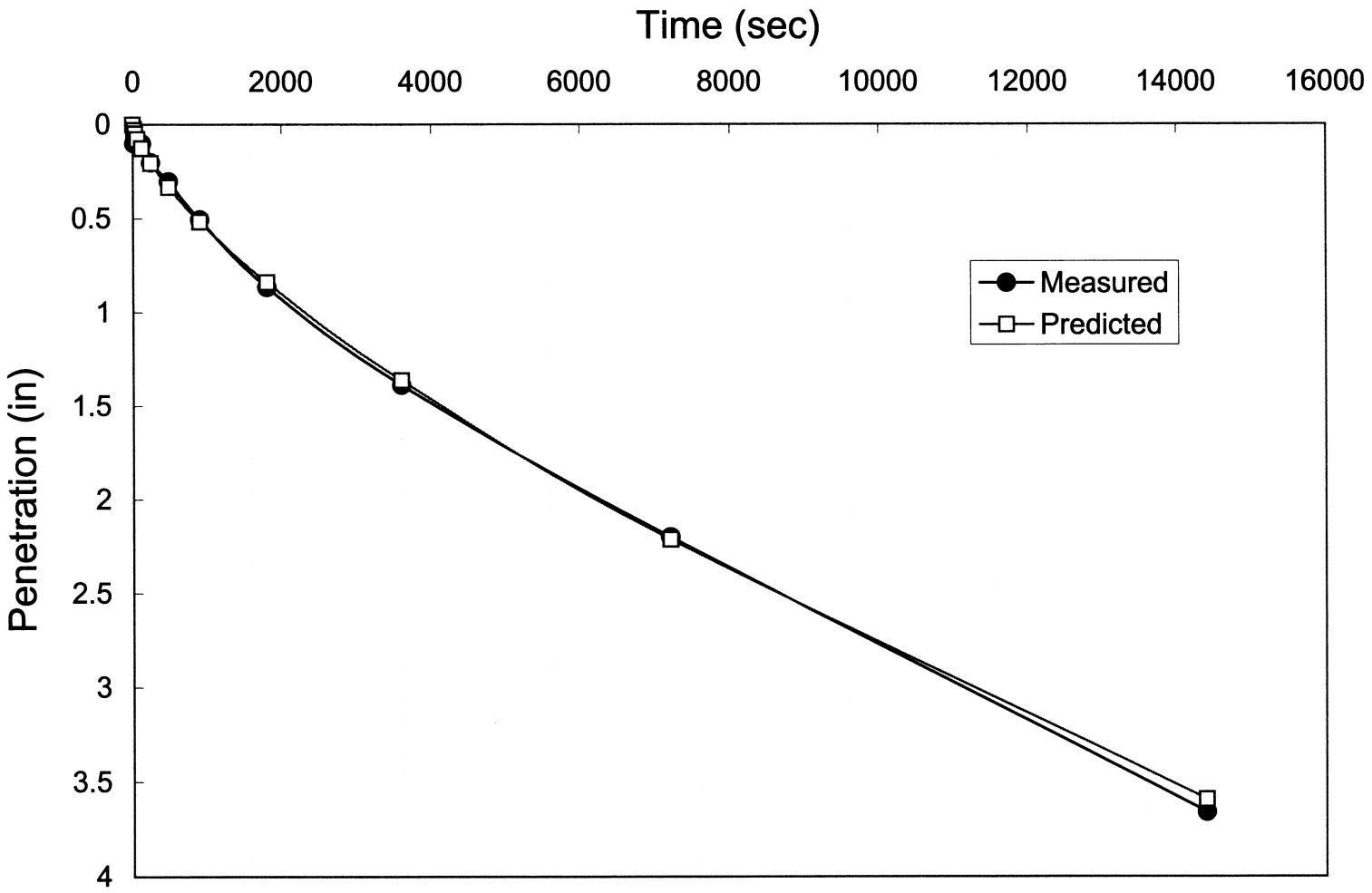

Figure 4.38 Attapulgite Slurry Penetration in Cohesionless Soil Under Pressure = 5 psi

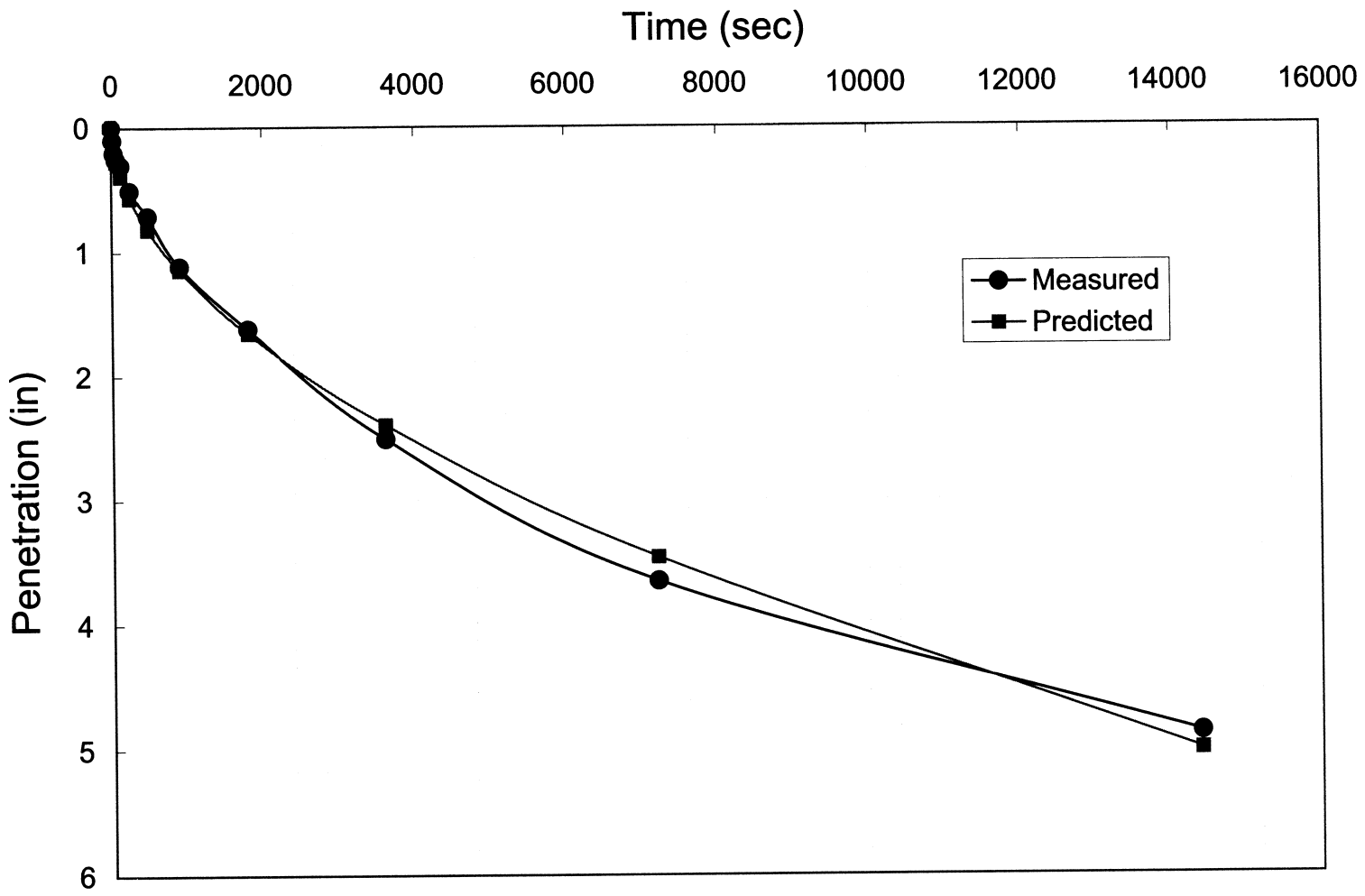

Figure 4.39 Attapulgite Slurry Penetration in Cohesionless Soil Under Pressure = 8 psi

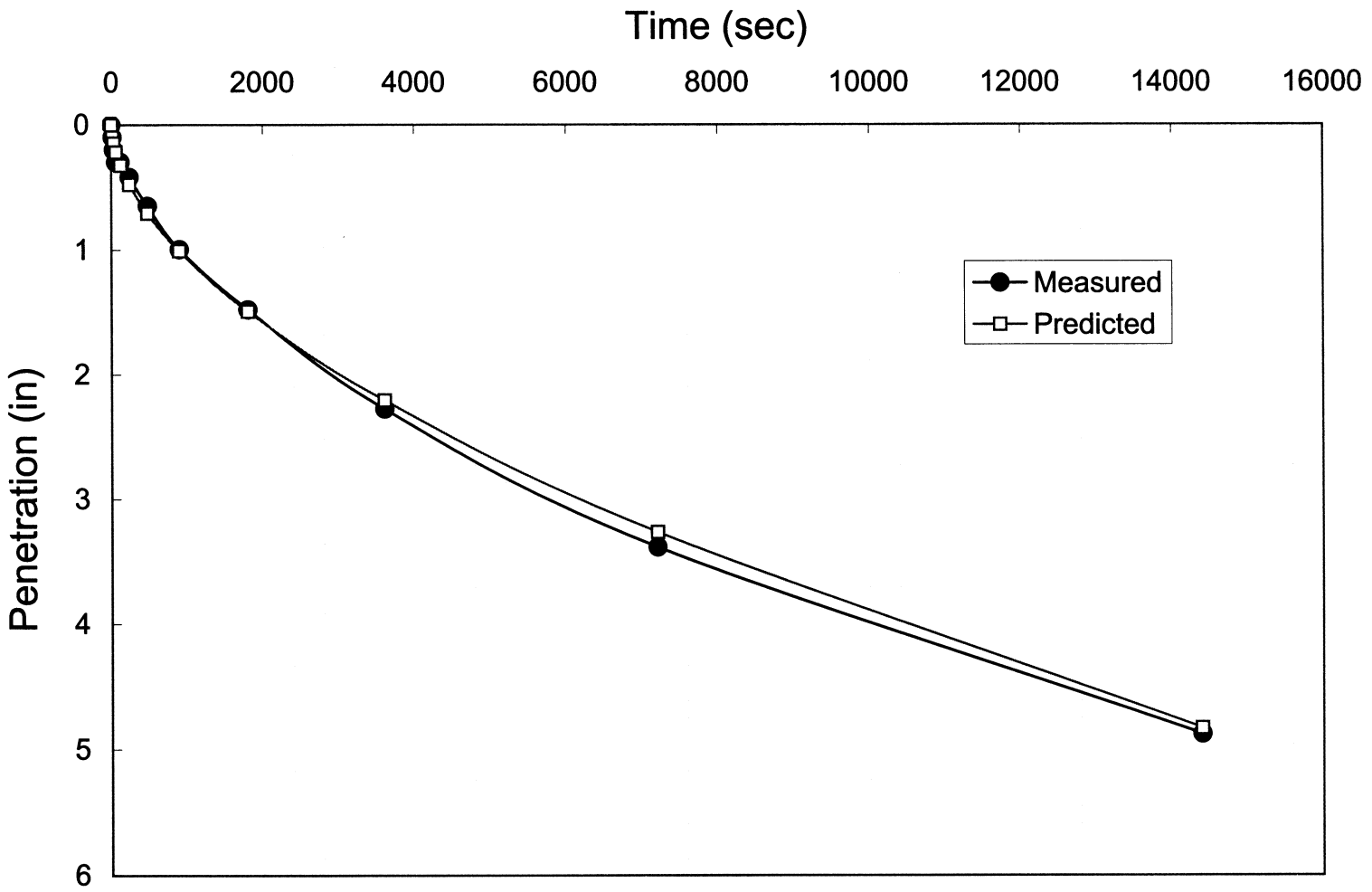

Figure 4.40 Attapulgite Slurry Penetration in Cohesionless Soil Under Pressure = 8 psi

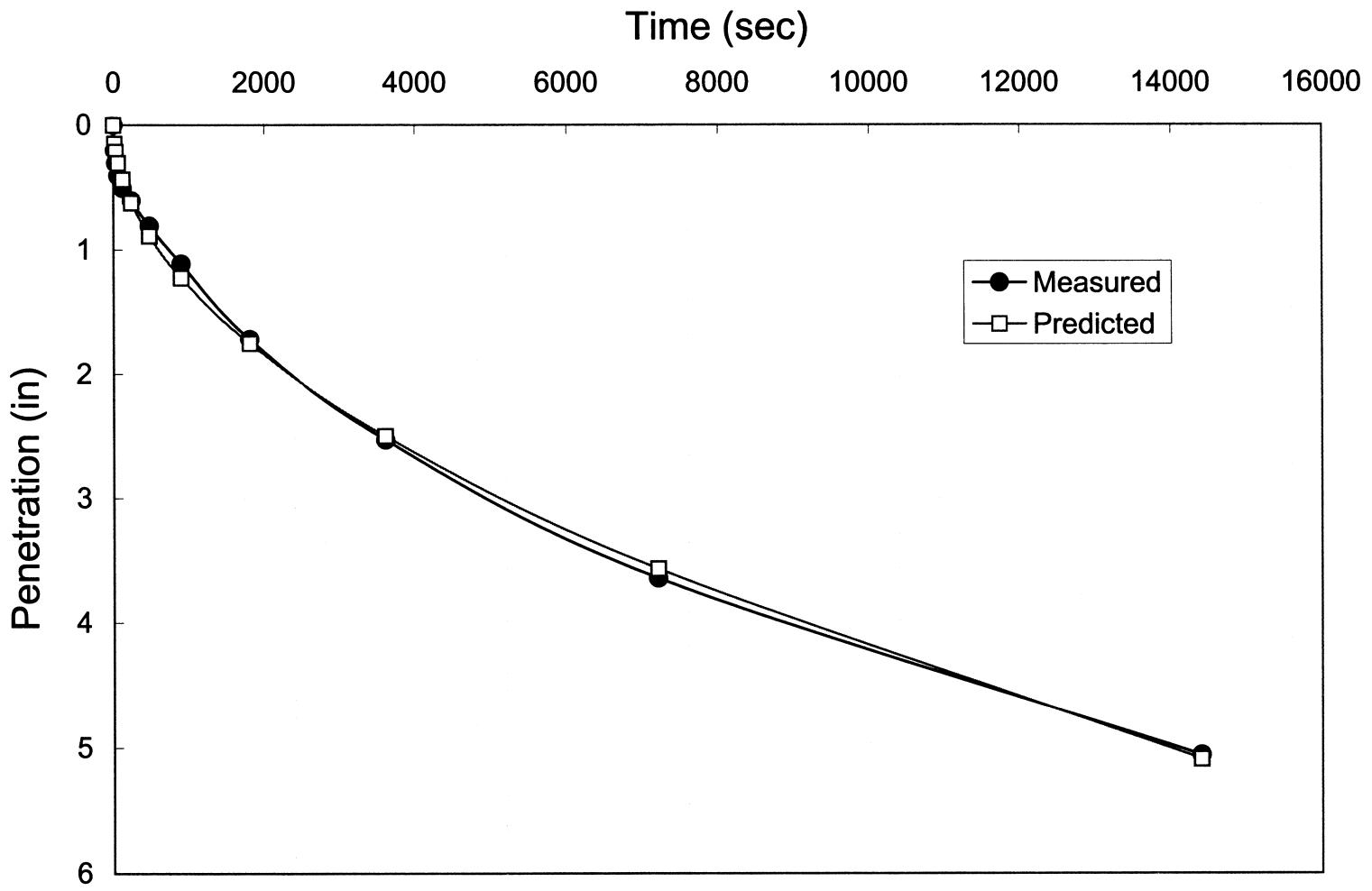

Figure 4.41 Attapulgite Slurry Penetration in Cohesionless Soil Under Pressure = 8 psi

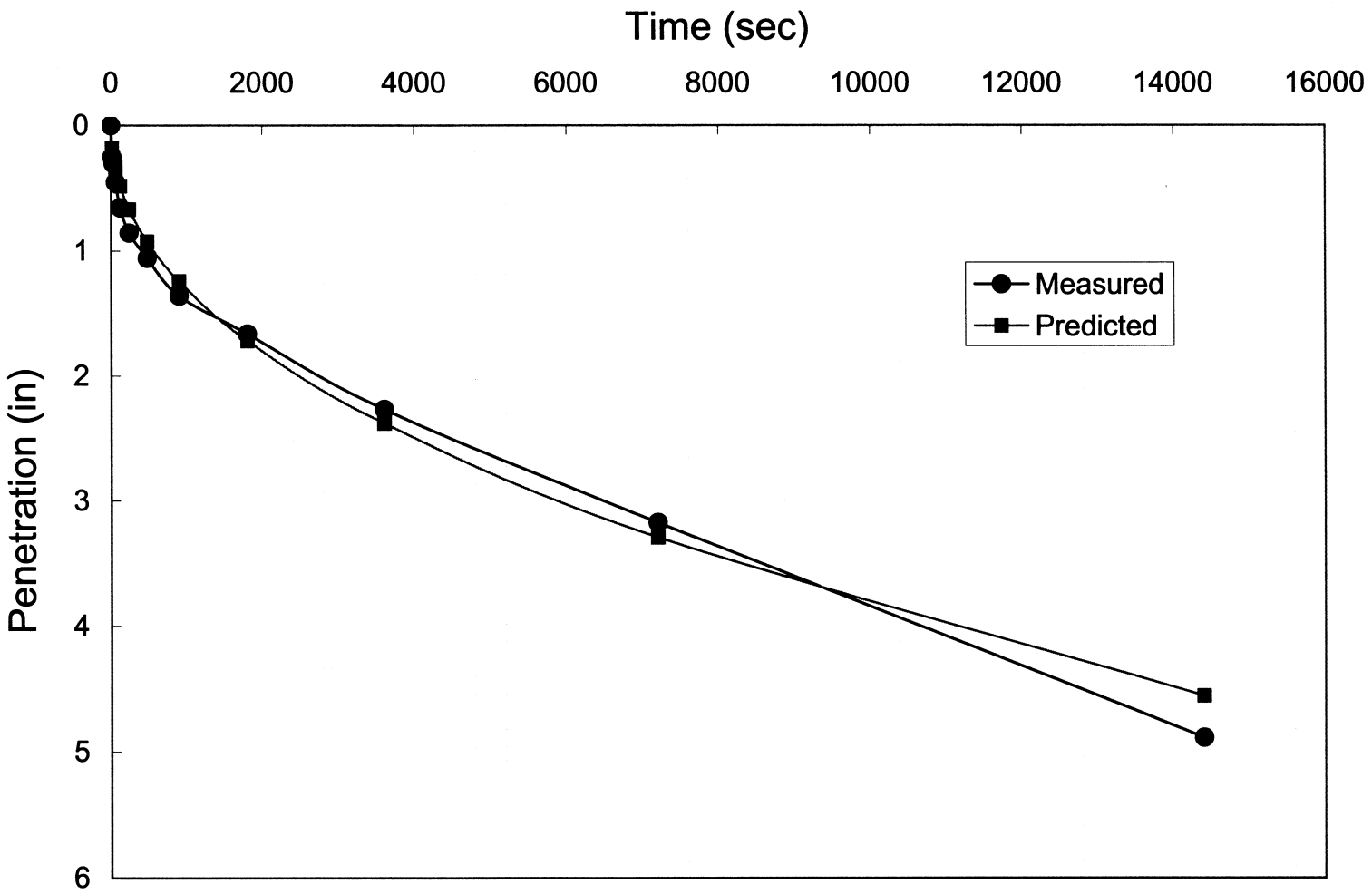

Figure 4.42 Attapulgite Slurry Penetration in Cohesionless Soil Under Pressure = 5 psi

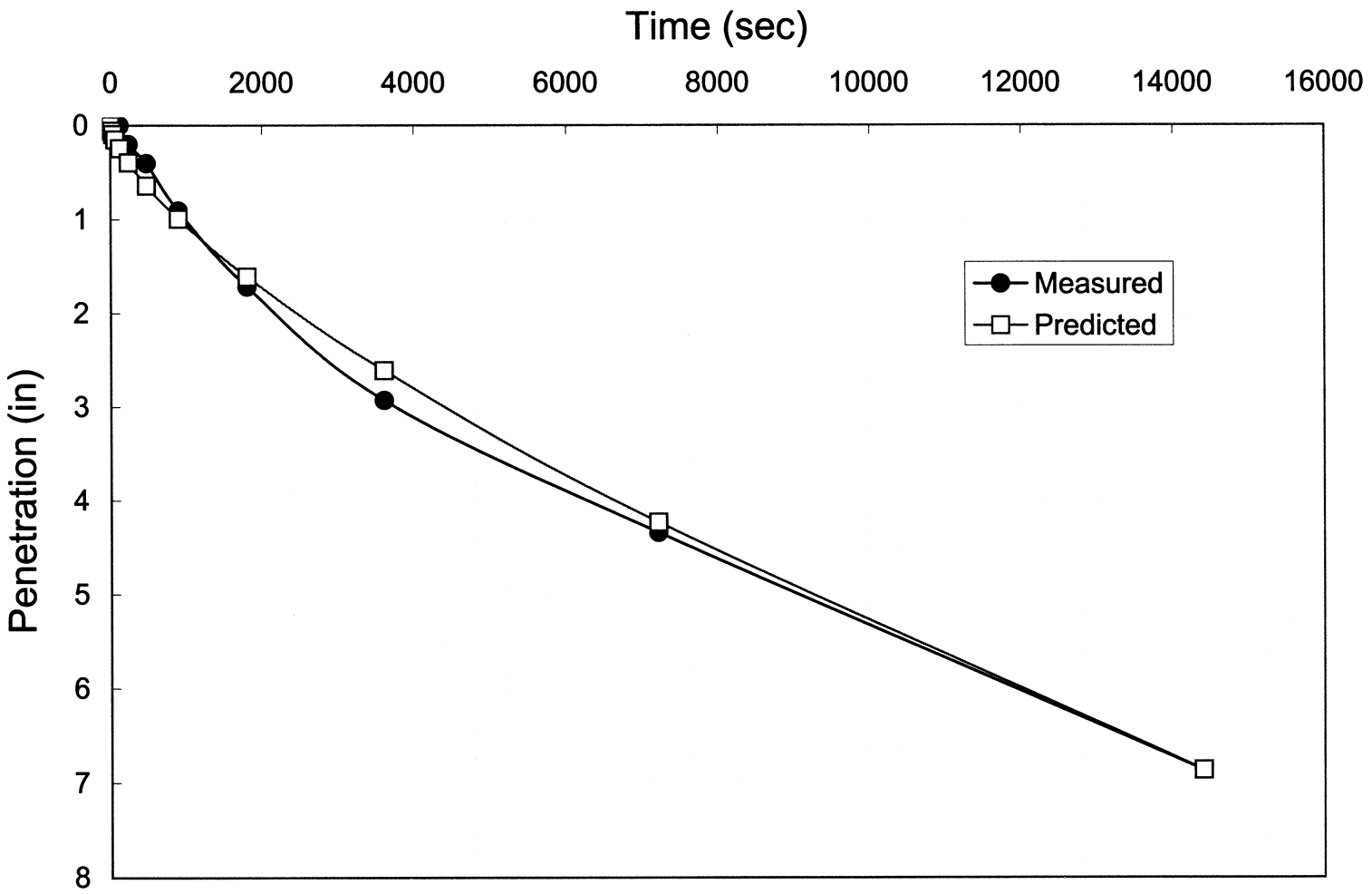

Figure 4.43 Attapulgite Slurry Penetration in Cohesionless Soil Under Pressure = 5 psi

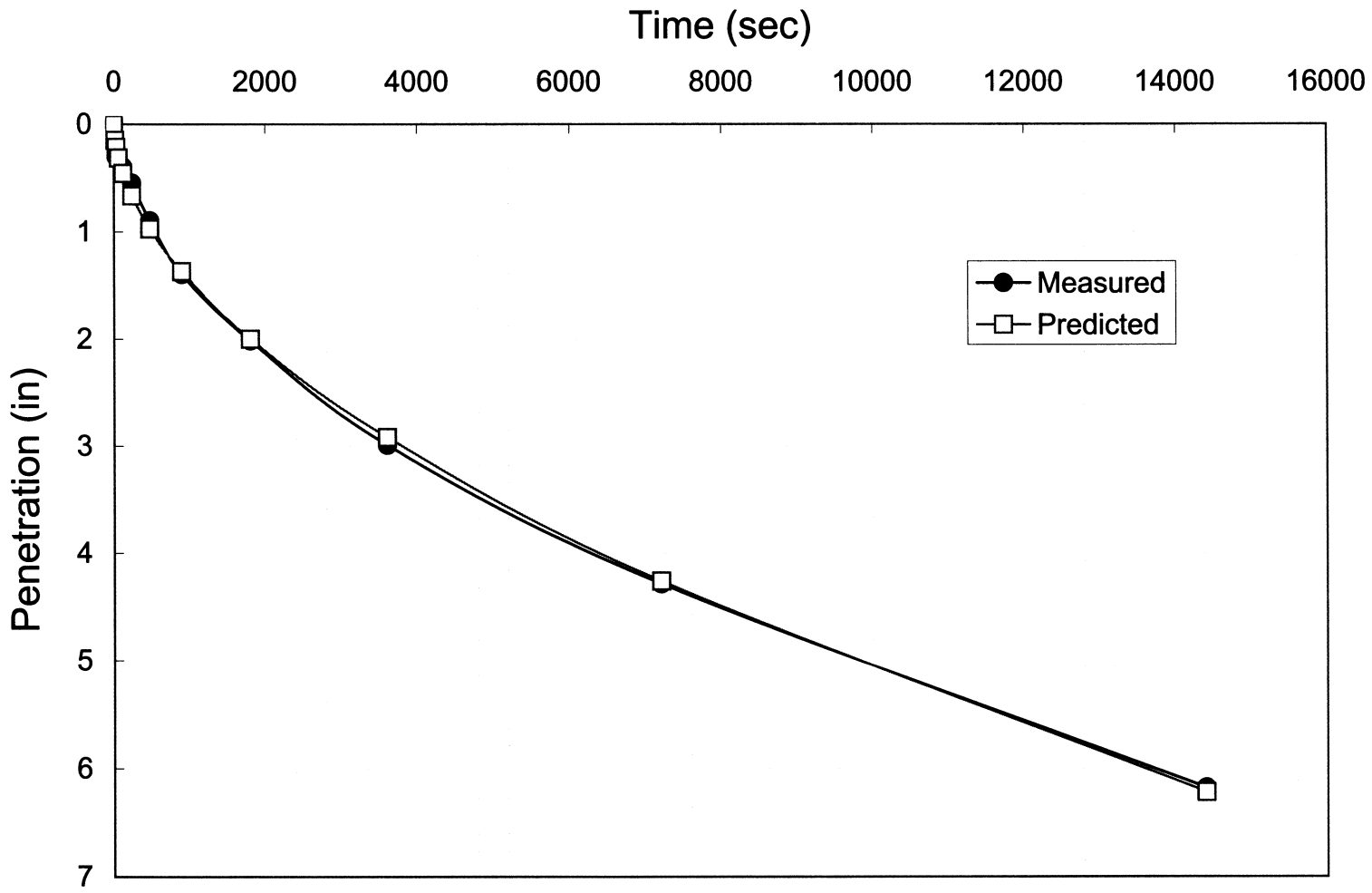

Figure 4.44 Attapulgite Slurry Penetration in Cohesionless Soil Under Pressure = 10 psi

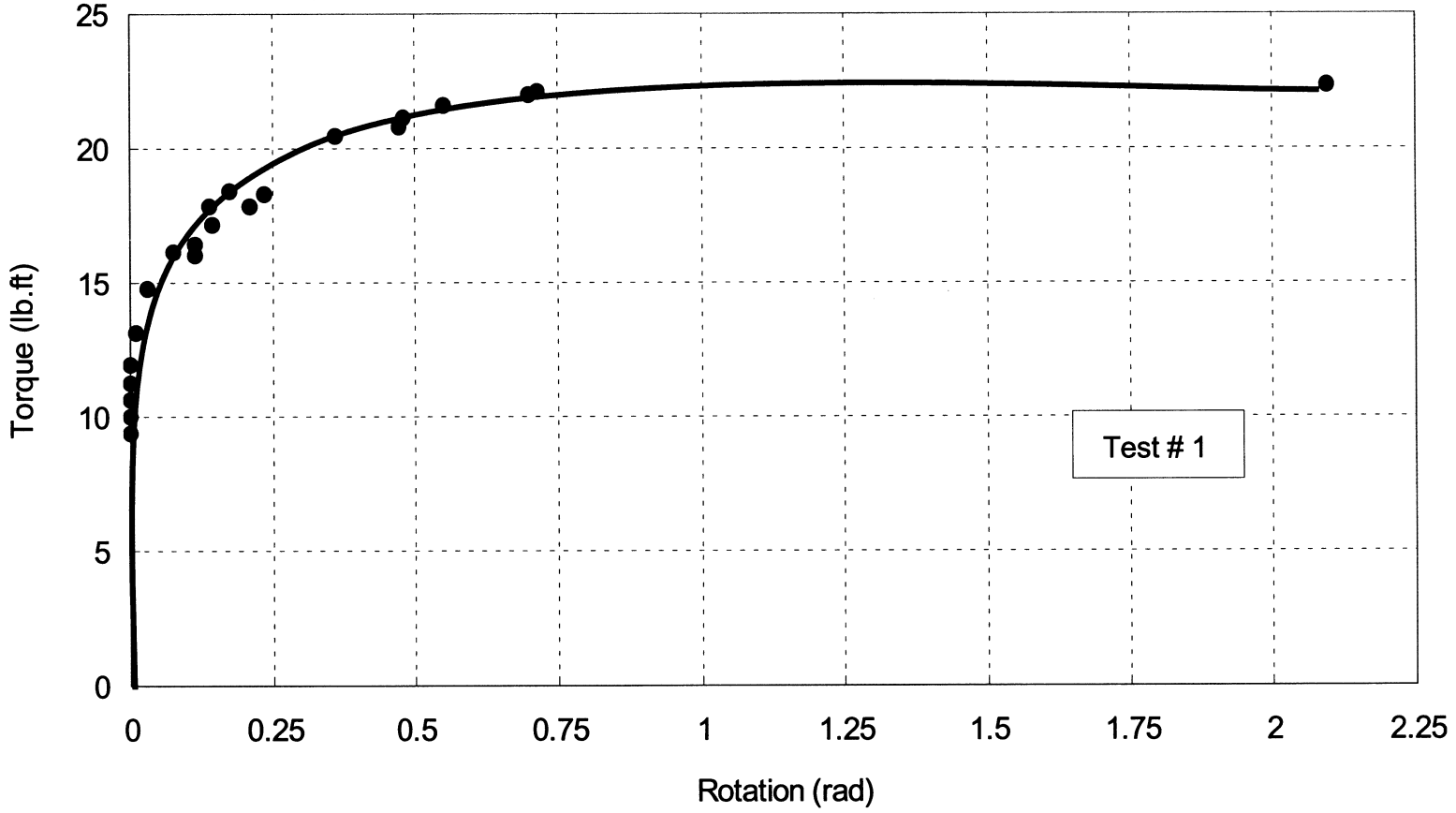

Figure 4.19. Simple Torsional Test on Scaled Model Shaft

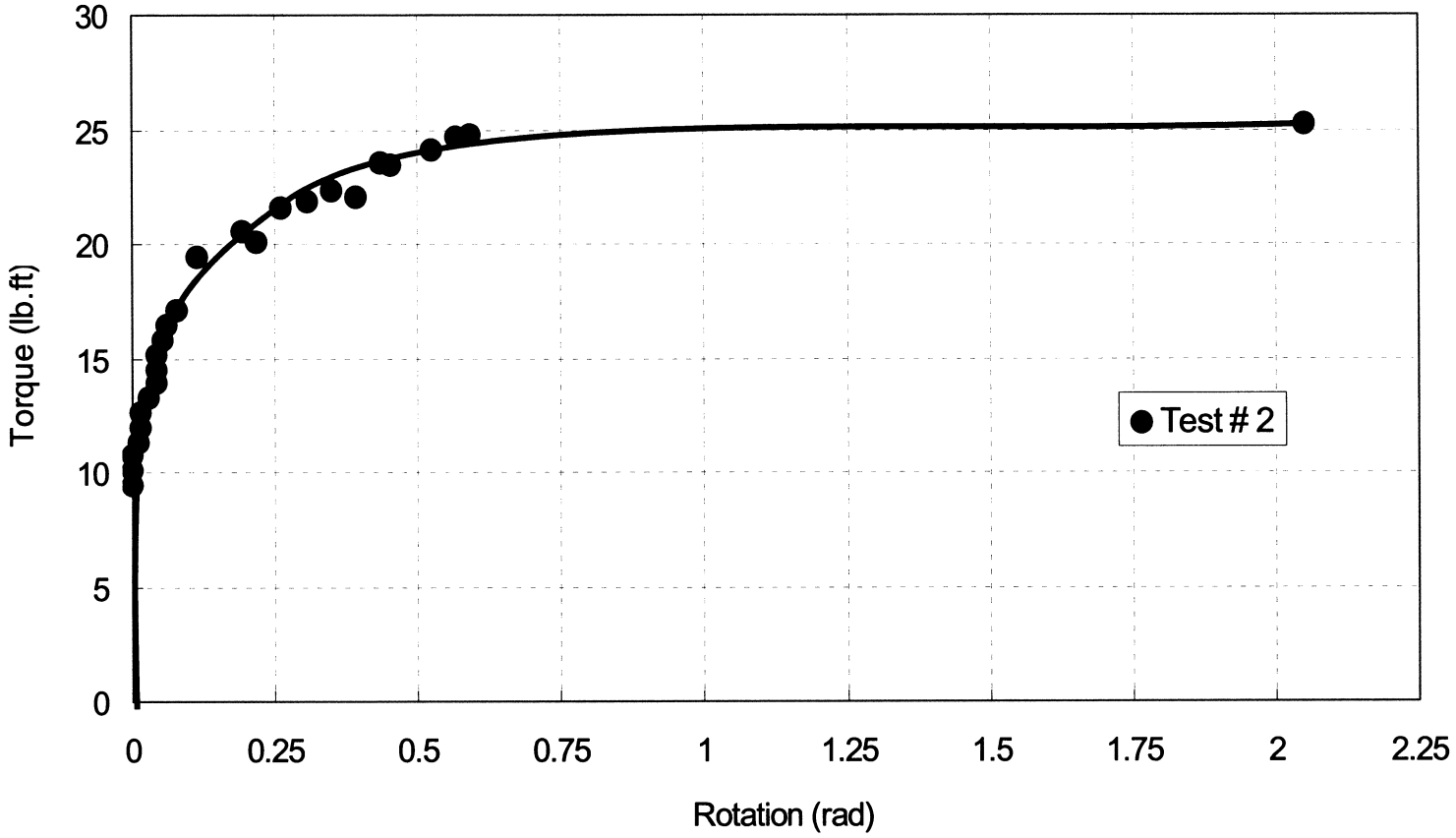

Figure 4.31 Simple Torsional Test on Scaled Model Shaft

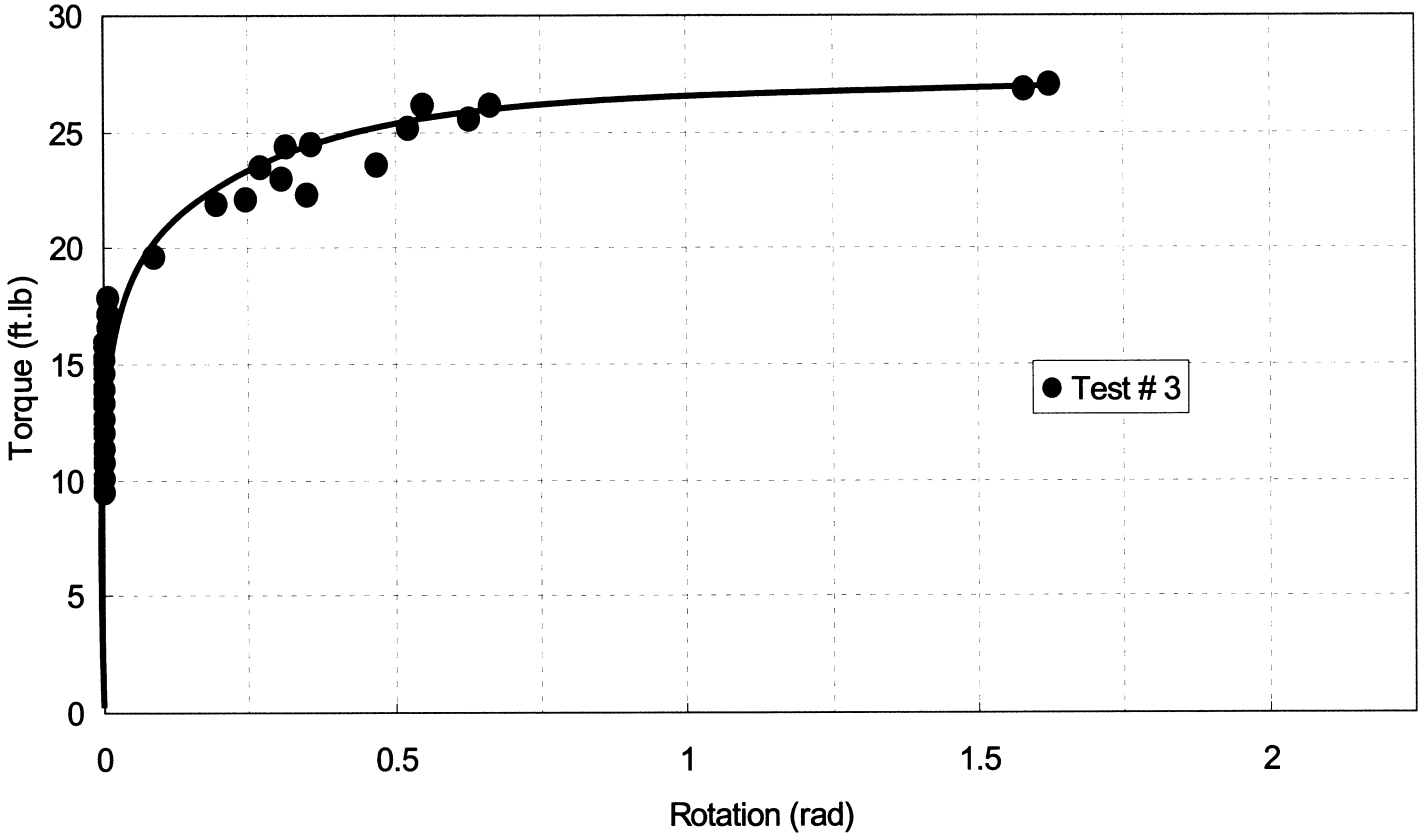

Figure 4.32 Simple Torsional Test on Scaled Model Shaft

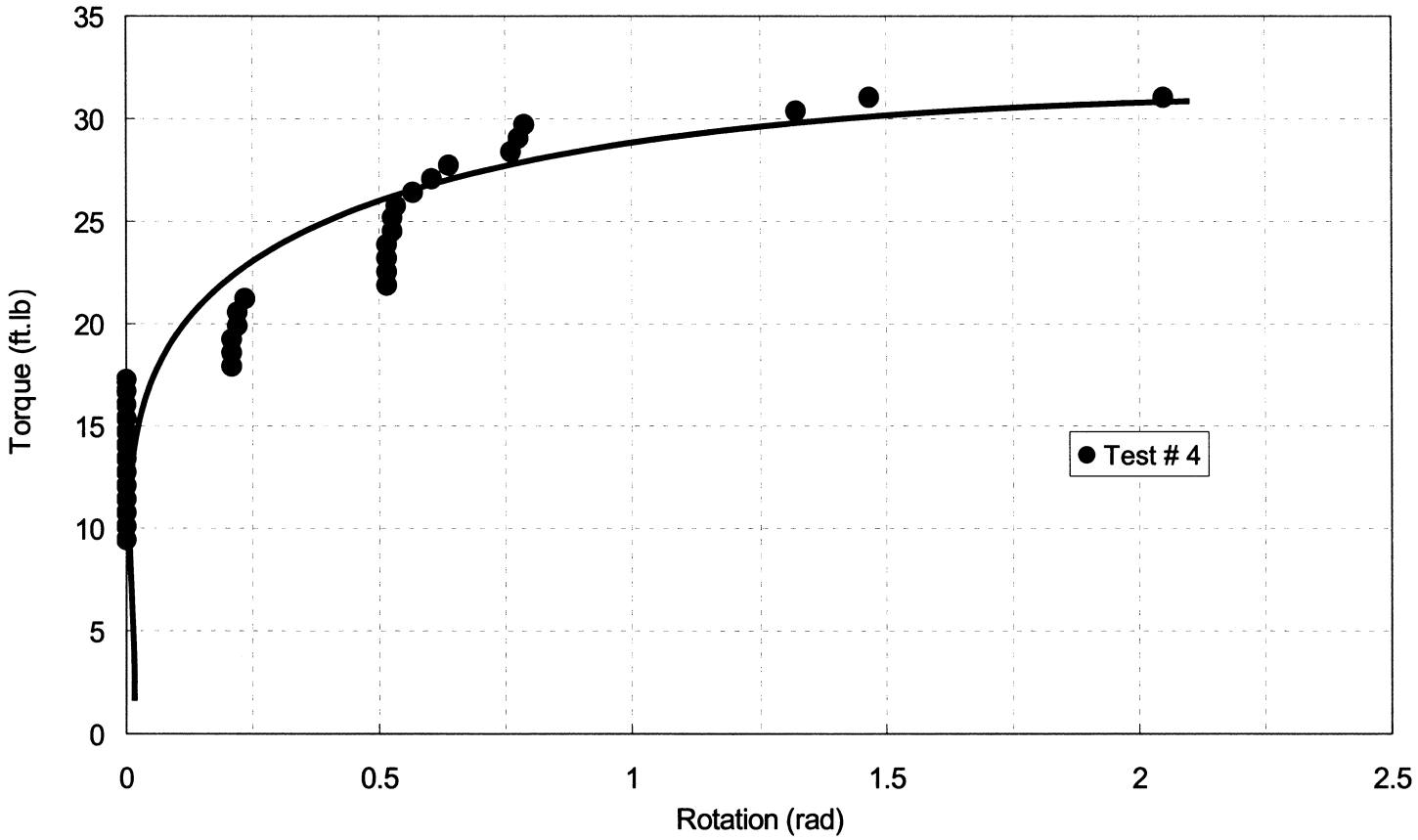

Figure 4.33 Simple Torsional Test on Scaled Model Shaft

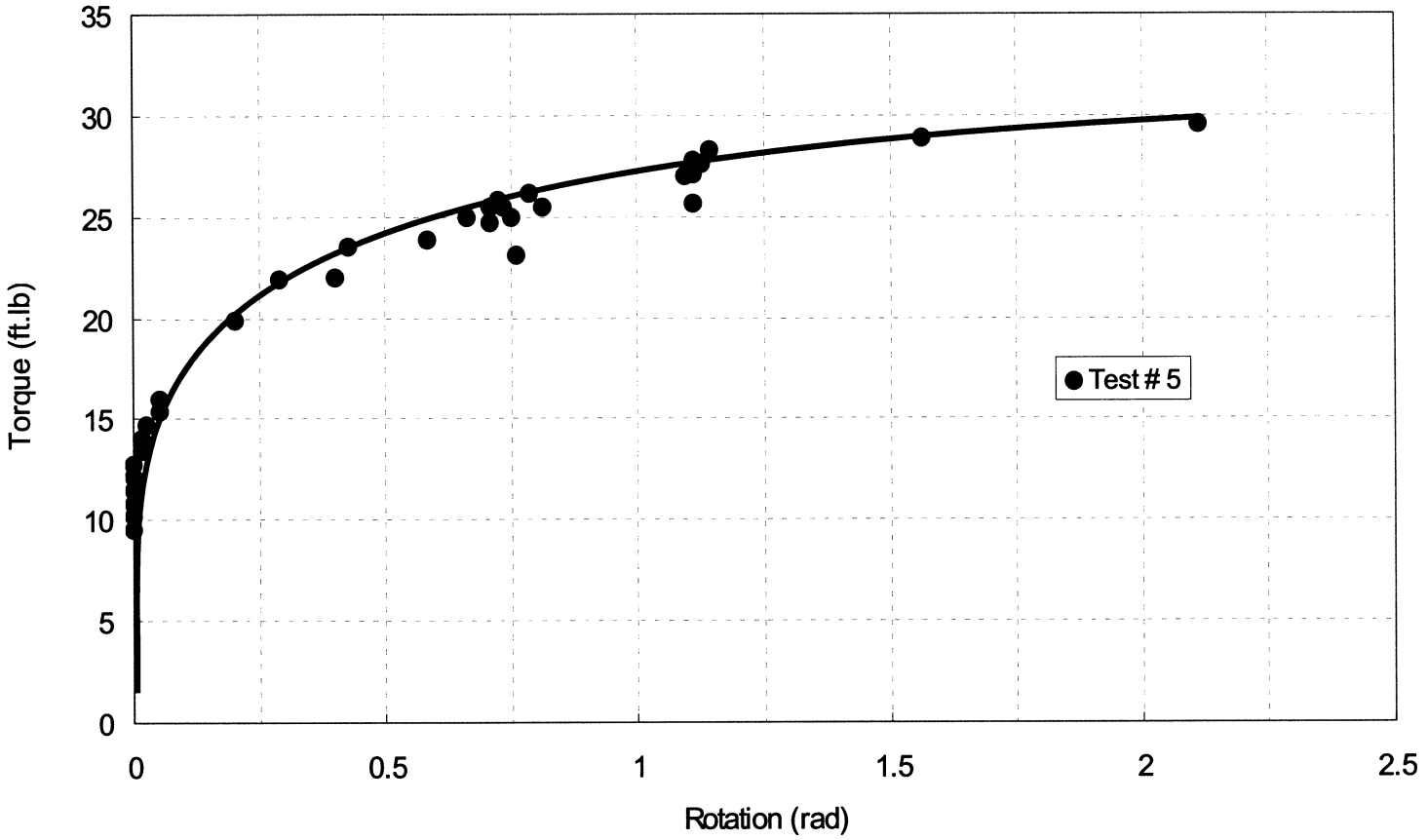

Figure 4.34 Simple Torsional Test on Scaled Model Shaft

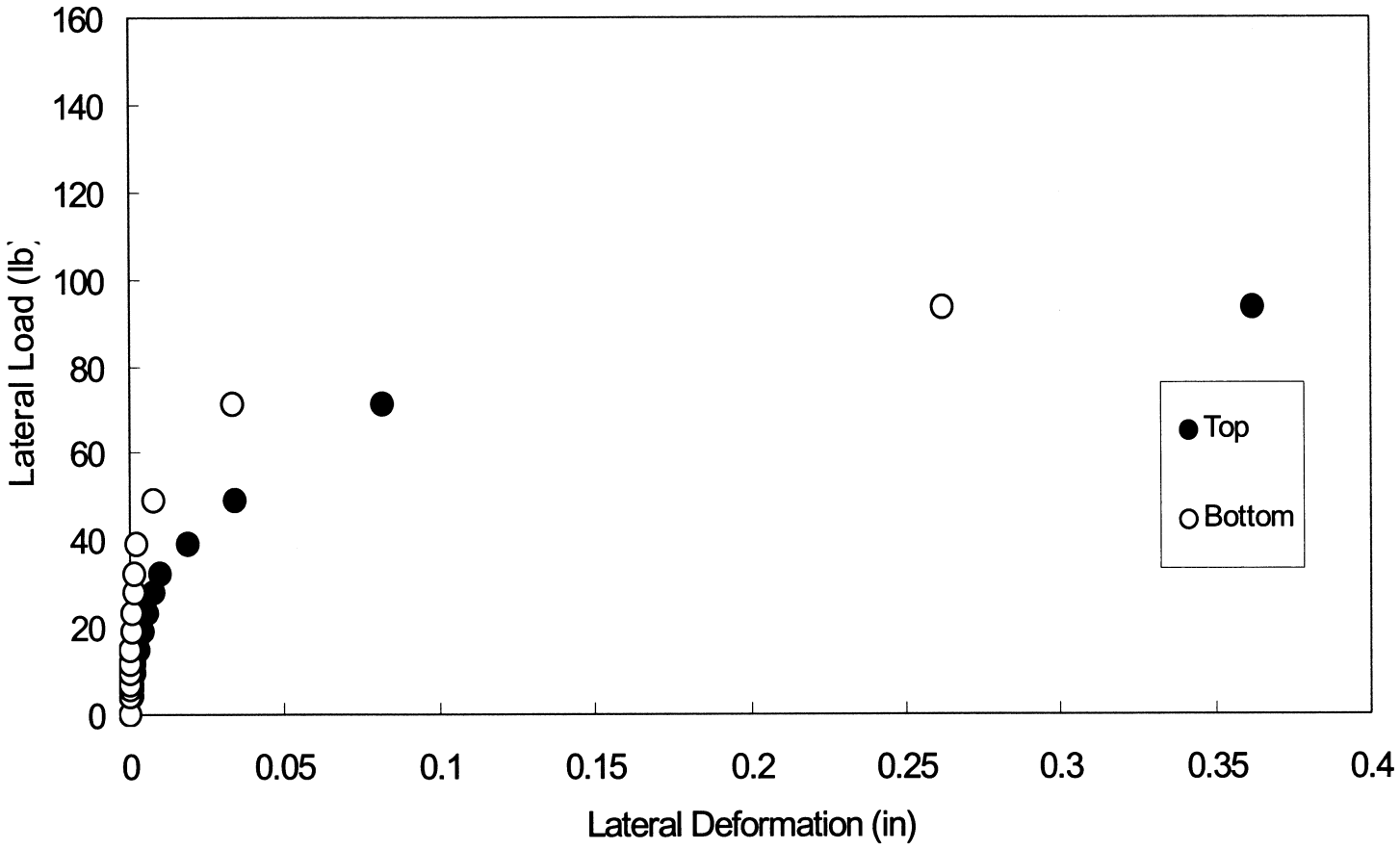

Figure 4.37 Test # 2 for Lateral Load vs. Lateral Deformation of Scaled Shaft

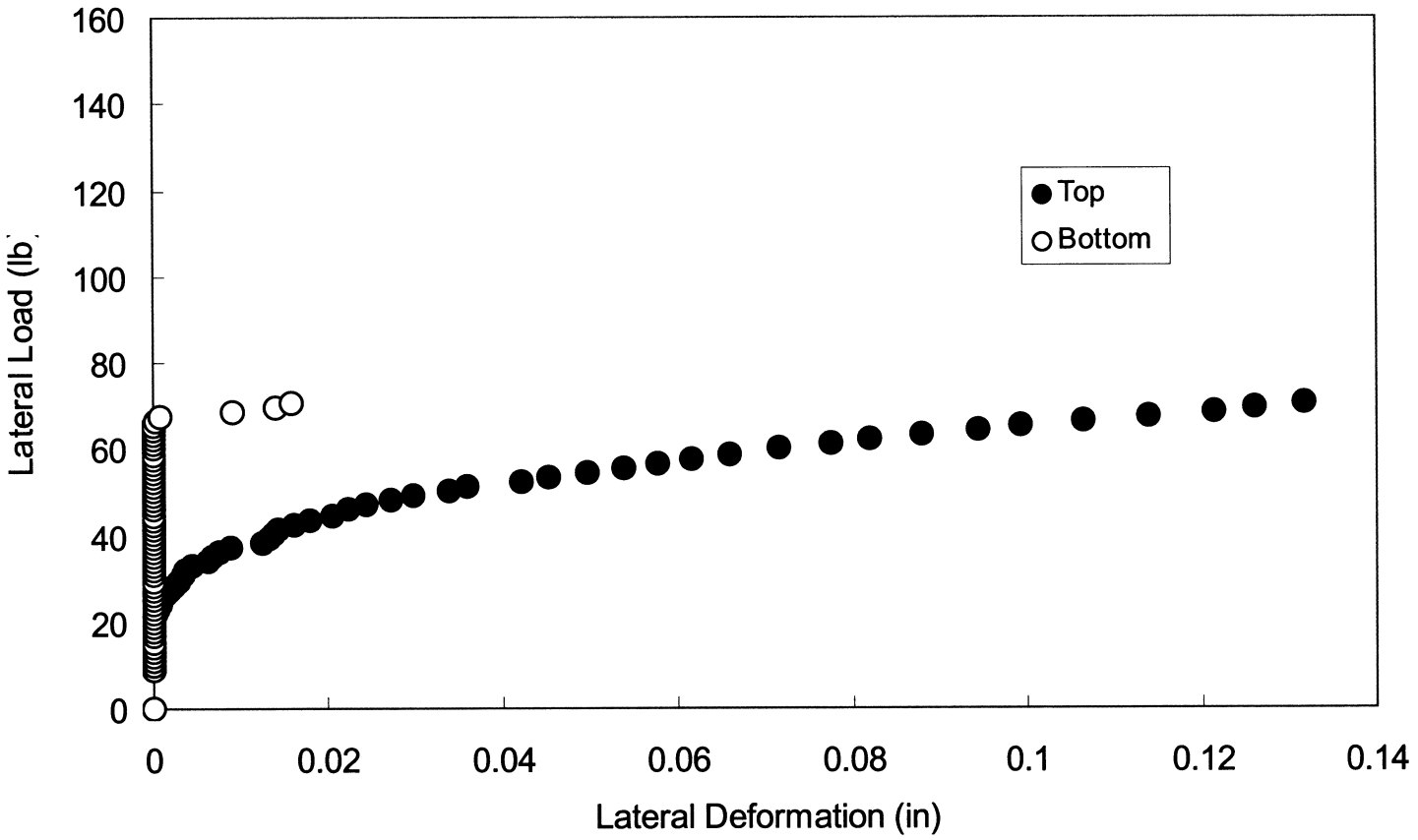

Figure 4.39. Test # 3 for Lateral Load vs. Lateral Deformation of Scaled Shaft

PCL XL error

Subsystem: KERNEL

Error: IllegalTag

Operator: 0x1b

Position: 2

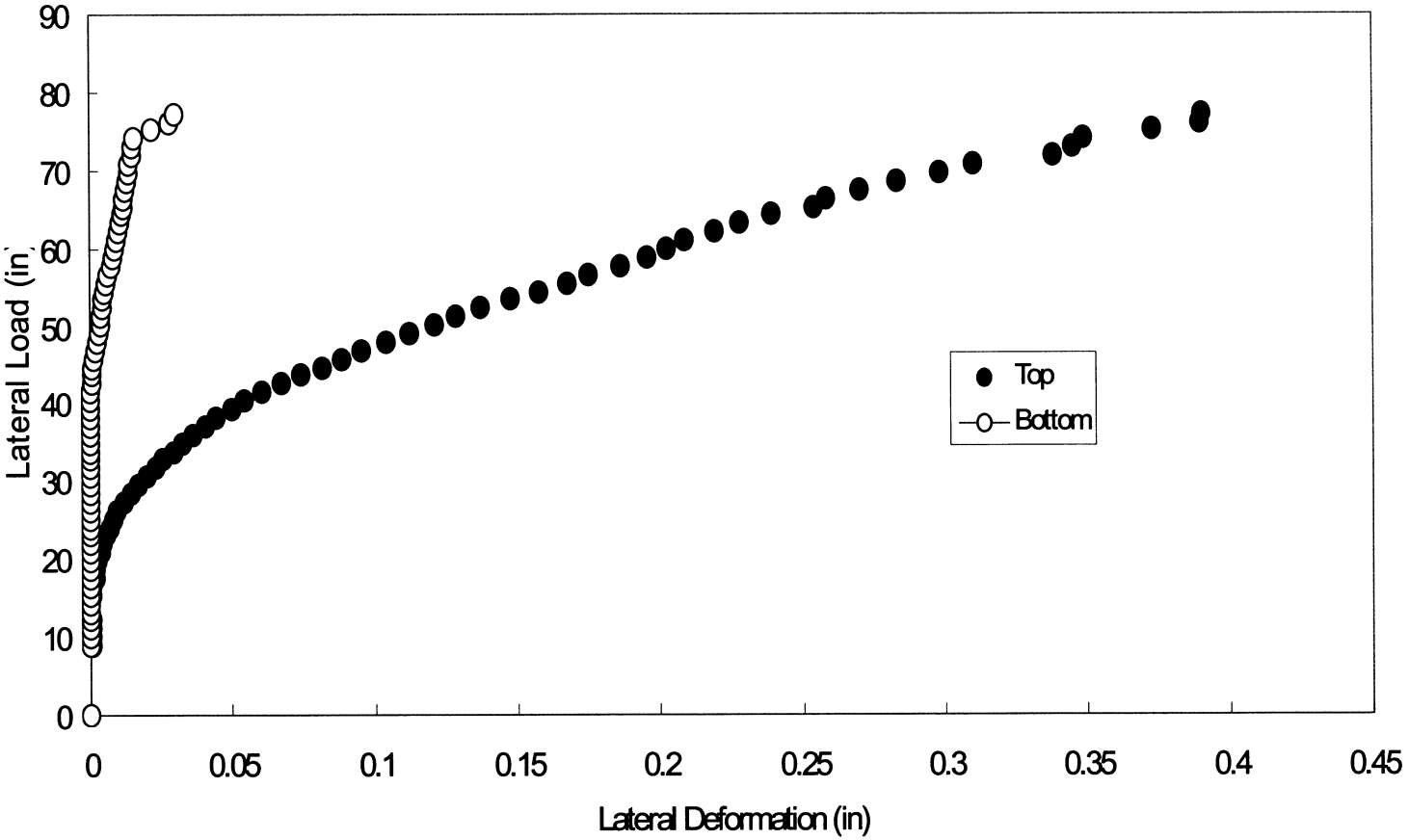

Figure 4.41 Test # 4 for Lateral Load vs. Lateral Deformation of Scaled Shaft

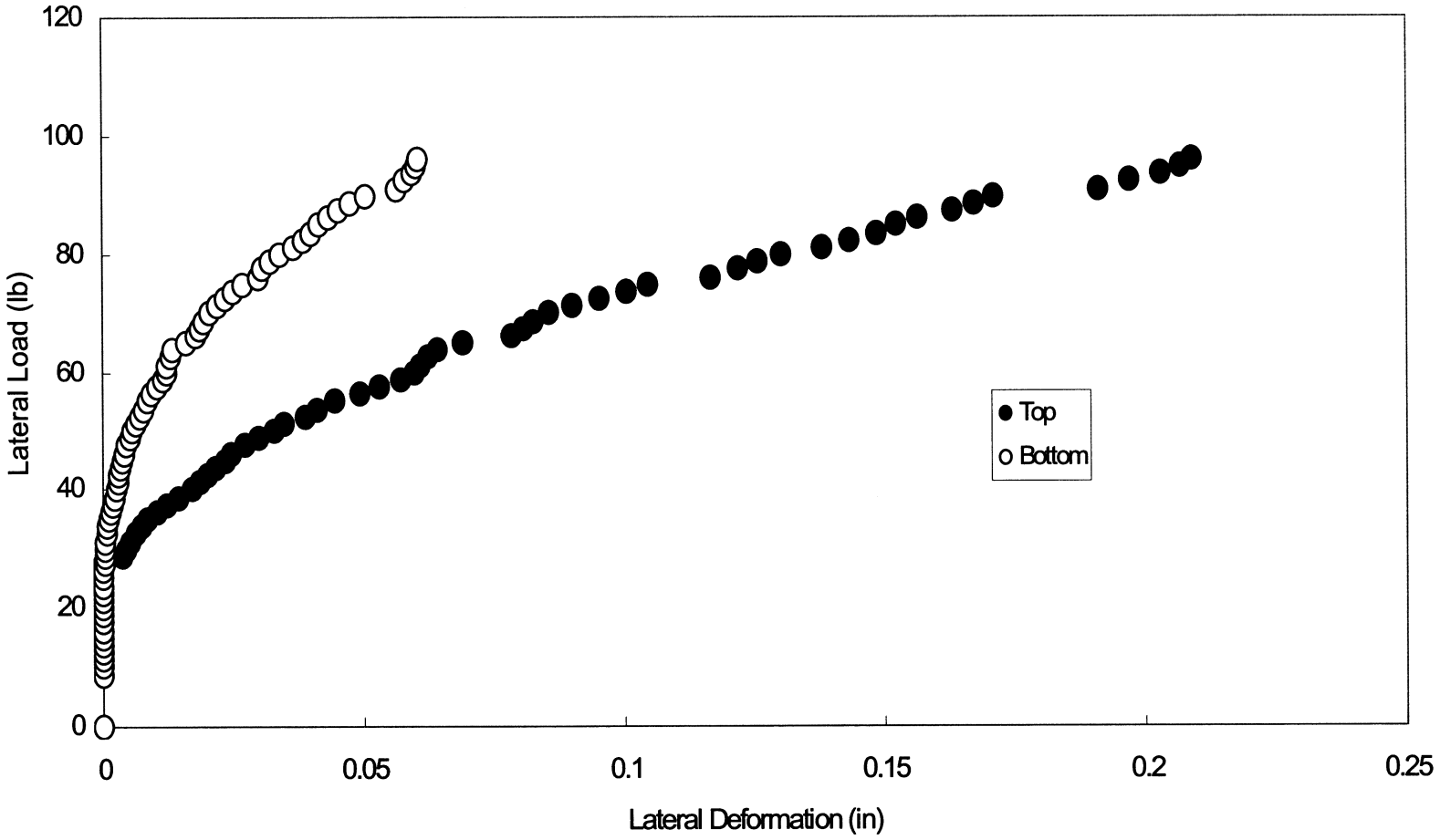

Figure 4.43 Test # 5 for Lateral Load vs. Lateral Deformation of Scaled Shaft

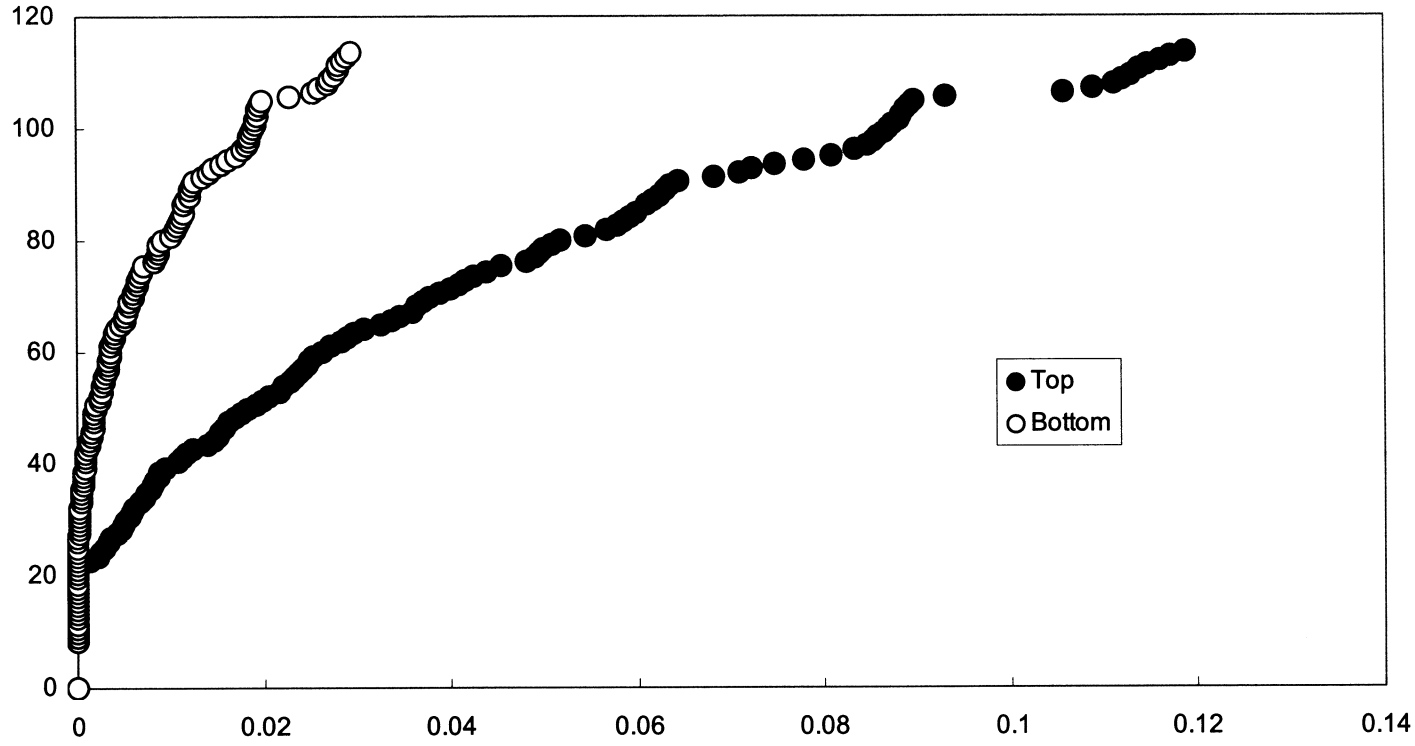

Figure 4.45 Test # 6 for Lateral Load vs. Lateral Deformation of Scaled Shaft

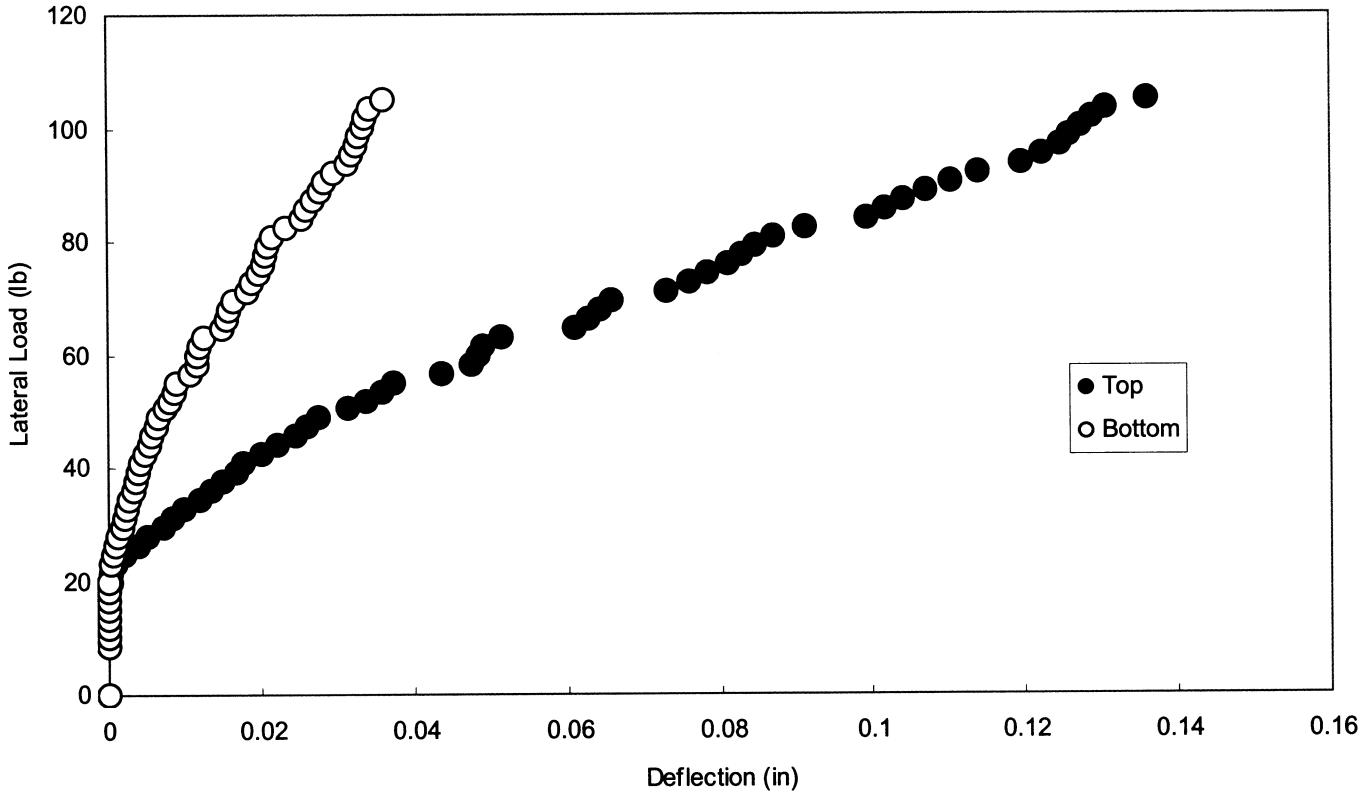

Figure 4.47 Test # 7 for Lateral Load vs. Lateral Deformation of Scaled Shaft

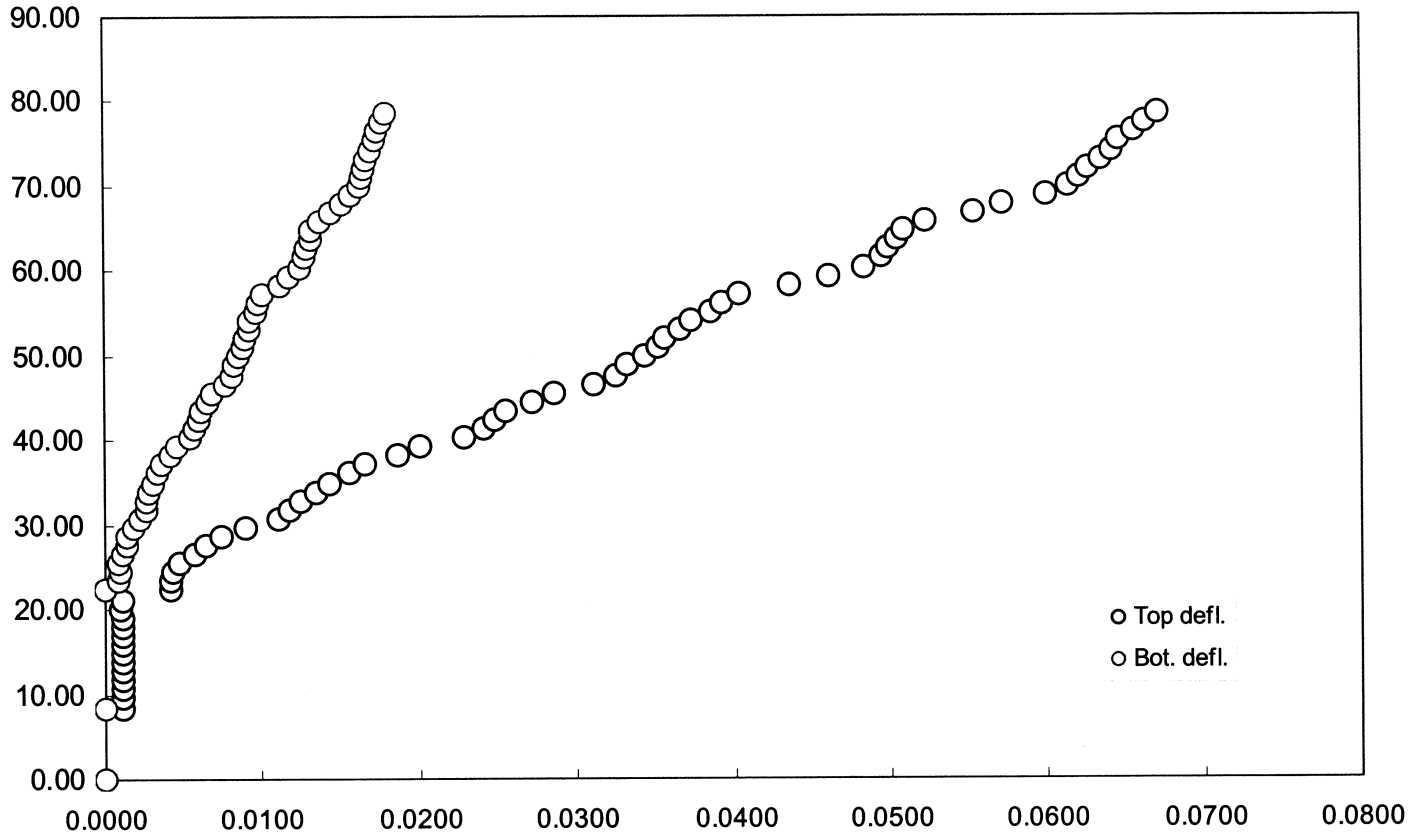

Figure 4.49 Test # 8 for Lateral Load vs. Lateral Deformation of Scaled Shaft

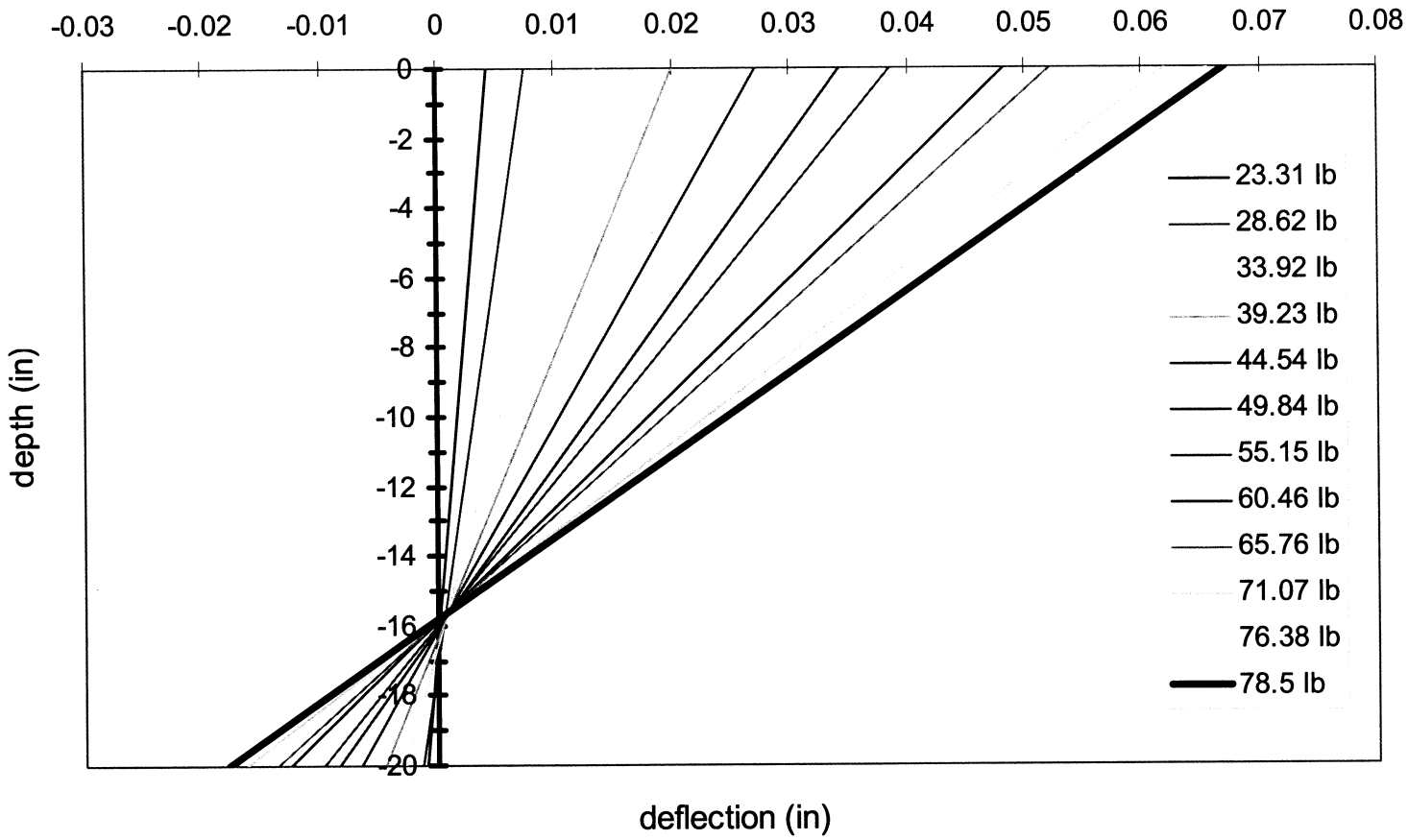

Figure 4.50 Test # 8 for Lateral Load vs. Lateral Deformation of Scaled Shaft
Depth vs. Deflection (lateral 8)

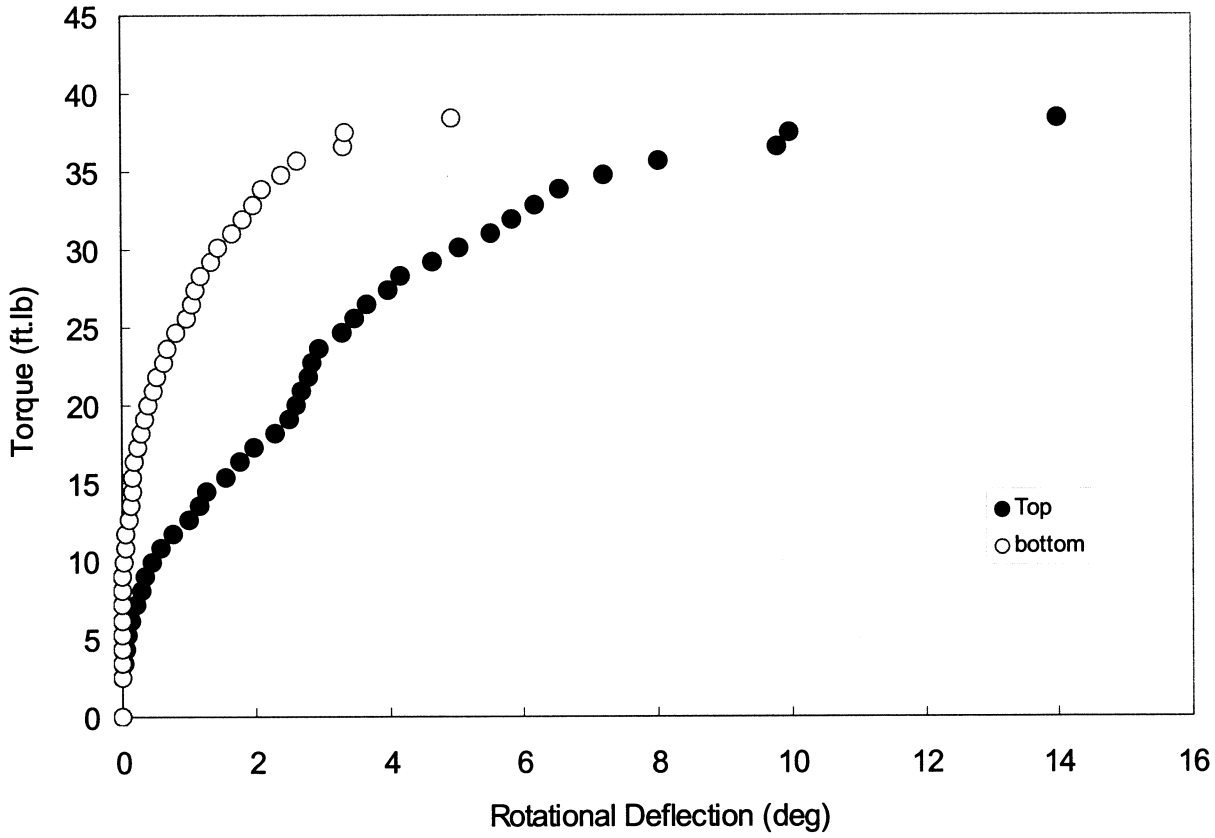

Figure 4.56 Test # 8 for Lateral Load & Moment Lateral First Then Torsional

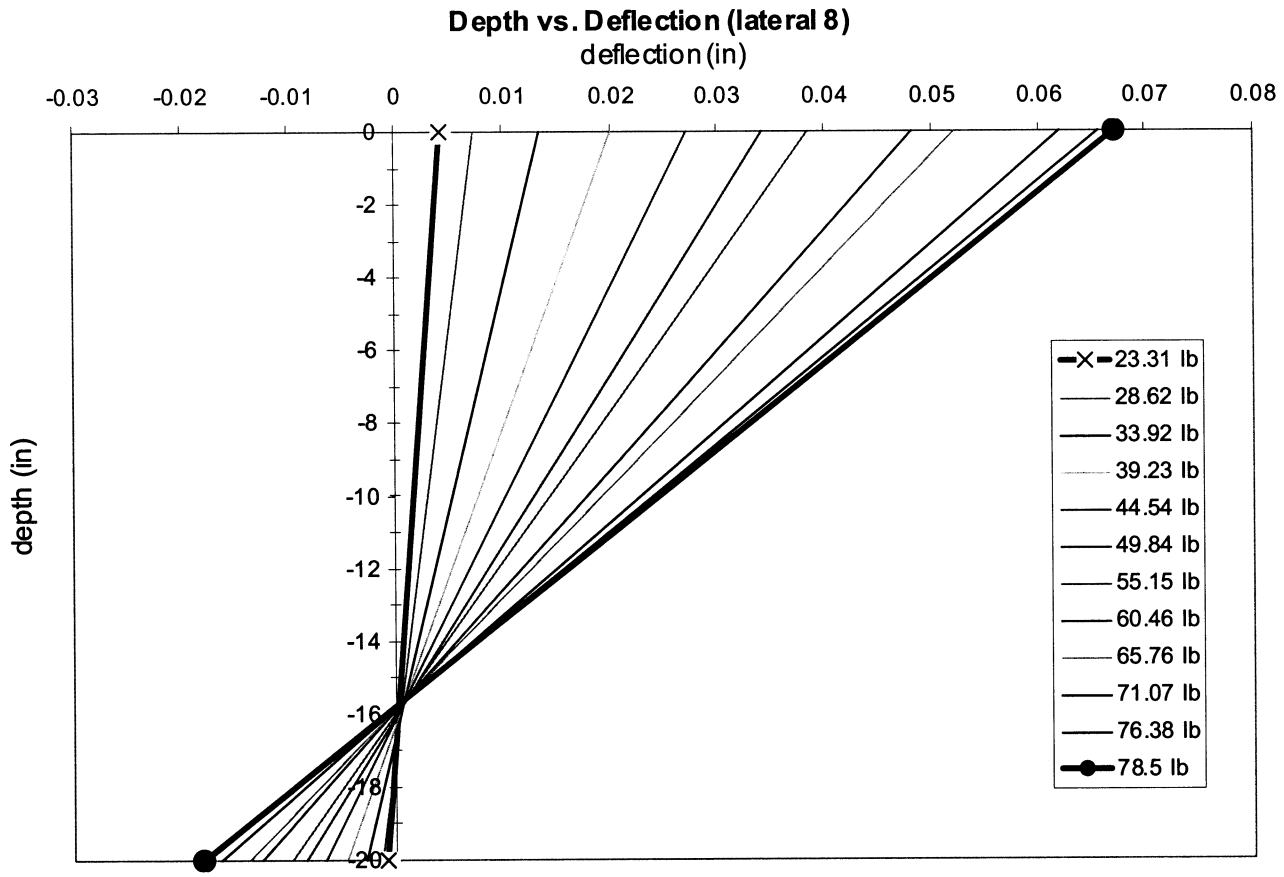

Figure 4.57 Test # 8 for Lateral Load & Moment Lateral First Then Torsional

APPENDIX B

FULL SCALE FIELD TESTING

Subsurface Soil Exploration
Bridge Foundation Drilled Shafts
FSU/FAMU Research Project
Tallahassee, Florida

Ardaman & Associates, Inc.

March 9, 1998
File No. 97-6341

Florida Department of Transportation
1901 S. Marion Street
Lake City, Florida 32025

Attention: Mr. Pasco Jarvis

Subject: Subsurface Soil Exploration
Bridge Foundation Drilled Shafts
FSU/FAMU Research Project
Tallahassee, Florida

Gentlemen:

As requested and authorized by you, we have completed subsurface soil exploration and laboratory testing for the subject project. The purposes of performing this exploration were to determine the general subsurface soil and groundwater conditions at selected locations and conduct laboratory testing to determine soil strength parameters. It is our understanding that this data will be used for a research project relative to drilled shaft foundations. This report documents our findings.

SITE LOCATION AND SITE DESCRIPTION

The site for the proposed facility is located on the north side of Levy Road near the FSU/FAMU Engineering Building in Tallahassee, Florida (Section 3, Township 1 S, Range 1 W). The general site location is shown superimposed on the 1970 (photorevised 1976) Tallahassee, Florida, U.S.G.S. quadrangle map presented on Figure 1.

The site is currently grass covered.

REVIEW OF SOIL SURVEY MAPS

Based on the 1981 Soil Survey for Leon County, Florida, as prepared by the U.S. Department of Agriculture Soil Conservation Service, the predominate soil type at the site is identified as the "Orangeburg Fine Sandy Loam" soil series which consists of well drained, gently sloping soils that occurs on the uplands. The internal drainage of the "Orangeburg Fine Sandy Loam" is moderately rapid in the surface layer and moderate in the subsoil. According to the Soil Survey, the seasonal high water table for the "Orangeburg Fine Sandy Loam" is typically greater than 72 inches below the natural ground surface.

FIELD EXPLORATION PROGRAM

The field exploration program consisted of performing 4 Standard Penetration Test (SPT) borings, 4 Dilatometer soundings and 4 Cone Penetrometer Test (CPT) soundings.

The SPT borings were performed at locations selected by the client. The borings were advanced to depths of 25 feet below the ground surface using the methodology outlined in ASTM D-1586. A summary of this field procedure is included in Appendix I. Split-spoon soil samples were recovered during performance of the borings continuously to a depth of 15 feet and every 2.5 feet thereafter. The samples were visually classified in the field and representative portions of the samples were transported to our laboratory in sealed sample jars for further classification and laboratory testing.

A total of 10 relatively undisturbed "Shelby" tube samples were retrieved from Borings TH-2, TH-3 and TH-4 for laboratory testing.

The CPT soundings were performed adjacent to the SPT borings to depths of 25 feet below ground surface using the methodology outlined in ASTM D-3441. They were conducted using a mechanical-type cone and cone rig mounted on a ballasted truck. For the cone soundings, both tip and shaft loads were recorded with depth. A summary of the CPT field procedure is also included in Appendix I.

The dilatometer soundings were also conducted adjacent to the SPT borings to depths of 25 feet. Readings were taken at 2-foot intervals during the soundings. A summary of this field procedure is also included in Appendix I.

The groundwater level at each of the SPT boring locations was measured upon completion of drilling.

The locations of the borings and soundings are schematically illustrated on a site plan shown on Figure 1. These locations were located in the field by representatives of the client.

LABORATORY TESTING PROGRAM

Representative soil samples obtained during our field sampling operation were packaged and transferred to our laboratory for further visual examination and classification. The soil samples were visually classified in general accordance with the Unified Soil Classification System (ASTM D-2488). The resulting soil descriptions are shown on the soil boring profiles presented on Figure 1.

Classification Tests

In addition to the visual examination of all samples, laboratory tests were conducted on representative samples to aid in classification. These tests included sieve analysis, percent fines, natural moisture and Atterberg limits. The results of these tests are presented on Figure 1 adjacent to the soil profiles at the respective depths from which the tested samples were recovered. The resulting sieve analysis curves are presented in Appendix II.

Direct Shear Tests

In addition to classification testing, direct shear tests were conducted on subsamples taken from the "Shelby" tube samples. The results of these tests are presented in Appendix III.

GENERAL SUBSURFACE CONDITIONS

General Soil Profile

The results of the field exploration and laboratory testing programs are graphically summarized on the soil boring profiles presented on Figure 1, the CPT sounding profiles presented in Appendix IV and the results of the dilatometer soundings represented in Appendix V. The stratification of the boring profiles represents our interpretation of the field boring logs and the results of laboratory examinations of the recovered samples. The stratification lines represent the approximate boundary between soil types. The actual transitions may be more gradual than implied.

The results of our SPT borings indicate the following general soil profile. Very loose to medium dense clayey silty fine sand and soft to stiff sandy clay were encountered below the topsoil to the termination depth of Boring TH-2 and to depths ranging from 17 to 21 feet in the remaining borings. Borings TH-1, TH-3 and TH-4 terminated in medium dense fine sand with silt and silty fine sand.

The results of the CPT and dilatometer soundings typically agreed with the results of the SPT borings.

The above soil profile is outlined in general terms only. Please refer to Figure 1 and Appendices IV and V for soil profile details.

Measured Groundwater Level

The groundwater level was not encountered on the day drilled. The absence of groundwater data at the boring locations indicates that groundwater was not encountered within the vertical reach of the borings on the date drilled. However, this does not necessarily mean that groundwater would not be encountered at some other time. Fluctuations in groundwater levels should be anticipated throughout the year primarily due to seasonal variations in rainfall and other factors that may vary from the time the borings were conducted.

CLOSURE

The data submitted herein are based upon the soil borings presented on Figure 1 and the CPT and dilatometer soundings presented in Appendices IV and V, respectively. This report does not reflect any variations which may occur adjacent to or between the borings and soundings.

This report has been prepared for the exclusive use of the Florida Department of Transportation in accordance with generally accepted soil engineering practices. No other warranty, expressed or implied, is given.

We are pleased to be of assistance to you on this phase of your project. When we may be of further service to you or should you have any questions, please contact us.

Very truly yours,
ARDAMAN & ASSOCIATES, INC.

Zan C. Bates, P.E.
Project Engineer
Florida Registration No. 49917

Charles H. Cunningham, P.E.
Division Manager
Florida Registration No. 38189

ZCB/CHC/jas
97-6341.SSE (ZCB #17)

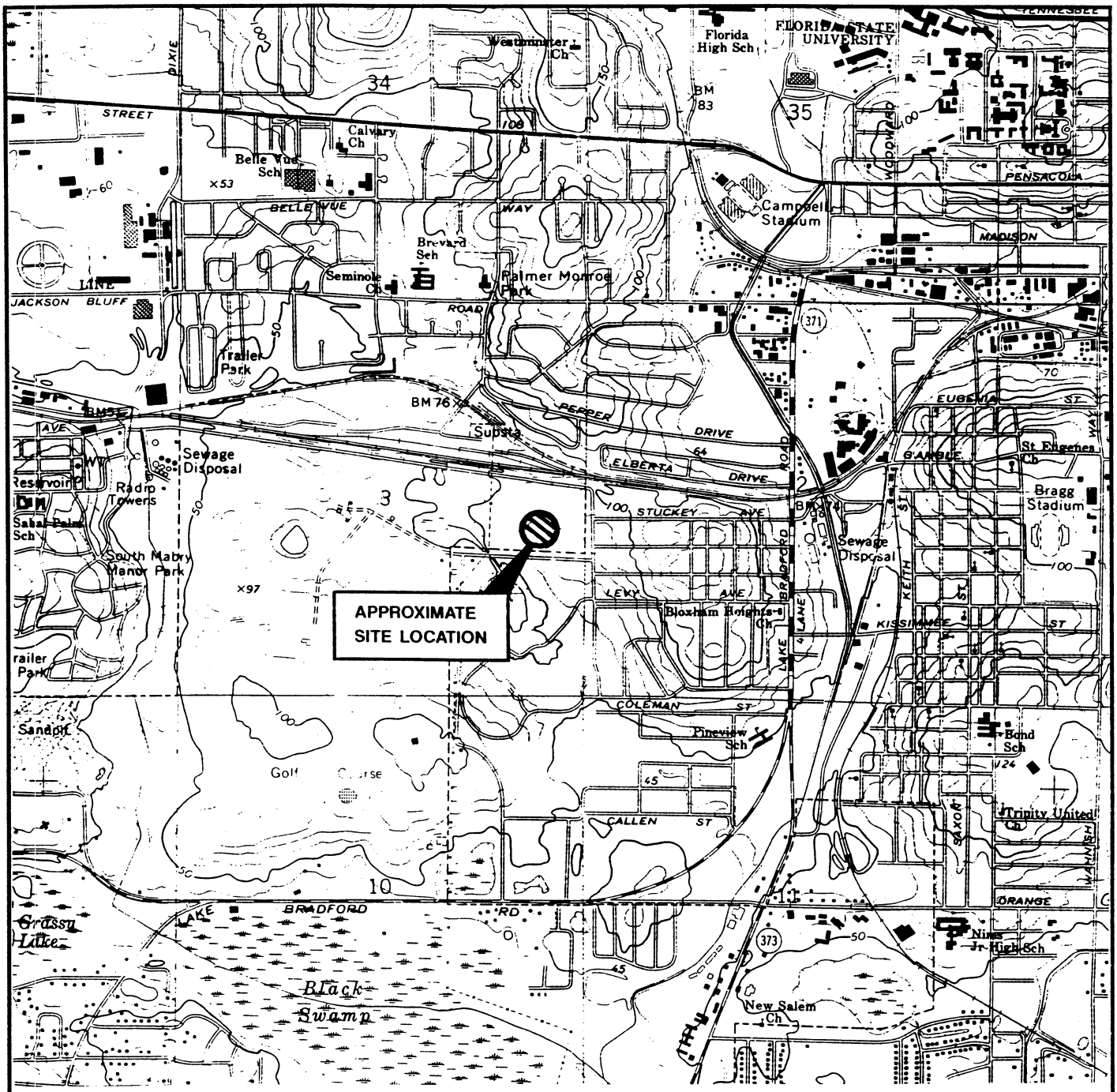

SECTION 3
TOWNSHIP 1 SOUTH
RANGE 1 WEST

OBTAINED FROM U.S.G.S. QUAD MAP: TALLAHASSEE, FLORIDA 1970
(PHOTOREVISED 1976)

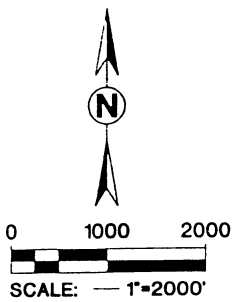

QUADRANGLE LOCATION

SITE LOCATION MAP

Ardaman & Associates, Inc.
Geotechnical, Environmental and Materials Consultants

SUBSURFACE SOIL EXPLORATION
BRIDGE FOUNDATION
DRILLED SHAFTS
F.S.U./F.A.M.U. RESEARCH PROJECT
TALLAHASSEE, FLORIDA

DRAWN BY: SEF	CHECKED BY:	DATE: 03/06/98
FILE NO. 97-6341	APPROVED BY:	FIGURE: 1

CADD FILE: DATE: 02/17/98 REVISED BY: SEF

SOIL BORING LOCATION PLAN

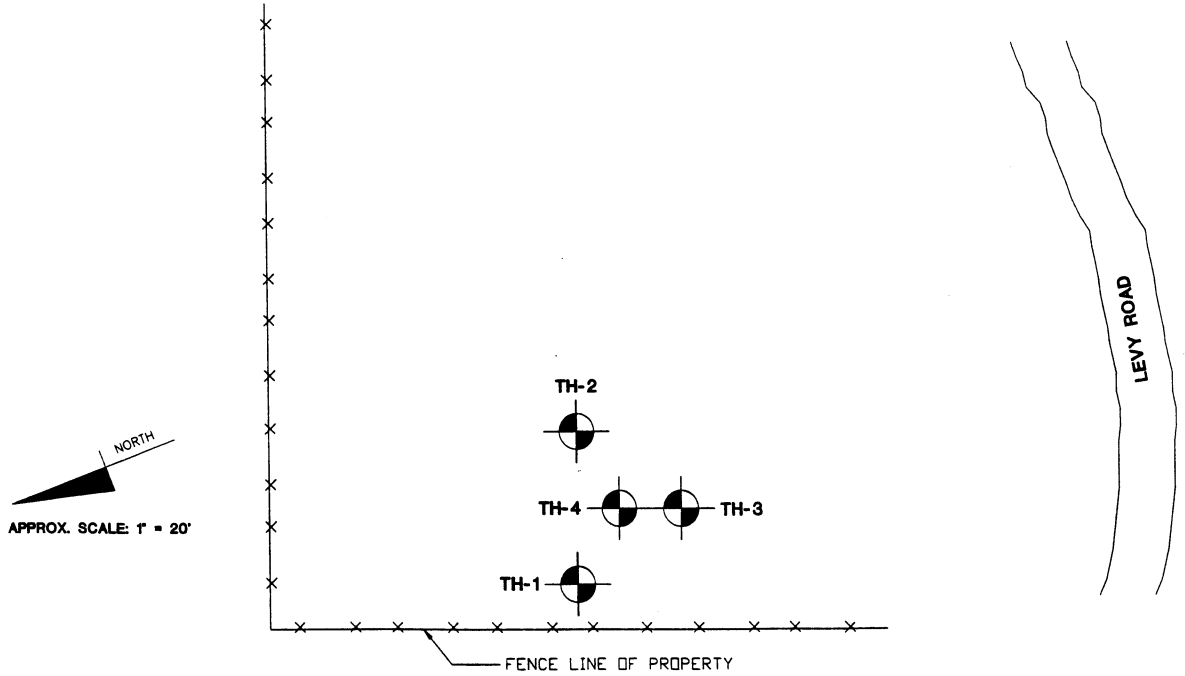

ENGINEERING CLASSIFICATION

I COHESIONLESS SOILS

DESCRIPTION	BLOW COUNT "N"
VERY LOOSE	0 TO 4
LOOSE	4 TO 10
MEDIUM	10 TO 30
DENSE	30 TO 50
VERY DENSE	>50

II COHESIVE SOILS

DESCRIPTION	UNCONFINED COMPRESSIVE STRENGTH, QU, TSF	BLOW COUNT "N"
VERY SOFT	<1/4	0 TO 2
SOFT	1/4 TO 1/2	2 TO 4
FIRM	1/2 TO 1	4 TO 8
STIFF	1 TO 2	8 TO 15
VERY STIFF	2 TO 4	15 TO 30
HARD	>4	>30

WHILE THE BORINGS ARE REPRESENTATIVE OF SUBSURFACE CONDITIONS AT THEIR RESPECTIVE LOCATIONS AND FOR THEIR RESPECTIVE VERTICAL REACHES, LOCAL VARIATIONS CHARACTERISTIC OF THE SUBSURFACE MATERIALS OF THE REGION ARE ANTICIPATED AND MAY BE ENCOUNTERED. THE BORING LOGS AND RELATED INFORMATION ARE BASED ON THE DRILLER'S LOGS AND VISUAL EXAMINATION OF SELECTED SAMPLES IN THE LABORATORY. THE DELINEATION BETWEEN SOIL TYPES SHOWN ON THE LOGS IS APPROXIMATE AND THE DESCRIPTION REPRESENTS OUR INTERPRETATION OF SUBSURFACE CONDITIONS AT THE DESIGNATED BORING LOCATIONS ON THE PARTICULAR DATE DRILLED.

LEGEND

TH	STANDARD PENETRATION TEST BORING
GNE	GROUNDWATER NOT ENCOUNTERED
N	BLOWS PER FOOT
NM	NATURAL MOISTURE (%)
-200	PERCENT PASSING No. 200 SIEVE
LL	LIQUID LIMIT (%)
PI	PLASTICITY INDEX (LL-PL)

SOIL BORING PROFILES

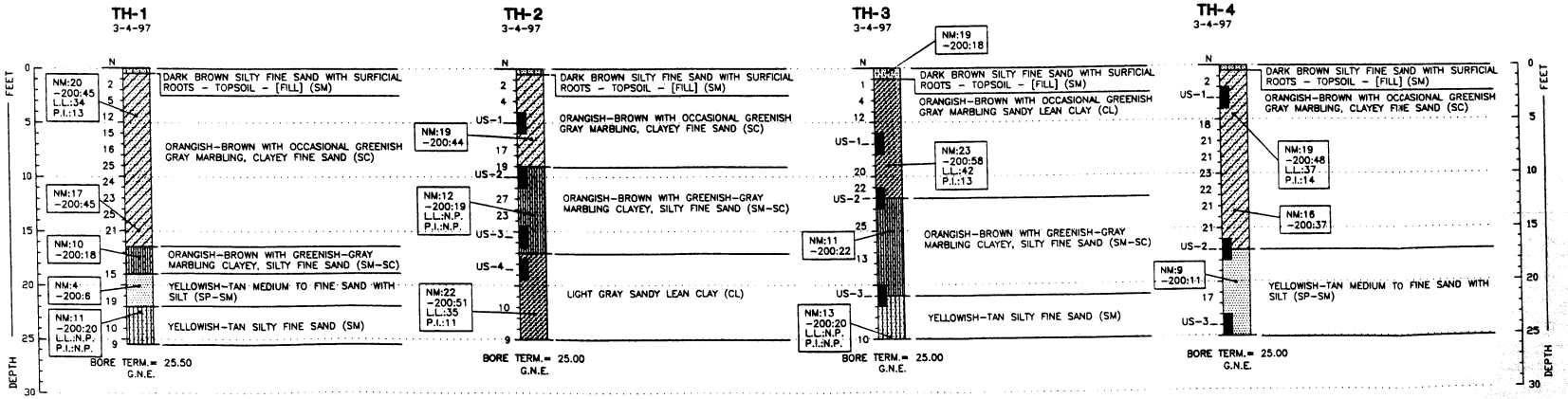

Ardaman & Associates, Inc.
Geotechnical, Environmental and Materials Consultants

SUBSURFACE SOIL EXPLORATION
BRIDGE FOUNDATION
DRILLED SHAFTS
F.S.U./F.A.M.U. RESEARCH PROJECT
TALLAHASSEE, FLORIDA

DRAWN BY: TEB	CHECKED BY:	DATE: 03-18-97
FILE NO. 97-6341	APPROVED BY:	FIGURE: 2

CAD FILE: 7800097 | DATE: 03/18/97 | PREVIOUS REVISION: SEP | DATE | LAST REVISION | DESCRIPTION OF LAST REVISION: DESCRIPTION

APPENDIX I

Field Exploration Procedures

DUTCH CONE PENETROMETER TESTS

The Dutch Cone Penetrometer is an *in situ* deep-testing device utilized to obtain information concerning the strength and compressibility of foundation soils. In the test, a shaft with a conical point is pushed into the soil. The resistance to penetration of the point and the friction developed on the circumference of the shaft are measured. The measured values constitute the test results. The cone apparatus does not recover soil samples. Originally developed and extensively used in Europe, the Dutch Cone has recently been accepted in the United States as a valuable geotechnical engineering tool (ASTM Special Technical Publication 479). Similar portable hand-operated penetrometers have been used extensively by our firm for many years as an alternate means for compaction control work and shallow subsurface soil exploration.

The Dutch Cone or Begemann penetrometer employs a 60°, hardened-steel cone point with a projected area of 10 square centimeters. The point is located at the end of a smooth cylindrical shaft which is free to move ahead of a second slightly large cylindrical shaft or friction sleeve. The testing assembly is attached to the end of a string of concentric inner and outer rods which connect it to the surface. The outer rods are used to push the testing assembly and the inner rods to the desired testing depth where they are disengaged and remain stationary while the test is being performed.

During the test, the inner rods are engaged and a hydraulic jack is used to push the cone point ahead of the friction sleeve. After a free travel of 1.5 inches, the friction sleeve engages and together with the cone tip they are pushed an additional 1.7 inches. Penetration speed is one to two centimeters per second. The thrust required to push the cone tip alone, and that required to push it and the friction sleeve together are measured by the operator at the surface with sensitive pressure gauges. After the completion of the test, the outer rods are reengaged and pushed, collapsing the telescoped testing device and carrying it to the next testing depth, which is usually 20 centimeters deeper, and the test is repeated. The value of the bearing pressure exerted by the cone point (q_{cone}) has been empirically correlated to various soil properties. The ratio of this value, q_{cone}, to the value of the frictional resistance of the disturbed soils surrounding the friction sleeve gives an indication of type of soil penetrated.

The mantle cone, which we occasionally use, is essentially a Dutch Cone without the friction sleeve. The conical top which bears directly upon the soil is like that of the Dutch Cone and the procedure of testing is similar to that described above, except that only the cone bearing value, q_{cone}, is obtained.

STANDARD PENETRATION TEST

The standard penetration test is a widely accepted test method of *in situ* testing of foundation soils (ASTM D-1586). A 2-foot long, 2-inch O.D. split-barrel sampler attached to the end of a string of drilling rods is driven 18 inches into the ground by successive blows of a 140-pound hammer freely dropping 30 inches. The number of blows needed for each 6 inches of penetration is recorded. The sum of the blows required for penetration of the second and third 6-inch increments of penetration constitutes the test result or N-value. After the test, the sampler is extracted from the ground and opened to allow visual examination and classification of the retained soil sample. The N-value has been empirically correlated with various soil properties allowing a conservative estimate of the behavior of soils under load.

The tests are usually performed at 5-foot intervals. However, more frequent or continuous testing is done by our firm through depths where a more accurate definition of the soils is required. The test holes are advanced to the test elevations by rotary drilling with a cutting bit, using circulating fluid to remove the cuttings and hold the fine grains in suspension. The circulating fluid, which is a bentonitic drilling mud, is also used to keep the hole open below the water table by maintaining an excess hydrostatic pressure inside the hole. In some soil deposits, particularly highly pervious ones, NX-size flush-coupled casing must be driven to just above the testing depth to keep the hole open and/or prevent the loss of circulating fluid.

Representative split-spoon samples from the soils at every 5 feet of drilled depth and from every different stratum are brought to our laboratory in air-tight jars for further evaluation and testing, if necessary. Samples not used in testing are stored for 30 days prior to being discarded. After completion of a test boring, the hole is kept open until a steady state groundwater level is recorded. The hole is then sealed, if necessary, and backfilled.

FLAT PLATE DILATOMETER TEST

The Flat Plate Dilatometer Test, developed by Dr. S. Marchetti of Italy, is an in-situ penetration and dilation/expansion test. It is utilized to obtain information concerning soil strength, stress, modulus, and consolidation characteristics quickly. In the test, a flat steel plate with a sharpened bottom edge is pushed into the soil, generally with cone penetration equipment, and stopped at suitable depths for testing. The thrust necessary to push the dilatometer to the desired depth is recorded. This is followed by the expansion of a circular, stainless steel membrane located on the side of the plate using gas pressure. No soil samples are obtained from this test.

During a test, the pressure necessary for the expansion of the membrane, is measured. The A-pressure is the pressure required to lift the membrane above its support and move it horizontally 0.05 mm into the surrounding soil. The B-pressure is the pressure required to move the membrane an additional 1.05 mm into the surrounding soil. An audio signal is utilized to inform the operator when to make the necessary readings using a sensitive pressure gauge. Calibration of the membrane is performed in the field by the operator both before and after each sounding. Tests during a dilatometer sounding are generally made at regular intervals (20 cm to 100 cm).

APPENDIX II

Sieve Analysis Curves

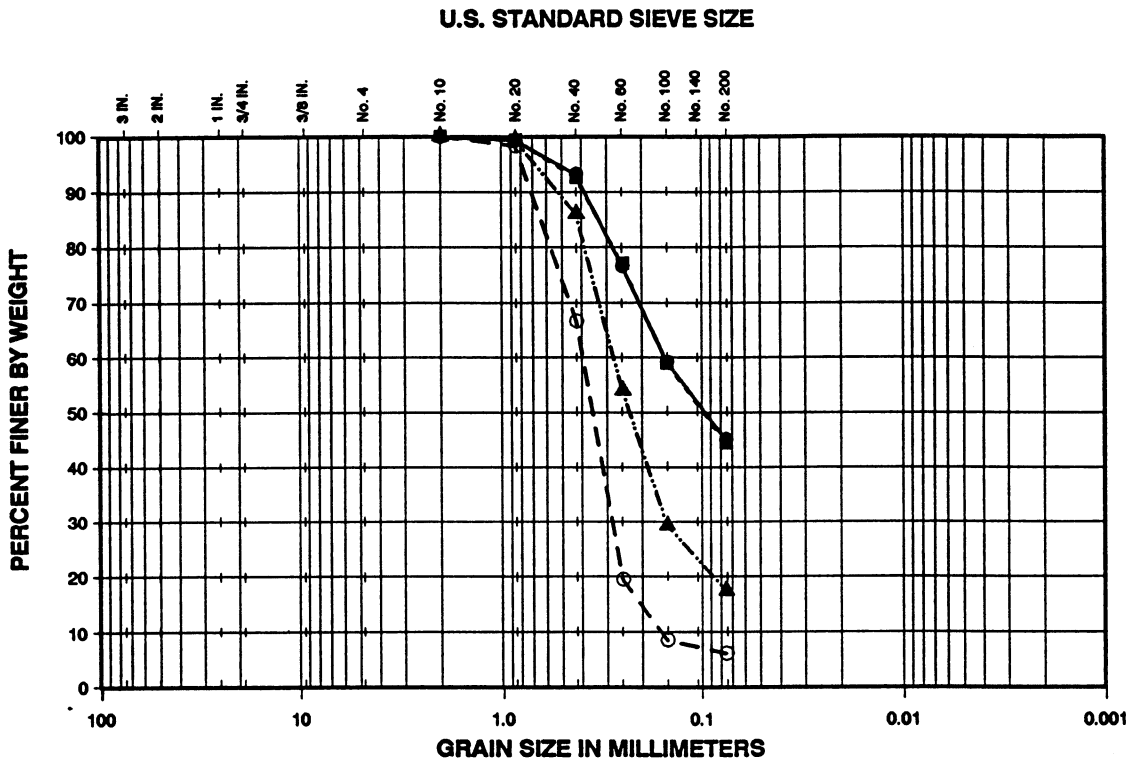

GRAVEL		SAND			SILT	CLAY
COARSE	FINE	COARSE	MEDIUM	FINE		

TEST HOLE NO.	SAMPLE NO.	DEPTH	SYMBOL	SAMPLE DESCRIPTION	UNIFIED CLASS.
TH-1	4	4.5'	●	ORANGISH-BROWN CLAYEY FINE SAND	SC
TH-1	11	15.0'	■	ORANGISH-BROWN CLAYEY FINE SAND	SC
TH-1	12	17.5'	▲	ORANGISH-BROWN CLAYEY, SILTY FINE SAND	SM-SC
TH-1	13	20.0'	○	YELLOWISH-TAN MEDIUM TO FINE SAND WITH SILT	SP-SM

GRAIN SIZE DISTRIBUTION

Ardaman & Associates, Inc.
Geotechnical, Environmental and Materials Consultants

GEOTECHNICAL EXPLORATION
F.S.U. / F.A.M.U. SITE
TALLAHASSEE, FLORIDA

DRAWN BY: TEB	CHECKED BY: WSJ	DATE: 3-20-97
FILE NO.: 97-6341	APPROVED BY:	FIGURE:

DISK #20 976341B 3-20-97

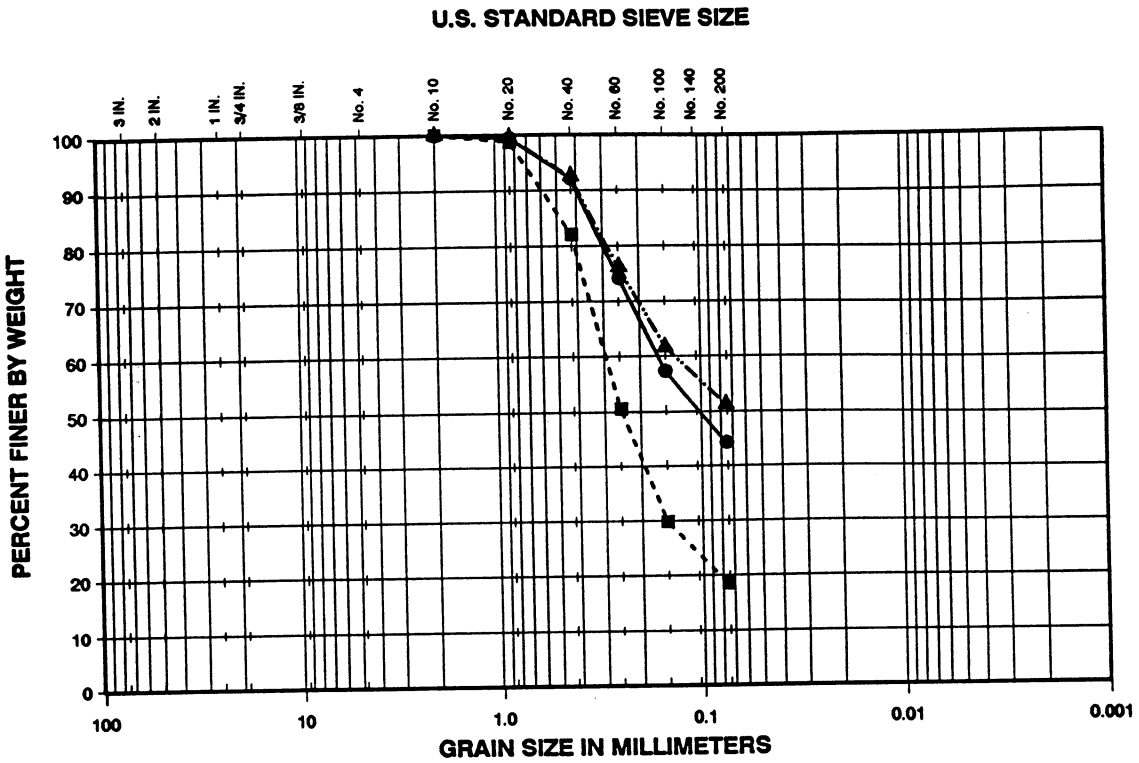

GRAVEL		SAND			SILT	CLAY
COARSE	FINE	COARSE	MEDIUM	FINE		

TEST HOLE NO.	SAMPLE NO.	DEPTH	SYMBOL	SAMPLE DESCRIPTION	UNIFIED CLASS.
TH-2	4	6.0'	●	ORANGISH-BROWN CLAYEY FINE SAND	SC
TH-2	7	13.5'	■	ORANGISH-BROWN CLAYEY, SILTY FINE SAND	SM-SC
TH-2	8	22.5'	▲	LIGHT GRAY SANDY LEAN CLAY	CL

GRAIN SIZE DISTRIBUTION

Ardaman & Associates, Inc.
Geotechnical, Environmental and Materials Consultants

GEOTECHNICAL EXPLORATION
F.S.U. / F.A.M.U. SITE
TALLAHASSEE, FLORIDA

DRAWN BY: TEB	CHECKED BY: WSJ	DATE: 3-20-97
FILE NO.: 97-6341	APPROVED BY:	FIGURE:

DISK #20 976341A 3-20-97

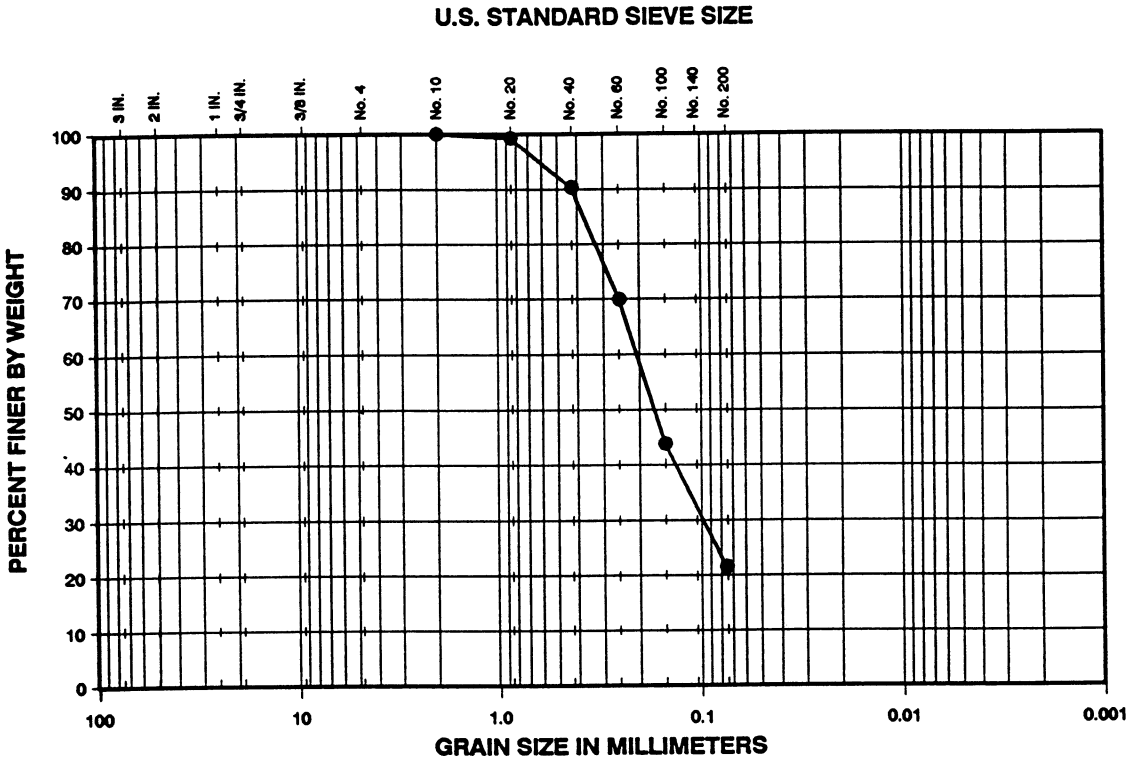

GRAVEL		SAND			SILT	CLAY
COARSE	FINE	COARSE	MEDIUM	FINE		

TEST HOLE NO.	SAMPLE NO.	DEPTH	SYMBOL	SAMPLE DESCRIPTION	UNIFIED CLASS.
TH-3	7	15.0'	●	ORANGISH-BROWN CLAYEY, SILTY FINE SAND	SM-SC

GRAIN SIZE DISTRIBUTION

Ardaman & Associates, Inc.
Geotechnical, Environmental and Materials Consultants

GEOTECHNICAL EXPLORATION
F.S.U. / F.A.M.U. SITE
TALLAHASSEE, FLORIDA

DRAWN BY: TEB	CHECKED BY: WSJ	DATE: 3-20-97
FILE NO.: 97-6341	APPROVED BY:	FIGURE:

DISK #20 976341C 3-20-97

APPENDIX III

Direct Shear Test Results

DIRECT SHEAR TEST RESULTS

Sample Location	Test Conditions		Initial Conditions		Peak Conditions			End of Test Conditions		
	Normal Stress (kg/cm^2)	Displacement Rate (cm/s)	Water Content (%)	Dry Density (pcf)	Stress Ratio	Horizontal Displacement (cm)	Friction Angle (degrees)	Stress Ratio	Horizontal Displacement (cm)	Friction Angle (degrees)
TH-2, US-2	0.27	0.03	14.3	109.8	0.93	0.09	42.9	0.62	0.58	31.9
	0.54	0.03	13.5	112.2	0.76	0.11	37.3	0.64	0.53	32.7
	0.81	0.03	12.6	114.5	0.69	0.16	34.8	0.59	0.54	30.4
TH-3, US-1	0.17	0.03	21.9	97.7	1.14	0.02	48.9	0.76	0.43	37.4
	0.37	0.03	22.7	91.7	0.74	0.17	36.4	0.69	0.58	34.8
	0.55	0.03	25.6	94.8	1.07	0.03	46.9	0.63	0.48	32.2
TH-4, US-1	0.085	0.01	20.5	100.5	1.14	0.032	48.8	0.78	0.50	38.0
	0.17	0.03	20.7	103.8	1.28	0.045	52.1	0.63	0.53	32.2
	0.26	0.03	21.4	103.4	1.14	0.08	48.7	0.78	0.56	37.9
TH-4, US-2	0.45	0.03	15.9	106.8	0.82	0.06	39.4	0.61	0.65	31.5
	0.90	0.03	13.8	113.4	0.77	0.11	37.4	0.61	0.45	31.3
	1.36	0.03	12.8	114.0	0.64	0.18	32.8	0.53	0.54	27.8

FAILURE ENVELOPE

Boring TH-2, US-2

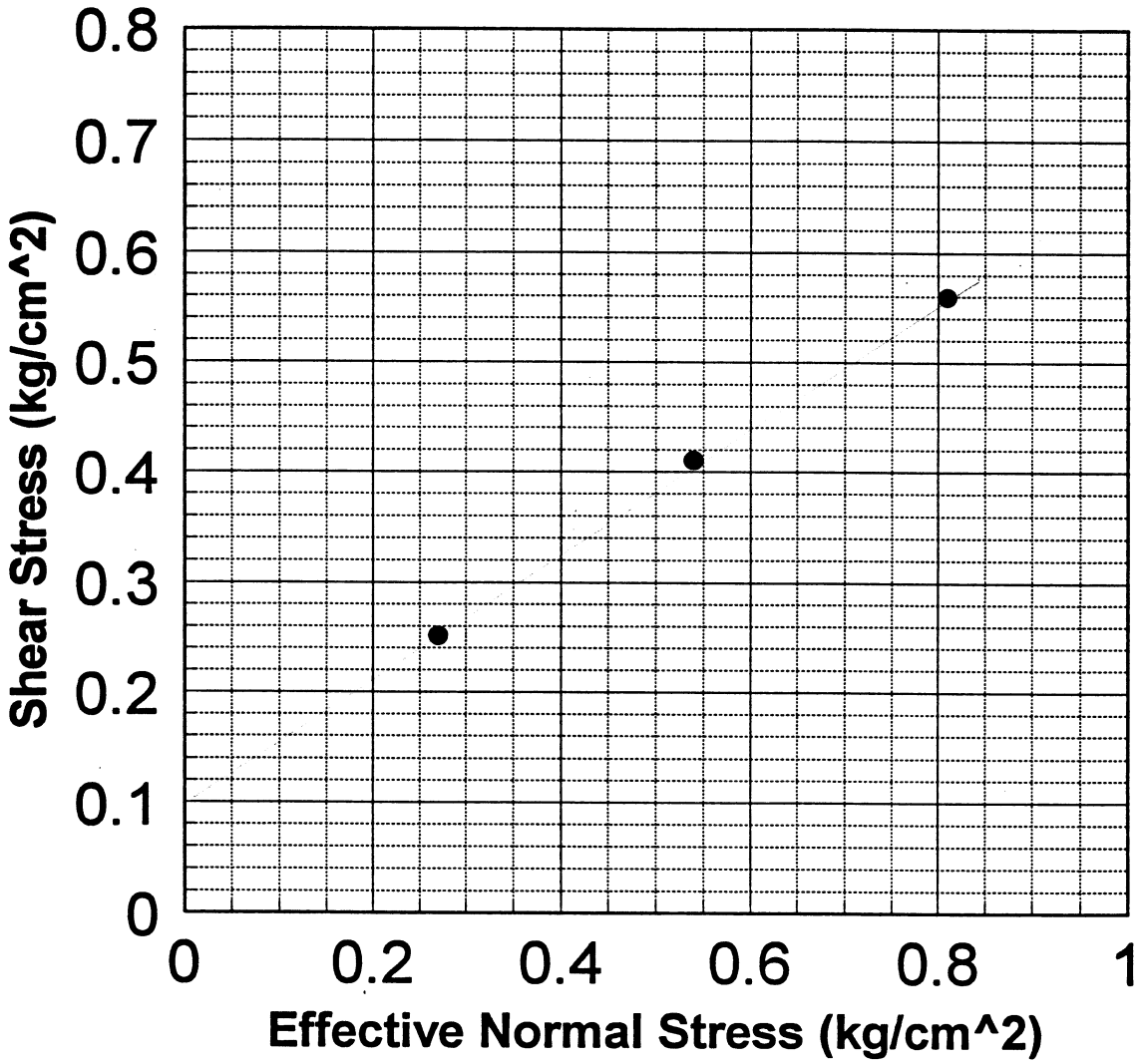

Ardaman & Associates, Inc.	Geotechnical, Environmental and Materials Consultants

GEOTECHNICAL ENGINEERING ANALYSIS
BRIDGE FOUNDATION DRILLED SHAFT PROJECT
TALLAHASSEE, FLORIDA

DRAWN BY:	ZCB	CHECKED BY:	DATE: 2/20/98
FILE NO.: 96-6341		APPROVED BY:	FIGURE NO.:

FAILURE ENVELOPE

Boring TH-3, US-1

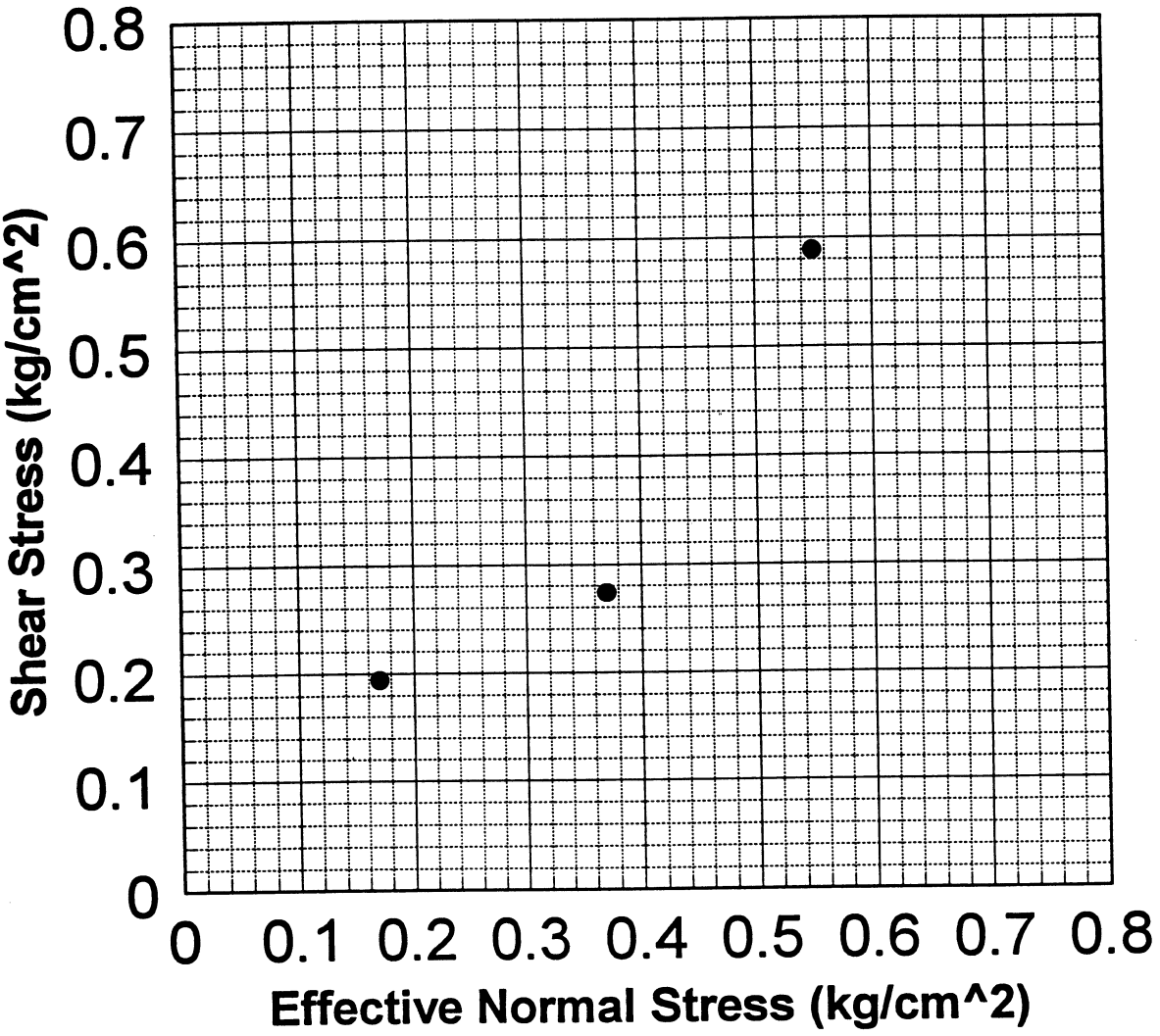

Ardaman & Associates, Inc.
Geotechnical, Environmental and Materials Consultants

GEOTECHNICAL ENGINEERING ANALYSIS
BRIDGE FOUNDATION DRILLED SHAFT PROJECT
TALLAHASSEE, FLORIDA

DRAWN BY: ZCB	CHECKED BY:	DATE: 2/20/98
FILE NO.: 96-6341	APPROVED BY:	FIGURE NO.:

PRI...DRW

FAILURE ENVELOPE

Boring TH-4, US-1

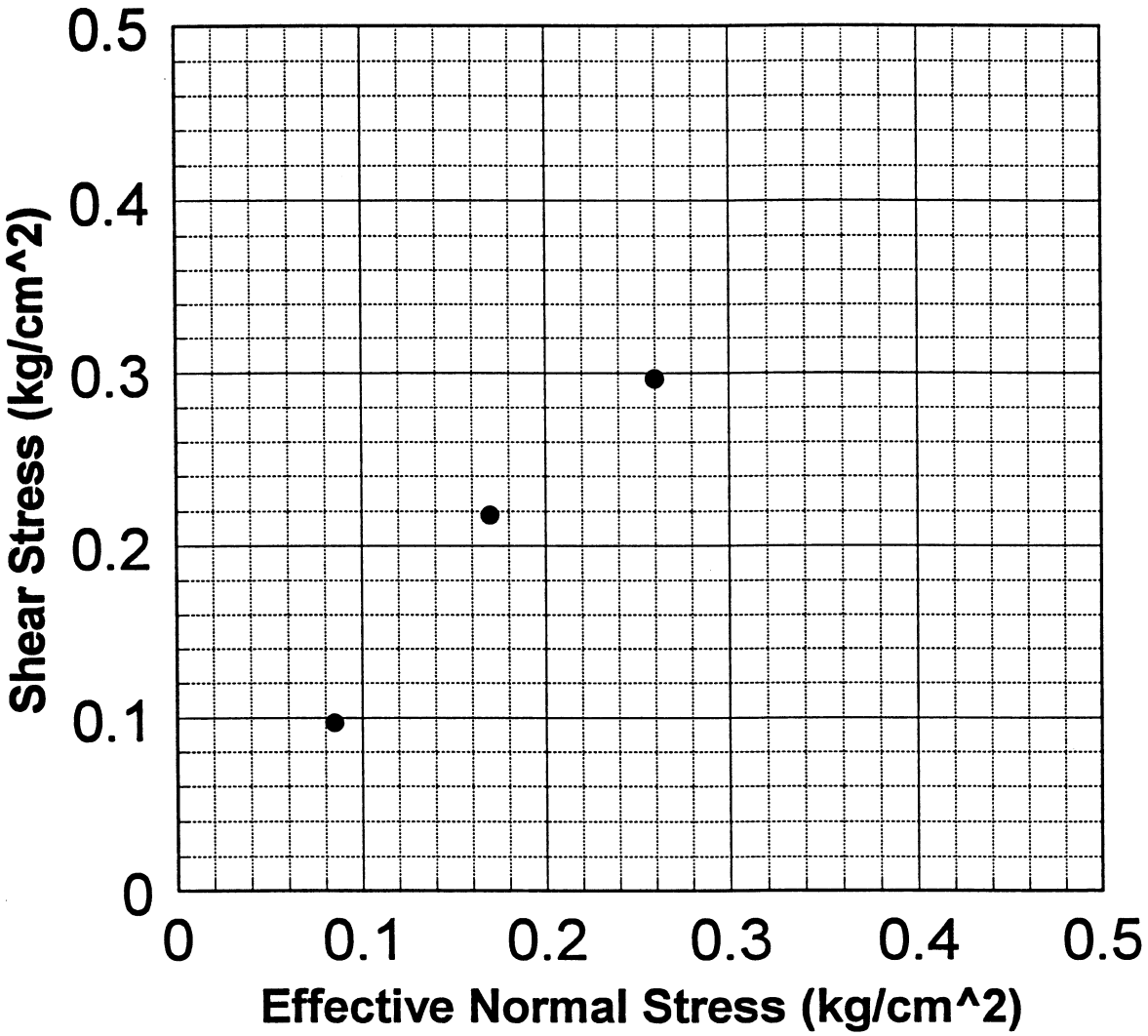

Ardaman & Associates, Inc.
Geotechnical, Environmental and Materials Consultants

GEOTECHNICAL ENGINEERING ANALYSIS
BRIDGE FOUNDATION DRILLED SHAFT PROJECT
TALLAHASSEE, FLORIDA

DRAWN BY: ZCB	CHECKED BY:	DATE: 2/20/98
FILE NO.: 96-6341	APPROVED BY:	FIGURE NO.:

JDRW

FAILURE ENVELOPE

Boring TH-4, US-2

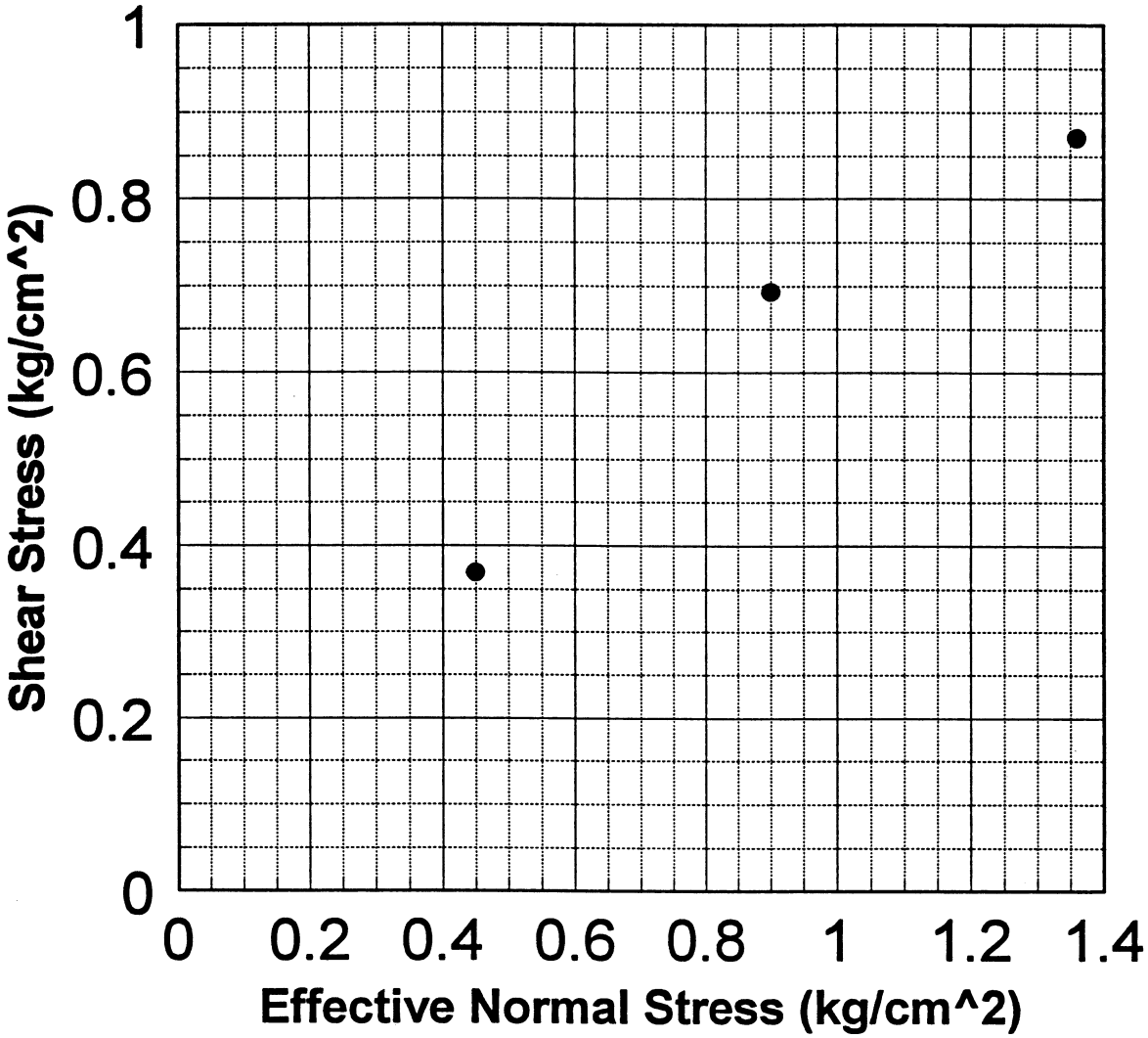

Note : Soil sample for direct shear test taken from clayey fine sand portion of tube sample.

Ardaman & Associates, Inc.
Geotechnical, Environmental and Materials Consultants

GEOTECHNICAL ENGINEERING ANALYSIS
BRIDGE FOUNDATION DRILLED SHAFT PROJECT
TALLAHASSEE, FLORIDA

DRAWN BY: ZCB	CHECKED BY:	DATE: 2/20/98
FILE NO.: 96-6341	APPROVED BY:	FIGURE NO.:

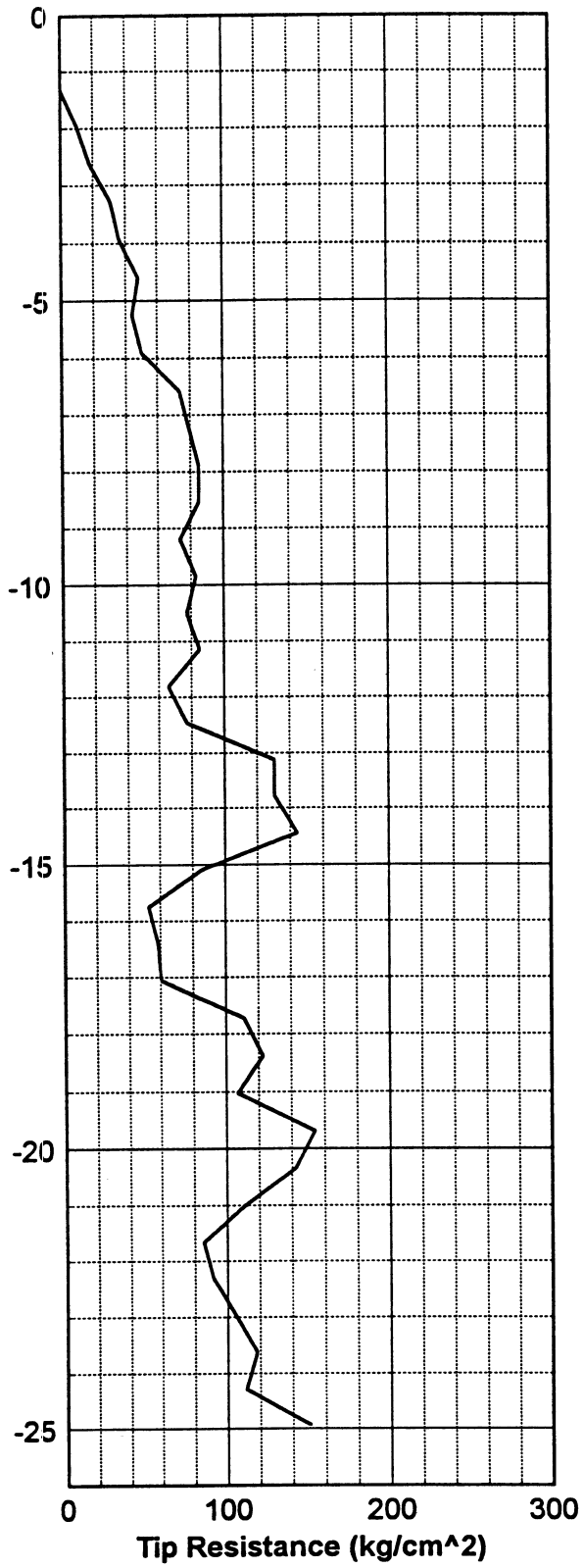

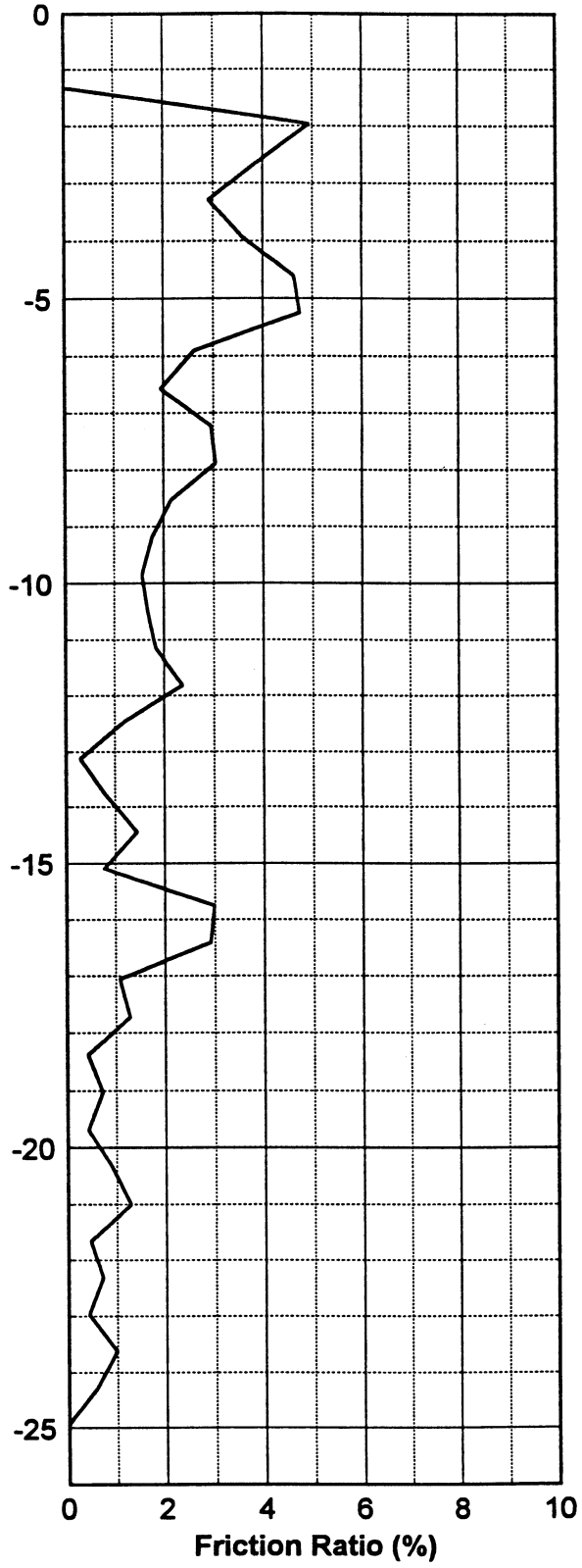

CPT-1

Ardaman & Associates, Inc.
Geotechnical, Environmental and Materials Consultants

MECHANICAL CONE SOUNDINGS
DRILLED SHAFT RESEARCH PROJECT
FSU / FAMU CAMPUS
LEON COUNTY, FLORIDA

DRAWN BY: ZCB	CHECKED BY:	DATE: 2/25/97
FILE NO.: 97-6341	APPROVED BY:	FIGURE NO.:

.O.DRW

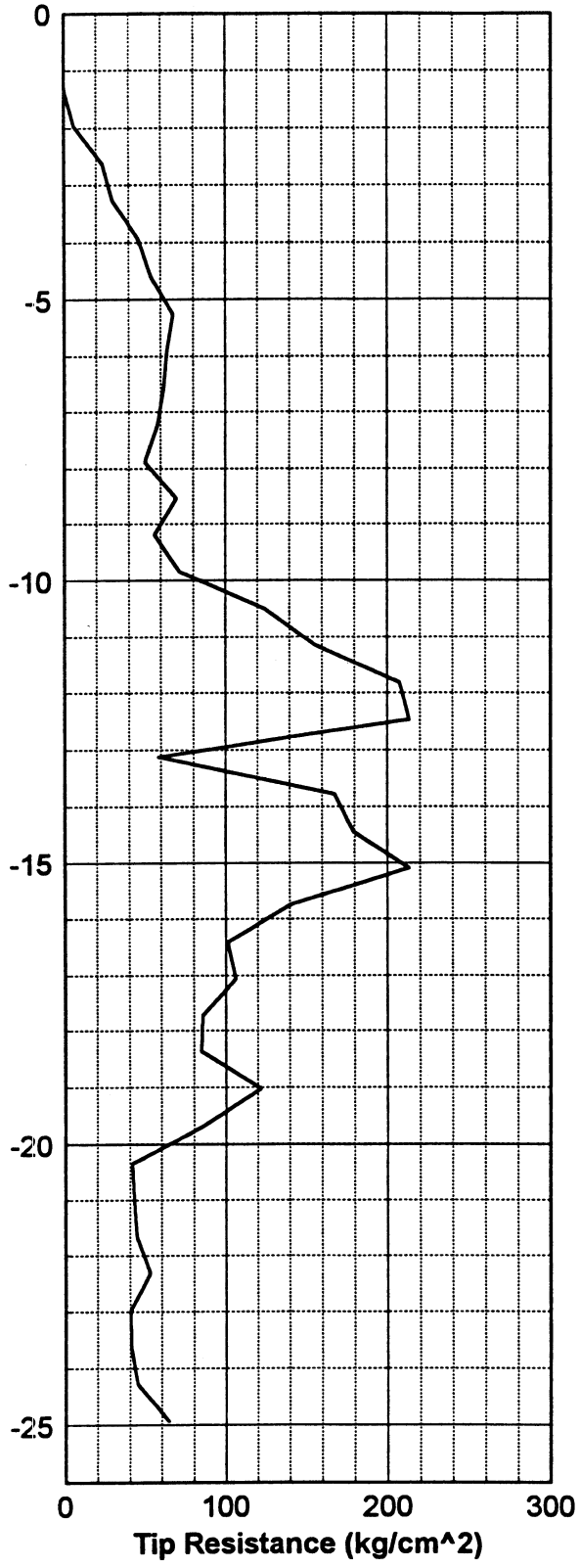

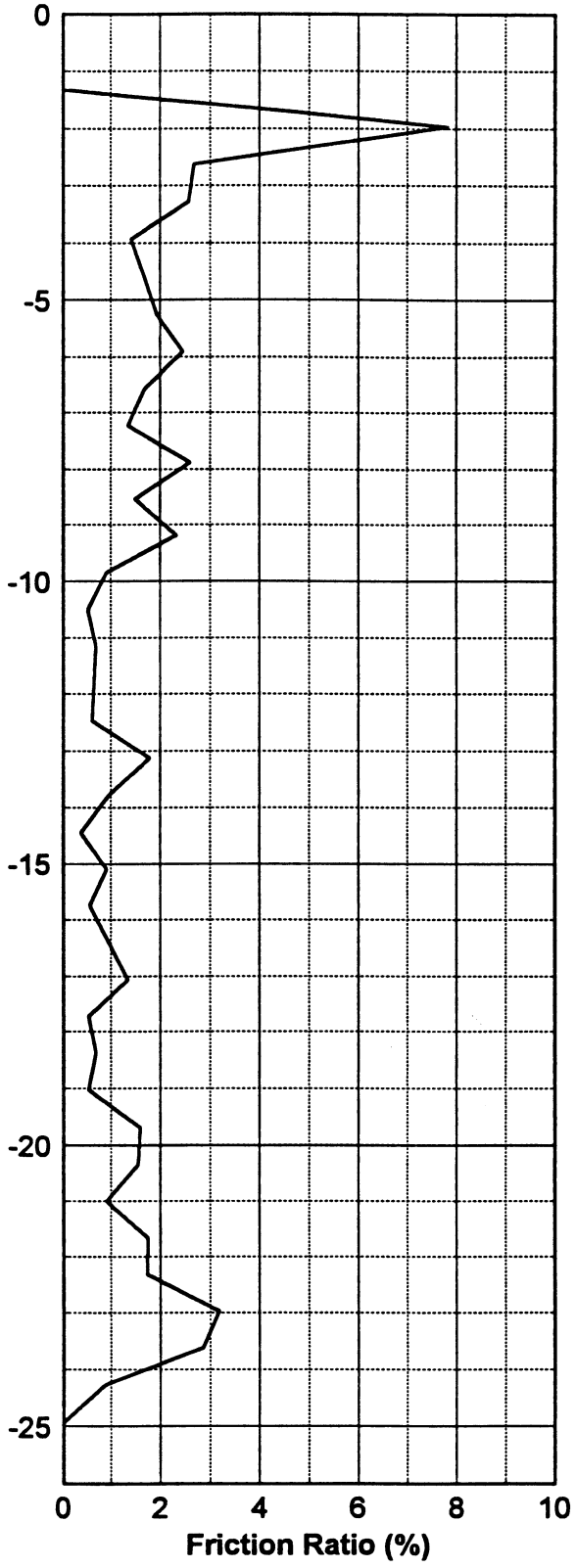

CPT-2

Ardaman & Associates, Inc.
Geotechnical, Environmental and Materials Consultants

MECHANICAL CONE SOUNDINGS
DRILLED SHAFT RESEARCH PROJECT
FSU / FAMU CAMPUS
LEON COUNTY, FLORIDA

DRAWN BY: ZCB	CHECKED BY:	DATE: 2/25/97
FILE NO.: 97-6341	APPROVED BY:	FIGURE NO.:

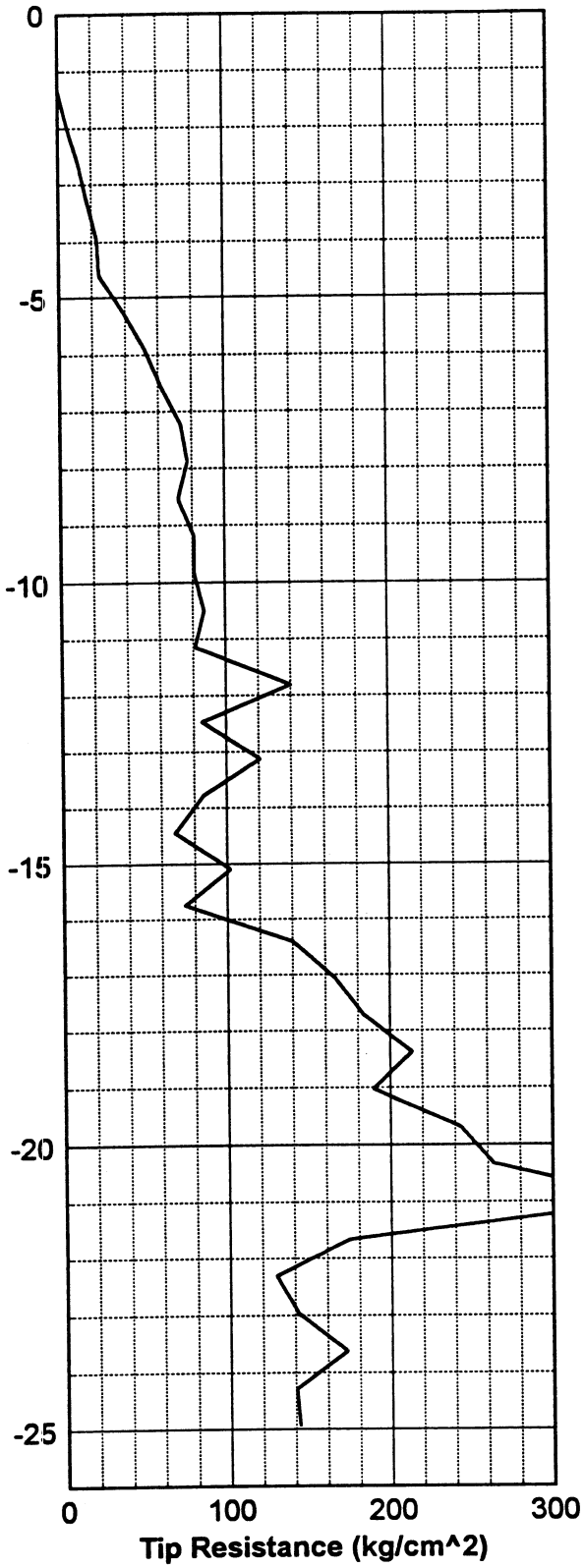

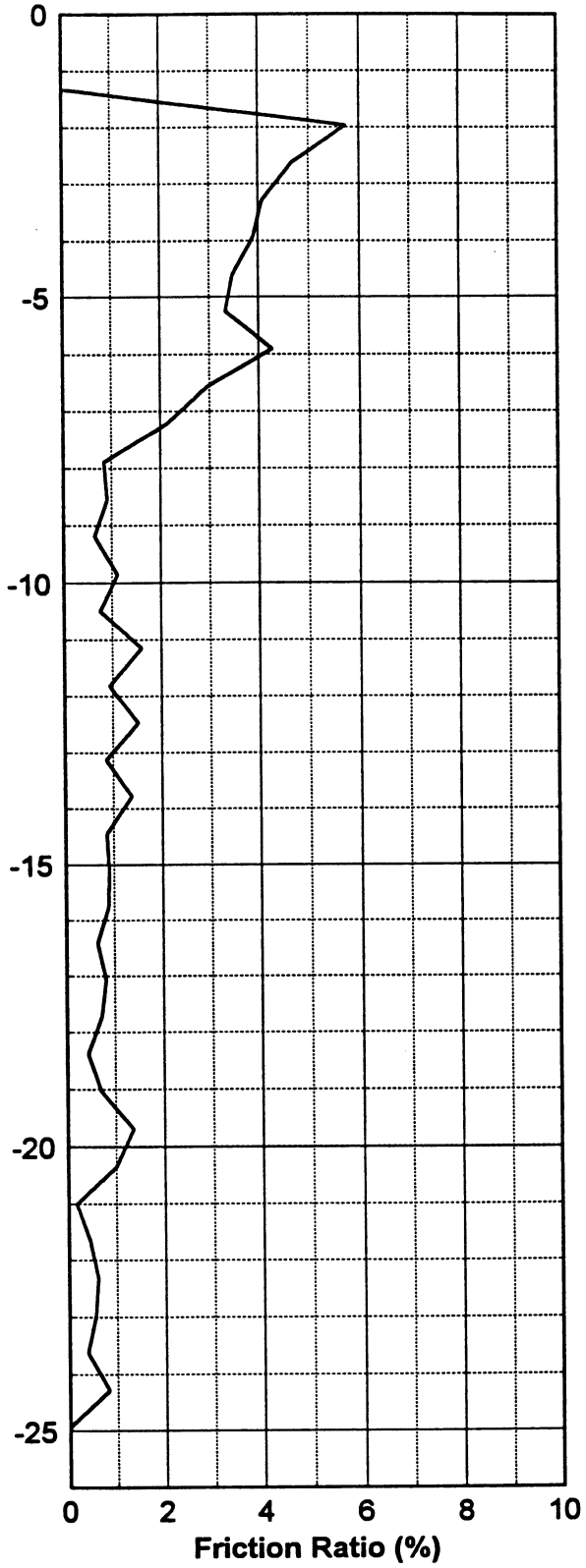

CPT-3

Ardaman & Associates, Inc.
Geotechnical, Environmental and Materials Consultants

MECHANICAL CONE SOUNDINGS
DRILLED SHAFT RESEARCH PROJECT
FSU / FAMU CAMPUS
LEON COUNTY, FLORIDA

DRAWN BY:	ZCB	CHECKED BY:	DATE: 2/25/97
FILE NO.: 97-6341		APPROVED BY:	FIGURE NO.:

J:DRW

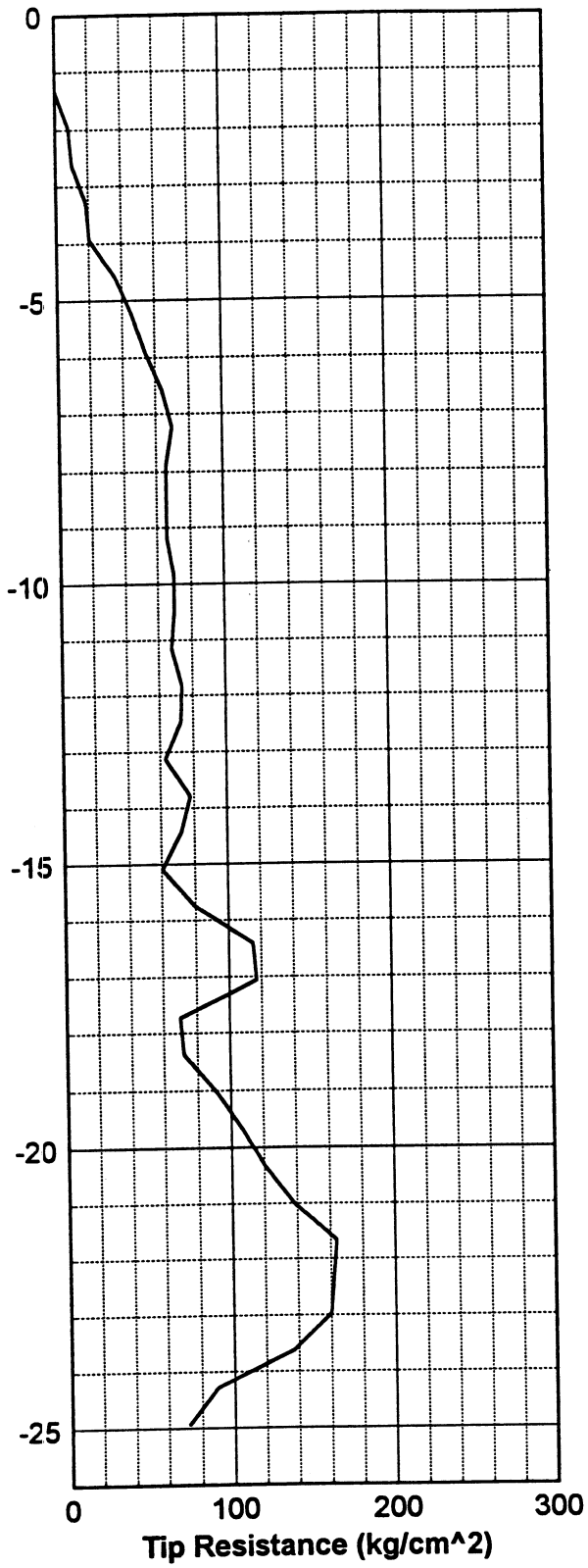

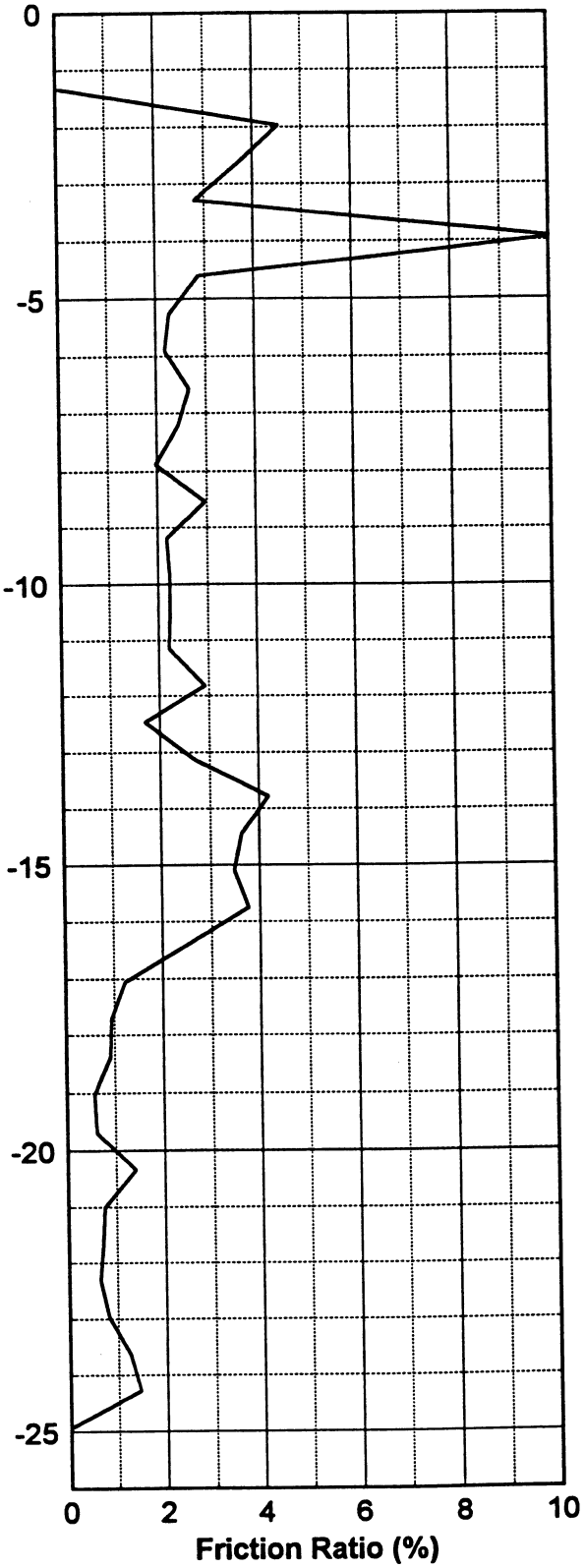

CPT-4

Ardaman & Associates, Inc.
Geotechnical, Environmental and Materials Consultants

MECHANICAL CONE SOUNDINGS
DRILLED SHAFT RESEARCH PROJECT
FSU / FAMU CAMPUS
LEON COUNTY, FLORIDA

DRAWN BY: ZCB	CHECKED BY:	DATE: 2/25/97
FILE NO.: 97-6341	APPROVED BY:	FIGURE NO.:

APPENDIX V

Dilatometer Sounding Results

ARDAMAN & ASSOCIATES TEST NO. DMT - 1

FILE NAME: FSU / FAMU DRILLED SHAFTS RESEARCH PROJECT

FILE NUMBER: 96-6341

RECORD OF DILATOMETER TEST NO. DMT - 1

USING DATA REDUCTION PROCEDURES IN MARCHETTI (ASCE,J-GED,MARCH 80)

KO IN SANDS DETERMINED USING SCHMERTMANN METHOD (1983)

PHI ANGLE CALCULATION BASED ON DURGUNOGLU AND MITCHELL (ASCE,RALEIGH CONF,JUNE 75)

PHI ANGLE NORMALIZED TO 2.72 BARS USING BALIGH'S EXPRESSION (ASCE,J-GED,NOV 76)

MODIFIED MAYNE AND KULHAWY FORMULA USED FOR OCR IN SANDS (ASCE,J-GED,JUNE 82)

LOCATION: BORING C1

PERFORMED - DATE: 2/26/97

BY: ZAN BATES

CALIBRATION INFORMATION:

DELTA A = .25 BARS DELTA B = .20 BARS GWT DEPTH= 8.50 M

LRGAGE 0 = -.08 BARS GAGE BREAK = 9.00BARS HRGAGE 0 = .20 BARS

ROD DIA.= 3.70 CM FR.RED.DIA.= 4.75 CM ROD WT.= 6.50 KG/M DELTA/PHI= .50 BLADE T=13.70 MM

1 BAR = 1.019 KG/CM2 = 1.044 TSF = 14.51 PSI ANALYSIS USES H2O UNIT WEIGHT = 1.000 T/M3

Z (M)	THRUST (KG)	A (BAR)	B (BAR)	ED (BAR)	ID	KD	UO (BAR)	GAMMA (T/M3)	SV (BAR)	PC (BAR)	OCR	KO	CU (BAR)	PHI (DEG)	M (BAR)	SOIL TYPE
.91	1.	2.35	6.44	133.	1.53	.83	.000	1.700	3.000						112.7	DSANDY SILT
1.52	1940.	5.75	14.95	309.	1.57	1.82	.000	1.950	3.109	5.17	1.66	.63		29.7	265.8	DSANDY SILT
2.13	3100.	13.10	22.50	326.	.74	3.93	.000	2.100	3.230	9.27	2.87	.97	1.655		506.0	DCLAYE SILT
2.74	2900.	12.85	23.40	368.	.86	3.69	.000	2.100	3.356	8.74	2.60	.93	1.589		550.4	VDCLAYE SILT
3.35	2900.	15.35	26.35	384.	.74	4.27	.000	2.100	3.482	11.37	3.27	1.04	1.978		628.9	VDCLAYE SILT
3.96	5400.	11.35	33.10	776.	2.16	2.86	.000	2.150	3.609	7.11	1.97	.59		36.8	1044.4	VRSILTY SAND
4.57	4300.	10.20	29.95	703.	2.18	2.48	.000	2.150	3.738	6.77	1.81	.59		35.0	855.2	VRSILTY SAND
5.18	4100.	10.25	24.80	514.	1.54	2.48	.000	2.100	3.865	7.22	1.87	.60		34.3	594.7	VDSANDY SILT
5.79	5300.	6.75	23.65	589.	2.71	1.57	.000	2.000	3.988	3.91	.98	.43		37.3	505.5	VRSILTY SAND
6.40	5000.	6.22	21.25	521.	2.57	1.42	.000	2.000	4.107	3.81	.93	.42		36.8	442.9	VRSILTY SAND
7.01	5000.	5.25	19.05	476.	2.79	1.17	.000	2.000	4.227	3.30	.78	.39		36.9	404.8	VRSILTY SAND
7.62	6700.	6.18	22.90	583.	2.94	1.31	.000	2.000	4.347	3.15	.72	.36		38.9	495.2	VRSILTY SAND

END OF SOUNDING

ARDAMAN & ASSOCIATES

TEST NO. DMT - 2

FILE NAME: FSU / FAMU DRILLED SHAFTS RESEARCH PROJECT
FILE NUMBER: 96-6341

RECORD OF DILATOMETER TEST NO. DMT - 2
USING DATA REDUCTION PROCEDURES IN MARCHETTI (ASCE,J-GED,MARCH 80)
KO IN SANDS DETERMINED USING SCHMERTMANN METHOD (1983)
PHI ANGLE CALCULATION BASED ON DURGUNOGLU AND MITCHELL (ASCE,RALEIGH CONF,JUNE 75)
PHI ANGLE NORMALIZED TO 2.72 BARS USING BALIGH'S EXPRESSION (ASCE,J-GED,NOV 76)
MODIFIED MAYNE AND KULHAWY FORMULA USED FOR OCR IN SANDS (ASCE,J-GED,JUNE 82)

LOCATION: BORING C2
PERFORMED - DATE: 2/26/97
BY: ZAN BATES

CALIBRATION INFORMATION:
DELTA A = .25 BARS DELTA B = .22 BARS GWT DEPTH= 8.50 M
LRGAGE 0 = -.08 BARS GAGE BREAK = 9.00BARS HRGAGE 0 = .20 BARS
ROD DIA.= 3.70 CM FR.RED.DIA.= 4.75 CM ROD WT.= 6.50 KG/M DELTA/PHI= .50 BLADE T=13.70 MM

1 BAR = 1.019 KG/CM2 = 1.044 TSF = 14.51 PSI ANALYSIS USES H2O UNIT WEIGHT = 1.000 T/M3

Z (M)	THRUST (KG)	A (BAR)	B (BAR)	ED (BAR)	ID	KD	UO (BAR)	GAMMA (T/M3)	SV (BAR)	PC (BAR)	OCR	KO	CU (BAR)	PHI (DEG)	M (BAR)	SOIL TYPE
.91	1020.	3.32	8.92	187.	1.59	1.13	.000	1.800	3.000	4.17	1.39	.66		24.8	158.9	DSANDY SILT
1.22	1960.	7.45	13.95	210.	.81	2.50	.000	1.950	3.000	4.24	1.41	.67	.871		229.8	DCLAYE SILT
1.52	2600.	8.55	17.25	290.	.98	2.77	.000	1.950	3.057	5.09	1.67	.74			352.8	D SILT
1.83	2300.	7.45	15.65	271.	1.06	2.38	.000	1.950	3.117	4.08	1.31	.64			290.4	D SILT
2.13		7.28	15.25	263.	1.05	2.28	.000	1.950	3.174	3.90	1.23	.62			270.8	D SILT
2.74		5.08	13.80	290.	1.67	1.52	.000	1.950	3.291						246.8	DSANDY SILT
3.35		5.14	18.75	469.	2.80	1.42	.000	2.000	3.409						398.3	VRSILTY SAND
3.96		7.22	24.10	588.	2.51	1.91	.000	2.000	3.529						593.5	VRSILTY SAND
4.57		4.35	19.75	534.	3.90	1.08	.000	2.000	3.649						453.7	VERYRIG SAND
4.88		5.92	20.95	520.	2.71	1.49	.000	2.000	3.709						442.2	VRSILTY SAND
5.18		5.32	21.85	575.	3.41	1.29	.000	2.000	3.768						488.7	VERYRIG SAND
5.49		5.13	19.75	505.	3.06	1.24	.000	2.000	3.829						429.6	VRSILTY SAND
5.79		5.04	19.38	495.	3.04	1.21	.000	2.000	3.888						420.9	VRSILTY SAND
6.40		4.68	10.35	179.	1.08	1.19	.000	1.800	4.002	1.78	.45	.30			152.4	D SILT
7.01		7.50	17.10	322.	1.26	1.80	.000	1.950	4.114						274.1	DSANDY SILT
7.62		6.38	16.00	323.	1.49	1.48	.000	1.950	4.231						274.7	DSANDY SILT

END OF SOUNDING

ARDAMAN & ASSOCIATES

TEST NO. DMT - 3

FILE NAME: FSU / FAMU DRILLED SHAFTS RESEARCH PROJECT
FILE NUMBER: 96-6341

RECORD OF DILATOMETER TEST NO. DMT - 3
USING DATA REDUCTION PROCEDURES IN MARCHETTI (ASCE,J-GED,MARCH 80)
KO IN SANDS DETERMINED USING SCHMERTMANN METHOD (1983)
PHI ANGLE CALCULATION BASED ON DURGUNOGLU AND MITCHELL (ASCE,RALEIGH CONF,JUNE 75)
PHI ANGLE NORMALIZED TO 2.72 BARS USING BALIGH'S EXPRESSION (ASCE,J-GED,NOV 76)
MODIFIED MAYNE AND KULHAWY FORMULA USED FOR OCR IN SANDS (ASCE,J-GED,JUNE 82)

LOCATION: BORING C3
PERFORMED - DATE: 2/26/97
BY: ZAN BATES

CALIBRATION INFORMATION:
DELTA A = .21 BARS DELTA B = .20 BARS GWT DEPTH= 8.50 M
LRGAGE 0 = -.05 BARS GAGE BREAK = 9.00BARS HRGAGE 0 = .20 BARS
ROD DIA.= 3.70 CM FR.RED.DIA.= 4.75 CM ROD WT.= 6.50 KG/M DELTA/PHI= .50 BLADE T=13.70 MM

1 BAR = 1.019 KG/CM2 = 1.044 TSF = 14.51 PSI ANALYSIS USES H2O UNIT WEIGHT = 1.000 T/M3

Z (M)	THRUST (KG)	A (BAR)	B (BAR)	ED (BAR)	ID	KD	UO (BAR)	GAMMA (T/M3)	SV (BAR)	PC (BAR)	OCR	KO	CU (BAR)	PHI (DEG)	M (BAR)	SOIL TYPE
*****	******	*****	*****	*****	*****	*****	******	******	******	*****	*****	*****	*****	*****	******	**********
.91	400.	1.75	5.85	134.	2.12	.61	.000	1.800	3.000	3.81	1.27	.76		16.8	114.3	RSILTY SAND
1.52	900.	2.98	6.65	119.	1.11	.99	.000	1.800	3.108	1.04	.33	.22			101.0	D SILT
2.13	2500.	11.10	21.10	349.	.95	3.30	.000	1.950	3.220	7.04	2.19	.85			485.4	D SILT
2.74	3000.	13.60	24.85	395.	.87	3.91	.000	2.100	3.341	9.51	2.85	.97	1.700		613.9	VDCLAYE SILT
3.35	4800.	6.05	26.25	712.	3.85	1.54	.000	2.000	3.464	3.23	.93	.41		37.5	622.8	VERYRIG SAND
3.96	4400.	5.25	20.70	539.	3.26	1.33	.000	2.000	3.584	3.10	.87	.41		36.8	458.0	VRSILTY SAND
4.57	4200.	8.22	20.15	411.	1.49	2.14	.000	1.950	3.702	5.60	1.51	.54		35.3	414.3	VDSANDY SILT
5.18	4400.	6.13	23.15	596.	3.08	1.46	.000	2.000	3.820	3.76	.98	.44		36.2	506.7	VRSILTY SAND
5.79	6100.	6.32	23.10	587.	2.93	1.47	.000	2.000	3.940	3.21	.82	.38		38.6	499.2	VRSILTY SAND
6.40	8600.	7.35	26.40	670.	2.89	1.65	.000	2.000	4.060	2.89	.71	.34		40.9	616.8	VRSILTY SAND
7.01	7000.	7.75	26.20	648.	2.62	1.70	.000	2.000	4.179	3.85	.92	.40		39.1	595.9	VRSILTY SAND
7.62	7100.	8.75	30.10	754.	2.72	1.85	.000	2.150	4.304	4.45	1.03	.42		38.9	758.0	VRSILTY SAND

END OF SOUNDING

ARDAMAN & ASSOCIATES

TEST NO. DMT - 4

FILE NAME: FSU / FAMU DRILLED SHAFTS RESEARCH PROJECT
FILE NUMBER: 96-6341

RECORD OF DILATOMETER TEST NO. DMT - 4
USING DATA REDUCTION PROCEDURES IN MARCHETTI (ASCE,J-GED,MARCH 80)
KO IN SANDS DETERMINED USING SCHMERTMANN METHOD (1983)
PHI ANGLE CALCULATION BASED ON DURGUNOGLU AND MITCHELL (ASCE,RALEIGH CONF,JUNE 75)
PHI ANGLE NORMALIZED TO 2.72 BARS USING BALIGH'S EXPRESSION (ASCE,J-GED,NOV 76)
MODIFIED MAYNE AND KULHAWY FORMULA USED FOR OCR IN SANDS (ASCE,J-GED,JUNE 82)

LOCATION: BORING C4
PERFORMED - DATE: 2/26/97
BY: ZAN BATES

CALIBRATION INFORMATION:
DELTA A = .23 BARS DELTA B = .20 BARS GWT DEPTH= 8.50 M
LRGAGE 0 = -.05 BARS GAGE BREAK = 9.00BARS HRGAGE 0 = .20 BARS
ROD DIA.= 3.70 CM FR.RED.DIA.= 4.75 CM ROD WT.= 6.50 KG/M DELTA/PHI= .50 BLADE T=13.70 MM

1 BAR = 1.019 KG/CM2 = 1.044 TSF = 14.51 PSI ANALYSIS USES H2O UNIT WEIGHT = 1.000 T/M3

Z (M)	THRUST (KG)	A (BAR)	B (BAR)	ED (BAR)	ID	KD	UO (BAR)	GAMMA (T/M3)	SV (BAR)	PC (BAR)	OCR	KO	CU (BAR)	PHI (DEG)	M (BAR)	SOIL TYPE
.91	600.	2.35	4.62	67.	.76	.85	.000	1.700	3.000	.78	.26	.16	.225		57.0	DCLAYE SILT
1.22	1100.	3.24	6.65	109.	.93	1.12	.000	1.800	3.000	1.22	.41	.27			92.3	D SILT
1.52	1520.	4.27	7.55	104.	.68	1.44	.000	1.800	3.053	1.84	.60	.38	.447		88.3	DCLAYE SILT
1.83	1800.	6.98	13.25	204.	.84	2.24	.000	1.950	3.110	3.72	1.20	.61	.790		202.1	DCLAYE SILT
2.13	2200.	9.65	18.35	301.	.94	2.93	.000	1.950	3.167	5.73	1.81	.77			381.8	D SILT
2.74	2400.	11.20	20.60	327.	.87	3.28	.000	1.950	3.284	7.11	2.17	.85	1.342		450.4	DCLAYE SILT
3.35	2700.	7.55	18.75	383.	1.51	2.15	.000	1.950	3.401	6.07	1.78	.62		31.8	389.0	VDSANDY SILT
3.96	3400.	8.85	24.10	531.	1.82	2.39	.000	2.000	3.519	6.48	1.84	.61		33.4	608.3	VRSILTY SAND
4.57	4000.	6.75	20.90	491.	2.23	1.75	.000	2.000	3.639	4.43	1.22	.49		35.4	439.9	VRSILTY SAND
5.18	4500.	7.18	21.90	512.	2.18	1.80	.000	2.000	3.759	4.53	1.20	.48		36.1	469.6	VRSILTY SAND
5.79	4300.	6.88	21.25	499.	2.22	1.67	.000	2.000	3.878	4.47	1.15	.48		35.7	426.1	VRSILTY SAND
6.40	3600.	5.05	15.45	354.	2.11	1.21	.000	2.000	3.998	3.76	.94	.45		34.6	301.0	RSILTY SAND
7.01	4800.	4.95	18.15	456.	2.86	1.12	.000	2.000	4.118	3.13	.76	.39		36.8	387.7	VRSILTY SAND
7.62	4900.	5.32	19.15	479.	2.79	1.17	.000	2.000	4.237	3.36	.79	.39		36.8	407.3	VRSILTY SAND

END OF SOUNDING

Figure 2.37 Checking the Plumpness of the Borehole During Construction

Figure 2.38 Drilling 4' Diameter x 20' Depth Borehole

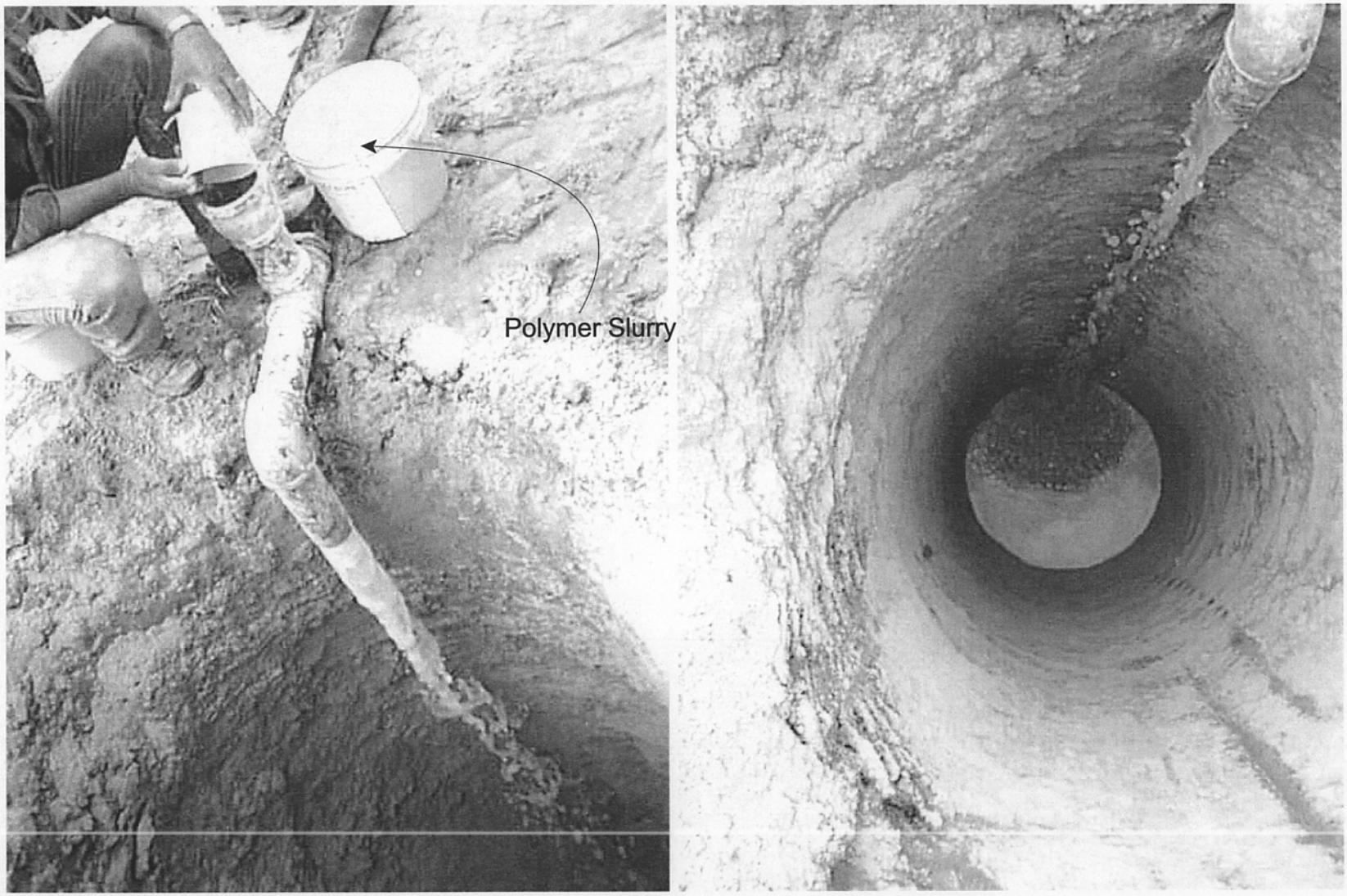

Figure 2.39 Adding SuperMud Slurry to the Borehole

Figure 2.40 Mixing Bentonite Slurry in the Tank Before Placing it in the Borehole

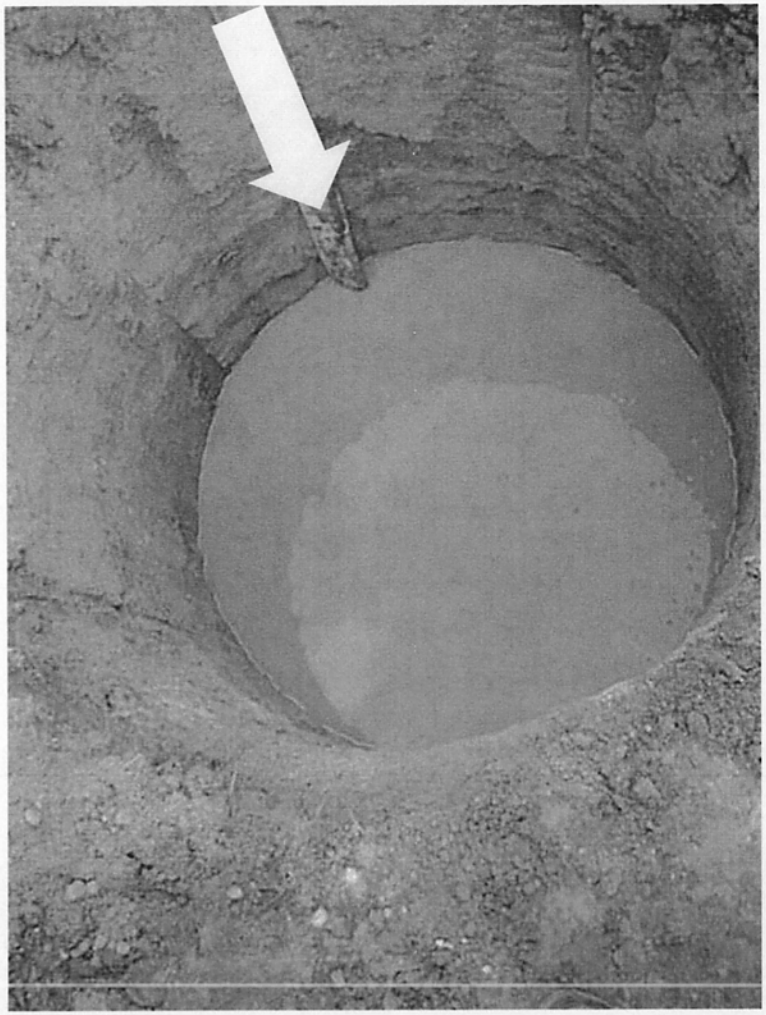

Figure 2.39 Adding BentoniteSlurry to the Borehole

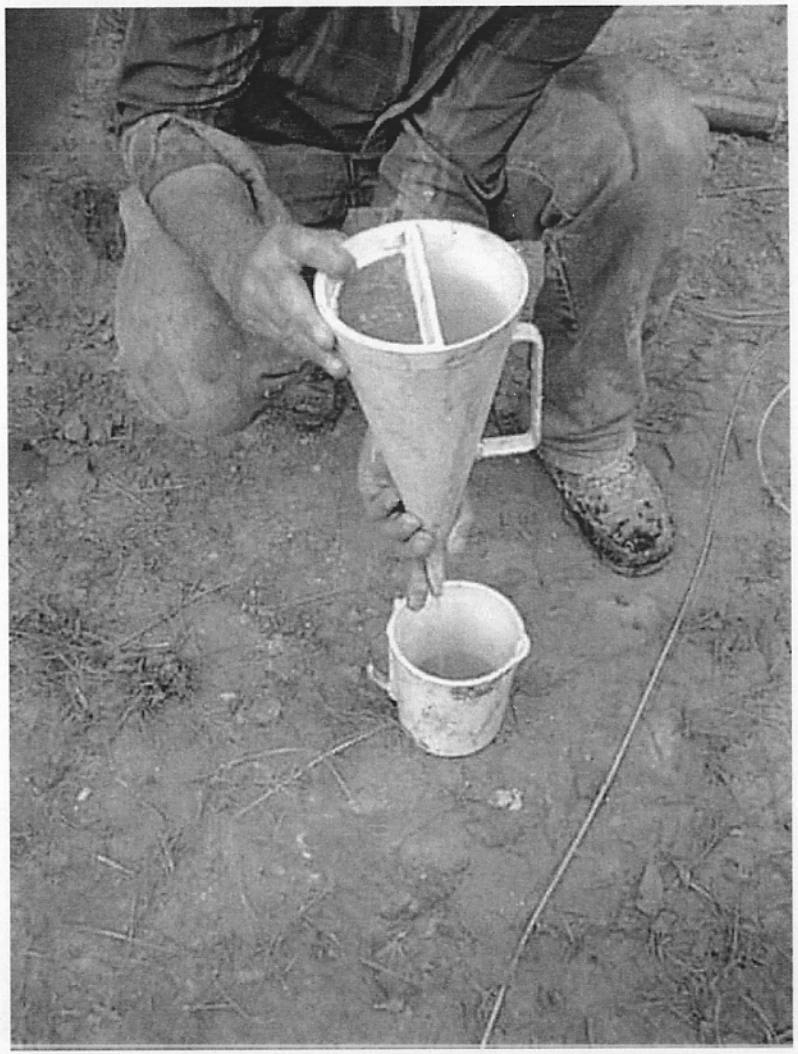

Figure 2.42 Checking the Viscosity of the Slurry using Marsh Funnel

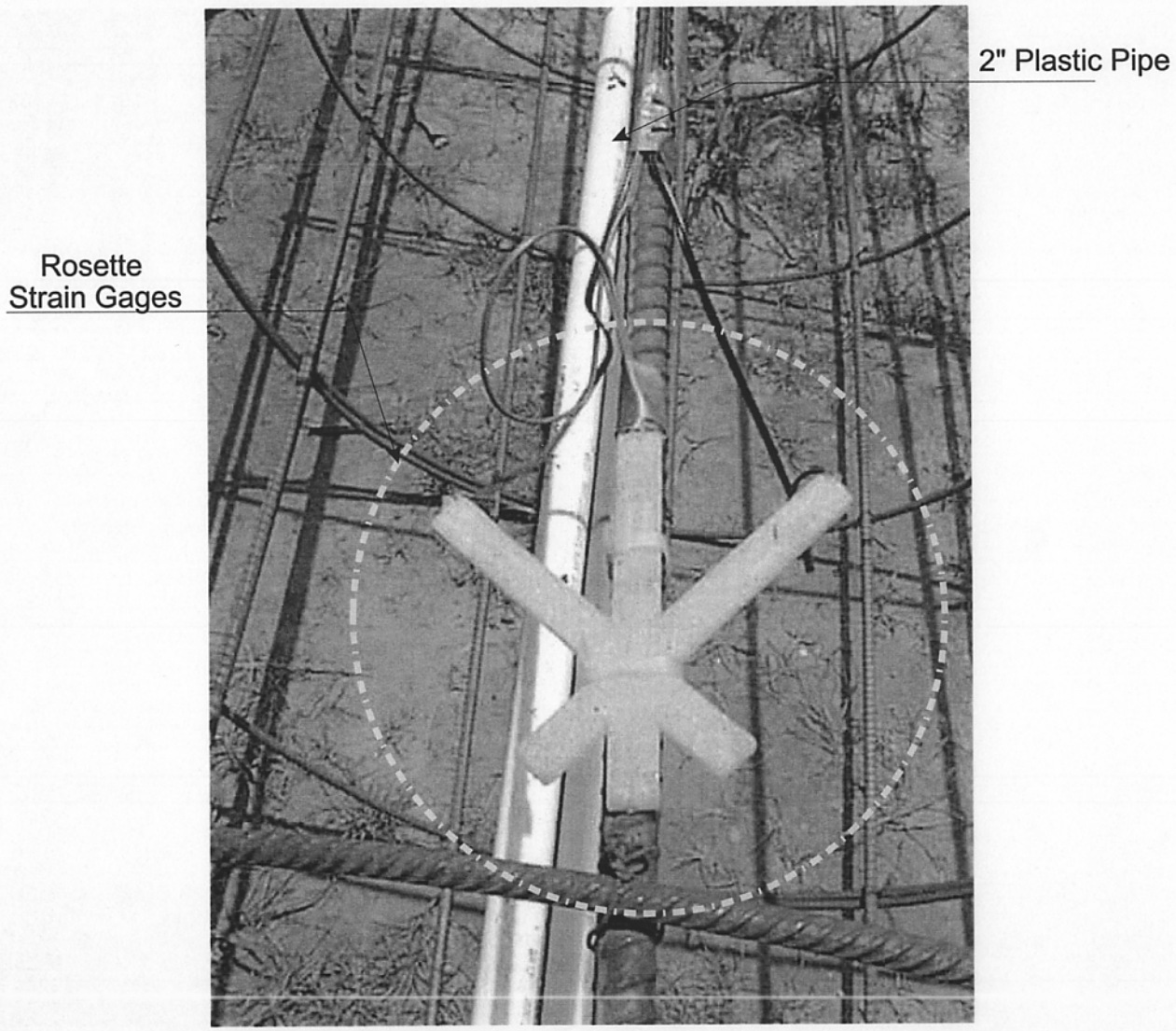

Figure 2.43 Embedded Gages used in the drilled Shafts

Figure 2.44 Lowering the Steel Cage in the Dry Hole

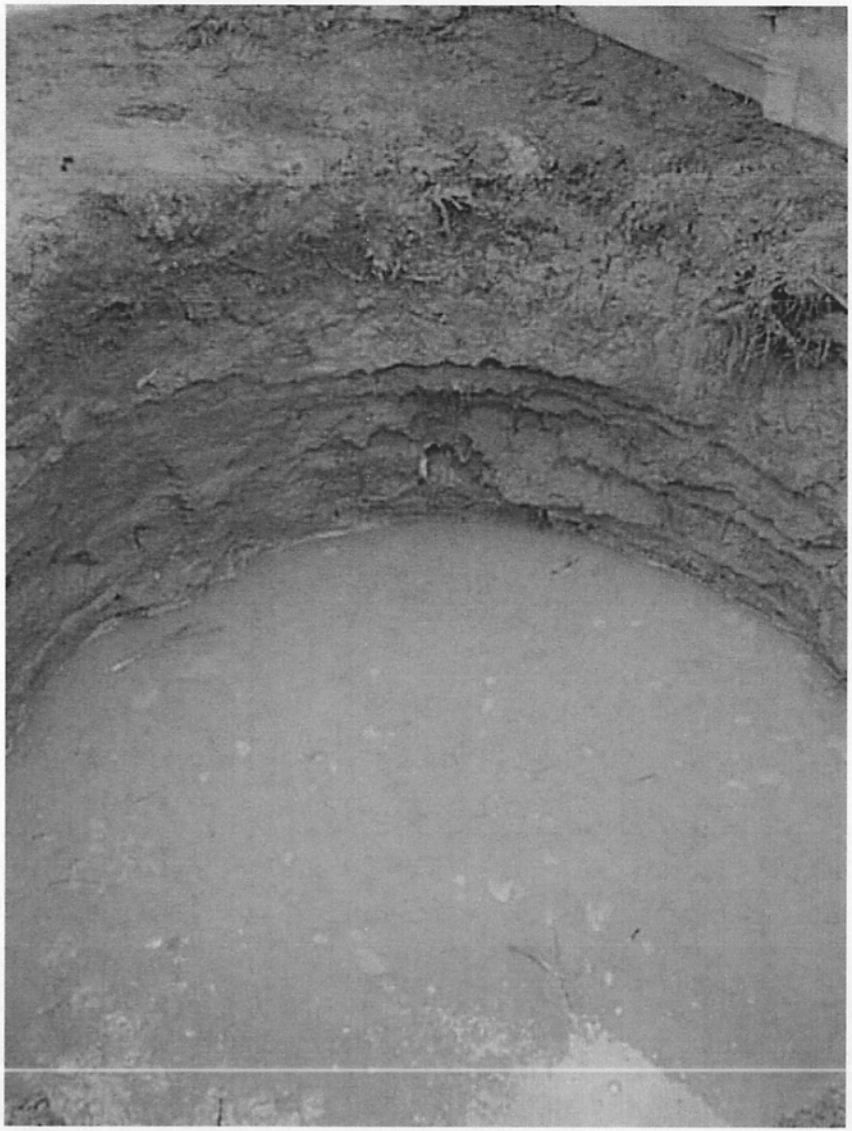

Figure 2.45 Fluid Loss After 18 Hours in the Bentonite Slurry Borehole

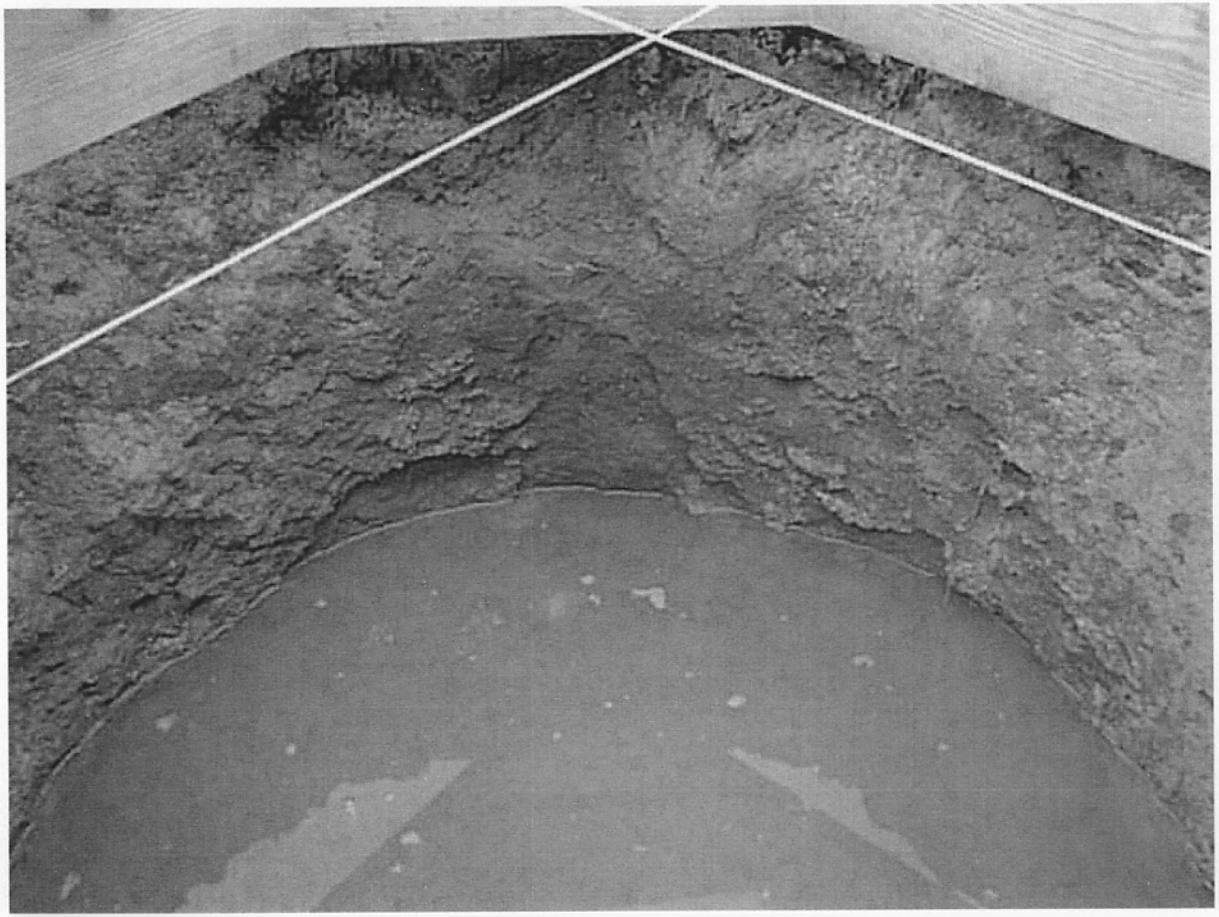

Figure 2.45 Fluid Loss After 18 Hours in the Polymer Slurry Borehole

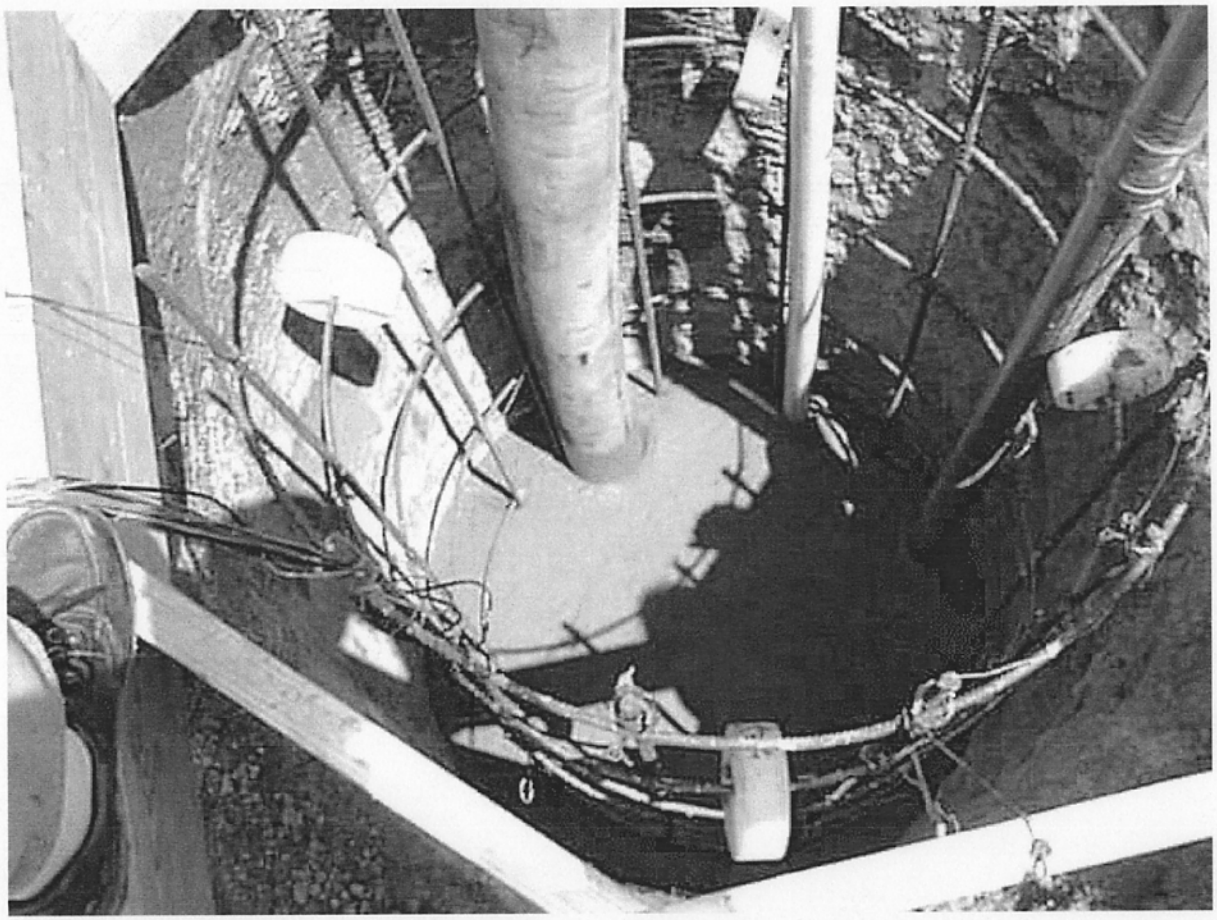

Figure 2.47 Concrete Placement in the Borehole using Concrete Pump

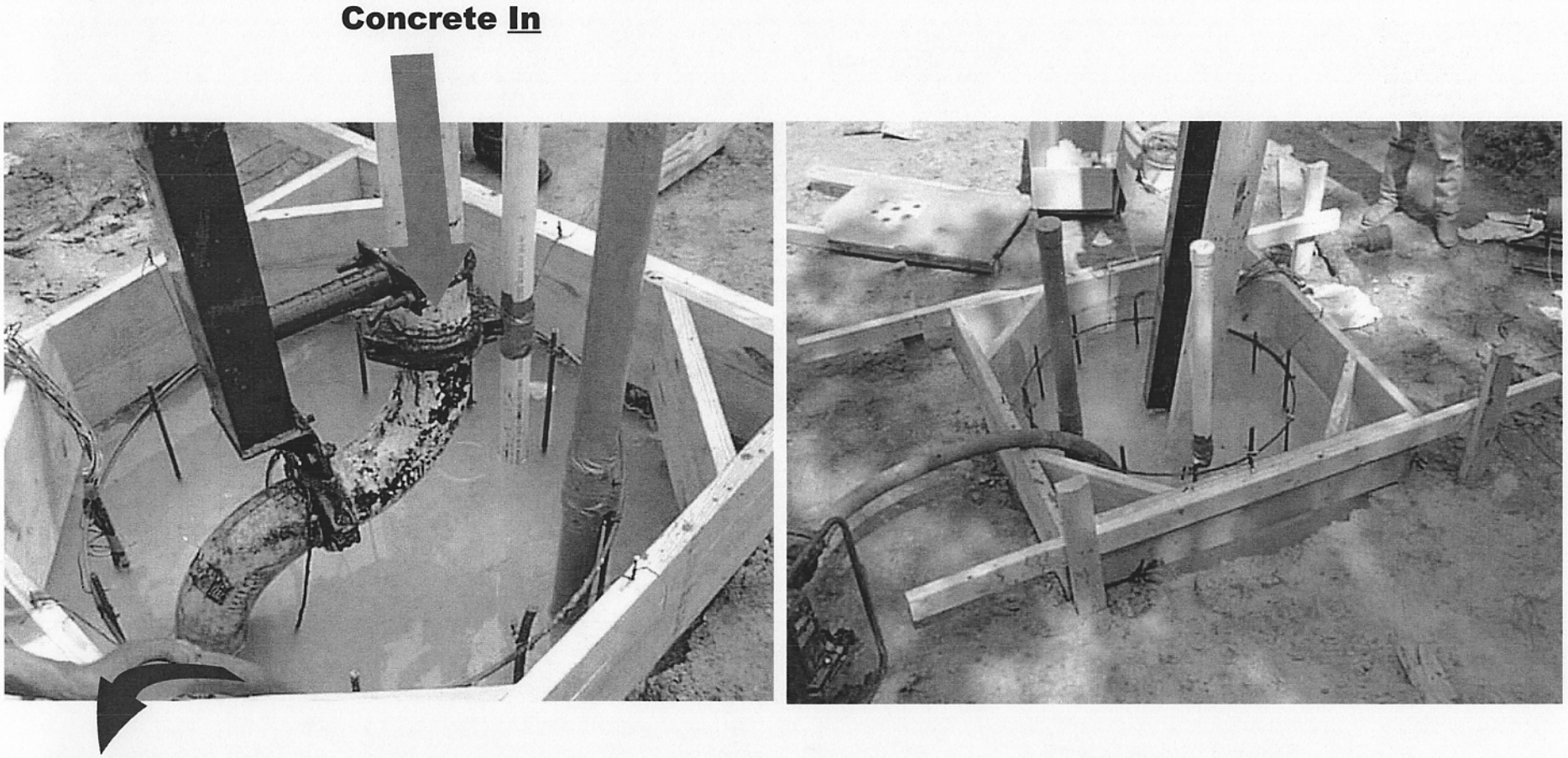

Figure 2.48 Rate of Concrete Placement > Rate of Pumping Ploymer Slurry

Figure 2.49 Overflow of the Polymer Slurry Due to the Slow Rate of Discharge.

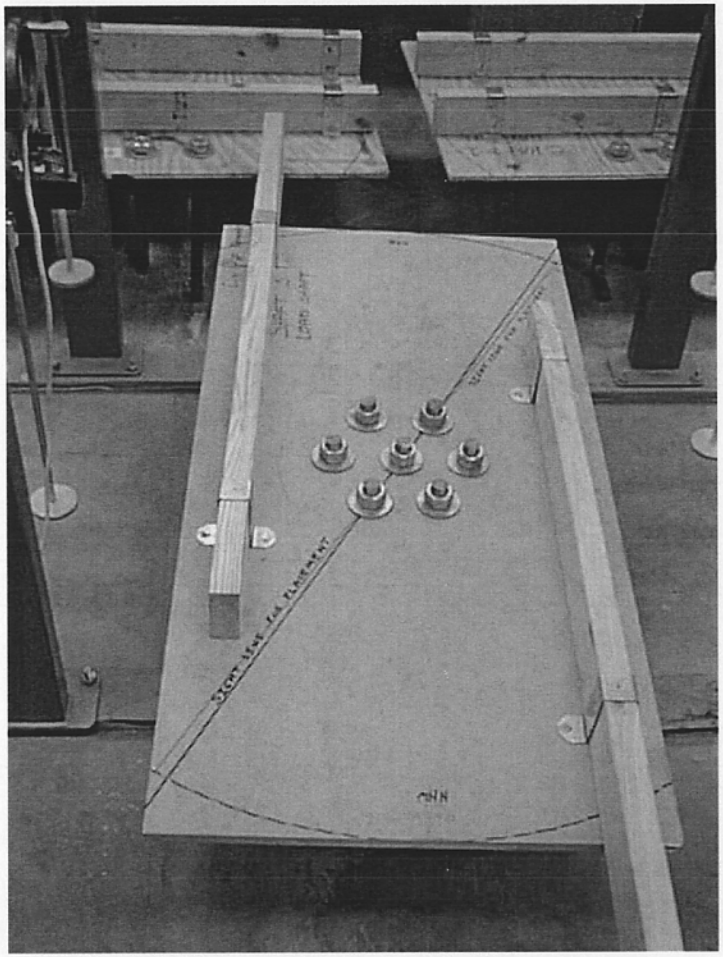

Figure 2.50 Anchor Bolt Template For the Load Support Shaft

Figure 2.51 Anchor Bolt Template For the Tested Shaft

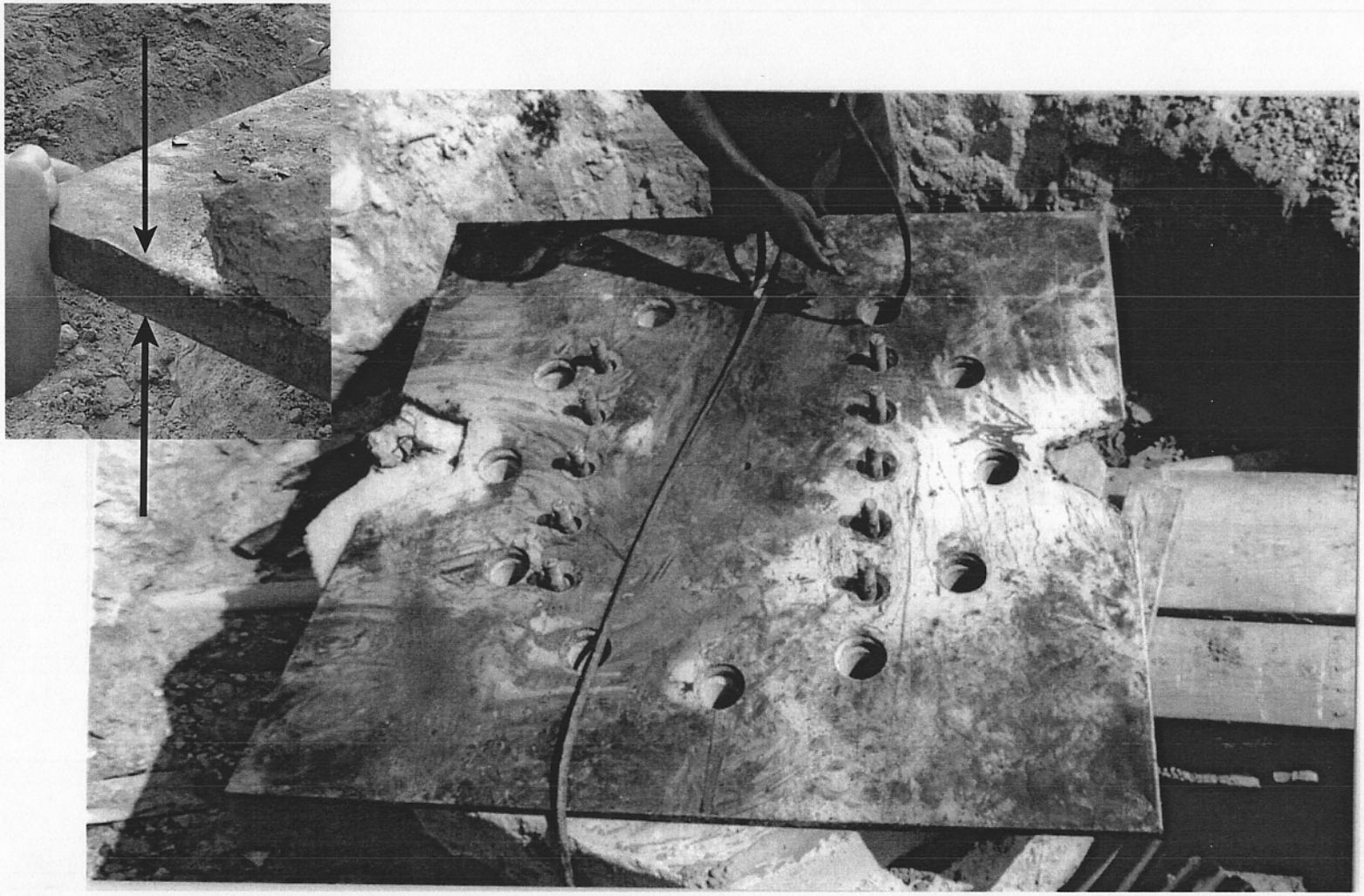

Figure 2.52 Top Plate for the Tested Shaft; Adding 2" Diameter x 24" Length Anchors

Figure 2.53 2" x 24 " Steel Anchors

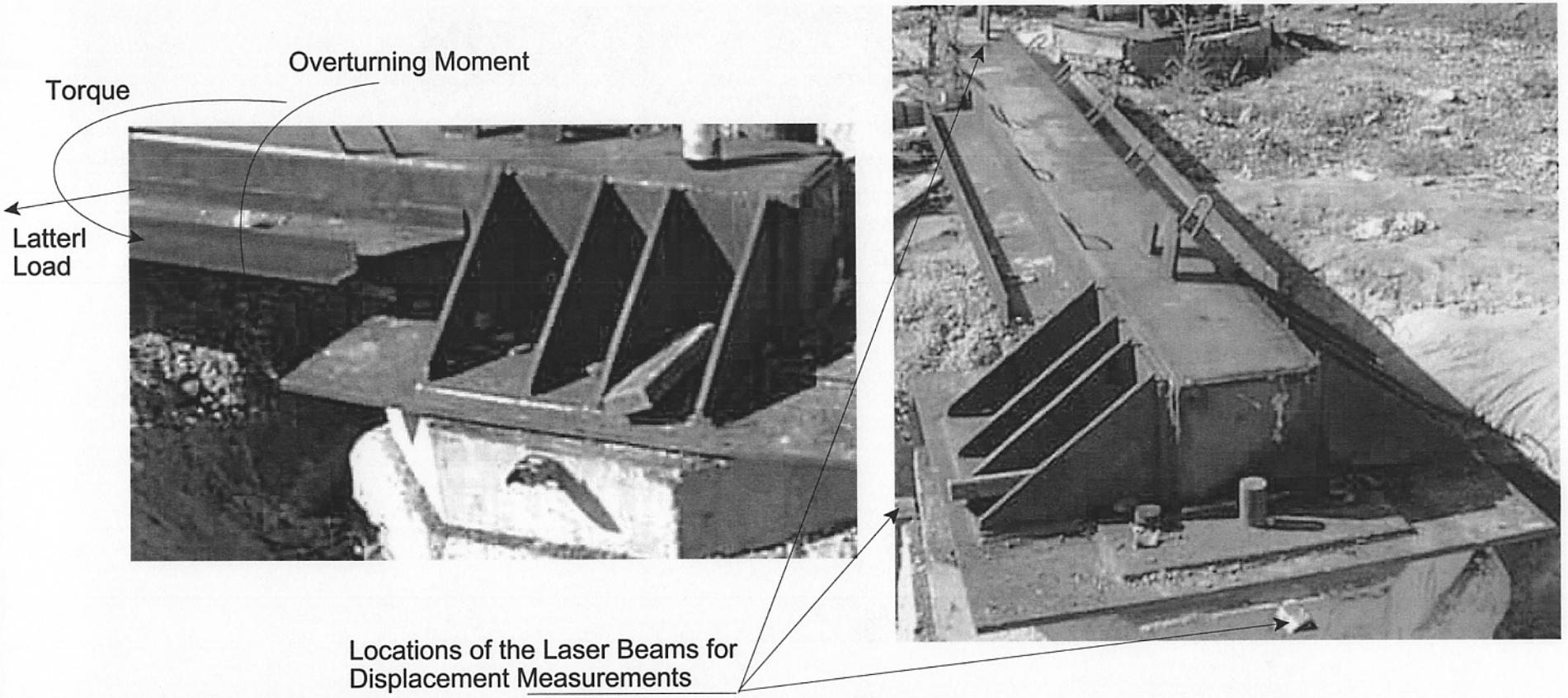

Figure 2.55 Torsional Test Arrangement for the Drilled Shafts

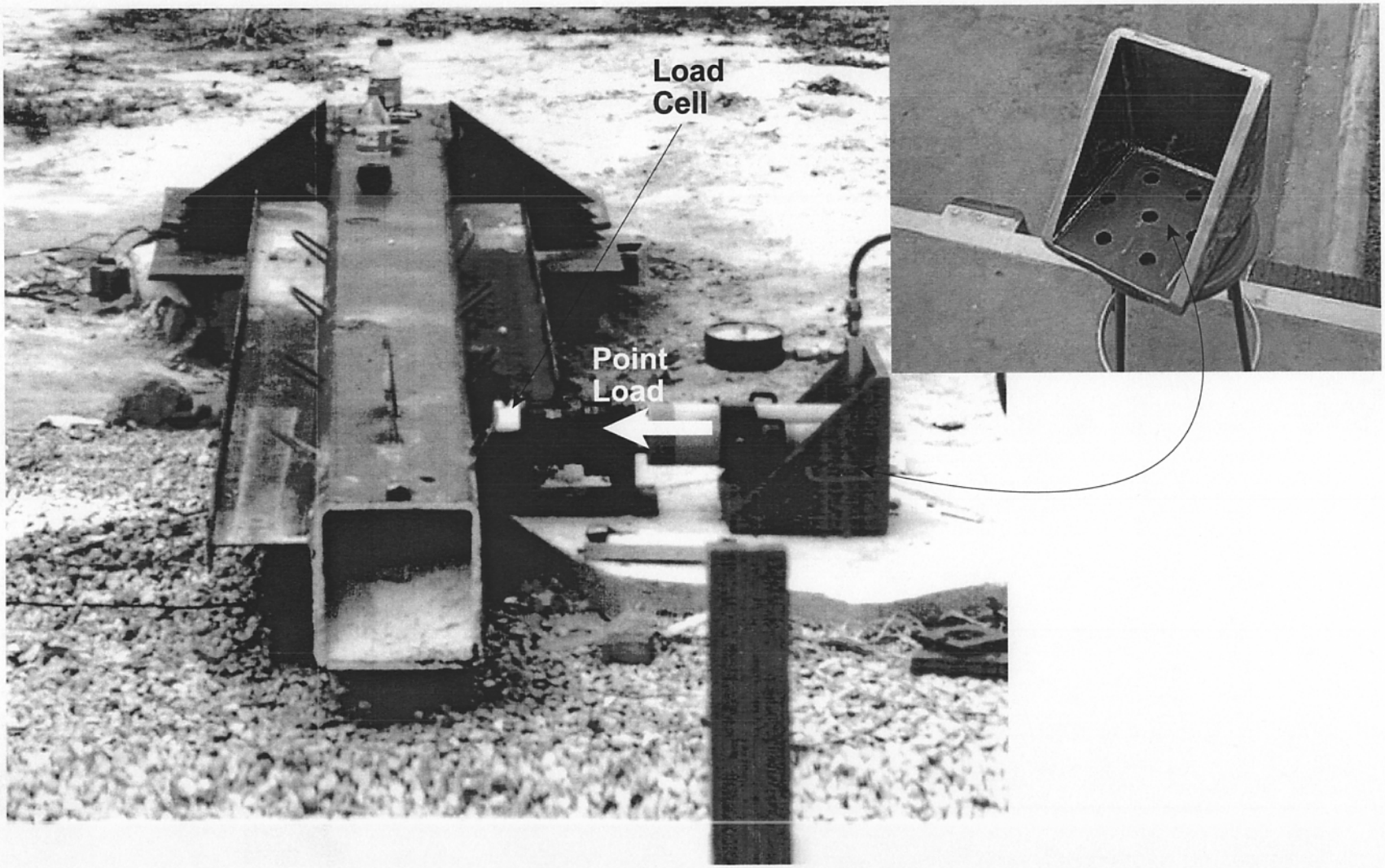

Figure 2.56 Load Application at The Arm

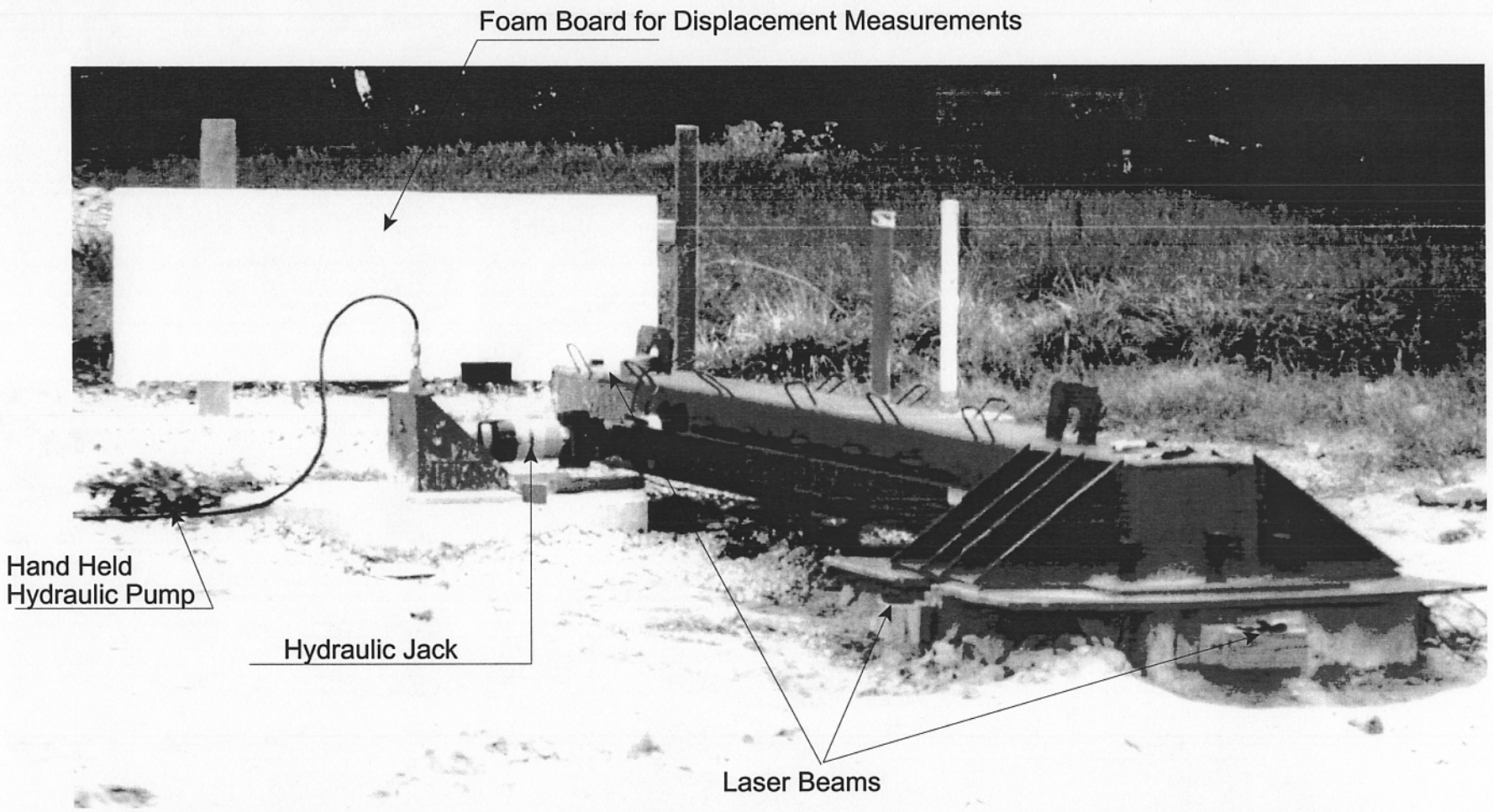

Figure 2.57 Torsional Testing on Drilled Shaft

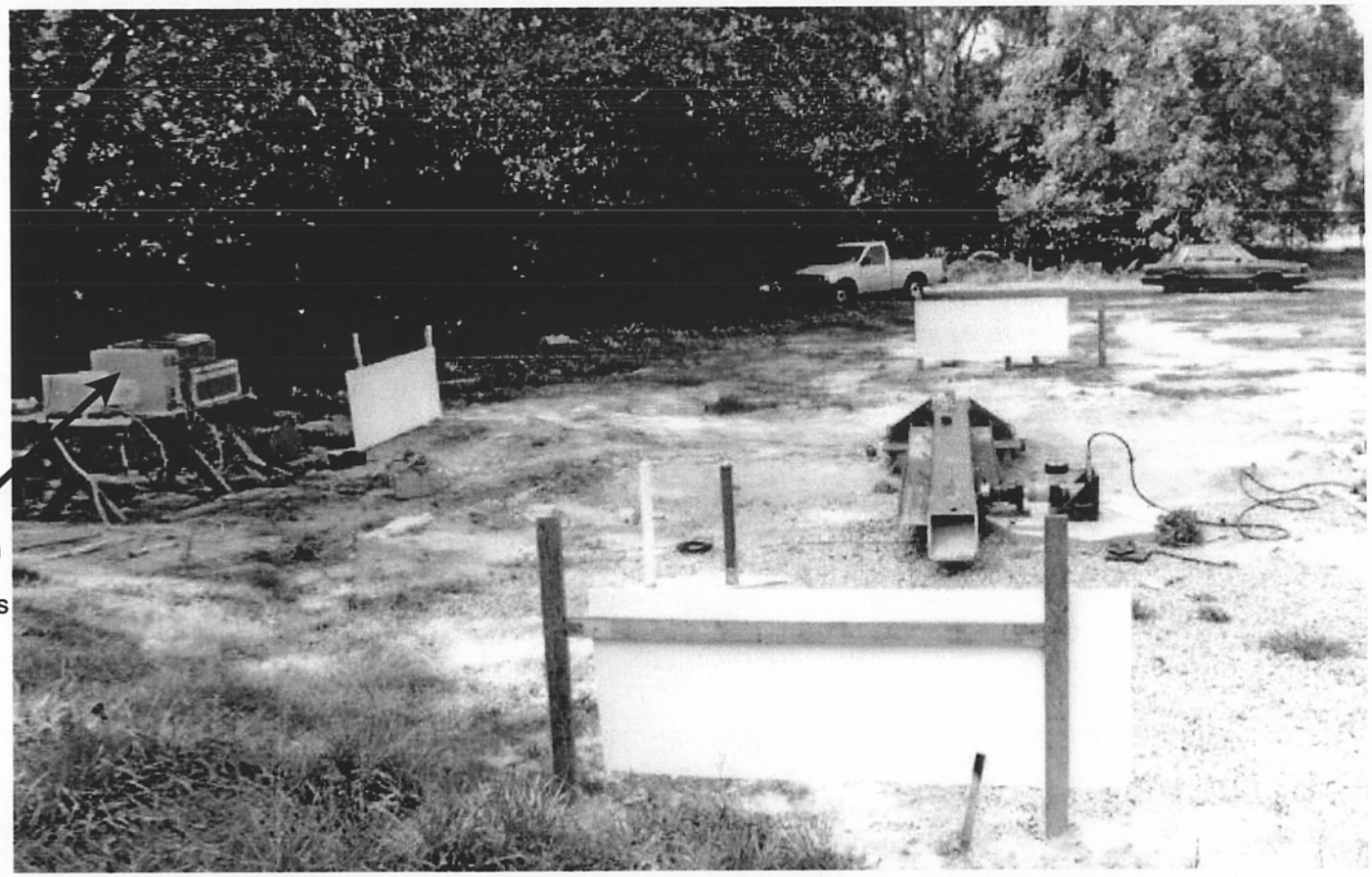

Figure 2.58 Load - Deformation Measurements During Torsional Testing on Drilled Shaft


CRAFTSMAN